UNIVERSITY OF KWAZULU-NATAL

DEVELOPMENT OF A SCALED DOWN LABORATORY TEST BED SYSTEM FOR USE IN THE OPTIMISATION OF CENTRIFUGAL FAN DRIVEN AIR VENTILATION SYSTEMS

by

Ashvir Harcharan

BSc. Eng

Submitted in fulfilment of the academic requirements for the degree of Master of Science in Engineering in the department of Electrical Engineering of the University of KwaZulu Natal in South Africa.

July 2010, Mr. G. Diana

As the candidate’s Supervisor I agree to the submission of this thesis.

Signed :_____

Gregory Diana

I hereby declare that the material incorporated into this thesis is my own original and unaided work except where specific reference is made by name or in the form of a numbered reference. The work contained herein has not been submitted for a degree at any other university.

Signed :_____

Ashvir Harcharan

ACKNOWLEDGEMENTS

The work presented in this thesis was carried out under the supervision of Mr. G. Diana of the Department of Electrical Engineering of the University of KwaZulu-Natal, Durban. I wish to thank Mr. G. Diana for his encouragement and constant support throughout my studies.

I also wish to thank:

- My parents and family for their constant support and encouragement through good times and bad.

- Mr. B Burton for providing technical advice and support.

- The postgraduate students of the School of Electrical, Electronic and Computer Engineering at the University of KwaZulu-Natal for providing encouragement and a stimulating work environment.

- The technical support staff of the Department of Electrical Engineering at the University of KwaZulu-Natal for aid in the construction of the test bed.

- National Power Contractors (NPC) for encouragement and for providing financial support.

- The South African National Energy Research Institute (SANERI) for providing financial support.

- The Technology and Human Resources for Industry Programme (THRIP) for providing financial support.

ABSTRACT

This thesis describes work that has been carried out to develop a scaled down laboratory test bed for use in the optimisation of fan driven air ventilation systems found at the various Anglo Coal South African mines. The present system involved in the movement of air underground comprises a fixed speed centrifugal fan driven damper controlled system. National Power Contractors (NPC) together with the University of KwaZulu-Natal (UKZN) proposed a variable speed automated controlled system, but the costs of installing Variable Speed Drives (VSD) and their impact on the energy consumption of a system prior to being installed are important. In addition deliverables required by the industrial partner NPC was to develop a calibrated simulation model where any fan system could be simulated showing potential energy savings.

A test bed was therefore constructed to evaluate the power usage of a VSD while driving a simulated fan. The test bed comprised of two Field Oriented Controlled induction machines. A ventilation system at Anglo Coal's Vlaklaagte colliery was proposed to be simulated by the test bed to develop the Measurement and Verification (M&V) methodology required to represent a business case, but since data from this fan system was not available two other fan systems were studied. One fan system was built at the UKZN whilst the other industrial fan system was at Anglo Coal's Greenside colliery.

TABLE OF CONTENTS

CHAPTER 3 CENTRIFUGAL FAN FUNDAMENTALS

CHAPTER 4 TEST BED HARDWARE AND INTERFACING

CHAPTER 5 TEST BED COMMISSIONING

CHAPTER 8 SIMULATION OF A 785 kW FAN BY THE TEST BED

CHAPTER 9 ENERGY COST INDICATOR AND AIR FLOW CONTROL

CHAPTER 10 SUMMARY AND CONCLUSIONS

LIST OF ABBREVIATIONS AND SYMBOLS

Common abbreviations and symbols used in this thesis are listed below:

Abbreviations

AC	Alternating Current
BOP	Basic Operator Panel
DB	Data Block
DC	Direct Current
DOL	Direct On Line
d-axis	direct axis
DP	Distributed Periphery
EMF	Electromotive Force
EMI	Electromagnetic Interference
ESCO	Energy Service Company
FB	Function Block
FC	Function
FOC	Field Oriented Control
HSC	High Speed Counter
IRR	Internal Rate of Return
MPI	Multi Point Interface
NPC	National Power Contractors
NPV	Net Present Value
OB	Organisation Block
PI	Proportional and Integral
PLC	Programmable Logic Controller
PV	Present Value
q-axis	quadrature axis
SCADA	Supervisory Control And Data Acquisition
SFB	System Function Block
SFC	System Function
UDT	User Defined Data Type

UKZN	University of KwaZulu-Natal
VFD	Variable Frequency Drive
VSD	Variable Speed Drive

Symbols

C_p	Pressure coefficient.
C_v	Fan flow rate coefficient.
C_w	Fan power coefficient.
d	Fan impeller diameter (m), rotor diameter (m).
e	Induced electromotive force (emf).
I_p	Phase current (A).
i_{ds}	Instantaneous d-axis stator current (A).
i_{qs}	Instantaneous q-axis stator current (A).
i_{dr}	Instantaneous d-axis rotor current (A).
i_{qr}	Instantaneous q-axis rotor current (A).
J	Inertia (kg-m^2).
l	Length (m).
L_e	Stator and referred rotor inductance (H).
L_m	Mutual inductance between the stator and the rotor (H).
L_1, L_s	Stator leakage inductance (H).
L_2, L_r	Rotor leakage inductance referred to the stator (H).
L_{11}	Stator self inductances (H).
L_{22}	Rotor self inductances (H).
m	mass (kg).
n	Fan speed, test bed speed (rad/s, rpm).
P_{ph}	Phase power (W, kW).
p	d/dt.
P	Power (W, kW).
P_s	Fan pressure (Pa).
$p\omega_r$	Rate of change of speed.
Q	Fan flow rate (m^3/s).
R_1, S_r	Stator resistance (Ω).
R_2, R_r	Rotor resistance (Ω).
R_e	Stator and referred rotor resistance (Ω).
r	Radius (m).

s	Slip.
t	Time (s).
T_{em}	Electromagnetic torque (Nm).
T_l	Load torque (Nm).
T_{mech}	Mechanical torque (Nm).
T_{wf}	Torque due to windage and friction (Nm).
Vp	Phase voltage (V).
v	Volume (m^3).
V_{ds}	d-axis stator voltage (V).
V_{qs}	q-axis stator voltage (V).
V_{dr}	d-axis rotor voltage (V).
V_{qr}	q-axis rotor voltage (V).
β	Frictional damping coefficient (N.m.s/rad).
ρ	Air density (kg/m^3).
(Wb)	Instantaneous winding flux linkage (Wb-t).
$\overline{\lambda_r}$	Rotor flux linkage space vector in the d-q reference frame (Wb-t).
λ	Amplitude of the rotor flux linkage per phase (Wb-t).
Ψ_λ	Phase angle of the winding flux linkage.
λ_{ds}	d-axis stator flux linkage (Wb-t).
λ_{qs}	q-axis stator flux linkage (Wb-t).
λ_{dr}	d-axis rotor flux linkage (Wb-t).
λ_{qr}	q-axis rotor flux linkage (Wb-t).
τ_{il}	Closed loop time constant.
τ_{ol}	Open loop time constant.
ω	Synchronous angular frequency.
ω_r	Angular rotational speed (rad/s).

CHAPTER 1

OVERVIEW OF THESIS

1.1 Introduction

Anglo Coal, a subsidiary of Anglo American is South Africa's largest coal producer with its 10 mines producing approximately 59 million tons [30] of coal out of the almost 244 million tons [11] of coal produced throughout South Africa in the year 2006. Each mine extracts coal and requires ventilation systems to remove the methane gas to provide a safe, healthy and productive working environment underground. There are between 35 to 40 air ventilation systems at Anglo Coal South Africa, each of which typically comprise three centrifugal fans as shown in Fig. 1.1 and Fig. 1.2 below ranging between 700 kW and 1.2 MW. Fig. 1.2 shows an existing fan ventilation system located at Anglo Coal's Vlaklaagte colliery above ground level and Fig. 1.5 shows this schematically with corresponding labels.

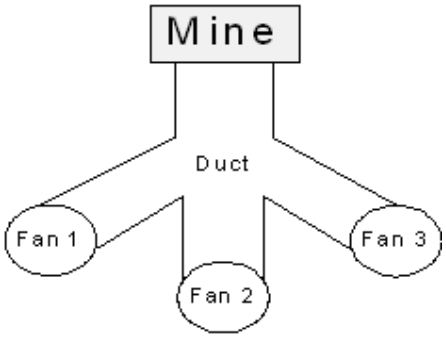

Fig. 1.1 Typical air ventilation system comprising of three centrifugal fans

Fig. 1.2 Existing air ventilation system at Vlaklaagte

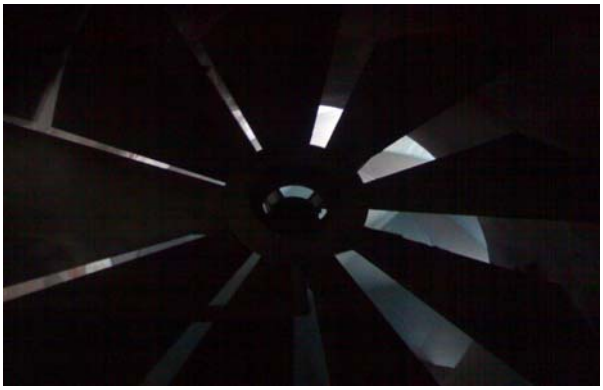

Fig. 1.3 Existing RVC damper (label 4 in Fig. 1.2 and Fig. 1.5) [12]

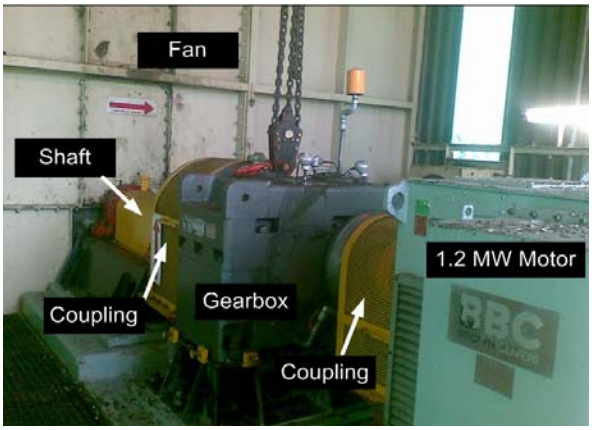

Fig. 1.4 Existing equipment driving a single fan-Fan 3 in Fig. 1.2 (label 1 in Fig. 1.2 and Fig. 1.5)

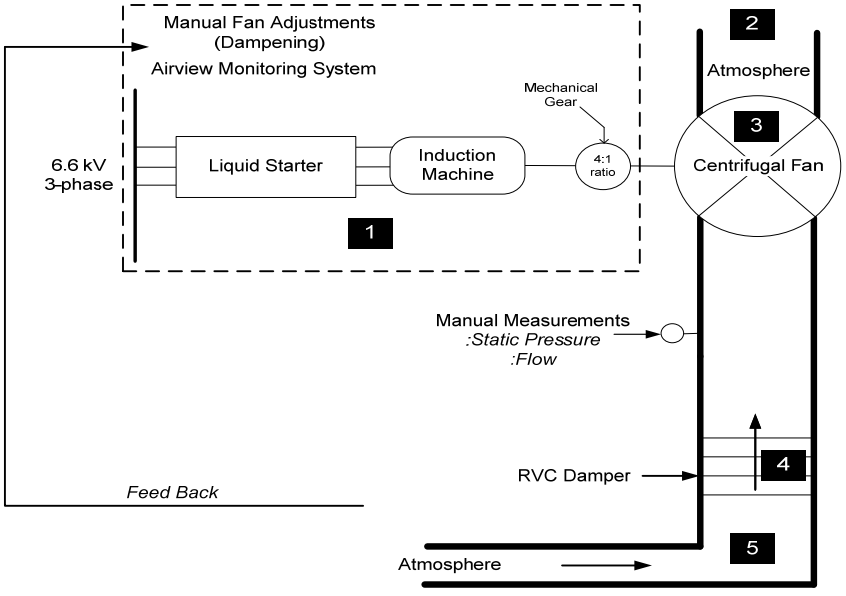

Fig. 1.5 Schematic of the existing air ventilation system [12]

1.2 Problem statement

The required underground ventilation is usually initially calculated for the lifespan of a mine. In the initial stages of a mine the airflow required underground is minimal but as the size of a mine increases the amount of air required underground increases to maintain a safe mining environment. It is therefore important that in the design of the fan ventilation system a method for dealing with the decrease in fan efficiency at flow rates that are lower than what the fan is optimally designed for is taken into account. Lower flow rates can be achieved by varying an inlet damper. Reference must be made to Fig. 1.3 and Fig. 1.5 above focusing on the Radial Vane Controlled (RVC) inlet damper. The disadvantage of utilising a damper to vary the air flow rate is that the power consumed by the fan is high, electronically uncontrolled and fairly stable across the damping range.

An investigation conducted by an Energy Service Company (ESCO) National Power Contractors (NPC) found most of the fan systems at Anglo Coal South Africa to be 45% damped. Contributing further to the inefficiency are air leaks caused by fissures in the underground rock face resulting in variable air flow rates and a loss of pressure throughout the existing mine air ventilation system. Air flow is also restricted in certain sections of the mine by regulators which divert the intake air into exhaust airways before it reaches the faces.

Previous research [1, 9, 23, 29] has shown that energy savings may be achieved through the use of Variable Frequency Drives (VFDs). Based on the initial investigation by NPC together with the knowledge that the ventilation systems are 45 % damped, NPC proposed considering the use of VFDs to improve operational efficiency and control the air flow rate. The possible energy savings through the use of VFDs are estimated in Fig. 1.6 using the universally known Fan laws [9]. From the Fan laws [9] it is known that air flow rate is proportional to the speed of the fan and the power drawn by the fan is proportional to the speed or air flow rate of the fan cubed as shown in Fig. 1.6.

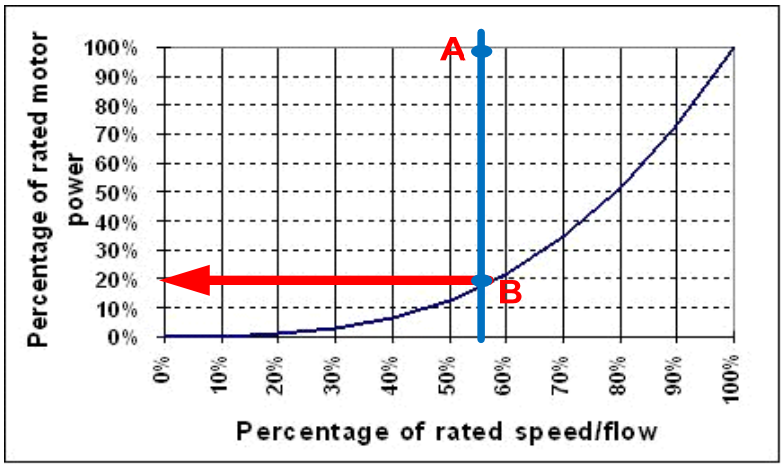

Fig. 1.6 Power Vs (Speed/Flow)^3 of a fan

With reference to Fig. 1.6, considering the fan ventilation system to be 45 % damped would result in the fan operating at point A. Now by reducing the speed of the fan with the use of a VSD and by following the fan laws [9], the fan should operate at point B to produce the same amount of air flow. This results in approximately 80 % saving of power. There are between 35 to 40 air ventilation systems at Anglo Coal South Africa each comprising typically three centrifugal fans.

1.3 Scope of the investigation

NPC approached the University of KwaZulu-Natal (UKZN) to conduct an investigation and develop the Measurement and Verification (M&V) methodology on the air ventilation system at Anglo Coal's Vlaklaagte colliery. This air ventilation system together with the equipment driving one of the centrifugal fans at Vlaklaagte was shown pictorially in Fig. 1.2, Fig. 1.3 and Fig. 1.4. The purpose of the M&V methodology is to test the feasibility of the project required to represent a business case for Anglo Coal.

Previous research [1] at the UKZN showed that a test bed could be used to replicate the operation of any pump or fan system. The UKZN therefore adopted this concept to develop the M&V methodology by developing a scaled down test bed that could replicate the operation of any fan ventilation system. The test bed is shown schematically in Fig. 1.7 comprising of two VFDs and two induction machines coupled together. Induction Machine1 represents the machine driving the fan while induction Machine2 represents the simulated fan.

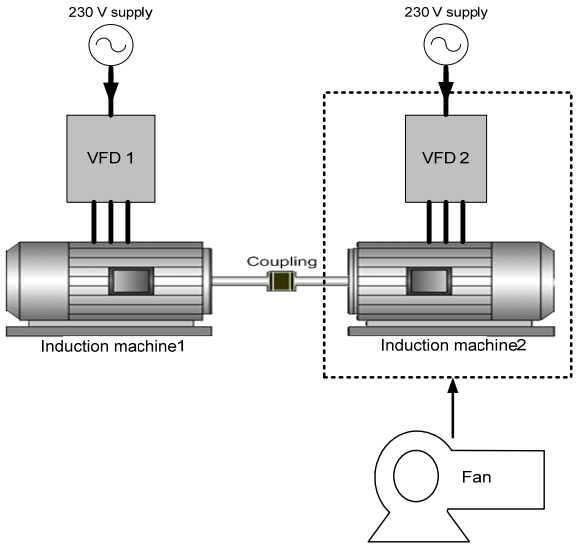

Fig. 1.7 Test bed

In addition to proving the energy savings achievable through speed control of the fan, NPC requested the UKZN to determine whether variable speed operation might afford more consistent air flow rates throughout the mine air ventilation system using a Programmable Logic Controller (PLC) based air feedback control system. This setup is shown schematically in Fig. 1.8 below.

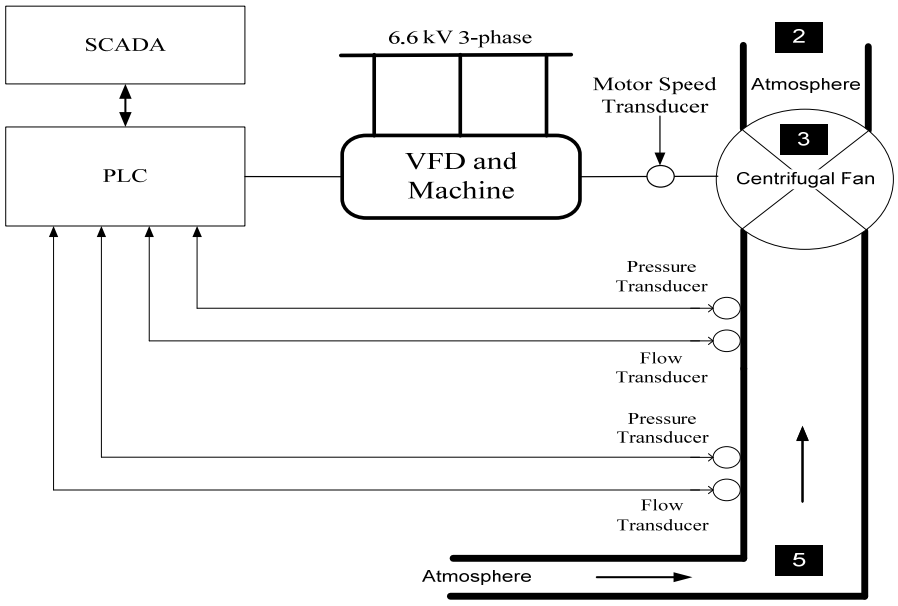

Fig. 1.8 Schematic of the proposed process controlled air ventilation system [12]

The work performed in this thesis will be carried out in four phases:

- The first phase is to gain an understanding of the induction machine and Field Oriented Control (FOC) required to simulate the test bed and to gain an understanding of the operation of centrifugal fans.

- The second phase involves the design, construction and commissioning of the test bed.

- The third phase involves Simulink™ simulations of the test bed replicating the fan, followed by the practical results gained from the test bed.

- The fourth phase involves simulations of an energy cost indicator. Air flow control through speed control of a fan is also investigated.

The overall objectives of this research are to obtain the results of the Simulink™ simulations and the practical results of the test bed. To then compare the results with the operations at the mines and ensure that they correlate with one another and reveal a reduction in energy usage through the intelligent use of VFDs.

1.4 Thesis outline

The thesis is structured as follows:

Chapter 1 discusses the problem statement, scope and objectives of the investigation to be carried out.

Chapter 2 presents the theory of induction machines and the theory of FOC.

Chapter 3 presents the relevant information required to understand the operation of centrifugal fans under damper control and speed control.

Chapter 4 involves the hardware and interfacing of the test bed.

Chapter 5 presents the commissioning of the test bed. This was carried out in two phases. The first phase identified and verified using Simulink™ simulations the induction machine's

electrical and mechanical parameters required to simulate the test bed under FOC; the second phase involved Simulink™ simulations of the test bed under FOC, followed by the practical results gained from the test bed.

Chapter 6 presents the results obtained from the test bed simulating the characteristics of a theoretical fan in Simulink™. The practical results gained from the test bed are then compared to the Simulink™ simulated results.

Chapter 7 discusses the design and construction of a 1.1 kW fan system at the UKZN. The characteristics of the fan system are determined and then simulated by the test bed in Simulink™. The practical results obtained from the test bed are then compared to the Simulink™ simulated results.

Chapter 8 discusses a 785 kW fan system tested at Anglo Coal's Greenside colliery. The fan system is simulated by the test bed in Simulink™. The practical results captured from the test bed are then compared to the Simulink™ simulated results.

Chapter 9 presents energy cost simulations in Simulink™ and in the PLC allowing for the energy consumed by the replicated fans under a specific duty cycle to be determined. Air flow control through speed control of the 1.1 kW fan is then presented.

Chapter 10 presents a summary and conclusion of the work performed in this study. The progress at Vlaklaagte, a business case and future work is also presented.

1.5 Research publications

Certain material in this thesis has been presented at a national conference [12] and two national conventions [13, 31].

CHAPTER 2

MODELLING OF THE INDUCTION MACHINE AND THE THEORY OF FIELD ORIENTED CONTROL

2.1 Introduction

In this chapter the 2-axis theory of the induction machine and the theory of FOC is provided. This theory is necessary for the design of the controllers required to simulate the induction machine under FOC in Chapter 5.

2.2 Hybrid model

In order to understand the principles of FOC and to illustrate how the controller design process enables the non-linear dynamic structure of the induction machine to be decoupled into a linear dynamic structure, the hybrid 2-axis model of the symmetric induction machine is used to develop a block diagram representation of the induction machine. The voltage and flux linkage equations representing the electrical model of the induction machine appear in Appendix A.2. The hybrid model uses the stator currents (i_{ds}, i_{qs}) and rotor flux linkages (λ_{dr}, λ_{qr}) as the state variables. The derivation of the hybrid model is presented in Appendix A.2 and the equations describing the hybrid model in the synchronous reference frame are shown in Eq. 2.1. The equivalent block diagram representation of the hybrid model is shown in Fig. 2.1.

$$\begin{bmatrix} v_{ds} \\ v_{qs} \\ 0 \\ 0 \end{bmatrix} = \begin{bmatrix} R_1 + L_{11}\sigma p & -\omega L_{11}\sigma & \frac{L_m}{L_{22}}p & -\omega L_m \\ \omega L_{11}\sigma & R_1 + L_{11}\sigma p & \omega\frac{L_m}{L_{22}} & \frac{L_m}{L_{22}}p \\ -R_2\frac{L_m}{L_{22}} & 0 & \frac{R_2}{L_{22}} + p & -s\omega \\ 0 & -R_2\frac{L_m}{L_{22}} & s\omega & \frac{R_2}{L_{22}} + p \end{bmatrix} \begin{bmatrix} i_{ds} \\ i_{qs} \\ \lambda_{dr} \\ \lambda_{qr} \end{bmatrix} \quad (2.1)$$

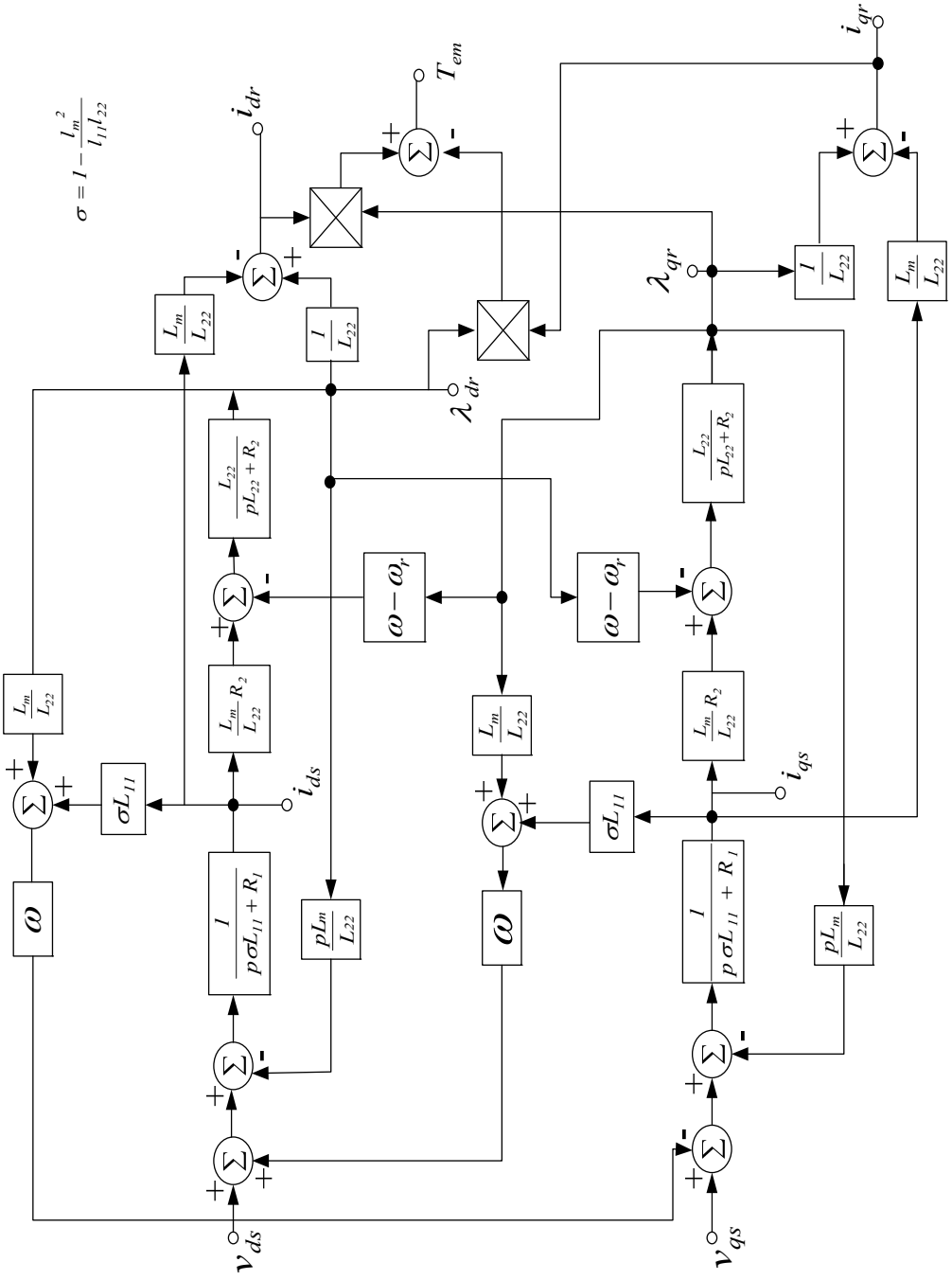

Fig. 2.1 Block diagram of the induction machine [8]

The hybrid model represents the electrical dynamics of the symmetric induction machine. To complete the induction machine's model, the mechanical dynamics of the rotor needs to be incorporated.

2.3 The mechanical model

The mechanical model of the induction machine is used to describe the mechanical dynamics of its shaft and any load that may be coupled to it. For the purpose of this thesis the loads to be considered are a centrifugal fan and another induction machine as shown in Fig. 2.2 and Fig. 2.3.

The electrical and mechanical dynamics of an induction machine are linked by the non-linear electromagnetic torque equation given in Eq. 2.2.

$$T_{em} = \frac{L_m}{L_{22}}(i_{qs}\lambda_{dr} - i_{ds}\lambda_{dr}) \tag{2.2}$$

The mechanical torque required to drive a load at a speed of ω_r is given by Eq. 2.3.

$$T_{mech} = Jp\omega_r + B\omega_r + T_l \tag{2.3}$$

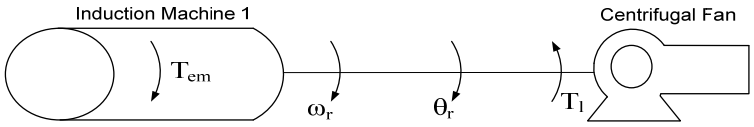

Fig. 2.2 Fan coupled to the machine

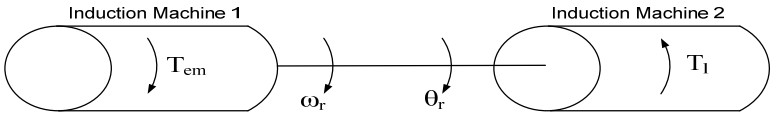

Fig. 2.3 Machines coupled together forming the test bed

Referring to Fig. 2.2 and Fig. 2.3, the shaft of Induction Machine1 is assumed to be rigidly coupled to either the Centrifugal Fan in Fig. 2.2 or Induction Machine2 in Fig. 2.3 and the moment of inertia of the machine (Induction Machine1) is combined with that of either the Centrifugal Fan or Induction Machine2 of the test bed to produce a lumped moment of inertia.

Therefore if we assume a completely rigid shaft we have at all times $T_{em}=T_{mech}$ and for a mechanical shaft speed of ω_r and shaft position of θ_r the equations given in Eq. 2.4 and Eq. 2.5 hold.

$$p\omega_r = \frac{T_{em} - B\omega_r - T_l}{J_m} \tag{2.4}$$

$$p\theta_r = \omega_r \tag{2.5}$$

The electrical and mechanical models together describe the complete induction machine dynamic model. The next section utilises the block diagram form of representation for the induction machine to explain the principles of FOC.

2.4 Principles of FOC

The induction machine has a complex dynamic structure as shown by Fig. 2.1 making speed and torque control difficult. FOC on the other hand is a method of control which enables the complex dynamic structure to be decoupled into that similar to a separately excited DC machine [8].

Referring to Fig. 2.4, FOC is achieved by controlling the q-axis rotor flux linkage (λ_{qr}) to be zero and by keeping the d-axis rotor flux linkage (λ_{dr}) constant [8]. λ_{qr} will only maintain a zero value by controlling the slip of the machine so as to force the angle (α) between the rotor flux linkage vector ($\underline{\lambda_r}$) and the stator current vector (i_s), such that under all conditions $\underline{\lambda_r}$ is aligned with the d-axis component of the stator current vector (i_{ds}) [8].

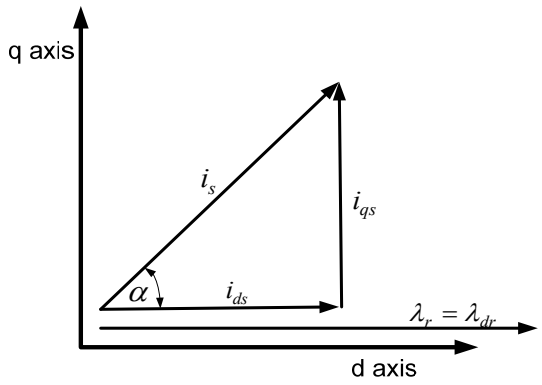

Fig. 2.4 Conditions of Field Oriented Control [8]

For the conditions of FOC in Fig. 2.4 to be met, the q-axis component of the rotor flux linkage (λ_{qr}) must be zero (point A, Fig. 2.5) [8]. If λ_{qr} equals zero then the input to the rotor transfer function has to also be zero (point B, Fig. 2.5). For point B to be zero the two inputs C and D must be equal (Fig. 2.5). This will only occur if the slip is held constant by some external controller resulting in the removal of all the bold lines and their associated blocks (Fig. 2.5) as they no longer contribute to the dynamics of the induction machine resulting in Fig. 2.6 [8].

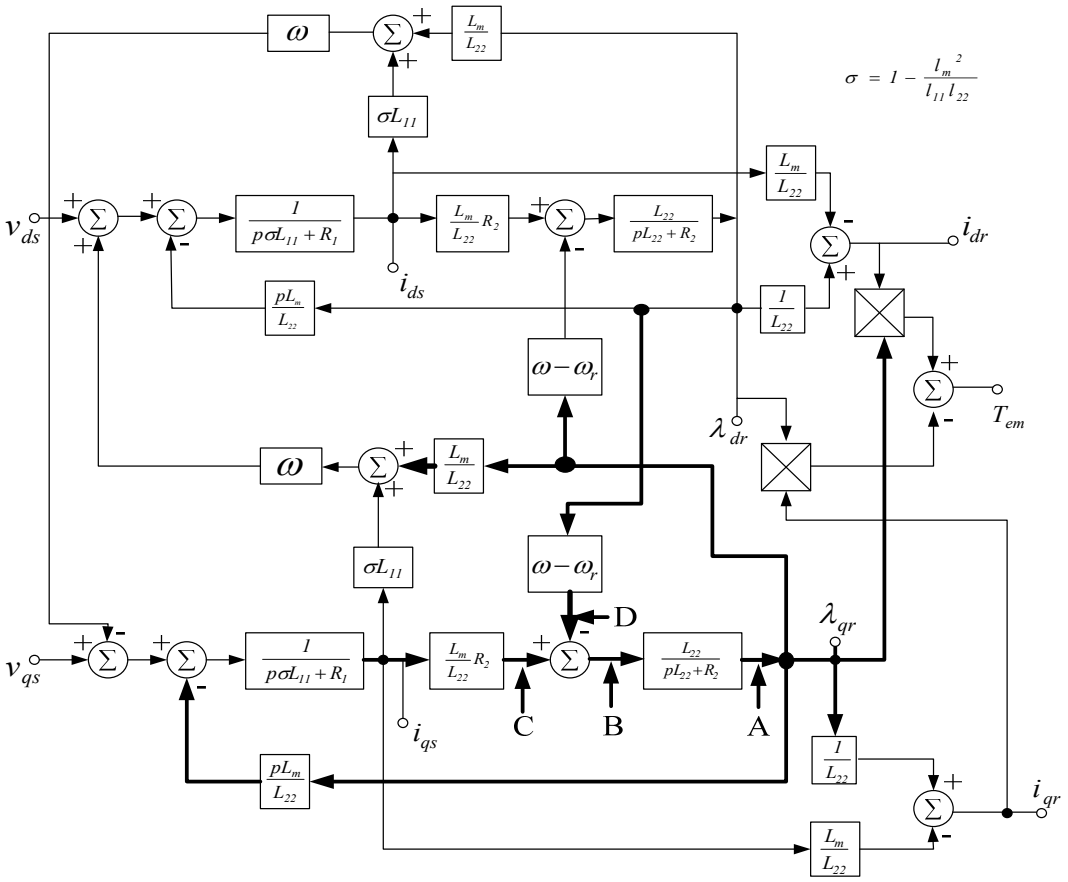

Fig. 2.5 Block diagram of the electrical dynamics of the induction machine [8]

With reference to Fig. 2.5, λ_{dr} can be calculated as given in Eq. 2.6. Eq. 2.6 will be used at a later stage to determine the condition that must be maintained to achieve FOC.

$$\lambda_{dr}(\omega - \omega_r) = \frac{L_m R_2 i_{qs}}{L_{22}} \tag{2.6}$$

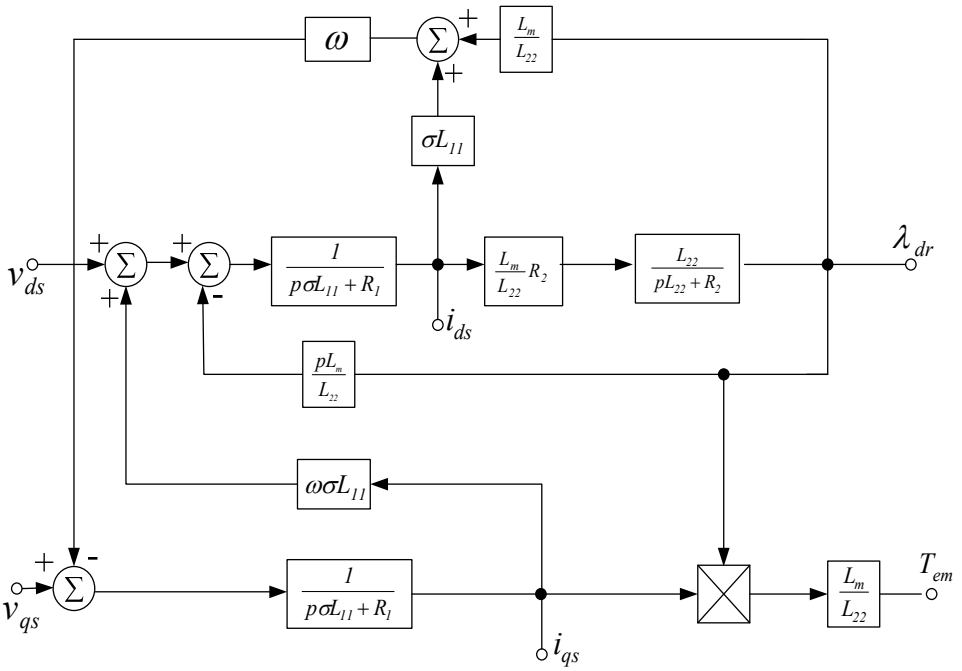

Fig. 2.6 Block diagram of the electrical dynamics of the induction machine when λ_{qr} equals zero

Now from Fig. 2.6 it is seen that:

$$\lambda_{dr} = \frac{L_m R_2 i_{ds}}{L_{22} p + R_2} \tag{2.7}$$

Under steady state conditions i_{ds} is maintained and with the d-axis rotor flux linkage (λ_{dr}) being constant, it results in $L_{22}p = 0$ allowing Eq. 2.7 to be reduced to Eq. 2.8.

$$\lambda_{dr} = L_m i_{ds} \tag{2.8}$$

$$\omega = \frac{R_2 i_{qs}}{L_{22} i_{ds}} + \omega_r \tag{2.9}$$

Eq. 2.9 represents the condition that must be maintained by a controller in steady state to achieve FOC.

Although the model has been reduced, non-linear interaction still exists between the d-axis and q-axis signal paths in the stator circuits [8]. To remove this non-linear interaction, appropriate terms of equal magnitude but opposite sign are added, by the controller, to the input of the

machine (i.e to v_{ds} and v_{qs}) as shown in Fig. 2.7. These pre-compensating terms further reduce the model causing the signal paths shown in bold in Fig. 2.7 to be removed as they no longer contribute to the dynamics of the machine resulting in the stator d and q-axis circuits to be decoupled as depicted in Fig. 2.8.

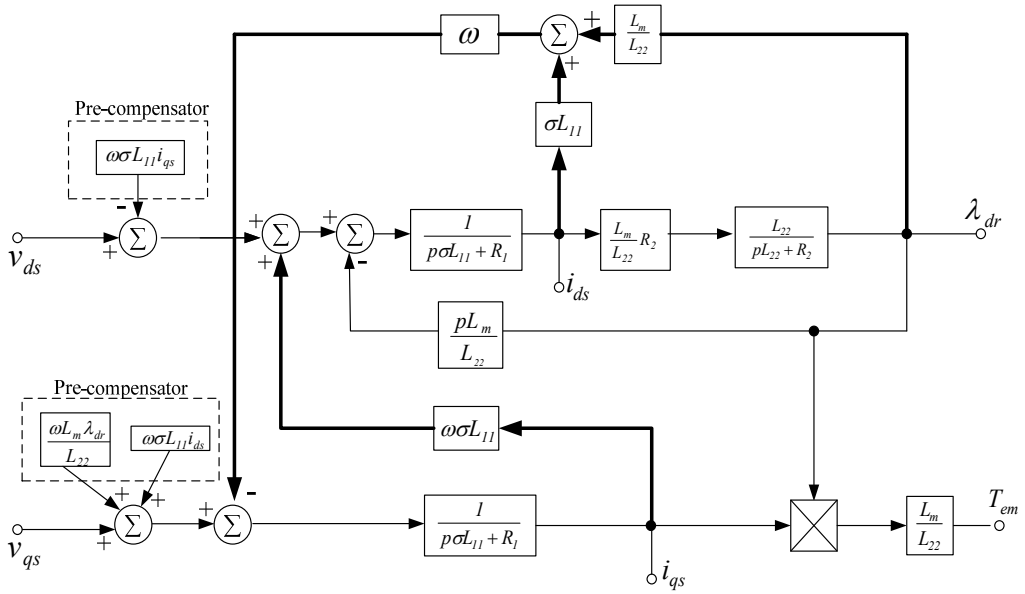

Fig. 2.7 Block diagram of the induction machine with the pre-compensating terms

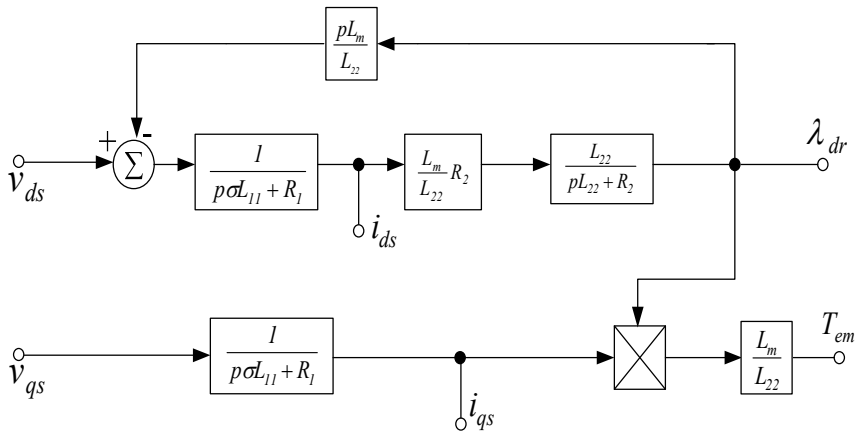

Fig. 2.8 Block diagram of the induction machine after successful compensation

The control of i_{ds} and i_{qs} is necessary to ensure FOC, but these currents are internal to the induction machine and are not directly accessible. External controllers have to be implemented

to control the stator voltages such that the actual currents (i_{ds} and i_{qs}) follow the reference currents (i_{ds*} and i_{qs*}) as closely as possible. These current controllers must be designed with a sufficiently high bandwidth [8].

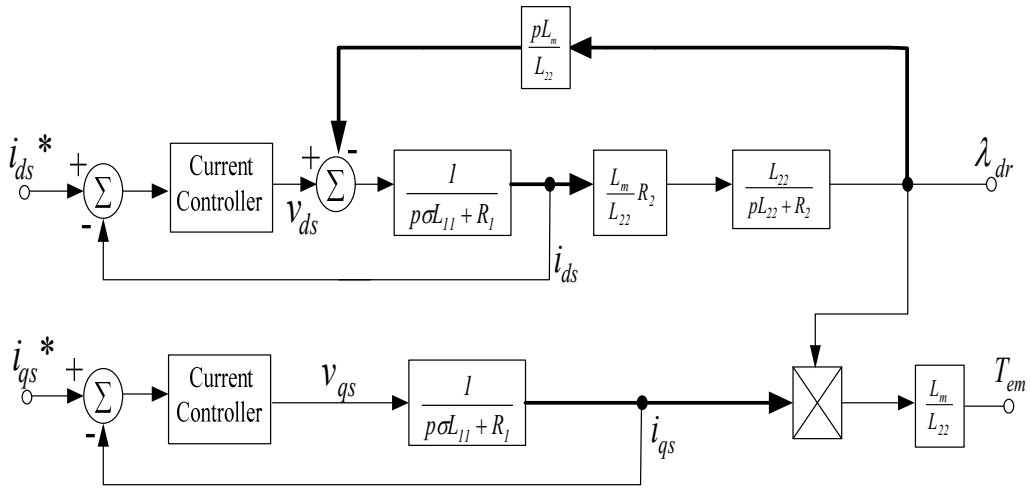

Fig. 2.9 Block diagram of the induction machine with stator current controllers

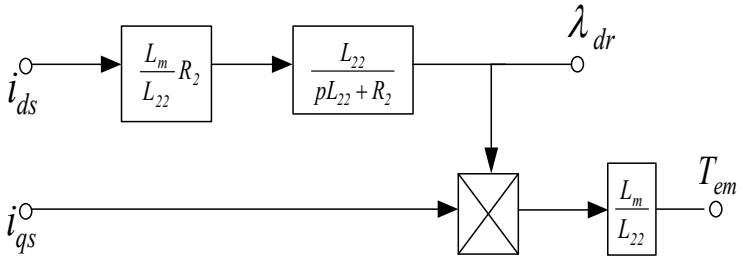

Fig. 2.10 Block diagram of the induction machine under FOC

Successful implementation of the current controllers results in a reduced model as shown in Fig. 2.10 enabling the induction machine to operate in the same manner as a separately excited DC machine. The d-axis stator current (i_{ds}) which under successful FOC produces the magnetising flux inside the induction machine is similar to the field current of a separately excited DC machine and the q-axis stator current (i_{qs}) which is used to regulate the torque produced, is similar to the armature current of a separately excited DC machine [8]. The electromagnetic torque produced by the induction machine under FOC is now given by Eq. 2.10.

$$T_{em} = \frac{L_m}{L_{22}} \lambda_{dr} i_{qs} \tag{2.10}$$

In summary the requirements for FOC can be achieved through:

1. Maintaining a particular value of slip frequency so that Eq. 2.9 holds true.

2. The current controllers exercising control over the stator currents to enable the machine to appear as if it is being supplied from a Current Source Inverter when it is actually fed from a Voltage Source Inverter, since the currents i_{ds} and i_{qs} become controlled inputs to the machine.

3. The d-axis rotor flux linkage (λ_{dr}) being kept constant by keeping i_{ds} constant, thus torque is controlled directly by the q-axis current (i_{qs}).

2.5 FOC controller design

Having described how FOC decouples the non-linear dynamic structure of the induction machine, the controller design process is now described. This section presents a generic design process of the stator current controllers, speed controller, voltage pre-compensating controllers and FOC controller. The design procedure for these controllers has been adopted from [34].

2.5.1 The q-axis current controller

This current controller is designed utilising Fig. 2.9. The q-axis current control loop is taken from Fig. 2.9 and is shown here as Fig. 2.11.

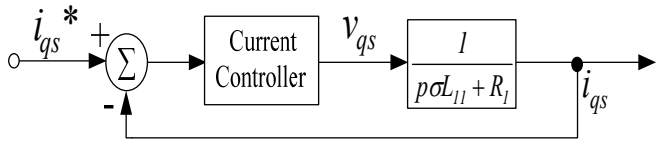

Fig. 2.11 q-axis current controller blocks as in Fig. 2.9

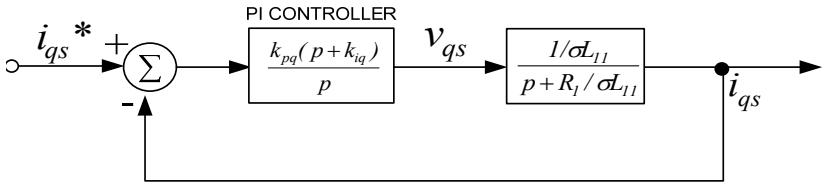

Fig. 2.12 Block diagram of the q-axis current controller

A Proportional and Integral (PI) controller is used to achieve a fast response with a zero steady state error. Choosing $k_{iq}=R_1/\sigma L_{11}$ results in a pole zero cancellation, since the zero of the PI controller cancels the stator pole so the q-axis current controller's integral gain is:

$$k_{iq} = \frac{R_1}{\sigma L_{11}} \tag{2.11}$$

Now:

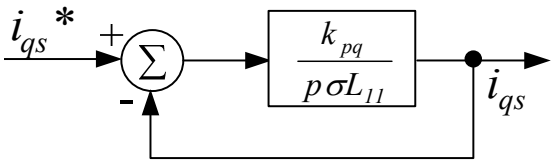

Fig. 2.13 q-axis K_{pq} transfer function

The open loop time constant is given as $\tau_{ol} = \sigma L_{11}/R_1$. Choosing the closed loop time constant τ_{il} to be 1 ms results in the q-axis current controller's proportional gain as given in Eq. 2.12.

$$k_{pq} = \frac{\sigma L_{11}}{1\times\ 10^{-3}\times 314.14} \tag{2.12}$$

2.5.2 The d-axis current controller

This current controller is also designed utilising Fig. 2.9. The d-axis current control loop is taken from Fig. 2.9 and is shown here as Fig. 2.14.

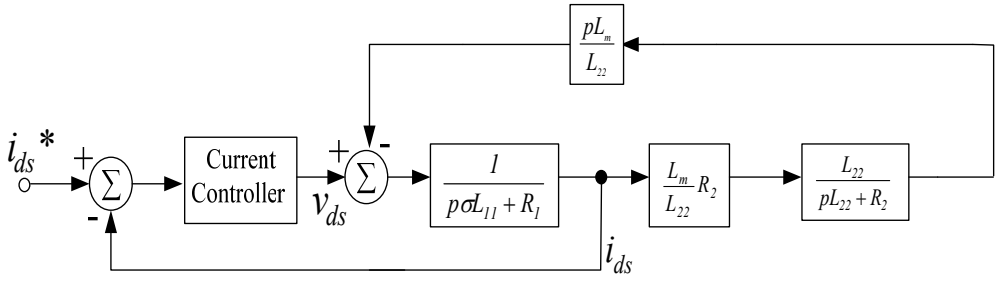

Fig. 2.14 d-axis current controller blocks as in Fig. 2.9

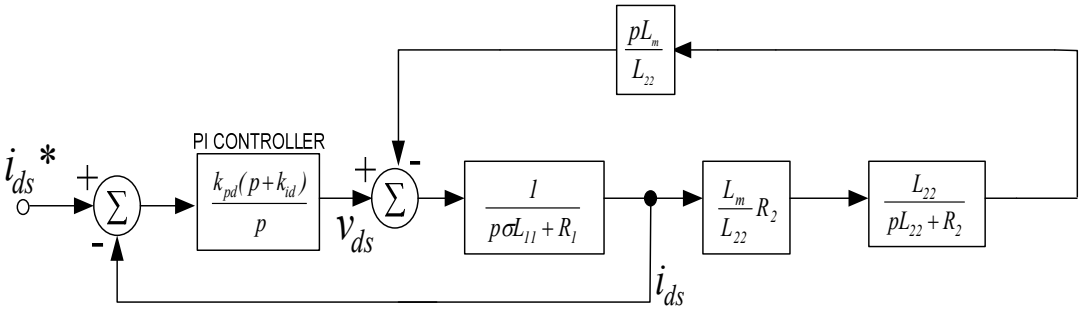

Fig. 2.15 Block diagram of the d-axis current controller

The d-axis transfer function (i_{ds}/i_{ds}^*) is more complicated than the q-axis transfer function (i_{qs}/i_{qs}^*) therefore the transfer function has to be reduced and rearranged as shown in Fig. 2.16 and Fig. 2.17 using the standard rules of block diagram reduction [22].

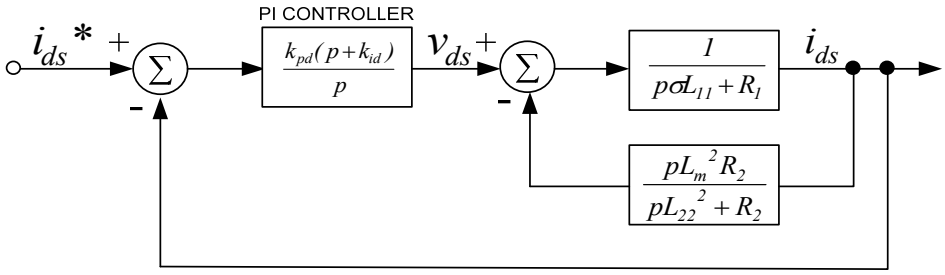

Fig. 2.16 Reduction of the block diagram in Fig. 2.15

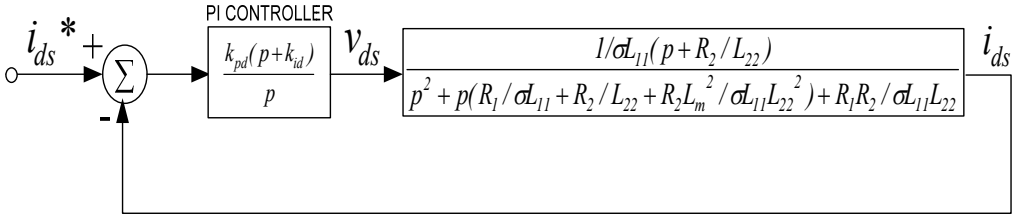

Fig. 2.17 Reduction of the block diagram in Fig. 2.16

The electrical parameters of the induction machine may now be substituted in the transfer function appearing in Fig. 2.17. The resulting transfer function is shown in Fig. 2.18, where *a, b* and *c* represent constants.

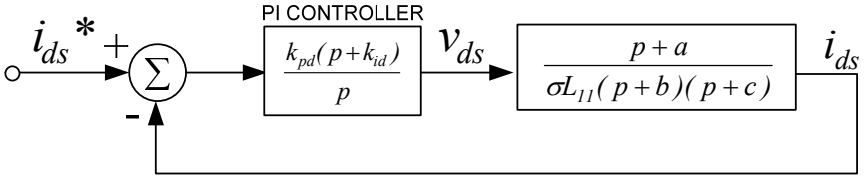

Fig. 2.18 d-axis transfer function after the substitution of the machine parameters

Referring to the transfer function shown in Fig. 2.18, a zero should be located close to a closed loop pole, thus the residue at the pole is small and the coefficient of the transient response term corresponding to this pole becomes small [22]. This means that a closely located pole and zero cancel each other out especially at high frequencies therefore the transfer function in Fig. 2.18 now reduces as shown in Fig. 2.19.

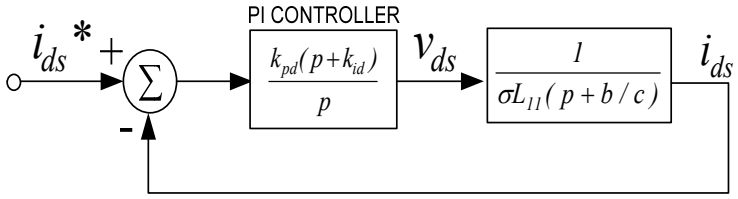

Fig. 2.19 d-axis transfer function

The d-axis current controller may now be designed in a similar manner to that of the q-axis current controller (Fig. 2.12) since the transfer functions are now similar.

Choosing $k_{id} = b/c$ causes the PI controller zero to cancel the stator pole.

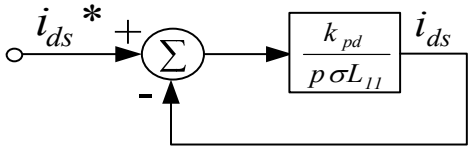

Fig. 2.20 d-axis K_{pd} transfer function

The transfer function in Fig. 2.20 now looks identical to the q-axis current controller transfer function shown in Fig. 2.13, therefore the proportional gain K_{pd} can be chosen to be the same as the proportional gain K_{pq}.

$$K_{pd} = K_{pq} \tag{2.13}$$

2.5.3 Speed controller

Under FOC the induction machine has a dynamic structure similar to that of a separately excited DC machine as explained in Section 2.4. The design procedure of the speed loop for a FOC induction machine is therefore similar to the design procedure of the speed loop for a separately excited DC machine. The transfer function in Eq. 2.14 may be obtained from Fig. 2.21.

$$\omega_r = \frac{T_{em}}{pJ + B} \tag{2.14}$$

In the design of this controller load torque $T_l = 0$.

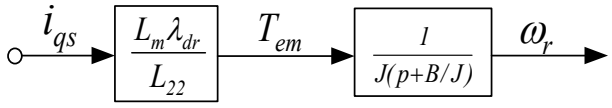

Fig. 2.21 Under FOC and current controllers the induction machine's dynamic structure

A PI controller is added to the transfer function in Fig. 2.21 similar to that of a DC machine as shown in Fig. 2.22.

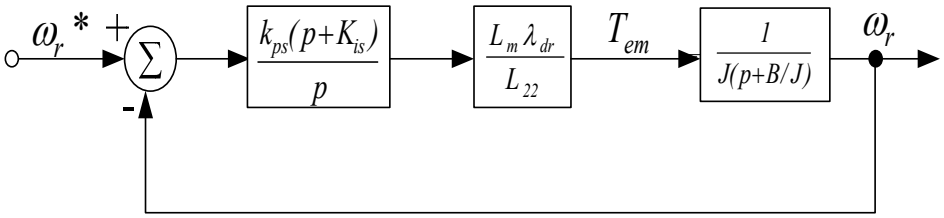

Fig. 2.22 Speed controller

$$k_{is} = \frac{B}{J} \tag{2.15}$$

Choosing $k_{is} = B/J$ results in a pole-zero cancellation.

Usually the closed loop speed time constant is chosen to be ten times larger than the time constants of the d and q-axis current controllers, both of which are equal to 1 ms [34]. The speed loop time constant is therefore equal to 10 ms.

Therefore: $k_{ps} = \dfrac{JL_{22}}{L_m \lambda_{dr} (10 \times 10^{-3})}$ (2.16)

For maximum torque production it is advantageous to maintain the flux linkage λ_{dr} at its rated value of λ_{dr}*. Refer to Appendix B for the procedure to calculate the rated rotor flux linkage.

2.5.4 Voltage pre-compensating controllers

The d-axis and q-axis stator signal paths have cross coupling effects existing between them [8]. The purpose of the pre-compensating controllers is to cancel these cross coupling effects by adding terms in the pre-compensator that have the same magnitude but opposite sign as the terms that have to be cancelled.

2.5.4.1 The q-axis voltage pre-compensator

The q-axis stator signal path together with its pre-compensating controller is shown in Fig. 2.23. Fig. 2.23 is reproduced from Fig. 2.7.

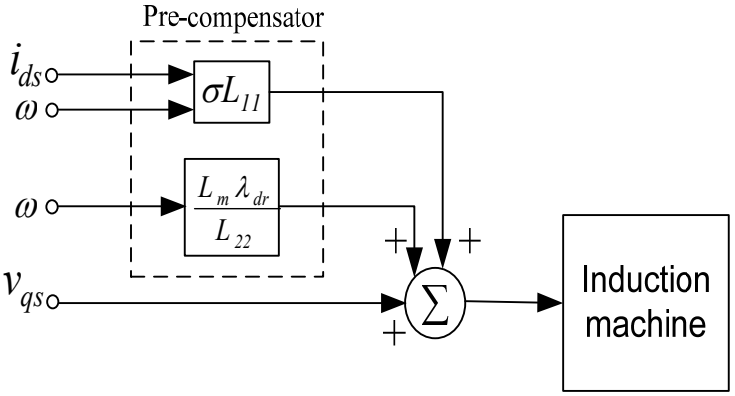

Fig. 2.23 The q-axis voltage pre-compensating controller

2.5.4.2 The d-axis voltage pre-compensator

The d-axis stator signal path together with its pre-compensating controller is shown in Fig. 2.24. Fig. 2.24 is reproduced from Fig. 2.7.

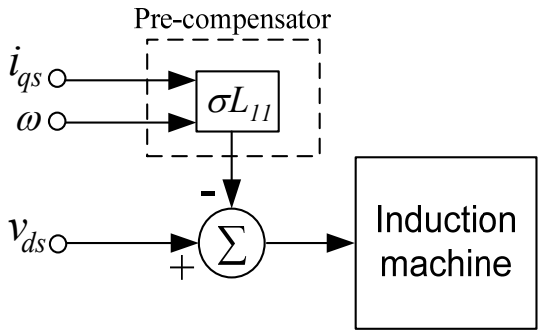

Fig. 2.24 The d-axis voltage pre-compensating controller

2.5.5 FOC controller

The main function of this controller is to ensure that Eq. 2.9 holds true at all times. Eq. 2.9 is repeated here as Eq. 2.17.

$$\omega = \frac{R_2 i_{qs}}{L_{22} i_{ds}} + \omega_r \tag{2.17}$$

2.6 Conclusion

In this chapter the 2-axis hybrid model of the induction machine was used to explain the principle of FOC enabling the induction machine to have a dynamic structure similar to that of a separately excited DC machine. The design procedure of the controllers required to implement FOC was then presented. This is necessary to simulate the two induction machines in the test bed under FOC. The simulations are presented in Chapter 5.

The next chapter introduces the main aspect of this thesis, which is fans and their associated characteristics.

CHAPTER 3

CENTRIFUGAL FAN FUNDAMENTALS

3.1 Introduction

Chapter 2 presented the two axis theory of an induction machine and described the method of FOC. Under FOC the induction machine behaves like a separately excited DC machine resulting in superior torque and speed control of the machine. This is necessary to accurately and easily control the machines in the test bed to replicate the various fan driven air ventilation systems.

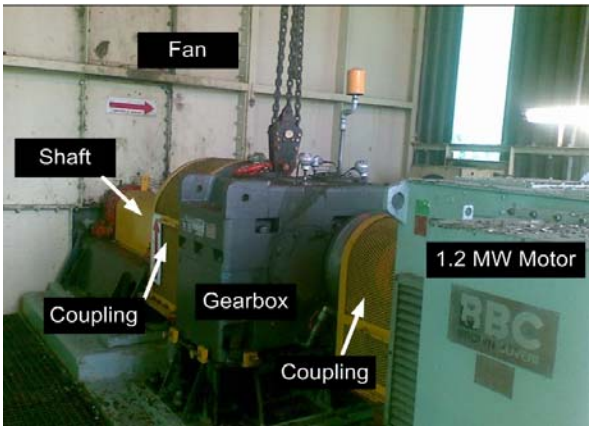

Fig. 3.1 Fixed speed slip ring induction machine at Vlaklaagte

Fixed speed induction machines are used by Anglo Coal at Vlaklaagte (Fig. 3.1) to drive centrifugal fans due to their high reliability, low cost and low maintenance with the air-flow rate being controlled via dampers or adjustable vanes resulting in large amounts of energy being consumed. In other cases the air-flow rate is controlled by regulating the speed of the fan, in which case energy savings may be realised.

The point of operation of any centrifugal fan is specific to the system in which it is deployed and is determined by both the fan characteristic (Fig. 3.4) and the system characteristic (Fig. 3.7). The fan characteristic is supplied by the manufacturer in the form of fan characteristic curves (Fig. 3.5). The system characteristic is a curve that represents the physical system (Fig. 3.6), which is dependant on the type of dampers or ducting used to transport the air. The fan and system characteristics are overlaid on one another and the intersection of the two characteristic curves represents the operating point (Fig. 3.8) of the fan. Varying a damper or adjusting the

speed of the fan changes the operating point of the fan. Therefore whether any energy savings are achievable through variable speed operation of the fan instead of fixed speed damper operation is dependant on the operating point of the fan. This chapter presents centrifugal fans and their associated characteristics showing the different operating points of a fan realised through variable speed and fixed speed damper operation.

3.2 Characteristics of Centrifugal fans

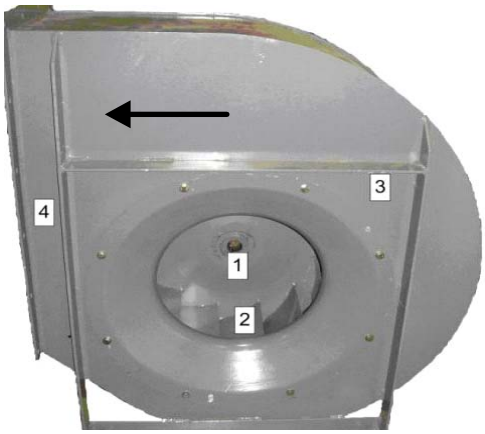

Fig. 3.2 Centrifugal fan depicting, (1) air inlet, (2) impeller, (3) spiral shaped casting, (4) air outlet

A centrifugal fan consists of an impeller (Fig. 3.3, wheel composed of a number of fan blades) running in a spiral casting as shown in Fig. 3.2. The angle or pitch of the fan blades determine the amount of work that the fan has to do in moving the air. The air enters parallel to the axis of the shaft and is accelerated towards the discharge periphery by the blades. There are three forms of impeller blades that a centrifugal fan can have as shown in Fig. 3.3 [9]:

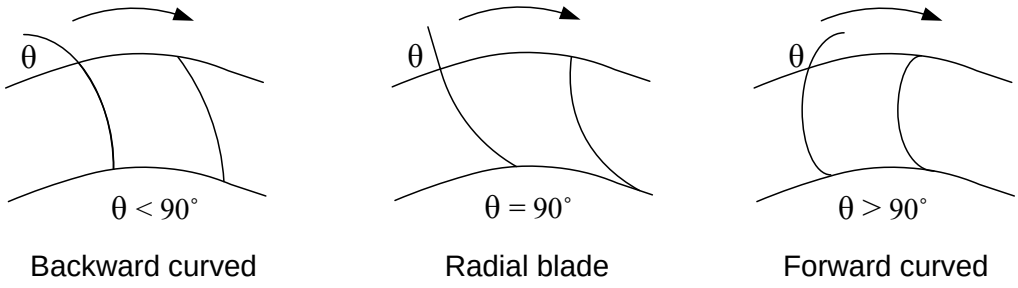

Fig. 3.3 Three forms of impeller blades [9]

1. Backward curved blade - The blade tips incline away from the direction of rotation; the blade angle θ is less than 90˚.

2. Radial blade - The blade tips are radial and the blade angle is equal to 90˚.

3. Forward curved blade - The blade tips incline towards the direction of rotation; the blade angle θ is greater than 90˚.

Forward curved fans are generally used in commercial buildings for ventilation [9]. Backward curved fans are likely to be used for ventilation on a large scale (mines and tunnels) due to their improved efficiency compared with forward curved and radial fans [9]. Radial fans are commonly used as draught fans on large boilers [9]. The centrifugal fans used for ventilation at Anglo Coal South Africa are backward bladed therefore only this type of centrifugal fan will be considered.

The performance of a fan in terms of pressure, volume flow and power absorbed depend on a number of factors [9]. The most important are:

- The design type and size of the fan.
- The point of operation of the fan.
- The speed of rotation of the impeller.
- The condition of the air passing through the fan.

3.2.1 Fan characteristic

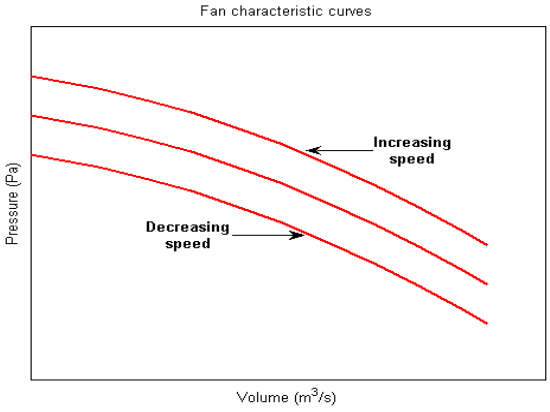

Fig. 3.4 Typical fan characteristic curves

Fig. 3.4 shows typical fan characteristic curves at various speeds.

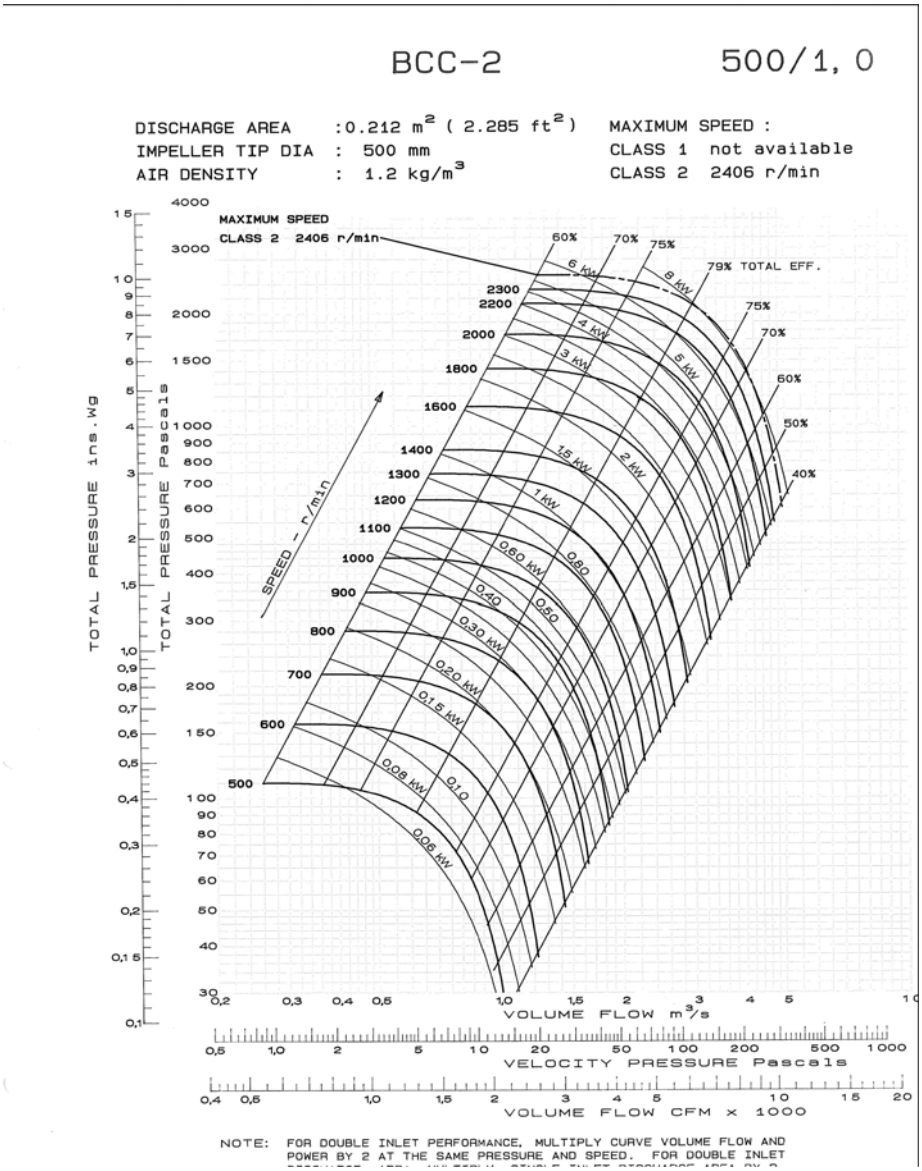

Fig. 3.5 Manufacturers fan characteristic curve [21]

A backward curved blade fan characteristic supplied by the manufacturer [21] for an 8 kW centrifugal fan is shown in Fig. 3.5. Numerous fan characteristic curves plotted at various speeds are shown in Fig. 3.5, together with lines of constant power and constant efficiency covering the expected range of operation of the fan. The relationship between pressure and flow cannot be expressed as a simple mathematical function; however by considering points on the manufacturer's fan characteristic curve (Fig. 3.5), it is possible to identify relationships known

as the Fan laws (Eq. 3.1 to Eq. 3.3) [9]. Eq. 3.1 represents the flow rate; Eq. 3.2 represents the fan pressure and Eq. 3.3 represents the power as the speed of the fan is varied.

$$Law\ 1: Q = C_v n d^3 \tag{3.1}$$

$$Law\ 2: P_s = C_p n^2 d^2 \rho \tag{3.2}$$

$$Law\ 3: P = C_w n^3 d^5 \rho \tag{3.3}$$

Once the data of a single point on the fan characteristic curve are known at a specific speed, the coefficients (C_v, C_p, C_w) in Eqs. 3.1 to 3.3 become known; hence the operating point of the fan at any speed may be determined. This concept of using the fan laws to determine new operating points of the fan is explained further using the next example. If 20 % more air is required then the fan speed needs to be increased by 20 % according to Eq. 3.1. The resulting static pressure will be 44% higher according to Eq. 3.2 and the resulting power will be 73 % higher according to Eq. 3.3. These laws only apply to the fan characteristic curve and not to the system as a whole. The curve that represents the system is known as the system characteristic curve which is discussed next in Section 3.2.2.

3.2.2 System characteristic

Fig. 3.6 Typical industrial air ventilation systems [24]

A system is any assembly of ducts, bends, dampers or any other equipment through which a fan draws in and discharges air as shown in Fig. 3.6. A system characteristic or resistance curve (Fig. 3.7) is a graphical representation of how the system reacts to a given air-flow. The system

resistance is therefore the sum of all pressure losses which could occur through the ducts, bends, dampers etc.

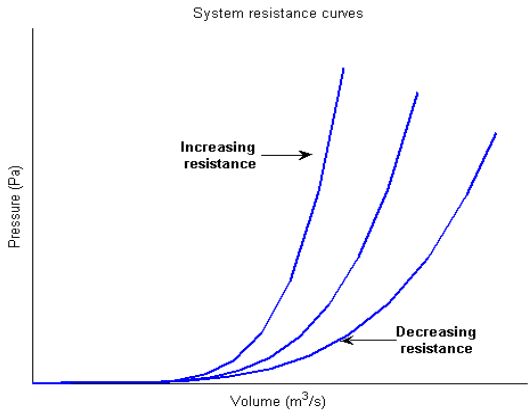

Fig. 3.7 Typical system resistance curves

Referring to Fig. 3.7, a system resistance curve always starts where the flow and static pressure are zero. In a system which is fixed, the pressure at a given flow varies as the square of the air-flow [9]. When a system physically changes the coefficient of the square law changes (see Eq. 3.2), such as if a damper is opened then the coefficient of the square law decreases and the system resistance is reduced resulting in a lower pressure. The closing of a damper or an obstruction in the duct increases the coefficient of the square law and the system resistance resulting in a higher pressure.

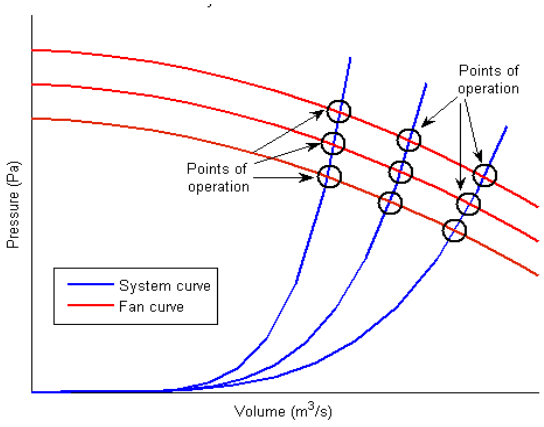

Fig. 3.8 Operating points of a fan

Once the system characteristic curve (Fig. 3.7) is determined, it may then be superimposed on the fan characteristic curve (Fig. 3.4) to determine the operating point of the fan in that specific system as shown in Fig. 3.8.

3.3 Flow control

Although there are numerous ways of controlling the required air-flow rate, only damper control and speed regulation are discussed for the purpose of this thesis. The manufacturer's fan characteristic curve shown in Fig. 3.5 is repeated in Fig. 3.9 having two system resistance curves drawn on it. The system resistance curves shown by the solid red line and solid blue line in Fig. 3.9 are assumed and drawn here to demonstrate the principle of a system resistance curve and how the operating point of a fan changes as the flow rate changes. It must be noted that the system resistance curve is drawn on the 70% efficiency line in Fig. 3.9 and is assumed to be linear for the ease of understanding.

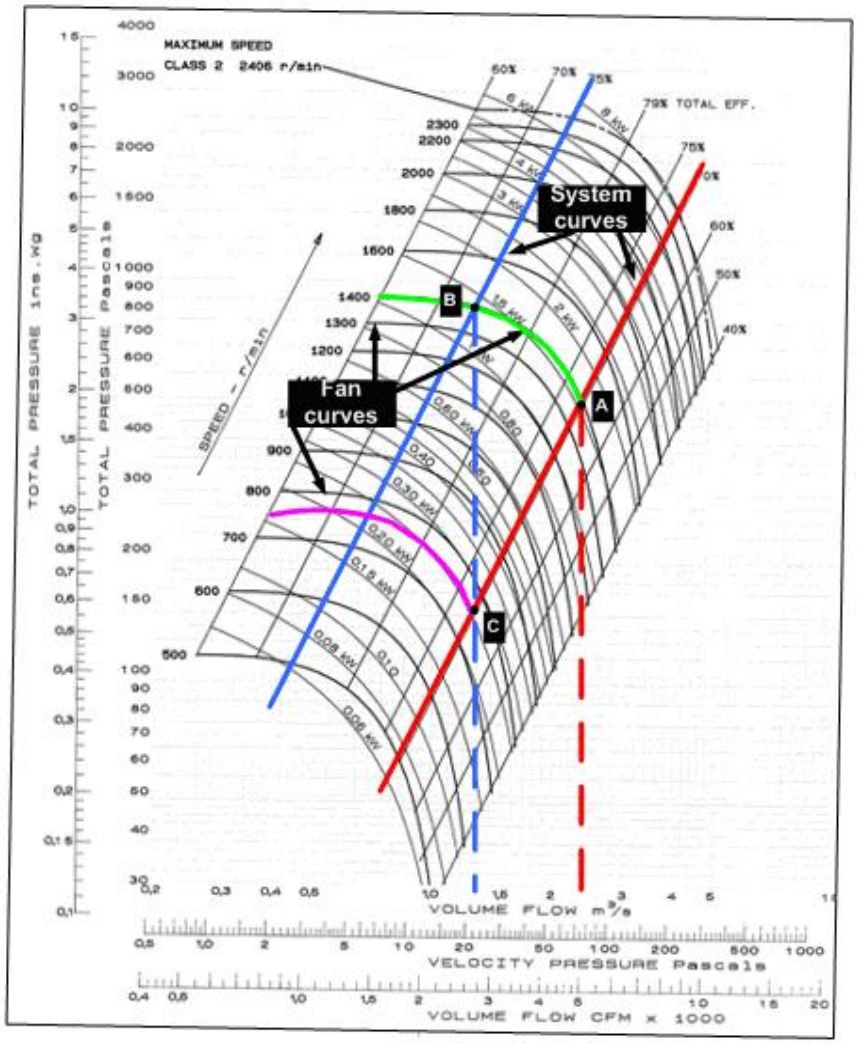

Fig. 3.9 System characteristic curve superimposed on the manufacturer's fan characteristic curve showing the effects of damper control and speed regulation

3.3.1 Damper control

Damper control is the simplest method of controlling the air-flow rate where the fan inlet or outlet area is shut off or dampened by a shutter. Closing or opening the damper effectively modifies the system characteristic curve.

Referring to Fig. 3.9 it is assumed that the fan is initially operating at point A where the green line is the chosen fan characteristic curve and the solid red line is the chosen system characteristic curve. Closing the damper effectively modifies the system characteristic curve causing it to move from point A along the green line towards Point B. The flow rate reduces from 2.38 m^3/s to 1.3 m^3/s and the new system characteristic curve is represented by the solid blue line. With this form of flow control the fan characteristic curve remains constant and the system characteristic curve changes. Between flow rates of 1.3 m^3/s and 3 m^3/s the chosen fan characteristic curve follows the 1.5 kW constant power curve whilst at flow rates below 1.3 m^3/s the fan power reduces to almost 1 kW. This method of flow control is simple, however it expends more energy compared to variable speed control of a fan and thereby incurs higher operating costs, especially where a wide range of flow rates are required since fan power remains almost constant over certain ranges of flow.

3.3.2 Speed regulation

Speed regulation is the most efficient method of flow control available for fans. This method of air volume control dispenses with the damper system. The air-flow rate is varied by regulating the speed of the VSD operated fan. The effect of changing the speed of the fan is depicted in Fig. 3.9.

Referring to Fig. 3.9, it is assumed again that point A is the initial point of operation where the green line is the chosen fan characteristic curve and the solid red line is the chosen system characteristic curve. To change to a flow rate of 1.3 m^3/s from a flow rate of 2.38 m^3/s, the operating point moves along the system characteristic curve towards point C. The power drawn by the fan at point C is 0.25 kW. With this form of air-flow control the fan characteristic curve changes and the system characteristic remains constant. The fan characteristic curve is now shown by the purple line. As the fan speed is varied between 500 rpm and 1400 rpm, the power of the fan varies in accordance with Eq. 3.3 and as depicted by the various constant power

curves in Fig. 3.9 therefore as the air-flow rate decreases, the power consumed by the fan decreases.

3.4 Torque-speed and power-flow representations

In Section 3.3 both damper control and speed regulation were discussed based on simplified assumptions. A graphical representation of how the torque and speed of the induction machine driving the fan changes and how the power drawn and air-flow rate produced by the fan varies when both forms of flow control are implemented is shown in this section in Fig. 3.10 and Fig. 3.11. This is based on the same assumptions as stated in Section 3.3, system resistance curve on the 70% efficiency line.

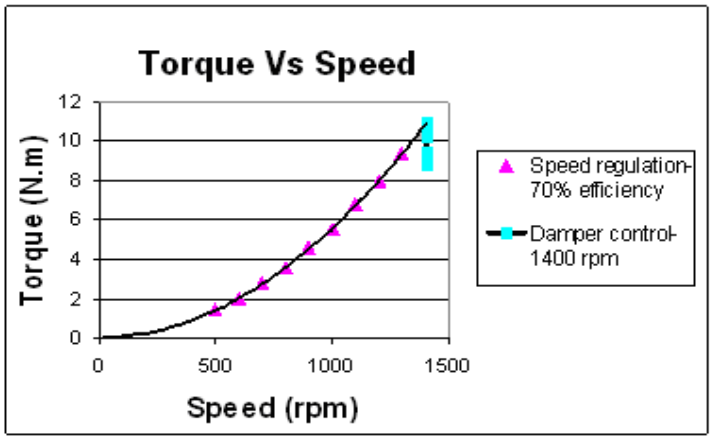

Fig. 3.10 Torque-speed of the motor

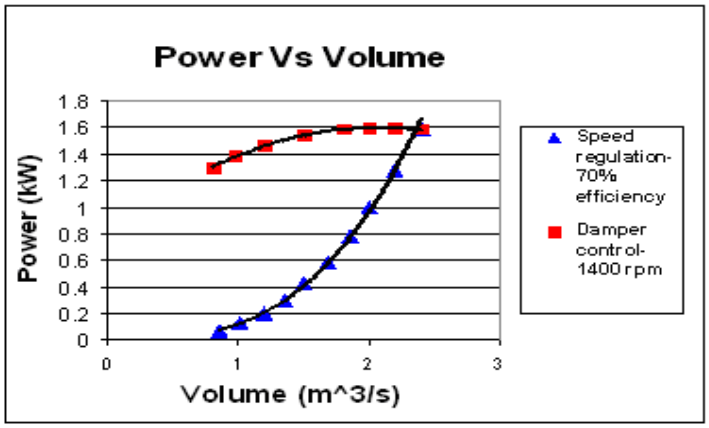

Fig. 3.11 Power-flow of the fan

Fig. 3.10 shows that the torque remains significantly high as the air-flow rate (Fig. 3.11) of the fan varies under damper control, while under speed regulation the torque reduces significantly. The power utilised by the fan under variable speed and damper operation is shown in Fig. 3.11. The saving of power through variable speed operation of the fan is clearly visible by this graphical representation shown in Fig. 3.11.

3.5 Conclusion

The different characteristics of the backward curved centrifugal fan have been presented and discussed since this type of fan is used at Anglo Coal South Africa. The manufacturer's fan characteristic curve for a backward curved centrifugal fan was shown and the effect of varying the air-flow rate of the fan through speed control and damper control were presented based on theoretical assumptions.

The next chapter describes the hardware and interfacing of the test bed.

CHAPTER 4

TEST BED HARDWARE AND INTERFACING

4.1 Introduction

Chapter 2 presented the two axes theory of the induction machine, the theory of FOC and the controller design process. Chapter 3 presented the characteristics of backward curved centrifugal fans and both damper and variable speed operation of these centrifugal fans were presented based on assumptions made on the manufacturer's fan characteristic curve.

A test bed that could replicate the operation of any fan ventilation system was required to develop the M&V methodology. Before any simulations could be performed, the test bed hardware and interfacing were required. This chapter describes the hardware and interfacing of a 3 kW test bed.

4.2 Test bed Hardware and Interfacing

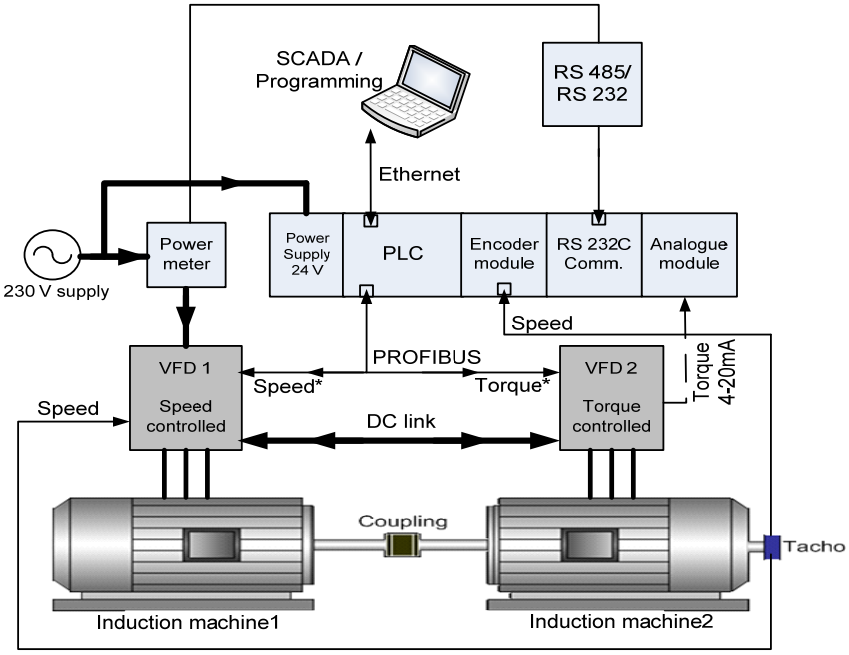

Fig. 4.1 Block diagram representation of the test bed

Fig. 4.1 depicts the test bed schematically. The narrow lines linking the components of the test bed represent communication and signal lines and the thick bold lines represent power lines. Hardware manufactured by Siemens was specified by NPC for use in the development of the test bed since similar hardware is used at Anglo Coal South Africa. The purpose of each component in the test bed is discussed below.

4.2.1 Programmable Logic Controller (PLC) and associated hardware

- **PLC**

Fig. 4.2 Programmable Logic Controller

A Siemens S7-315 2PN/DP PLC shown in Fig. 4.2 performs some of the supervisory logic and control in the project. The module has 256 kB of working memory and a micro memory card to store the user defined programmable software. The PLC has two ports available, one being a Multi Point Interface (MPI)/Distributed Peripheral (DP) port while the other is an Ethernet port. The MPI/DP port is used for PROFIBUS communication. PROFIBUS is an international, open field bus communication profile used for high speed data transmission using low cost connections [16]. It is a bus which allows several automation, visualisation or engineering systems with field devices to operate together [16]. PROFIBUS is used to communicate with the two FOC Drives as shown in Fig. 4.1. The Ethernet port is used for programming the PLC and for linking the test bed to a SCADA program. PROFIBUS and Ethernet were chosen as the communication mediums in the test bed since the same communication media are used at Anglo Coal South Africa.

- **High Speed Counter module**

The High Speed Counter (HSC) expansion module of the PLC is used to read the speed signals (pulses) received from the incremental encoder attached to the shaft of Machine2 in the test bed as shown in Fig. 4.1. The HSC module calculates speed by counting the number of pulses per encoder revolution within a dynamic measuring time [17].

- **RS 232C module**

The RS 232C serial expansion module of the PLC is used to provide the communication link between the power meter and the PLC as shown in Fig. 4.1. The serial expansion module enables all the quantities measured by the power meter to be accessed by the PLC.

- **Analogue module**

The analogue module shown in Fig. 4.1 is a 4 input/2 output 8 bit module. The module allows for both voltage inputs/outputs and current inputs/outputs. The torque calculated by VFD2 in the test bed is sent to the PLC via the current interface of the analogue module as shown in Fig. 4.1.

4.2.2 Variable Frequency Drive and associated hardware

- **VFD**

The main objective of a VFD is to provide a variable frequency output. The main hardware components which assist in achieving this objective are shown schematically in Fig. 4.3.

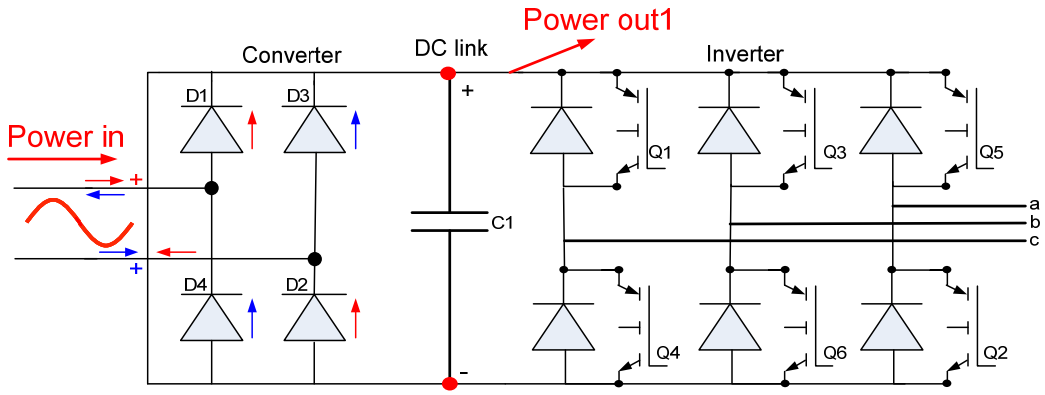

Fig. 4.3 Schematic of the VFD

Referring to Fig. 4.3, the supply is rectified to DC via the diodes labelled D1-D4. The capacitor (C1) assists in maintaining a constant DC link voltage and also ensures a near sinusoidal current output for superior torque performance of the machine. The transistors Q1-Q6 are intelligently gated to produce the variable frequency output.

Fig. 4.4 3 kW Micromaster 440 VFD

The two VFDs used in the test bed are identical and are commercially available MICROMASTER 440 3 kW VFDs manufactured by Siemens as shown in Fig. 4.4. The input voltage of the VFD is 230 V 50 Hz single phase. The output voltage of the VFD is three phase with an output frequency range of 0 Hz to 650 Hz [14].

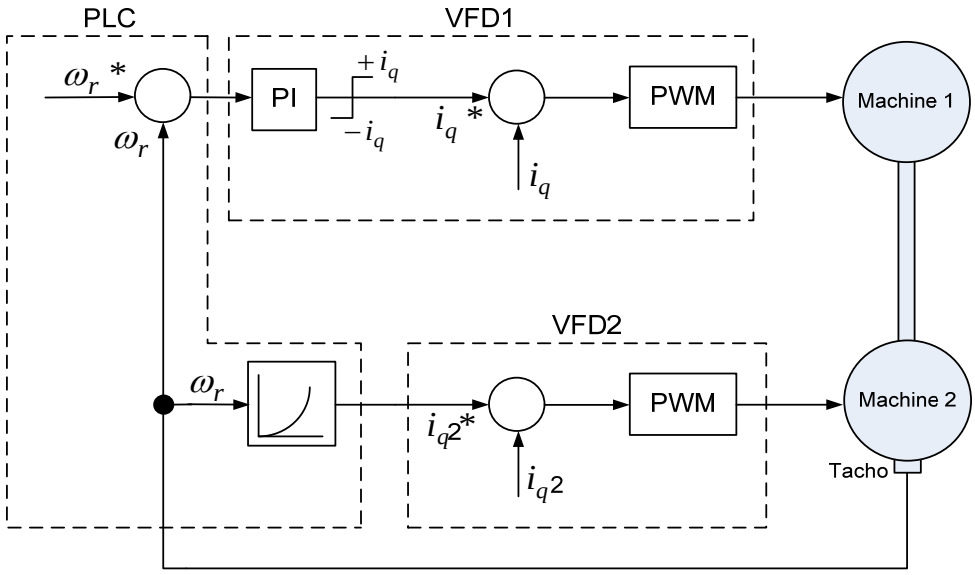

Fig. 4.5 Software integration

The MICROMASTER 440 VFDs are used to control Machine1 and Machine2 of the test bed under FOC. Referring to Fig. 4.5, the required speed and torque setpoints are calculated in the PLC and sent via PROFIBUS to VFD1 and VFD2 respectively. VFD1 operates Machine1 under Speed Control using speed feedback from the incremental encoder discussed in Section 4.2.3

and VFD2 operates Machine2 under Torque Control enabling Machine1 to represent the machine driving a fan and Machine2 to represent the fan.

- **Power flow in the test bed**

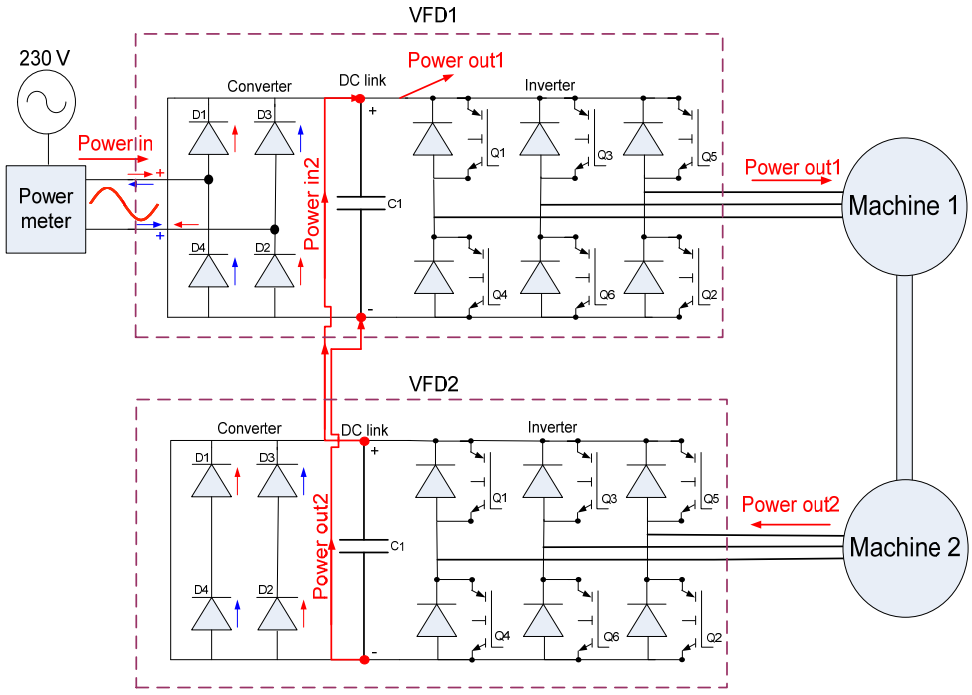

Fig. 4.6 Power flow in the test bed

The power flow in the test bed is described using Fig. 4.6. Machine1 of the test bed operates as a motor while Machine2 operates as a generator. The DC links on both VFD's of the test bed are connected enabling the power generated by Machine2 to be fed back into the system as shown in Fig. 4.6. The power flowing into the DC link of VFD1 from VFD2 has to equal the power flowing out of the DC link of VFD1 for the voltage across the DC link capacitor of VFD1 to remain constant. The power drawn from the mains supply is therefore only used to replace electrical and mechanical losses in the test bed. Referring to Fig. 4.6, the power (Power out1) flowing out of VFD1 therefore comprises the power (Power in from the mains supply) required to replace the losses in the test bed and the power (Power in 2) flowing in the DC link of VFD1 from VFD2. The power drawn from the supply to replace these losses is measured using the power meter discussed next.

- **Power meter**

A Satec single phase AC power meter shown in Fig. 4.7 is used to measure the input power of the test bed. Due to Machine1 operating as a motor, Machine2 operating as a generator and having the DC links linked on both VFDs, the power meter only measures the power required to replace losses in the system.

Fig. 4.7 Satec power meter

The electrical connection of the power meter to VFD1 is shown schematically in Fig. 4.8 [19].

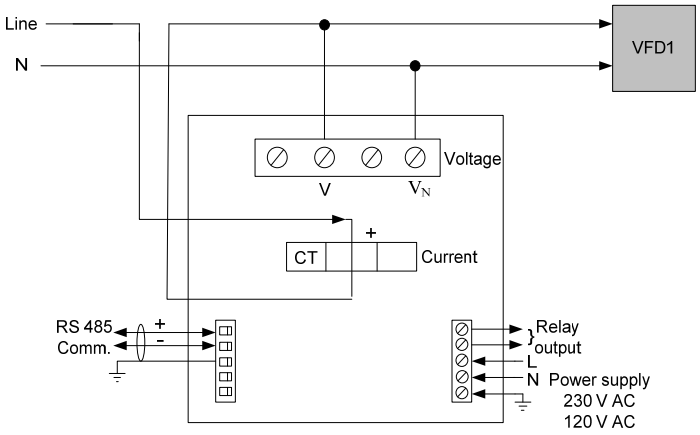

Fig. 4.8 Schematic of the power meter terminals and connections [19]

Referring to Fig. 4.8, using the power meter's RS 485 serial port all the measured quantities are accessed and made available by the PLC via its RS 232C serial communication module. Additional Moxa hardware shown in Fig. 4.9 was utilised to convert the RS 485 signal transmitted from the power meter to RS 232. The electrical connection of the power meter to the RS 232C serial module via the Moxa is shown in Fig. 4.10.

Fig. 4.9 RS 485 to RS 232 signal converter

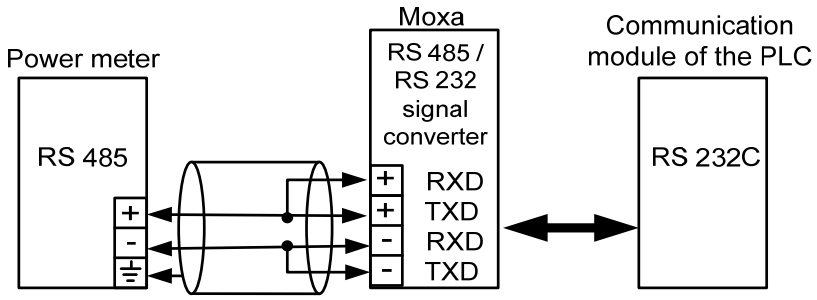

Fig. 4.10 Connection diagram for the serial port conversion

- **Control terminals**

The MICROMASTER VFD has a set of control terminals as shown in Fig. 4.11. The control terminals provide the analogue output (Terminals 12 and 13) required to send the torque calculated by VFD2 of the test bed to the PLC via its analogue module as shown in Fig. 4.1

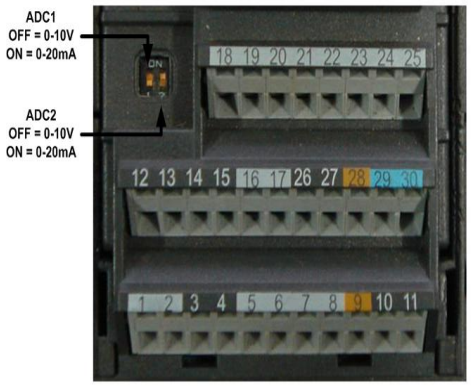

Fig. 4.11 Control terminals available on the VFD [14]

- **PROFIBUS module**

To enable the PLC to communicate with each VFD of the test bed, an additional PROFIBUS module is attached to each VFD. A picture of this PROFIBUS module is depicted in Fig. 4.12.

Fig. 4.12 PROFIBUS module for the VFD

4.2.3 Incremental encoder

The incremental encoder used to provide speed feedback from the test bed is a 24 V 50 mA encoder (Fig. 4.13). The maximum counting frequency of the encoder is 300 kHz. Single evaluation (1024 pulses per revolution) of the encoder signals are enabled, since the HSC module does not support both double evaluation (2048 pulses per revolution) and quadruple evaluation (4096 pulses per revolution) of the encoder signals. The incremental encoder is connected directly to VFD1 and the HSC module.

Fig. 4.13 Leine and Linde speed transducer

4.3 Earthing strategy

Large currents are switched through the power electronic devices in each VFD; therefore the generation of Electromagnetic Interference (EMI) is very high. The EMI generated can manifest itself in two ways: the first is noise being induced into the signal wires (signals of the speed transducer); and secondly is ground loops. Ground loops result in circulating currents flowing in the signal cable shielding and system framework. Ground loops may cause damage to equipment due to volt drops generated between ground points in the loop.

The problem of EMI induced in the signal cables (speed signal) was addressed with the use of screened cables. The screened cables were only earthed on the return side of the signal cable to avoid ground loops.

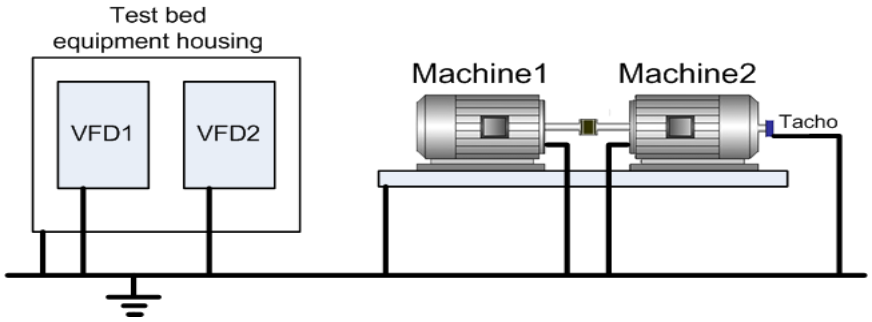

Fig. 4.14 Earthing strategy

The problem of ground loops was addressed by earthing the VFDs, housing box, test bed machines and encoder shielding individually, employing a 'tree' like earthing structure as shown in Fig. 4.14. All earth leads used were kept as short as possible to limit the resistance in the earth paths, in order to limit the volt drops generated by any earth currents.

4.4 Complete test bed

The two induction machines shown schematically in Fig. 4.1 are shown stiffly coupled together in Fig. 4.15. The framework which holds both induction machines together was made out of iron. Both induction machines are identical, therefore no special modifications had to be done on the framework since the shafts of the machines lined up perfectly for direct coupling.

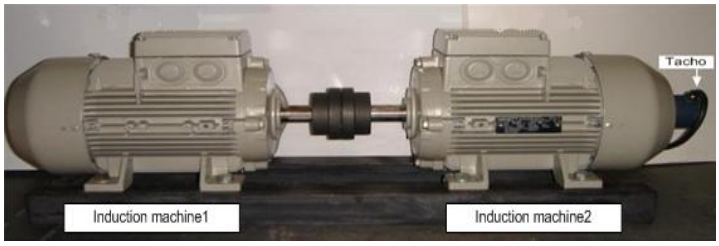

Fig. 4.15 Induction machines coupled together

The control and monitoring components of the test bed that were discussed in Section 4.2 are shown below in Fig. 4.16.

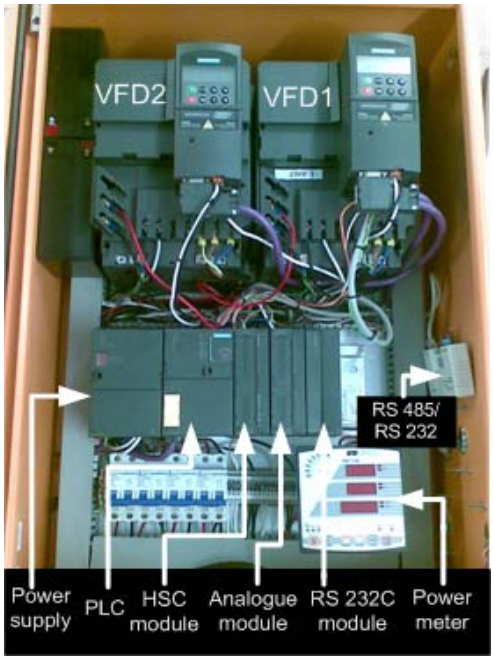

Fig. 4.16 Equipment housing

The induction machines shown in Fig. 4.15 and the equipment shown in Fig. 4.16 together form the complete test bed.

4.5 Conclusion

This chapter described the hardware and interfacing of the components required to operate and monitor the test bed.

The next chapter discuses the commissioning of the test bed.

CHAPTER 5

TEST BED COMMISSIONING

5.1 Introduction

In Chapters 2 and 3 the theory of the induction machine, the principles of FOC and the characteristics of centrifugal fans were presented. This was followed by the hardware and interfacing of the test bed in Chapter 4.

This chapter presents the commissioning of the test bed. The commissioning was carried out in two phases. The first phase involves the calculation and verification of the electrical and mechanical parameters for the induction machine model. The machine's parameters are first calculated by doing manual tests and are then calculated by the VFD. The parameters are then verified by simulating the response of the machine and comparing it to the actual measured response of the machine. The machine parameters are necessary because they are used in the second phase of commissioning which involves a computer simulation of the test bed under FOC. The parameters are therefore required in the design of the controllers utilised to implement FOC. The practical results gained from the test bed are then presented. The two induction machines of the test bed have the same nameplate data therefore for Phase 1 of the commissioning process the results of only one machine is shown to avoid repetition. The differences in the electrical and mechanical parameters of the two machines are negligible.

PHASE 1

5.2 Manual tests

Three manual tests were performed to determine the electrical and mechanical parameters of the induction machine using the IEEE Standard Test Procedure for Polyphase Induction Machines and Generators (Std 112-1984) [6]. These tests are briefly described below stating the final results obtained from each specific test. Refer to Appendix D for the full calculations and results obtained from testing the machine. The stator windings of the machine were connected in delta for the tests described in Sections 5.2.1 to 5.2.3 since the VFDs in the test bed are connected in delta.

5.2.1 No load test

The no load test was performed to measure the parameters R_m (core losses) and L_m (mutual inductance). The rated voltage (230 V) of the machine was applied while the machine ran on no load. The measured data is shown in Appendix D, Fig. D.3 resulting in a R_m of 605.55 Ω and L_m of 0.187 H.

5.2.2 Locked rotor test

The locked rotor test measured the parameters R_e (stator and referred rotor resistance) and L_e (stator and referred rotor inductance). A reduced voltage was applied to the machine until the rated current flowed in its stator windings as shown in Appendix D, Fig. D.5. The results showed R_e to be 3.74 Ω and L_e to be 0.0222 H at the rated current (11.1 A) of the machine. L_e may decrease at higher currents especially during a DOL start-up due to the machine saturating.

5.2.3 Windage and Friction loss test

Some of the losses present in an induction machine are:

- copper losses in the stator and rotor windings.

- mechanical losses due to bearing friction and the cooling fan.
- hysteresis and eddy current losses.

The no load loss due to friction and the cooling fan at synchronous speed of the machine as shown in Appendix D, Fig. D.6 is 22.975 W.

A rundown curve of the machine under no load presented in Fig. D.7 and Fig. D.8 (Appendix D) showed the rate of change of speed to be -31.751 rad/s^2. This enabled the machine's inertia (J) and frictional damping coefficient (B) to be calculated; J was found to be 0.00459 kg.m^2 and B 0.00093 Nms/rad.

Measured parameters		
Parameter name	**Parameter symbol**	**Value**
Stator resistance	R_1	2.3 Ω
Referred rotor resistance	R_2'	1.440199 Ω
Stator leakage inductance	L_1	0.01111 H
Referred rotor leakage inductance	L_2'	0.01111 H
Magnetising resistance	R_m	605.55 Ω
Mutual inductance	L_m	0.187 H
Inertia	J	0.00459 kg-m^2
Frictional damping coefficient	B	0.00093 N.m.s/rad

Table 5.1: Measured machine parameters

5.3 VFD calculated machine parameters

The MICROMASTER VFDs used in the test bed are commercially available Siemens VFDs that may be programmed to perform a number of functions. One of the functions that the VFD can perform is to determine the electrical and mechanical parameters of the induction machine connected to it. Specialised software called Drive Monitor available for use with the MICROMASTER VFDs is used to display the measured data from the VFD and set the various available programmable functions. A screen captured from Drive Monitor is shown in Fig. 5.1 displaying the electrical and mechanical parameters of the induction machine that were determined by the VFD. The extreme left of the screen shown in Fig. 5.1, the green and yellow blocks, show the parameter number of a specific parameter. The second last column from the left displays the value of a specific parameter.

P0307	Rated motor power	+	000	1st. Drive data set (DDS)	3.00	
P0308	Rated motor cosPhi	+	000	1st. Drive data set (DDS)	0.820	
P0309	Rated motor efficiency	+	000	1st. Drive data set (DDS)	82.5	%
P0310	Rated motor frequency	+	000	1st. Drive data set (DDS)	50.00	Hz
P0311	Rated motor speed	+	000	1st. Drive data set (DDS)	1425	min⁻¹
r0313	Motor pole pairs	+	000	1st. Drive data set (DDS)	2	
P0314	Motor pole pair number	+	000	1st. Drive data set (DDS)	0	
P0320	Motor magnetizing current	+	000	1st. Drive data set (DDS)	0.0	%
r0330	Rated motor slip	+	000	1st. Drive data set (DDS)	5.00	%
r0331	Rated magnetization current	+	000	1st. Drive data set (DDS)	3.188	A
r0332	Rated power factor	+	000	1st. Drive data set (DDS)	0.820	
r0333	Rated motor torque	+	000	1st. Drive data set (DDS)	20.10	Nm
P0335	Motor cooling	+	000	1st. Drive data set (DDS)	0 Self-cooled	
P0340	Calculation of motor parameters	+	000	1st. Drive data set (DDS)	0 No calculation	
P0341	Motor inertia [kg*m^2]	+	000	1st. Drive data set (DDS)	0.0055	
P0342	Total/motor inertia ratio	+	000	1st. Drive data set (DDS)	1.000	
P0344	Motor weight	+	000	1st. Drive data set (DDS)	25.0	kg
r0345	Motor start-up time	+	000	1st. Drive data set (DDS)	0.073	s
P0346	Magnetization time	+	000	1st. Drive data set (DDS)	0.145	s
P0347	Demagnetization time	+	000	1st. Drive data set (DDS)	0.362	s
P0350	Stator resistance (line-to-line)	+	000	1st. Drive data set (DDS)	2.81051	Ohm
P0352	Cable resistance	+	000	1st. Drive data set (DDS)	0.40896	Ohm
P0354	Rotor resistance	+	000	1st. Drive data set (DDS)	1.51172	Ohm
P0356	Stator leakage inductance	+	000	1st. Drive data set (DDS)	10.46875	
P0358	Rotor leakage inductance	+	000	1st. Drive data set (DDS)	11.00000	
P0360	Main inductance	+	000	1st. Drive data set (DDS)	209.500	

Fig. 5.1 Parameters of the machine calculated by the VFD

Referring to parameter P0350 and parameter P0352 in Fig. 5.1 the machine's stator resistance is calculated as shown in Eq. 5.1:

$$R_1 = P0350 - P0352 \tag{5.1}$$

$$R_1 = R_{line} - R_{cable}$$

$$R_1 = 2.81051 - 0.408$$

$$R_1 = 2.4\Omega$$

With reference to Fig. 5.1, the induction machine's parameters are repeated in Table 5.2.

VFD calculated parameters		
Parameter name	**Parameter symbol**	**Value**
Stator resistance	R_1	2.4 Ω
Rotor resistance	R_2	1.51172 Ω
Stator leakage inductance	L_1	0.010469 H
Rotor leakage inductance	L_2	0.011 H
Mutual inductance	L_m	0.209 H
Inertia - Method 1	J	0.0055 kg-m^2

Table 5.2: VFD calculated machine parameters

5.4 Direct On Line start-up current and speed

For the purposes of verifying the induction machine's parameters calculated by doing manual tests and by the VFD, the Direct On Line (DOL) stator current and speed responses of the induction machine were captured on an oscilloscope and imported to Matlab. The machine's terminals were connected in Star for this test with a reduced voltage of 300 V to prevent the machine's iron parts from saturating during start-up since saturation of the machine will not occur with the simulation model.

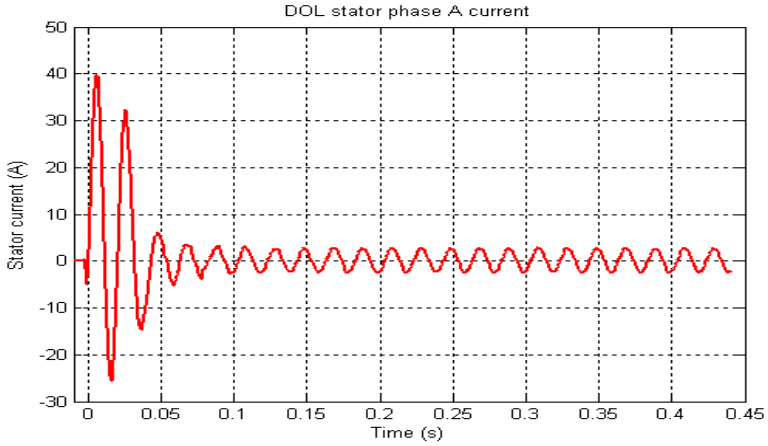

Fig. 5.2 DOL start-up current peaking at 40 amps

A rapid rise in the stator phase A current is shown in Fig. 5.2 which accurately describes an induction machine since the start-up current of an induction machine during a DOL start-up is approximately 5 to 8 times greater than the rated current (6.4 A, Appendix A.1) of the machine. The maximum current at the first peak of the current signal is 40 A.

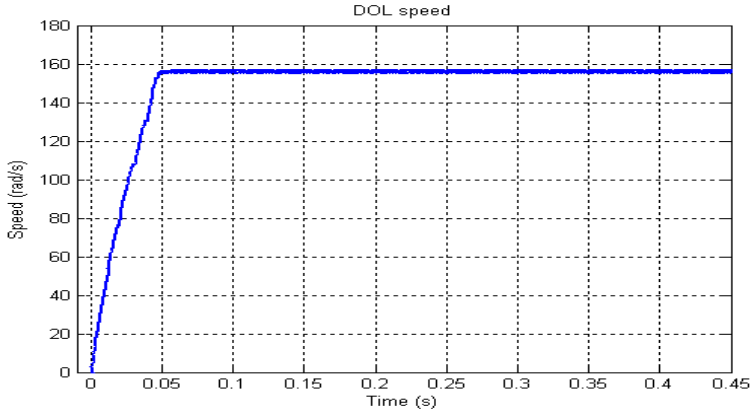

Fig. 5.3 DOL start-up speed with a final speed of approximately 157 rad/s

Fig. 5.3 depicts the DOL speed response of the machine. The machine reaches no load speed in approximately 0.05s.

5.5 DOL start-up Simulink™ simulation of the machine using the measured and VFD calculated parameters

The parameters of the machine have been determined by doing manual tests and by the VFD. The measured DOL start-up of the machine has been presented in the previous section. In this section the DOL start-up of the machine using the two sets of machine parameters is simulated using software called Simulink™. The simulated DOL start-up is then compared to the measured DOL start-up to verify the accuracy of the machine's parameters.

Fig. 5.4 shows the Simulink™ model comprising a 300 V three phase source, connected to a circuit breaker, connected directly to a star connected induction machine. The speed and current responses of the machine are viewed via the scope connected to the machine output in Fig. 5.4.

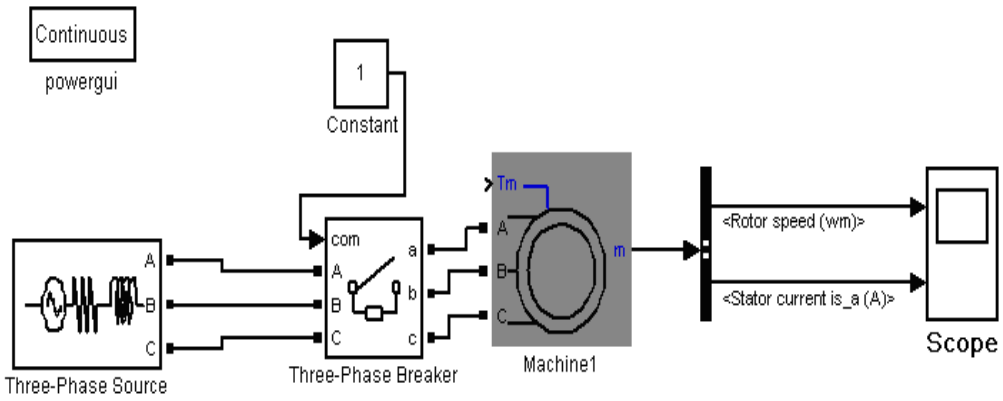

Fig. 5.4 Simulink™ model for a DOL start-up

The DOL start-up of the machine is first simulated using the manually measured parameters and compared to the actual DOL start-up responses (Fig. 5.2 and Fig. 5.3) as shown in Fig. 5.5 and Fig. 5.6.

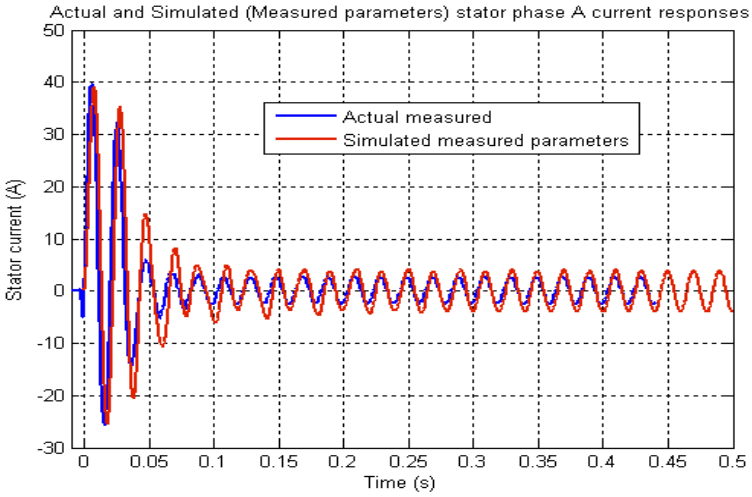

Fig. 5.5 Comparison of the stator phase A current response

Fig. 5.5 compares the simulated DOL start-up response to the measured DOL start-up response (Fig. 5.2). The stator phase A currents shown in Fig. 5.5 follow one another accurately.

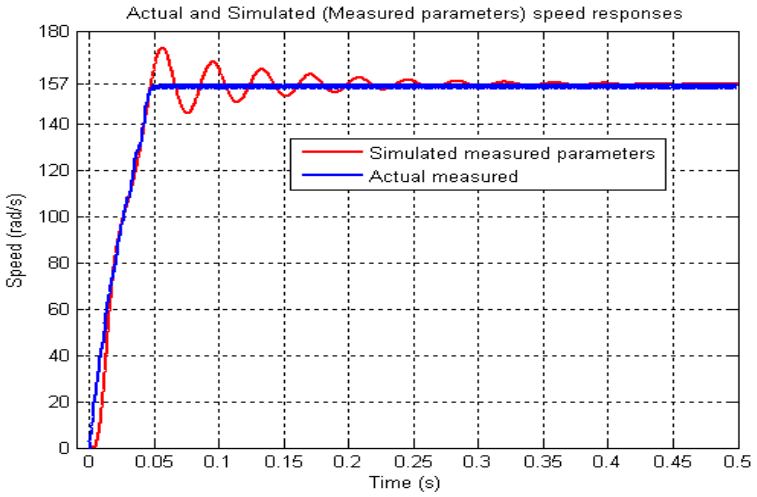

Fig. 5.6 Comparison of the speed response

The simulated DOL start-up speed response of the machine is compared to the measured (Fig. 5.3) DOL start-up speed response in Fig. 5.6. There are oscillations in the simulated speed response causing the machine to reach no load speed after approximately 0.3s.

The simulated DOL start-up responses of the machine using the VFD calculated parameters as shown in Section 5.3 and the measured frictional damping value given in Section 5.2 are now

compared to the actual DOL start-up responses (Fig. 5.2 and Fig. 5.3). These comparisons are presented below in Fig. 5.7 and Fig. 5.8.

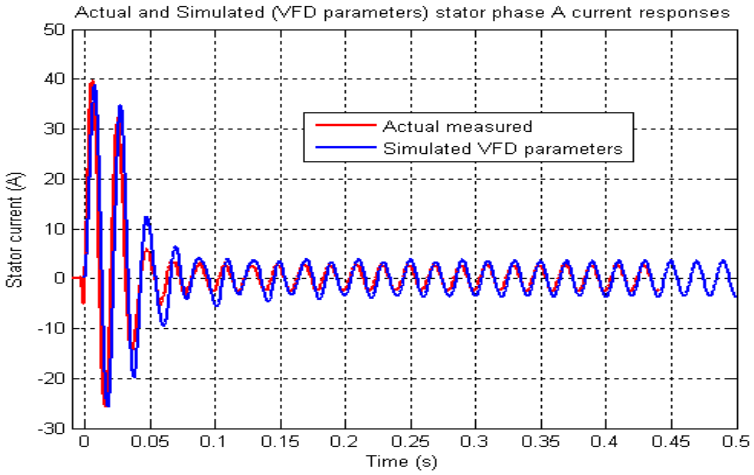

Fig. 5.7 Comparison of the stator phase A current response

The simulated and measured DOL start-up stator phase A current responses are compared in Fig. 5.7. The stator phase A currents follow each other accurately.

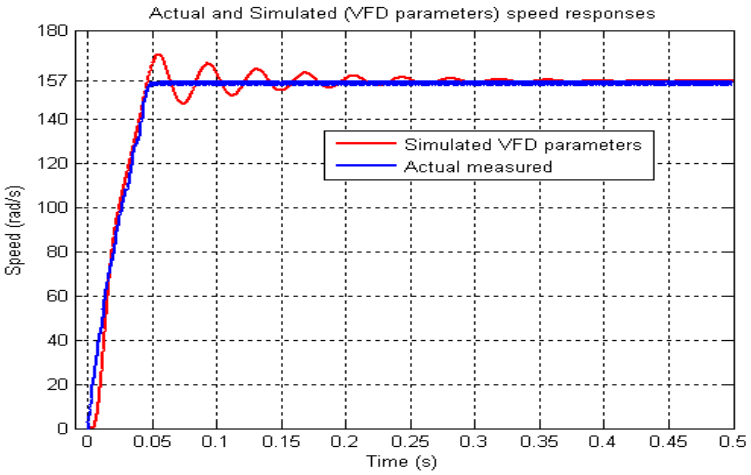

Fig. 5.8 Comparison of the speed response

Fig. 5.8 compares the measured DOL start-up speed response (Fig. 5.3) to the simulated DOL start-up speed response of the machine. The simulated speed response also has oscillations causing the machine to reach no load speed after approximately 0.3s similar to when the measured parameters of the machine were used as the input data for the Simulink™ model shown in Fig. 5.4.

5.6 Identification of the machine's parameters using the Optimisation toolbox for Simulink™

Two sets (Measured and VFD calculated) of parameters were used to simulate the machine starting up DOL. The Simulink™ simulations were then compared to the measured DOL responses which showed discrepancies in the speed response of the machine. The next step was to try and get better correlation as it was obvious the parameters were incorrect. This was done using the Optimisation toolbox for Simulink™ in Matlab™.

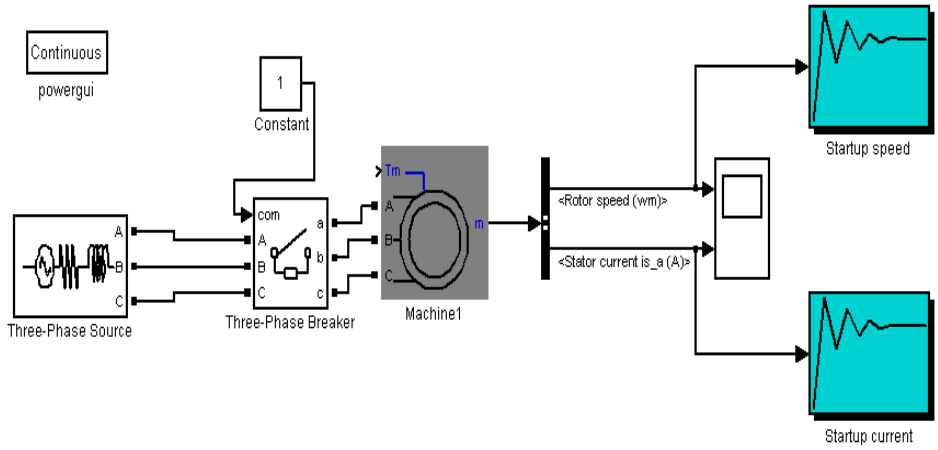

Fig. 5.9 Setup of the machine with signal constraints connected to the machine's output

To try and achieve better correlation between the measured and simulated DOL start-up responses, the measured DOL start-up responses were imported to Simulink™. The DOL start-up stator phase A current and speed responses were imported to the signal constraint blocks shown in Fig. 5.9 labelled 'start-up speed' and 'start-up current' as shown in Fig. 5.10 and Fig. 5.11. The measured DOL start-up responses are shown in grey and the black lines around the grey curves are the signal boundaries which I have set. At the bottom of the signal constraint figures shown in Fig. 5.10 and Fig. 5.11 there are two boxes which have been ticked, namely 'enforce signal bounds' meaning restrict the simulated response to within the black lines and 'track reference signal' in other words, try and follow the grey curves as closely as possible.

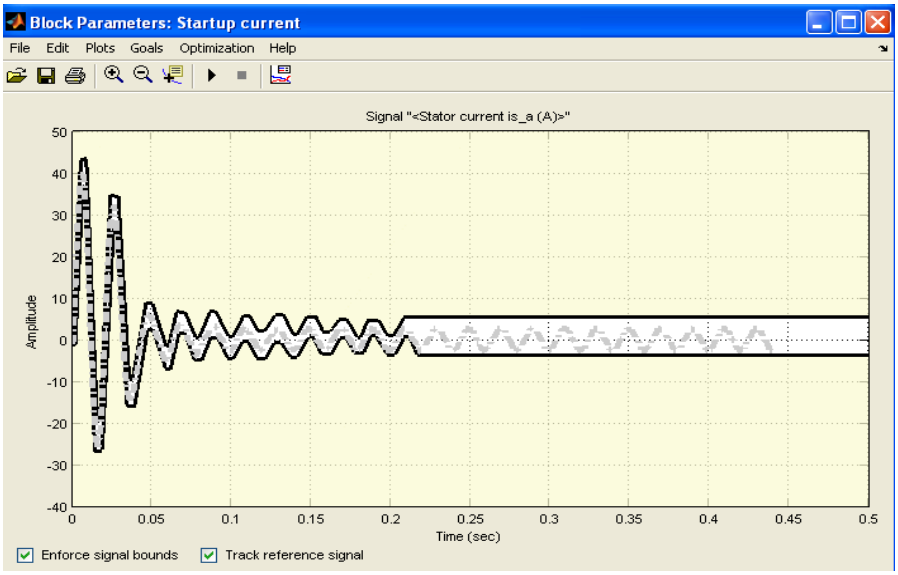

Fig. 5.10 Current constraint window of the model

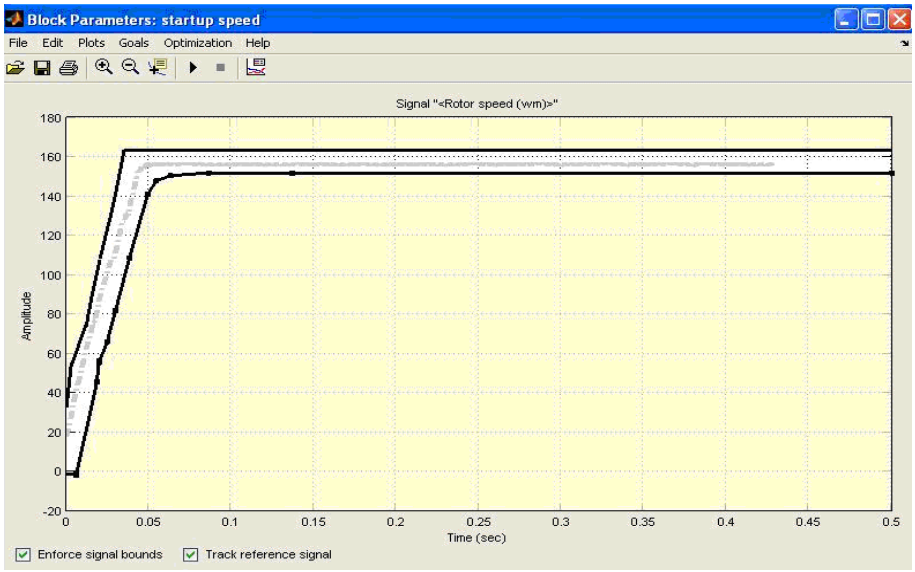

Fig. 5.11 Speed constraint window of the model

The parameter identification process starts by simulating the current and speed responses of the induction machine using the initial measured parameters from Section 5.2. The parameter identification process then adjusts the machine's parameters *Rr, Lr*, Sr, *Lm, Ls, B* and *J* until there is a better correlation between the actual and simulated responses. The various simulated response curves are shown by the different colour curves in Fig. 5.12 and Fig. 5.13.

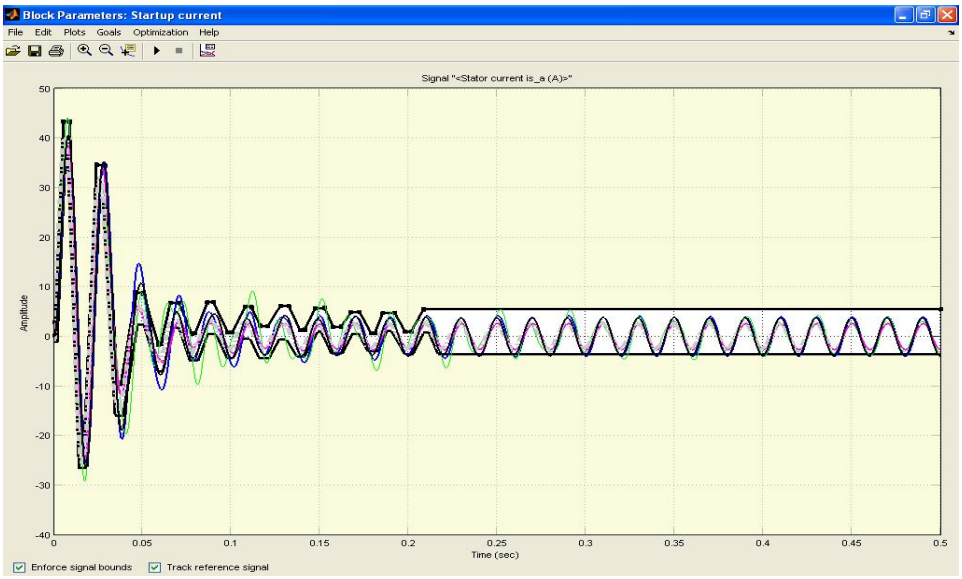

Fig. 5.12 Optimisation of the current response as shown by the various different colour curves

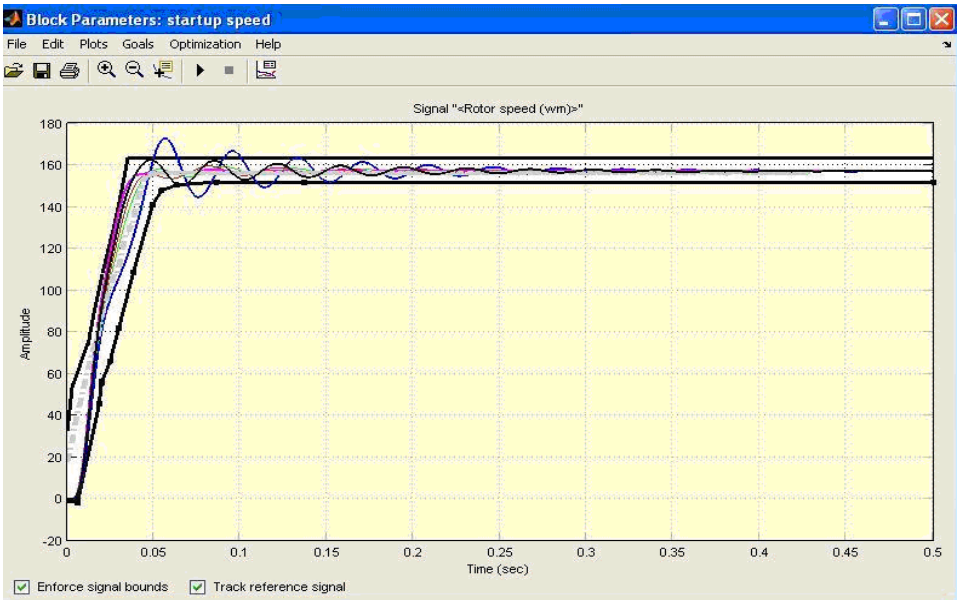

Fig. 5.13 Optimisation of the speed response as shown by the various different colour curves

Referring to Fig. 5.12 and Fig. 5.13, the blue curve represents the first simulation of the machine with the initial parameters and the last simulation is depicted by the solid black curve. These black curves are shown in Fig. 5.14 and Fig. 5.15 for clarity purposes.

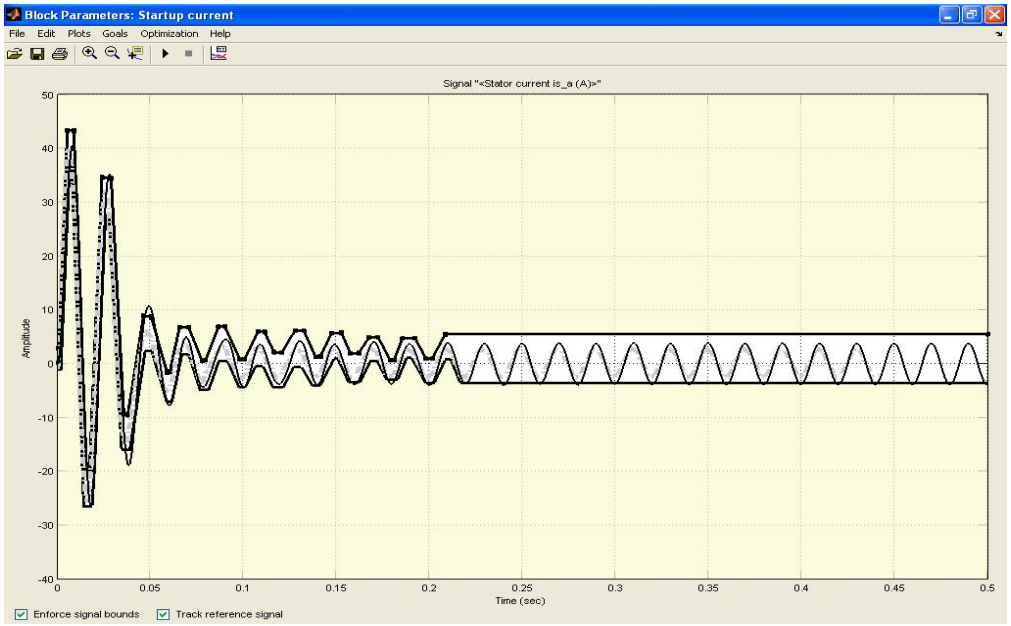

Fig. 5.14 Final current signal solution obtained by optimisation

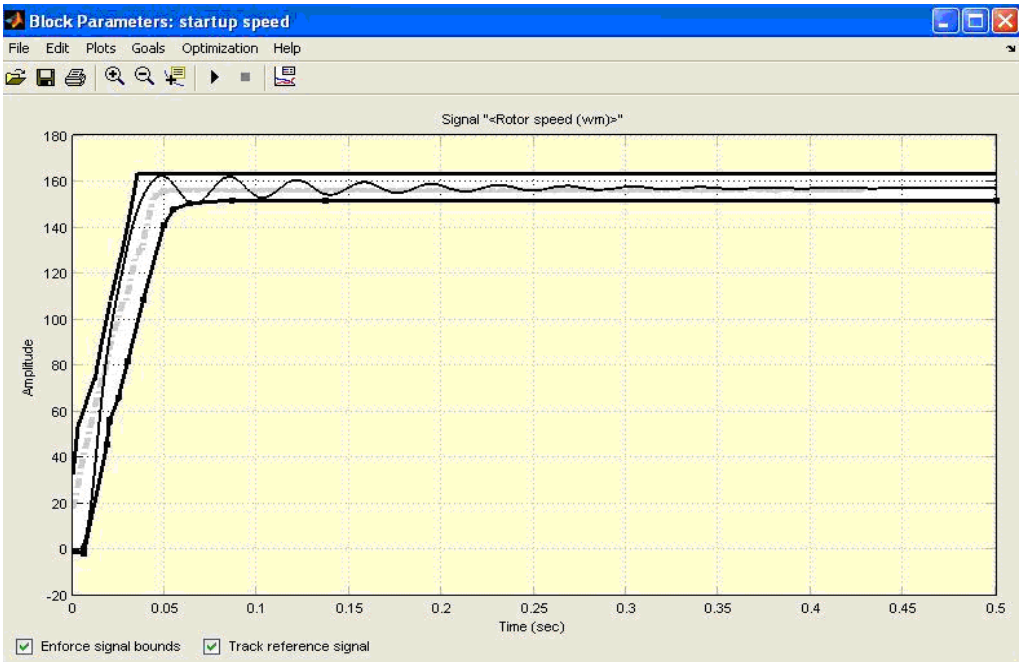

Fig. 5.15 Final speed signal solution obtained by optimisation

The final parameters of the machine obtained at the end of the optimisation identification process are shown in Fig. 5.16.

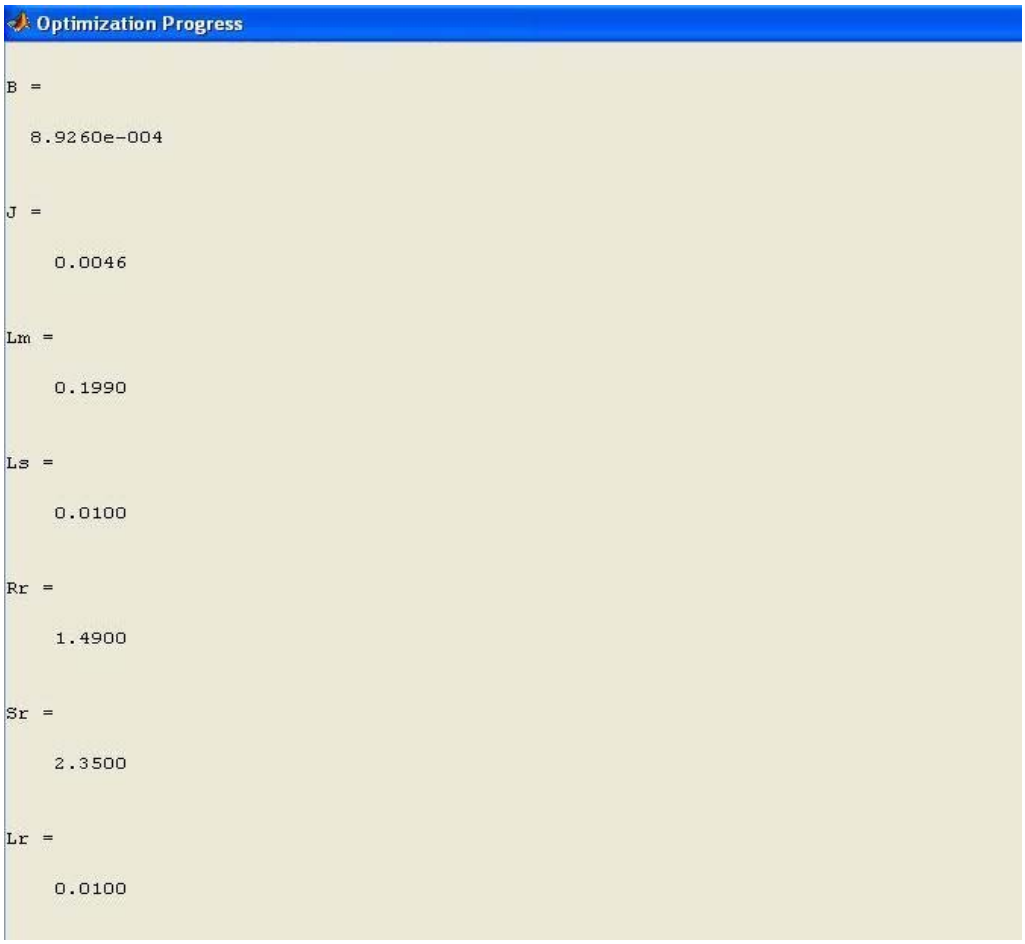

Fig. 5.16 Identified machine parameters as shown by the optimisation window available during the optimisation identification process

5.7 DOL start-up simulation of the machine with the Optimisation toolbox identified parameters

The same Simulink^{TM} model of the machine (source supplying 300 V for a star connected machine) as depicted in Fig. 5.4 was used to simulate the machine starting up DOL using the Optimisation toolbox identified parameters as the input data for the machine model. The simulated stator phase A current and speed responses of the machine are compared to the measured DOL start-up responses as shown in Fig. 5.17 and Fig. 5.18.

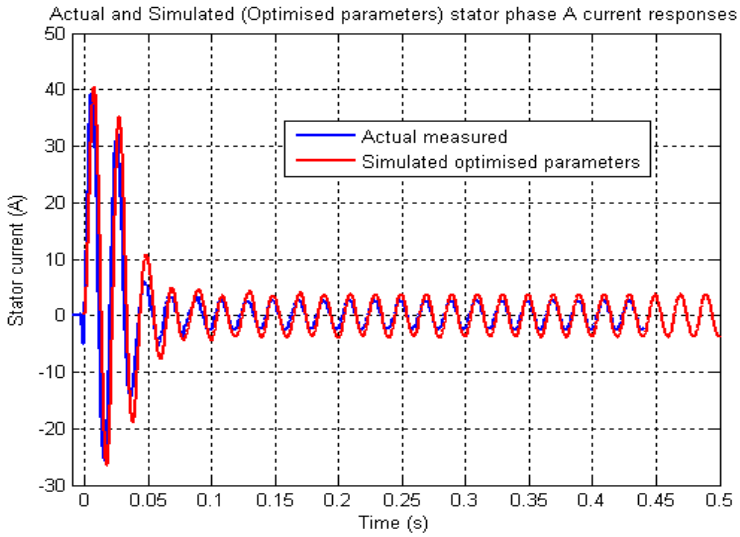

Fig. 5.17 Comparison of the stator phase A current response

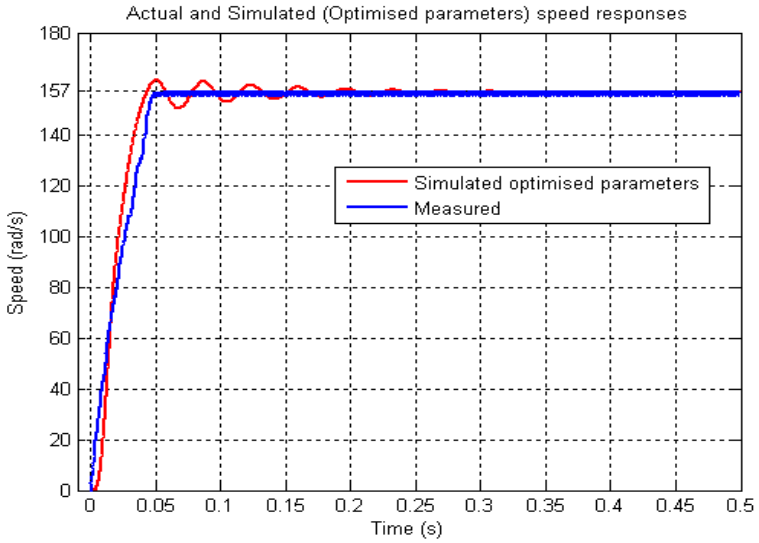

Fig. 5.18 Comparison of the speed response

Fig. 5.17 depicts the stator phase A currents tracking each other accurately. Fig. 5.18 shows the measured DOL start-up speed response 'approximately' matching the simulated DOL start-up speed response. The simulated speed response is still oscillatory unlike the actual response of the machine; however the oscillations are not as large as compared to the previously simulated responses of the machine shown in Fig. 5.6 and Fig. 5.8.

5.8 Parameter discrepancies

Parameter Symbol	Measured	VFD calculated	Optimisation toolbox identified
R_1	2.3 Ω	2.4 Ω	2.35 Ω
R_2	1.440199Ω	1.51172 Ω	1.49 Ω
L_1	0.01111H	0.010469 H	0.01 H
L_2	0.01111H	0.011 H	0.009987 H
L_m	0.187 H	0.209 H	0.199 H
J (method 1)	0.00459 kg-m^2	0.0055 kg-m^2	0.0046 kg-m^2
B	0.00093 N.m.s/rad	-	0.0008926 N.m.s/rad

Table 5.3: The various sets of machine parameters

Referring to Table 5.3, there are small differences between the measured, VFD calculated and Optimisation toolbox identified parameters. The differences in the actual speed response of the induction machine compared to the simulated speed responses of the induction machine are due to using a digital encoder (Fig. 4.13) to capture the speed signal. The digital speed signal from the encoder is passed through the PLC which converts the signal to analogue to be displayed and captured on an oscilloscope. The active filters on the digital to analogue converter and the slow sampling rate of the PLC could not capture the fast true start-up response of the machine.

The next section discusses the second phase of commissioning.

PHASE 2

5.9 Test bed simulation

The measured, VFD calculated and Optimisation toolbox identified parameters of the machine have small variances. Any set (whether VFD calculated, measured or Optimisation toolbox identified) of the electrical and mechanical parameters of the induction machine could therefore be used to design the controllers and simulate the test bed under FOC. The Optimisation toolbox identified parameters were used to design the controllers and to simulate the test bed machines under FOC. All the variables are plotted in physical units and not on a per unit based system of units.

Following the design procedure outlined in Chapter 2, Section 2.5 the controller gains were calculated as shown in Appendix C and are provided in Table 5.4 below. The inverter is assumed to be ideal and has an input voltage of 220 V AC. The DC link voltage of the inverter is 311 V DC but the DC link voltage in the d-q reference frame is 311*√(3/2) V DC. The inverter is neglected in the simulations therefore the gains of the current controllers are increased by a factor of 311*√(3/2).

Controller gains	
k_{iq}	120.9
k_{pq}	0.062*311*√(3/2)
k_{id}	193.1
k_{pd}	0.062*311*√(3/2)
k_{is}	0.194
k_{ps}	0.662

Table 5.4: Controller gains calculated using the optimised machine parameters

To show the decoupling of the induction machine under FOC and to verify the accuracy of the controller design process, the test bed is simulated under FOC using the above controller gains. Fig. 5.19 and Fig. 5.20 show the Simulink™ block diagrams of Machine1 operating under Field Oriented Speed Control and Machine2 operating under Field Oriented Torque Control respectively. The machines in the test bed are coupled therefore the block diagrams shown in Fig. 5.19 and Fig. 5.20 are combined to represent the test bed as shown in Fig. 5.21.

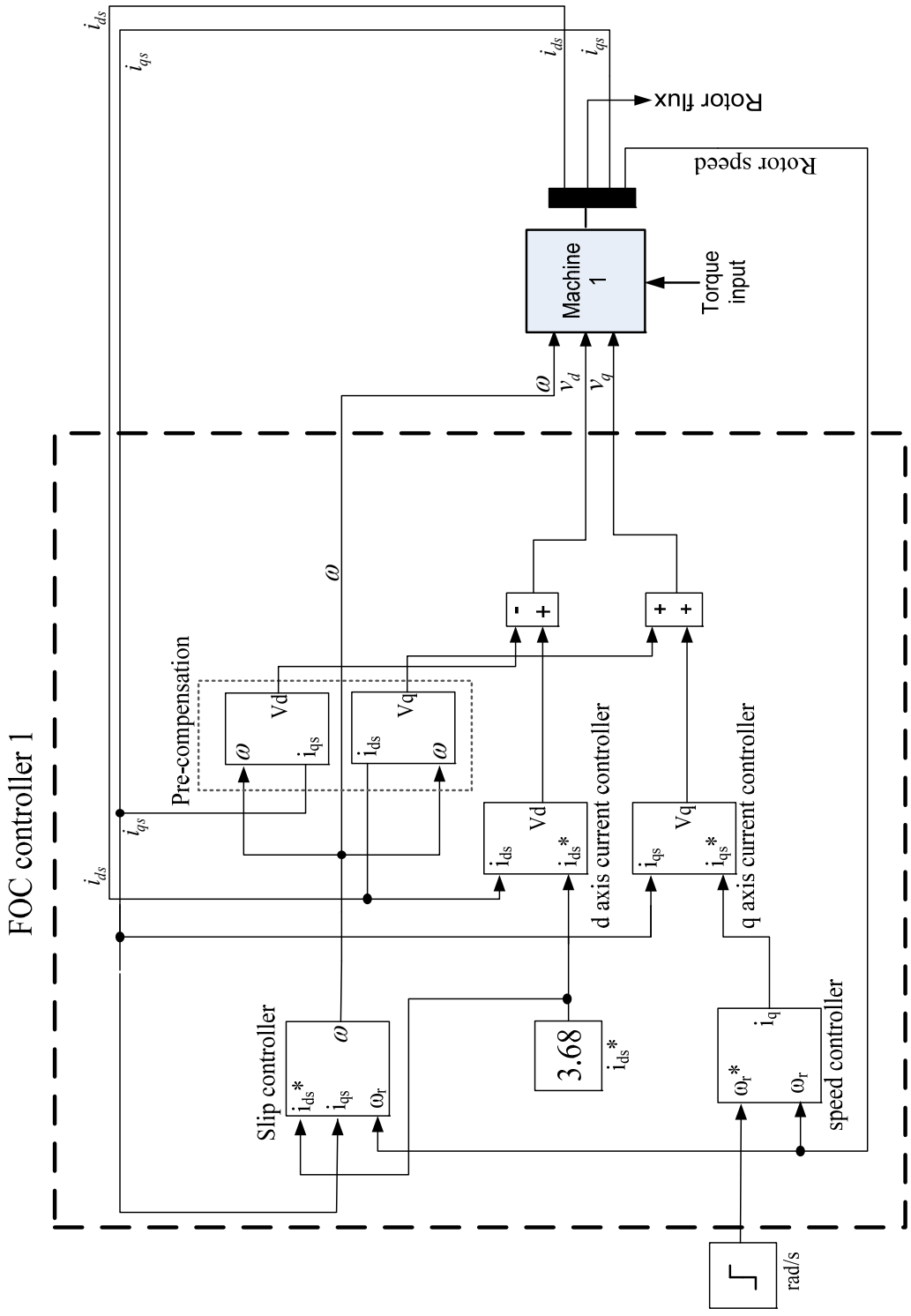

Fig. 5.19 Simulink™ block diagram representation of Machine1 operating under speed control

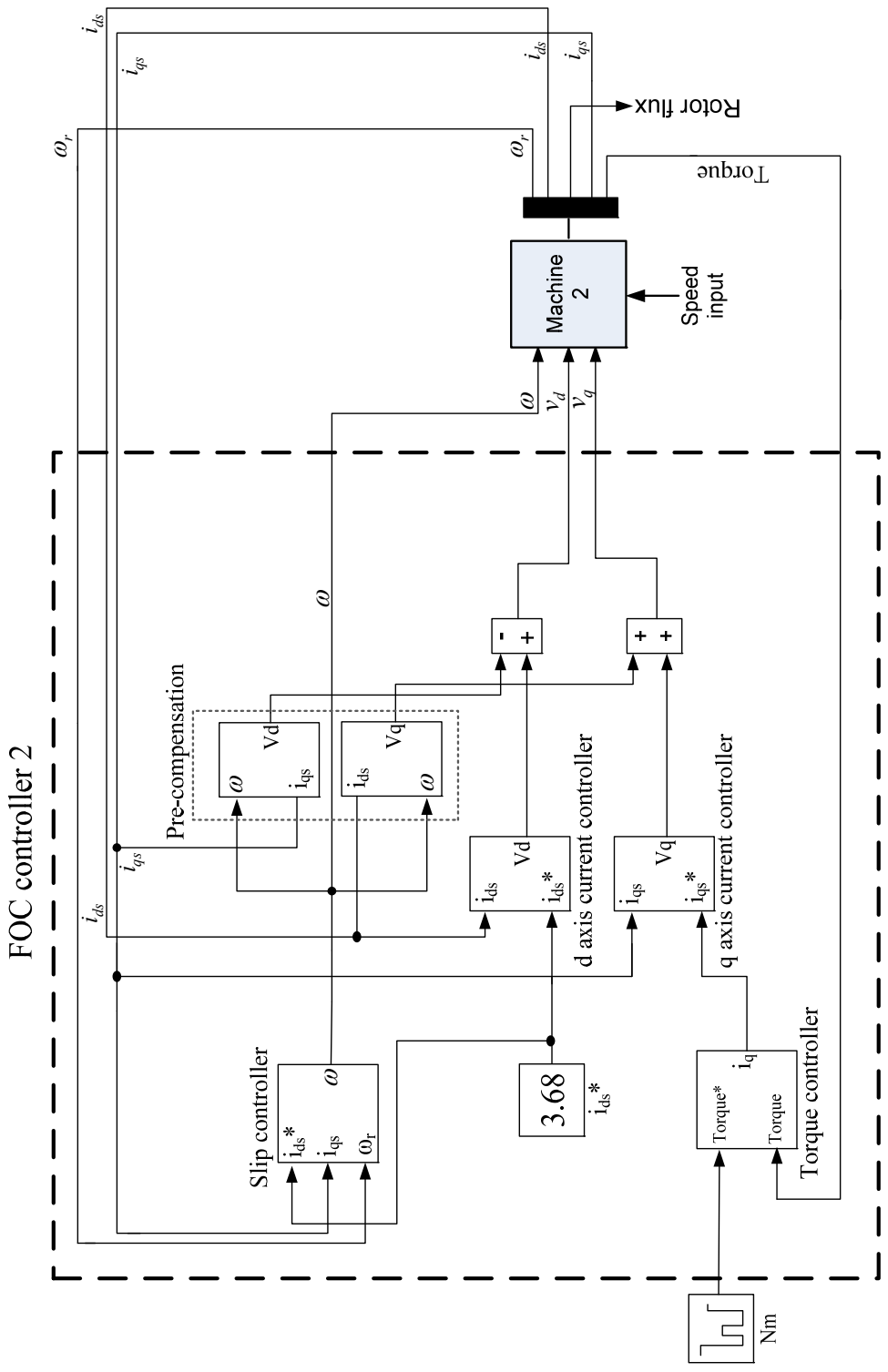

Fig. 5.20 Simulink™ block diagram representation of Machine2 operating under torque control

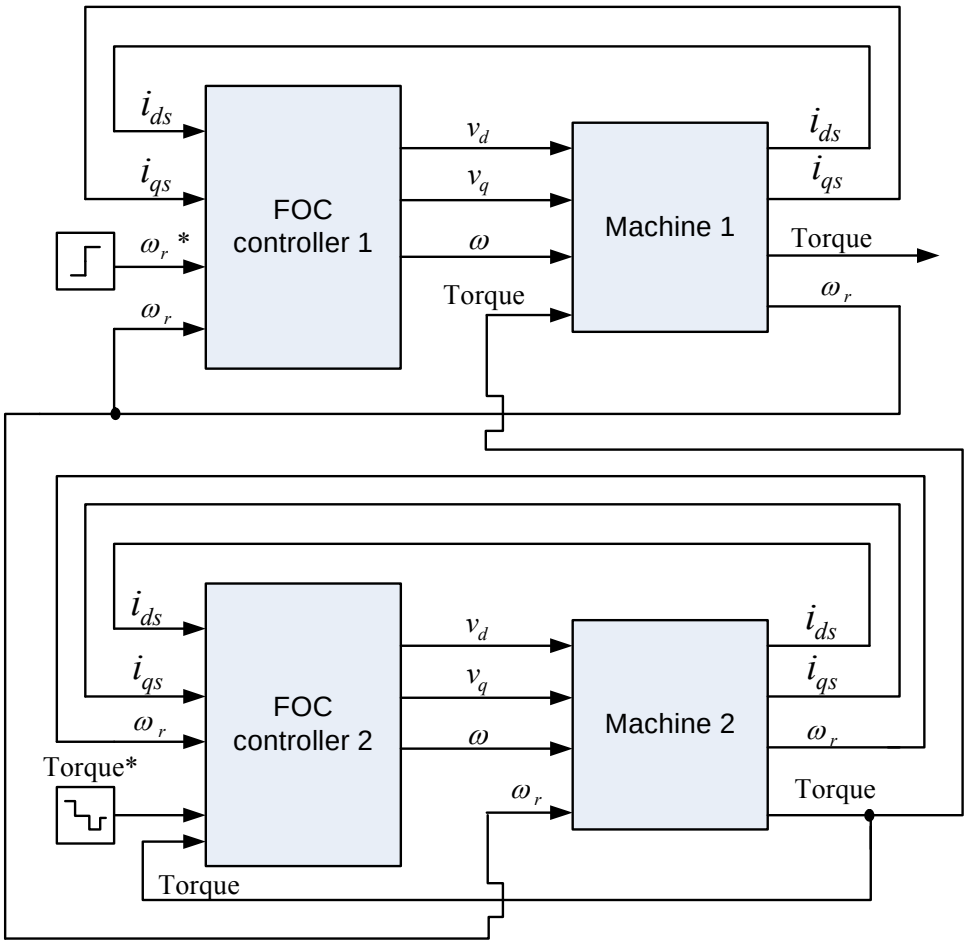

Fig. 5.21 Simulink™ block diagram representation of the test bed

Referring to Fig. 5.21, a step input (157 rad/s) to the speed reference (ω_r*) is applied to Machine1 after 1s and a time varying, stepped torque load is commanded from Machine2 after 1.5s. A torque load of 5 Nm was demanded at time = 1.5s, 7 Nm at time = 1.7s and finally 3 Nm at time = 2s. The simulated responses of Machine1 and Machine2 are presented and discussed in Section 5.9.1 and Section 5.9.2 respectively.

5.9.1 Machine1-Speed controlled

The responses of Machine1 under speed control are presented and discussed in this section whilst subjected to a step input to the speed reference after 1s as shown in Fig. 5.22.

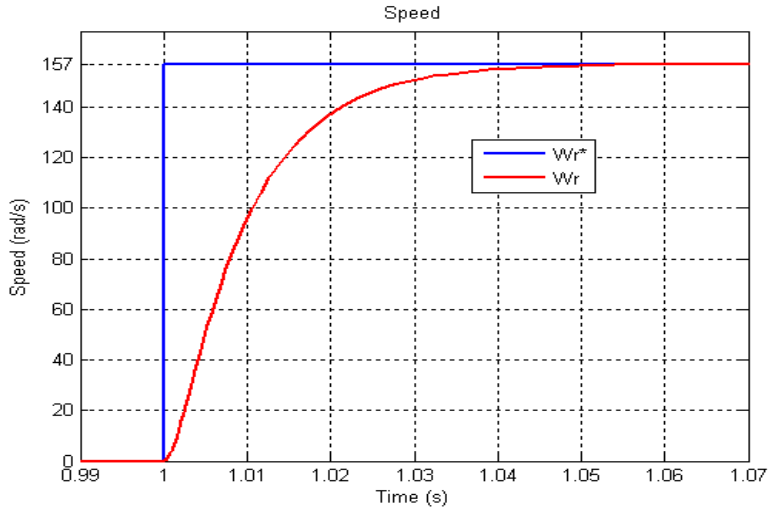

Fig. 5.22 Speed response of Machine1

The speed response of Machine1 shown in Fig. 5.22 has no oscillations in it as the speed (ω_r) of both the test bed machines increase from zero to the reference speed (ω_r*) of 157 rad/s demanded due to the uniformity of torque (see Fig. 5.27) that is produced.

The d-axis stator transient current response is depicted in Fig. 5.23 when subjected to a step change of 3.68 A in the d-axis current reference (i_{ds}*) producing the required rated rotor flux linkage of 0.73 Wb as shown in Fig. 5.24. Refer to Appendix B for the calculation of the rated rotor flux linkage.

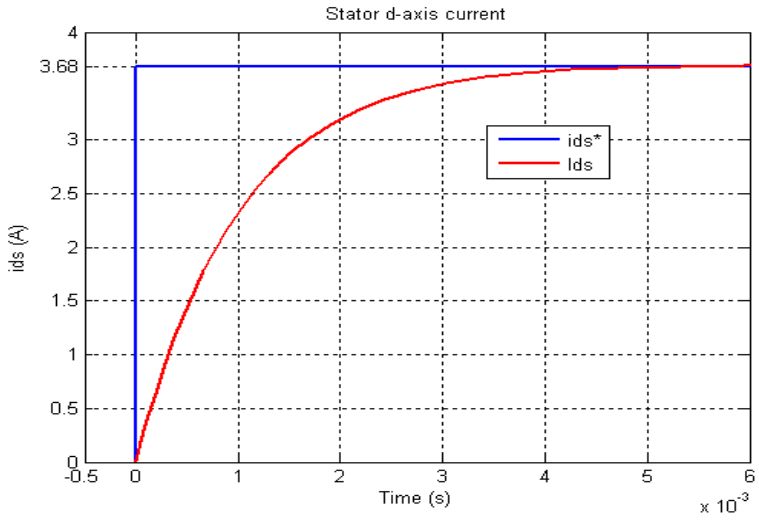

Fig. 5.23 d-axis stator current (i_{ds}) of Machine1

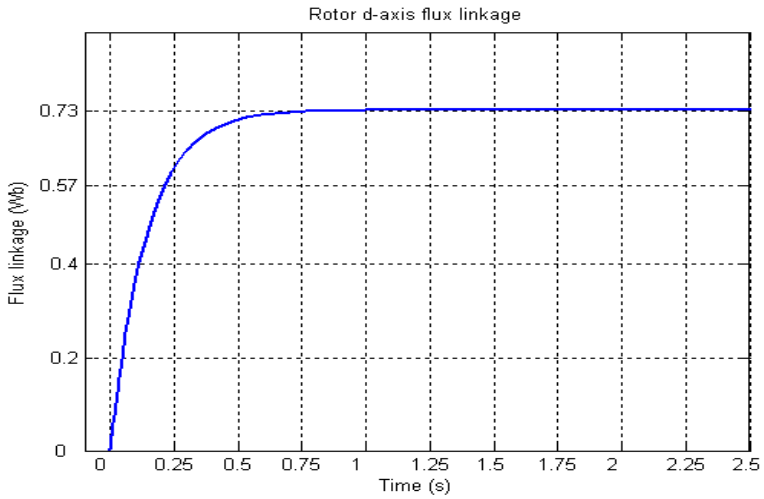

Fig. 5.24 d-axis rotor flux linkage (λ_{dr}) of Machine1

Fig. 5.25 and Fig. 5.26 depict the q-axis stator current response. During an initial period of one second the machine is pre-fluxed by holding the q-axis stator current reference (i_{qs}*) to zero. This allows for the d-axis rotor flux linkage (λ_{dr}) to build up to its rated value of 0.73 Wb; the machine will now be able to respond with full torque if required. A step in the speed (ω_r*) reference is applied after the pre-fluxing period as shown in Fig. 5.22 causing the q-axis reference current (i_{qs}*) and the actual q-axis current (i_{qs}) to rise rapidly reaching its limit of 12.24 A. The induction machine is protected by limiting the q-axis current until the actual speed (ω_r) of the machine reaches the specified reference speed (ω_r*) demanded. After 1.5s torque is again produced by the machine due to the load applied by Machine2 therefore the stator q-axis current changes according to the amount of torque required to match the load. The torque response of the machine is shown in Fig. 5.27.

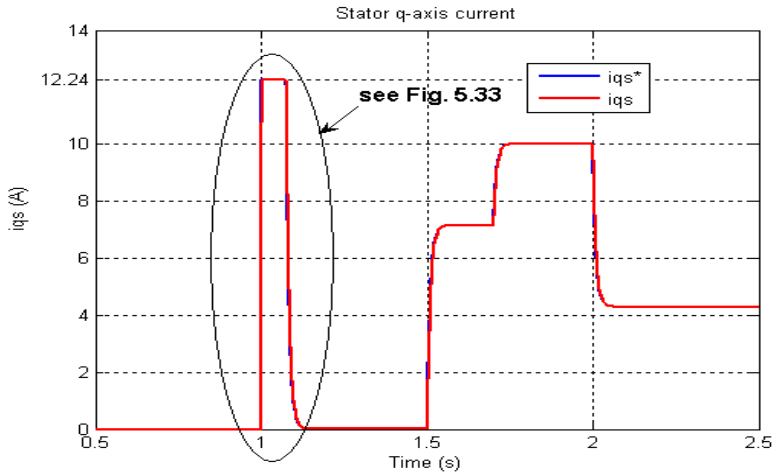

Fig. 5.25 q-axis stator current (i_{qs}) of Machine1

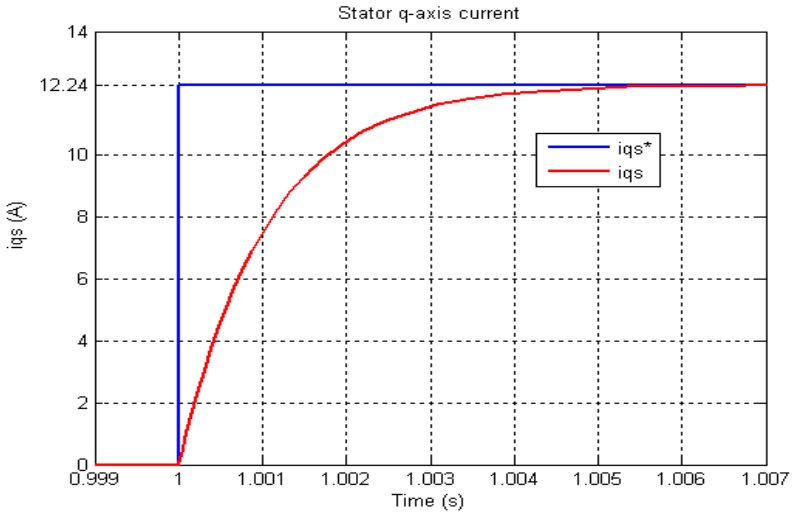

Fig. 5.26 Enlarged view of Fig. 5.25 from 0.99s to 1.007s

The torque response shown in Fig. 5.27 has a similar shape to that of the q-axis stator current response clearly illustrating the relationship between the two as given in Eq. 2.10 in Chapter 2. The decoupled structure of the induction machine gives rise to a linear torque response. After 1s the torque rises rapidly and settles down to almost 0 Nm once the reference speed demanded shown in Fig. 5.22 is reached. After 1.5s torque is applied by the machine to match the load applied by Machine2. According to Eq. 2.10 which is repeated here as Eq. 5.2, 0.695 A of current produces 1 Nm of torque. This relationship is verified by the q-axis stator current response shown in Fig. 5.25 and the torque response shown in Fig. 5.27; 12.24 A of current results in a torque of 8.5 Nm.

$$T_{em} = 0.695 i_{qs} \tag{5.2}$$

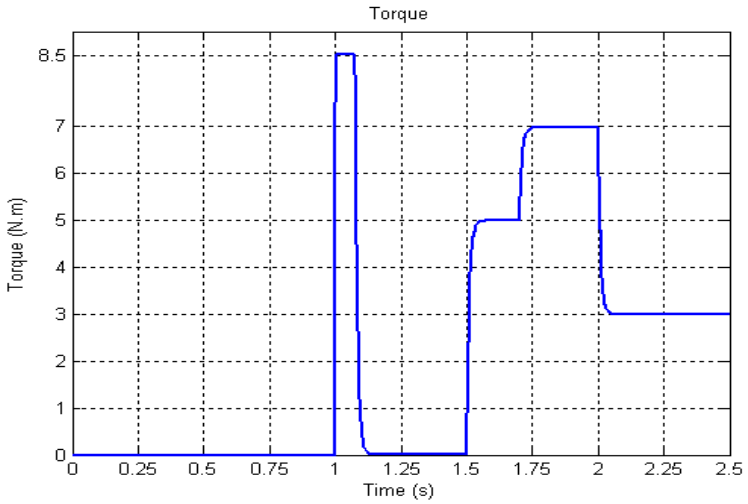

Fig. 5.27 Torque response of Machine1

The q-axis rotor flux linkage (λ_{qr}) response shown in Fig. 5.28 is zero.

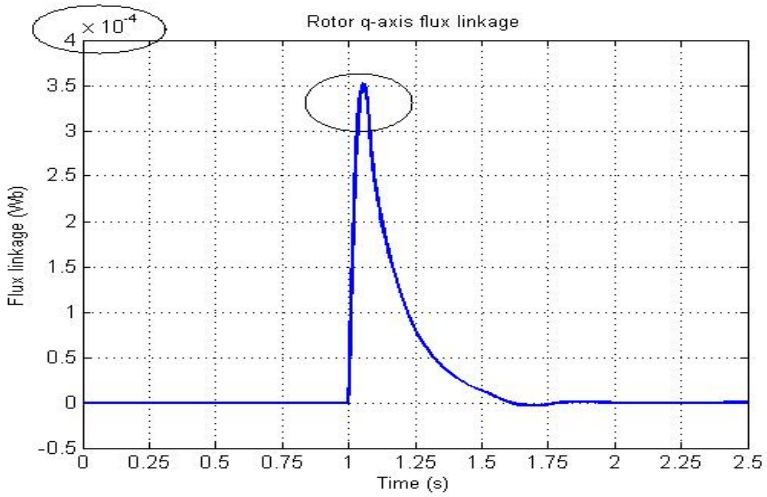

Fig. 5.28 q-axis rotor flux linkage (λ_{qr}) of Machine1

The linear torque response, λ_{dr} being maintained at its rated value and λ_{qr} equalling zero shows the correct application of FOC.

5.9.2 Machine2-Torque controlled

The responses of Machine2 under torque control are presented and discussed in this section whilst subjected to a time varying, stepped torque input as shown in Fig. 5.29. A torque load of 5 Nm was demanded at time = 1.5s, 7 Nm at time = 1.7s and 3 Nm at time = 2s.

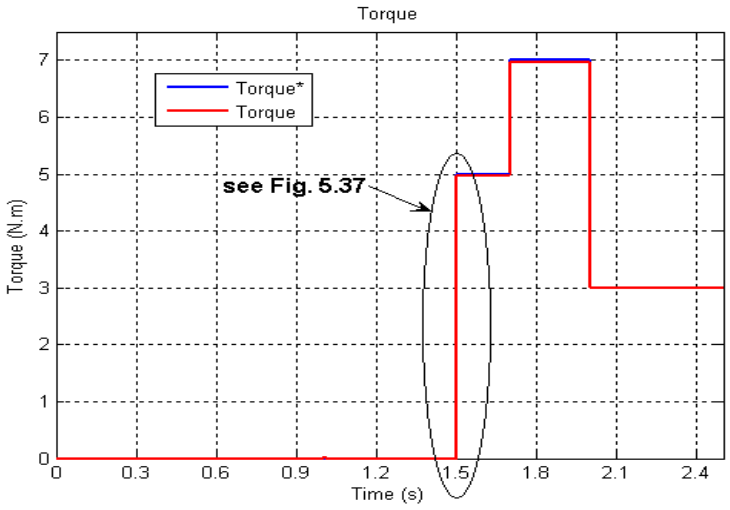

Fig. 5.29 Torque response of Machine2

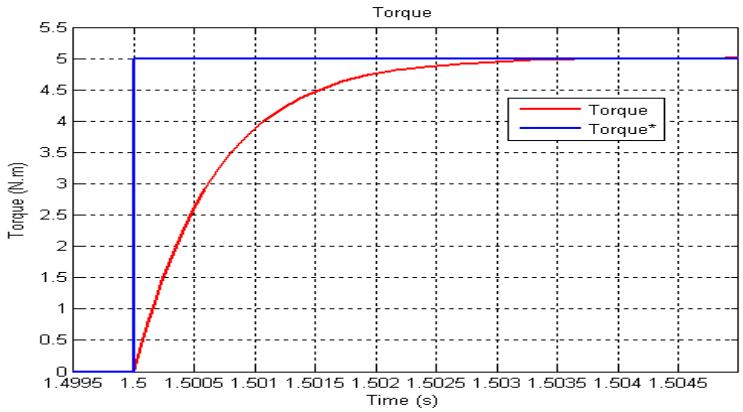

Fig. 5.30 Enlarged view of Fig. 5.29 from 1.4995s to 1.5046s

Fig. 5.31 depicts the d-axis stator transient current response when subjected to a step change of 3.68 A in the d-axis current reference (i_{ds}*) producing the required rated rotor flux linkage of 0.73 Wb as shown in Fig. 5.32. Refer to Appendix B for the calculation of the rated rotor flux linkage.

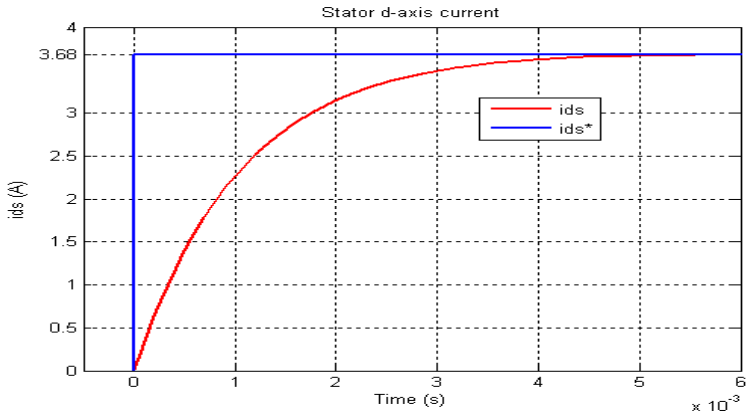

Fig. 5.31 d-axis stator current (i_{ds}) of Machine2

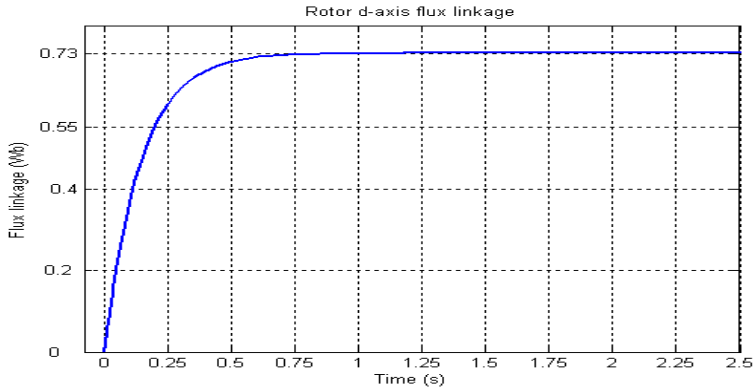

Fig. 5.32 d-axis rotor flux linkage (λ_{dr}) of Machine2

The q-axis stator current response is depicted in Fig. 5.33 and Fig. 5.34. After 1.5s a step in the torque reference (*Torque**) causes the q-axis reference current (i_{qs}*) to rise rapidly until the actual torque (*Torque*) of the machine reaches the specified reference torque (*Torque**). The q-axis stator current changes depending on the torque demanded. To produce 5 Nm of torque, 7.2 A of current is required as shown in Fig. 5.33. The ratio of torque to current is the same as that defined in Eq. 5.2.

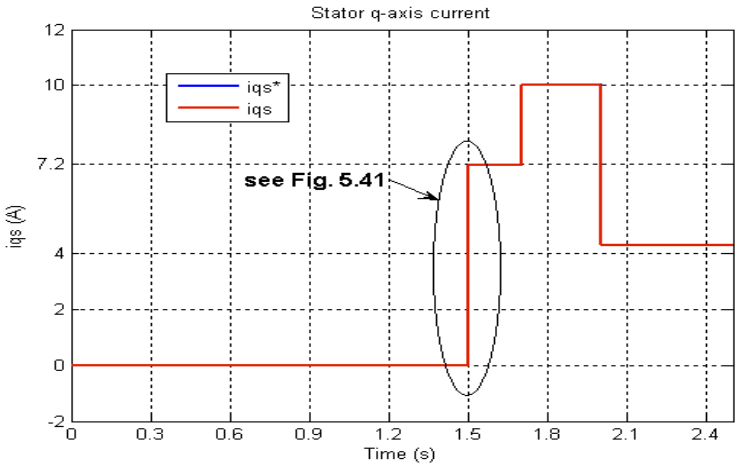

Fig. 5.33 q-axis stator current (i_{qs}) of Machine2

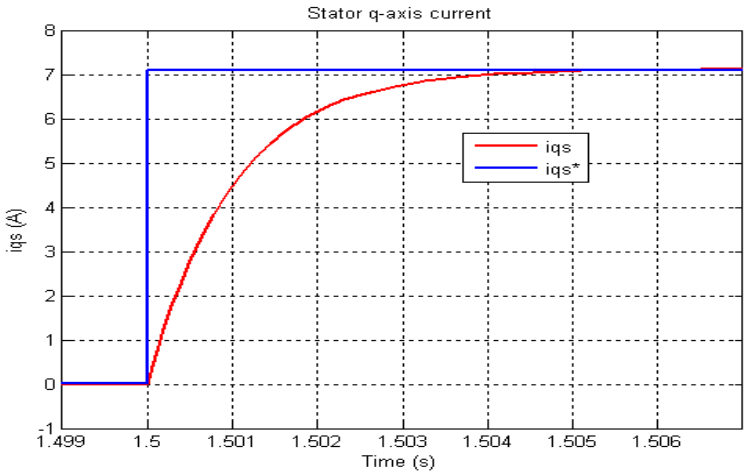

Fig. 5.34 Enlarged view of Fig. 5.33 from 1.499s to 1.507s

The speed response of Machine2 is shown in Fig. 5.35. Due to Machine1 being stiffly coupled to Machine2 the speed response of Machine2 corresponds to the speed response of Machine1. The speed response of Machine1 and Machine2 is therefore the response of the test bed and not the individual machines.

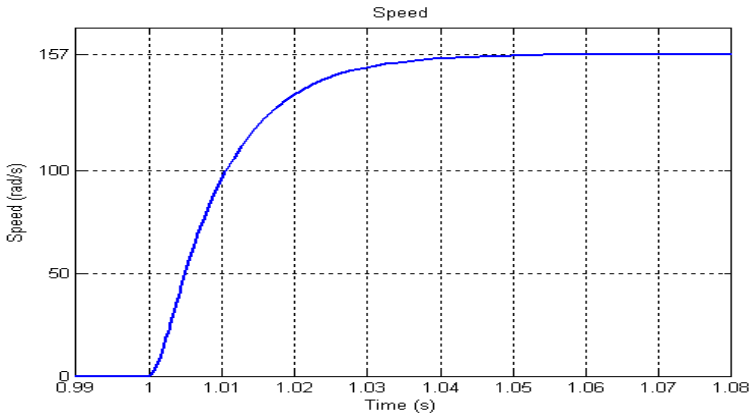

Fig. 5.35 Speed response of Machine2

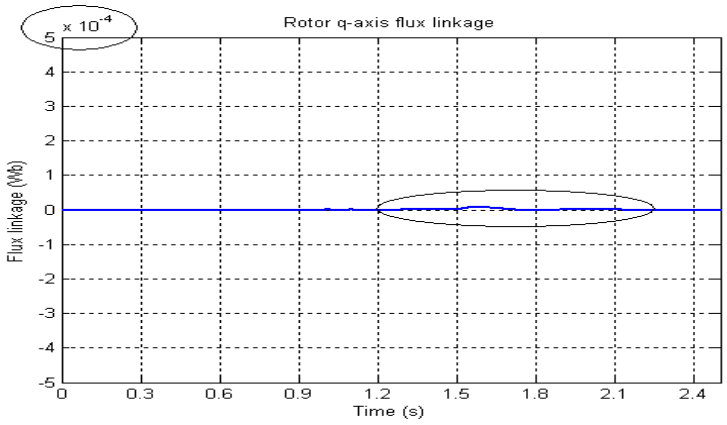

Fig. 5.36 q-axis rotor flux linkage (λ_{qr}) of Machine2

The q-axis rotor flux linkage (λ_{qr}) equals zero as depicted in Fig. 5.36 showing the correct application of FOC.

5.10 Practical results gained from the test bed

Following the Simulink^{TM} simulations of the induction machine under FOC, the test bed VFDs were programmed. VFD1 and VFD2 were configured such that both Machine1 and Machine2 operate under FOC. The various internal control loops of each VFD which allow speed and torque control of the induction machines are shown in Fig. 5.37 to Fig. 5.39. The inputs and outputs to the blocks presented in Fig. 5.37 to Fig. 5.39 show the parameter name, parameter number and the defined range of the parameter to be set using the Siemens Drive monitor software. Note that Fig. 5.37 to Fig. 5.39 have been reproduced from the 'MICROMASTER 440, Parameter list' manual [15].

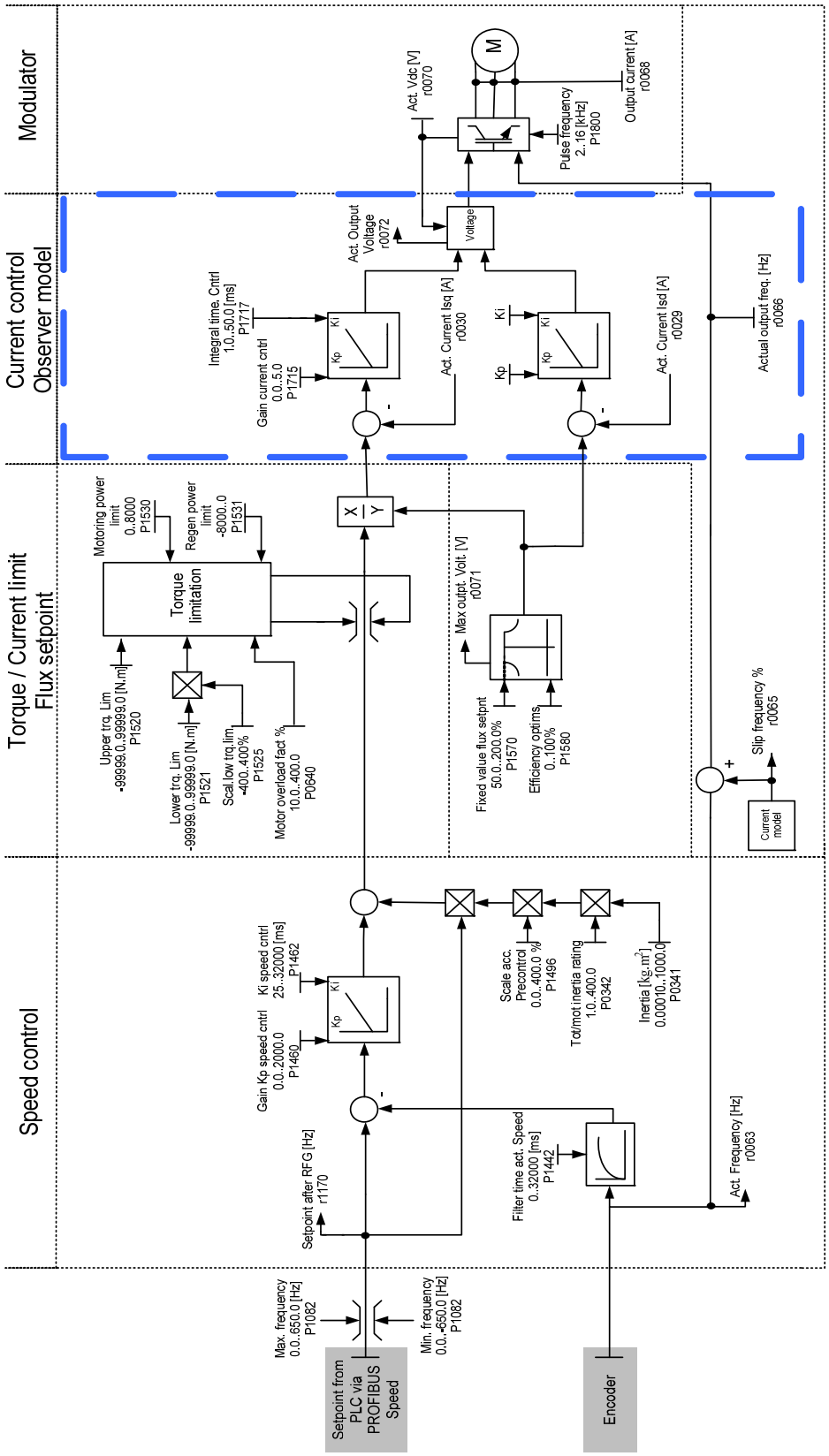

Fig. 5.37 Overview of the speed controller [15]

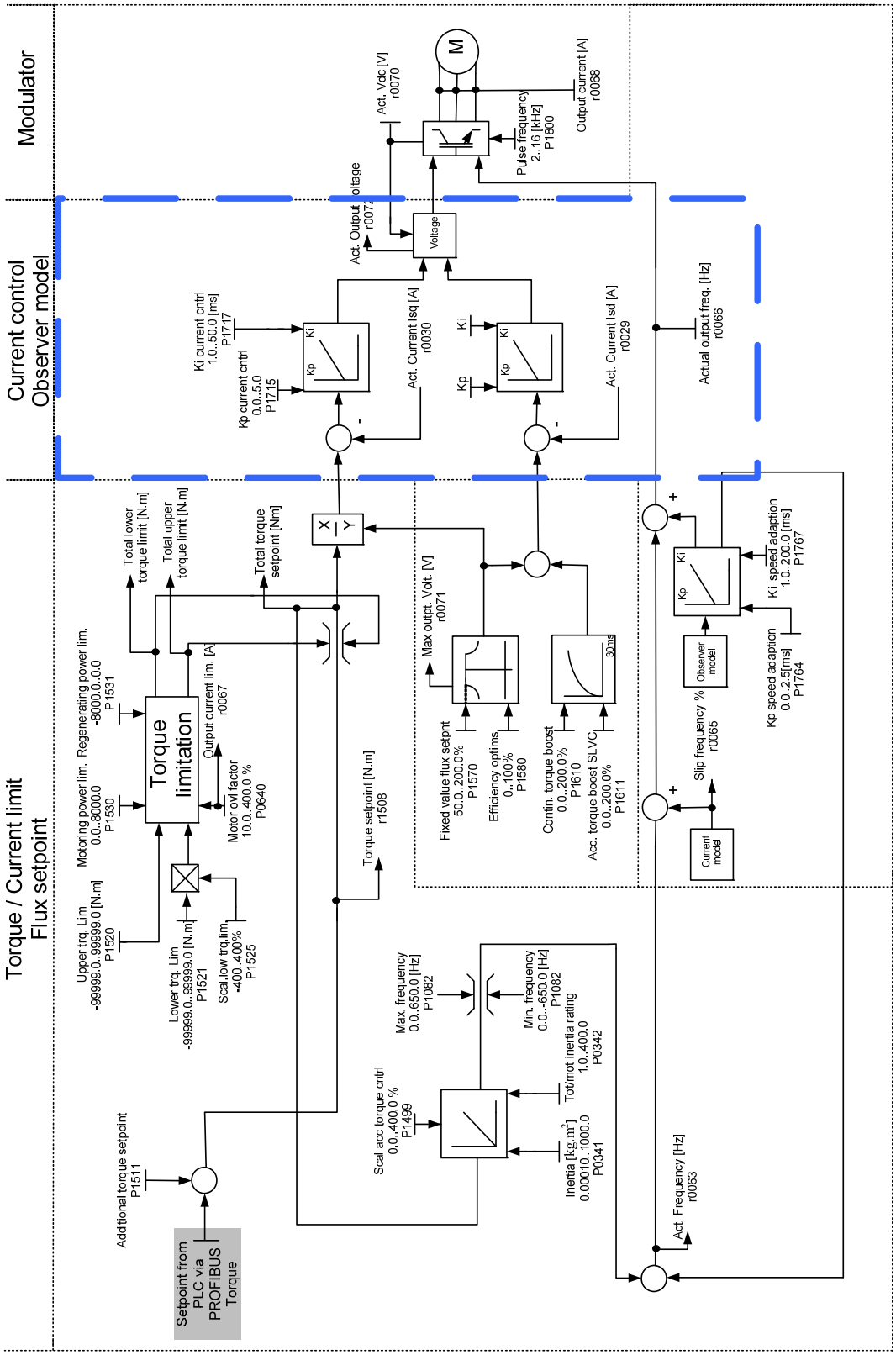

Fig. 5.38 Overview of the torque controller [15]

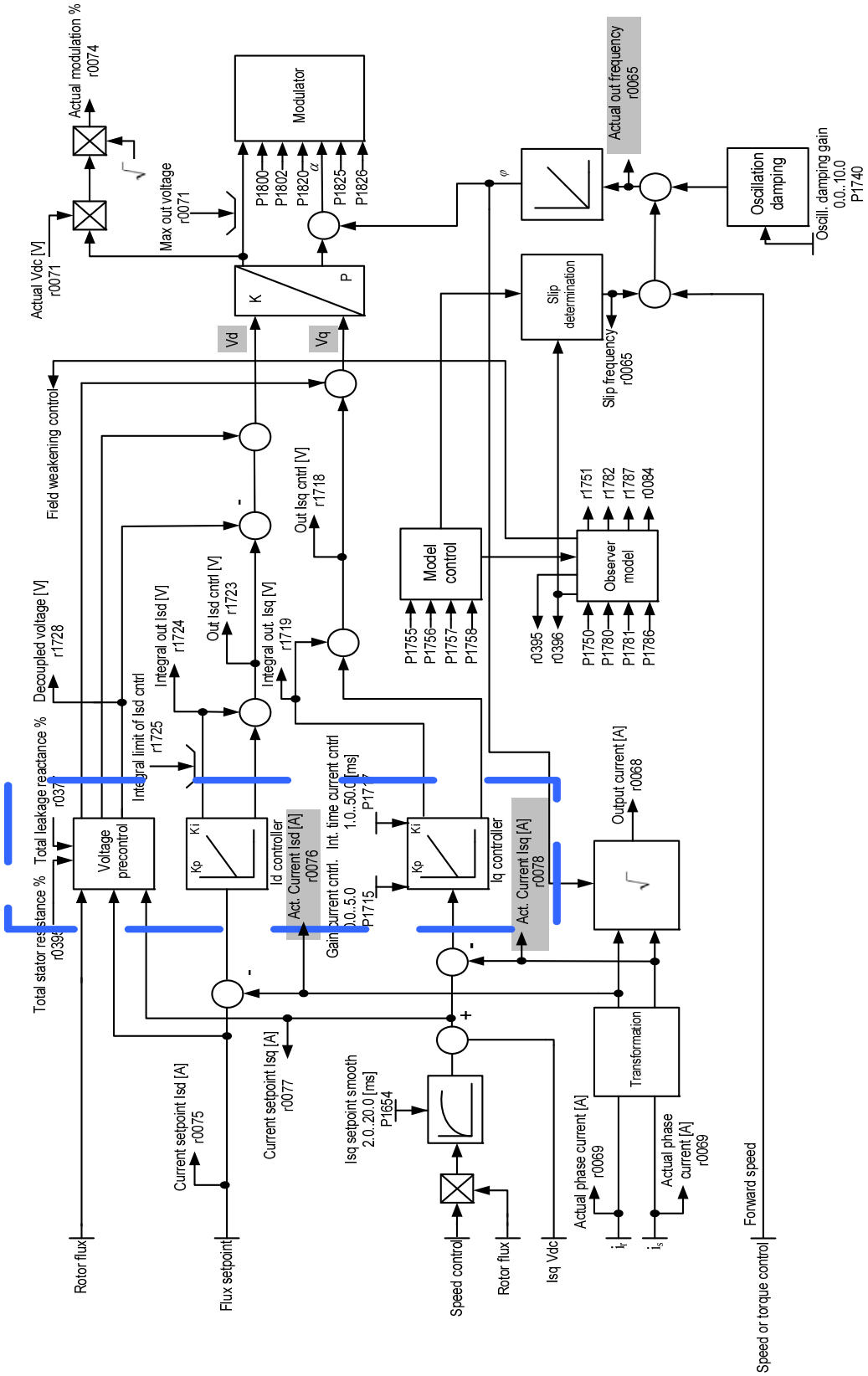

Fig. 5.39 Current control Observer model [15]

Referring to Fig. 5.37 through to Fig. 5.39, the main control loops blocked in blue form the heart of FOC and correspond to the control loops designed in Chapter 2, Section 2.5. All additional blocks provide improved control of the machine resulting in a technologically advanced VFD. The actual d-axis stator current (Parameter r0075 in Fig. 5.39) and q-axis stator current (Parameter r0078 in Fig. 5.39) responses of Machine1 and Machine2 were output to an oscilloscope using the analogue outputs available on each VFD. 50 ms filters were active on the analogue outputs of each VFD when the stator current responses shown in Fig. 5.40 to Fig. 5.43 were captured.

A step input (1450 rpm) to the speed reference (ω_r*) was applied to Machine1 to obtain the d-axis stator current response of Machine1. Once this response was obtained, a step torque input (7 Nm) to the torque reference (T*) was applied to Machine2 to obtain its d-axis stator current response while Machine1 continued to operate at 1450 rpm. The d-axis stator current responses of Machine1 and Machine2 are shown in Fig. 5.40 and Fig. 5.41 respectively.

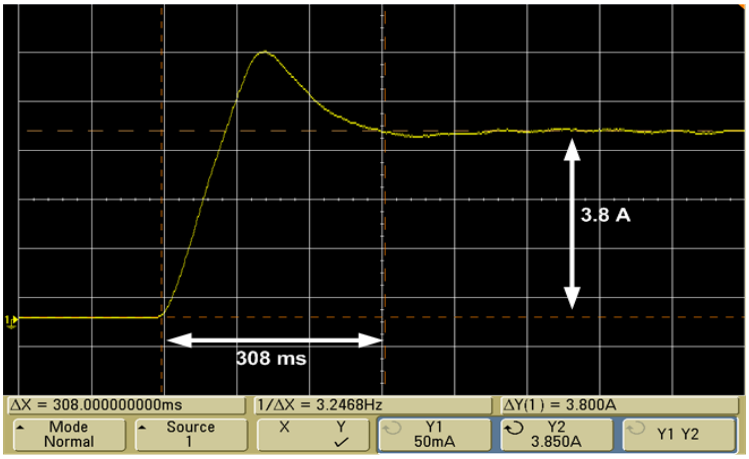

Fig. 5.40 d-axis stator current response - i_{ds} of Machine1

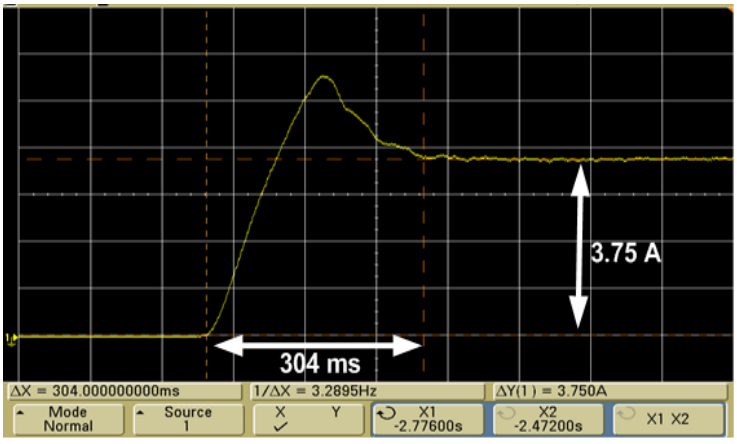

Fig. 5.41 d-axis stator current response - i_{ds} of Machine2

The d-axis stator current response of Machine1 is shown in Fig. 5.40 rising to 3.8 A in 308 ms while for Machine2 the d-axis stator current rose to 3.75 A in 304 ms as shown in Fig. 5.41.

To obtain the q-axis stator current responses of Machine1 and Machine2 a load of approximately 4 Nm was applied to Machine 1, while a load of 4 Nm was demanded from Machine2. These responses are shown in Fig. 5.42 and Fig. 5.43.

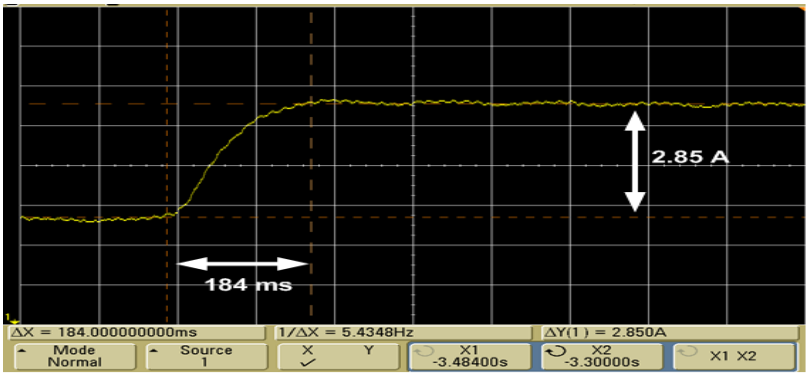

Fig. 5.42 q-axis stator current response - i_{qs} of Machine1

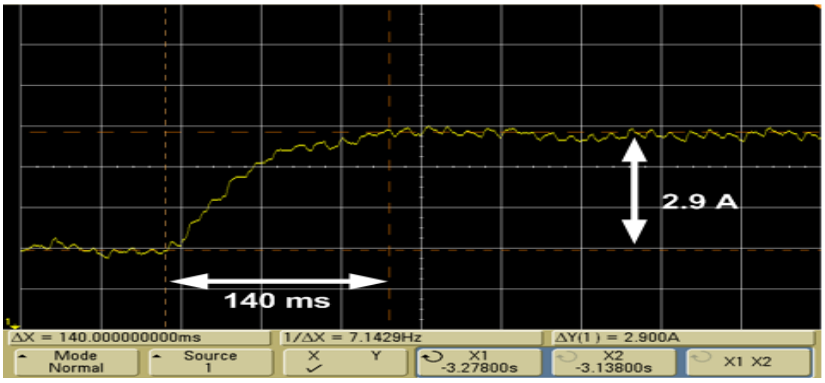

Fig. 5.43 q-axis stator current response - i_{qs} of Machine2

The q-axis stator current response of Machine1 is shown in Fig. 5.42 reaching 2.85 A in 184 ms. The q-axis stator current of Machine2 reached 2.9 A in 140 ms as shown in Fig. 5.43.

With reference to Section 5.9, the Simulink™ simulated d-axis stator current responses of Machine1 and Machine2 each rose to 3.68 A in 4 ms. The Simulink™ simulated q-axis stator current response of Machine1 peaked at 12.24 A in 4 ms when a step input to the speed reference was applied and for Machine2 the Simulink™ simulated q-axis stator current response peaked at 7.2 A in 4 ms when a step torque input to the torque reference was applied. The actual d-axis and q-axis stator current responses are much slower than the simulated responses of the

machine due to the time constants in the d-axis and q-axis current controllers being slow. The time constants could not be changed in the VFDs due to the restricted access of these parameters and safety limitations implemented by Siemens. Nevertheless the slow response of the test bed machines is not significant in the context of the test bed being used to replicate the characteristics of centrifugal fan systems.

The stator d-axis and q-axis currents of both Machine1 and Machine2 were then monitored and captured while Machine1 was loaded by Machine2 as shown in Fig. 5.44 to Fig. 5.47.

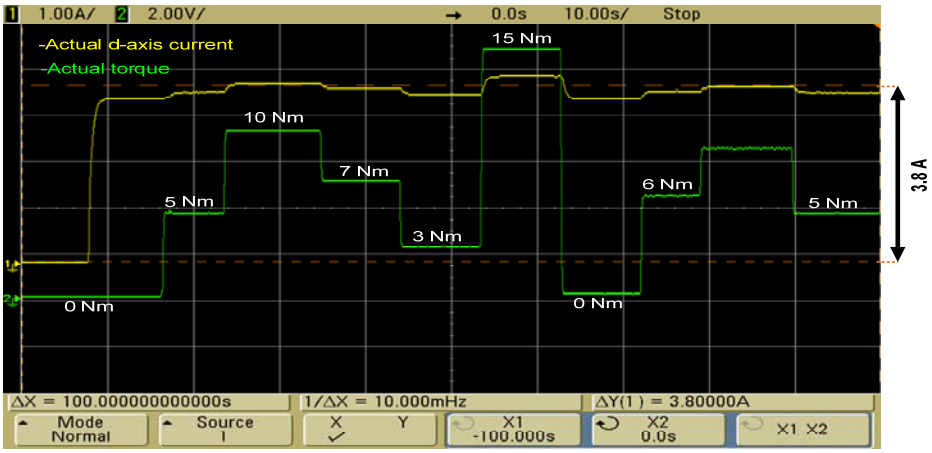

Fig. 5.44 d-axis stator current - i_{ds} of Machine1 under various loads

The d-axis stator current of Machine1 remained at approximately 3.8 A while the machine was subjected to various loads as shown in Fig. 5.44. The minimum and maximum d-axis stator currents recorded were 3.55 A and 3.9 A respectively. The d-axis stator current is not constant due to the ineffectiveness of the pre-compensator shown in Fig. 5.39 resulting in cross coupling between the d-axis and q-axis stator signals.

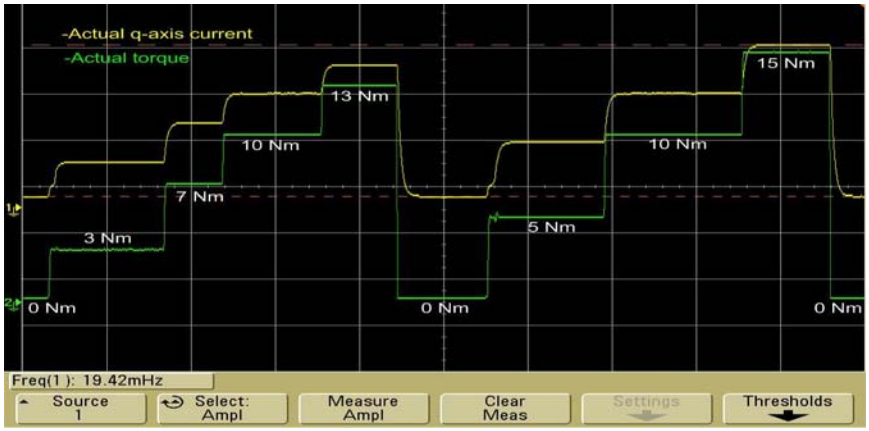

Fig. 5.45 q-axis stator current - i_{qs} of Machine1 under various loads

With reference to Fig. 5.45, the q-axis stator current of Machine1 changed according to the torque the machine had to produce to match the load applied by Machine2.

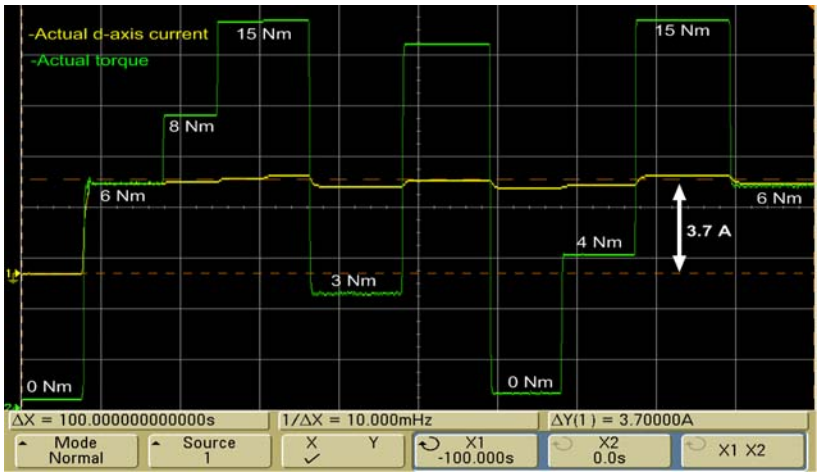

Fig. 5.46 d-axis stator current - i_{ds} of Machine2 producing various loads

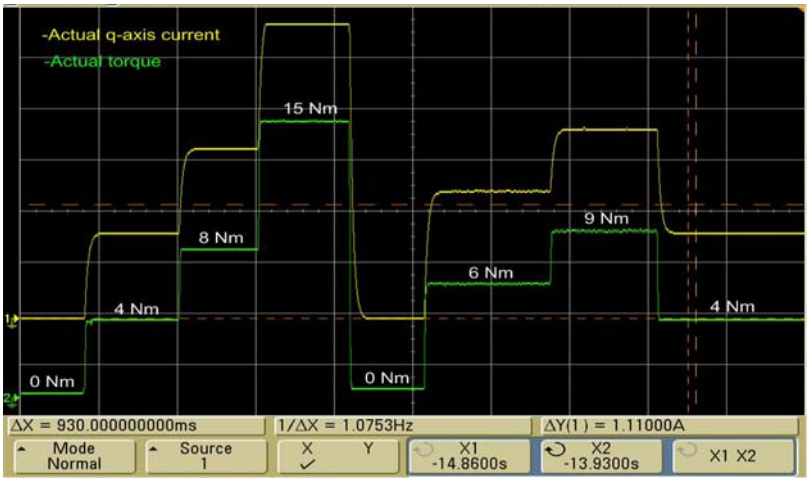

Fig. 5.47 q-axis stator current - i_{qs} of Machine2 producing various loads

With reference to Fig. 5.46, the d-axis stator current of Machine2 is shown equaling approximately 3.7 A while the machine was applying various loads. The pre-compensation implemented by VFD2 is also not as effective as shown by the varying d-axis stator current. The q-axis stator current of Machine2 changed according to the amount of torque demanded as shown in Fig. 5.47.

The speed response of the test bed (Machine1 coupled to Machine2) was captured on an oscilloscope and is shown in Fig. 5.48. The ability of the test bed to maintain the speed demanded under various loads is then shown in Fig. 5.49 and Fig. 5.50.

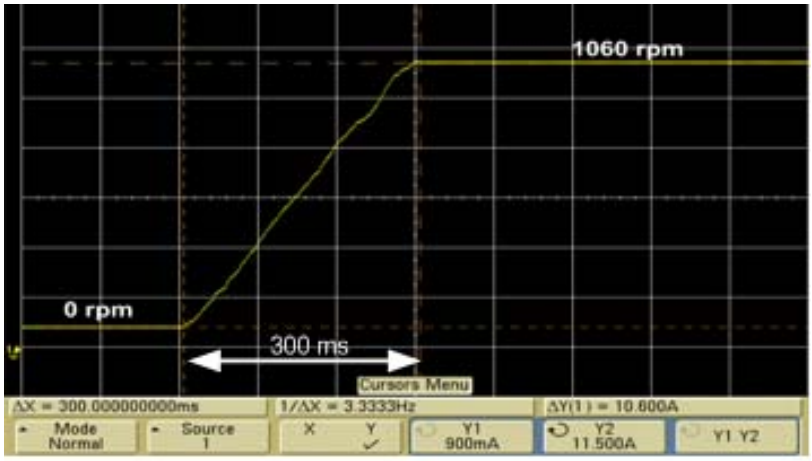

Fig. 5.48 Speed response of the test bed-ramp-up time 300 ms

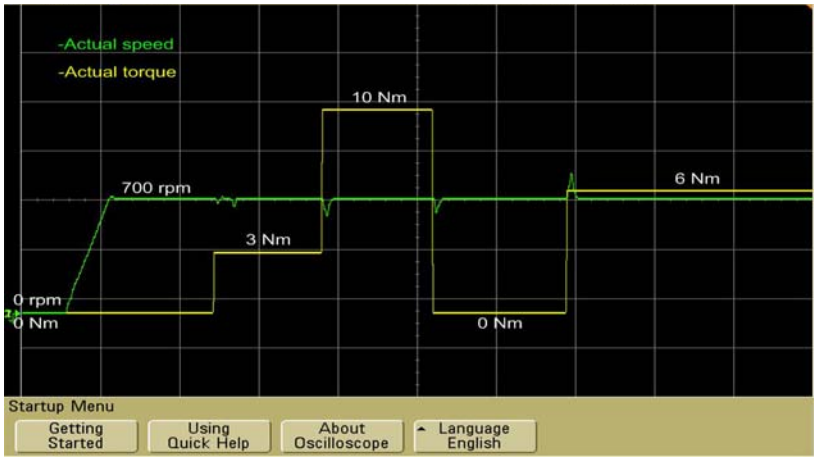

Fig. 5.49 Speed (700 rpm) response of the test bed under various loads

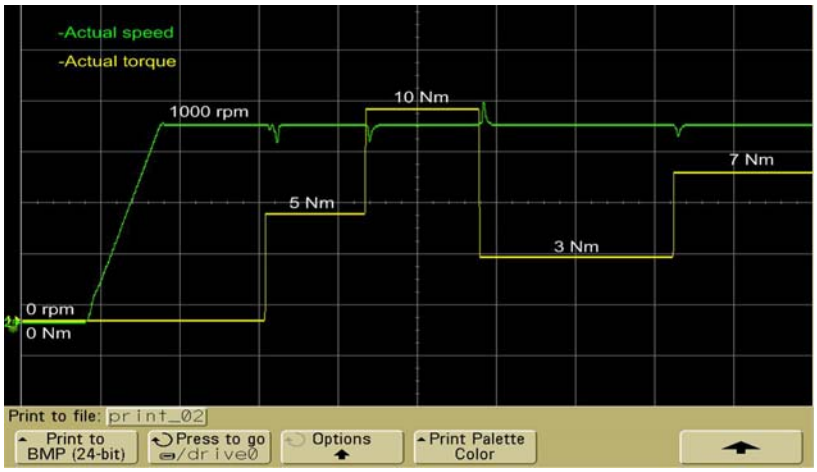

Fig. 5.50 Speed (1000 rpm) response of the test bed under various loads

The speed response of the test bed from 0 rpm to 700 rpm and 1000 rpm while being subjected to various step torque loads is shown in Fig. 5.49 and Fig. 5.50 respectively. In both cases the disturbances in the speed responses are due to the speed controller taking a finite time to readjust to the new condition each time local torque changes. This proves speed control has been applied correctly.

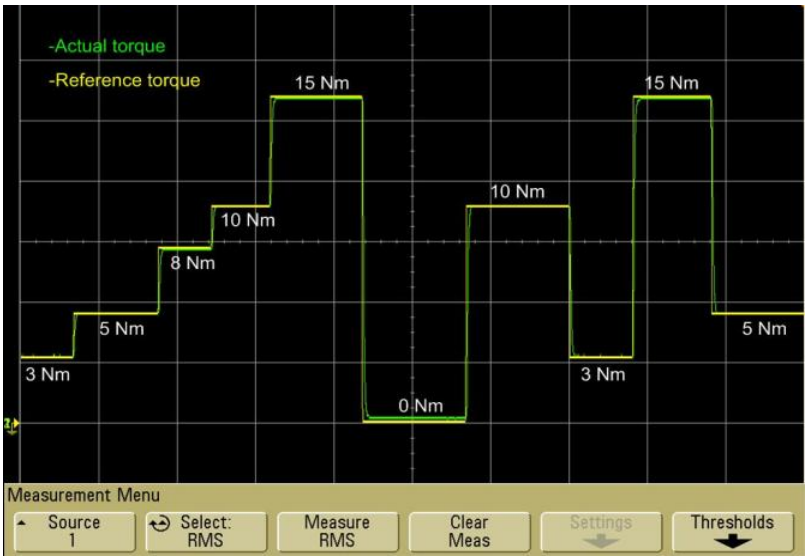

Fig. 5.51 Torque response of Machine2

The demanded torque and actual torque responses produced by Machine2 are shown in Fig. 5.51 displaying variances which are negligible between the two torque signals. This shows torque control has been applied correctly.

5.11 Conclusion

Three different methods were used to identify and verify the machine's electrical and mechanical parameters required for the design of the controllers necessary to implement FOC. The results have shown similarities in the machine's parameters. The simulated DOL start-up stator phase A current responses using all three sets of parameters matched the measured DOL start-up stator phase A current response accurately. The DOL Simulink^{TM} simulation of the machine using the measured and VFD calculated parameters displayed oscillations in the speed responses of the machine. Using the Optimisation toolbox identified machine parameters for the DOL simulation of the machine resulted in a speed response that had less oscillation causing the measured DOL start-up and simulated DOL start-up speed responses to approximately match.

The optimised machine parameters were therefore used in the designing of the controllers required to implement FOC.

The machines of the test bed were first simulated under FOC in Simulink™ which displayed torque control and improved dynamic characteristics of the machine. The machines of the test bed were then programmed to operate under speed control and torque control. The actual responses of both Machine1 and Machine2 of the test bed have been shown proving the correct application of FOC. The speed response of Machine1 showed the machine trying to maintain a constant speed under various loads and the torque response of Machine2 showed the reference and actual torque signals approximately matching each other.

The next chapter presents Simulink™ simulations of the test bed replicating a theoretical fan, followed by the practical results gained from the test bed replicating this fan.

CHAPTER 6

SIMULATION OF A THEORETICAL FAN BY THE TEST BED

6.1 Introduction

The test bed was constructed as discussed in Chapter 4 and commissioned as in Chapter 5. Commissioning showed that Machine1 could be accurately speed controlled and Machine2 could be accurately torque controlled so as to act as a configurable load to Machine1. The next step was to control Machine2 to act as an arbitrary fan load since the data from Vlaklaagte was not available at this time. For this purpose the torque-speed and power-flow curves from Chapter 3 are used.

This chapter presents Simulink™ simulations of the test bed replicating the arbitrary theoretical fan followed by the practical results gained from the test bed.

6.2 Simulink™ simulation of the test bed replicating the theoretical fan

To simulate the test bed replicating the theoretical fan, the torque-speed and power-flow curves from Chapter 3 need to be replicated. These torque-speed (Fig. 3.11) and power-flow curves (Fig. 3.12) are repeated here as Fig. 6.1 and Fig. 6.2 respectively. The Simulink™ block diagram used to simulate the test bed replicating the theoretical fan is presented in Fig. 6.3 and is similar to the Simulink™ block diagram shown in Fig. 5.21. The torque-speed and power-flow curves of the theoretical fan are programmed in the Simulink™ block labelled 'Fan model' shown in Fig. 6.3. Refer to Appendix E.1 for the contents of the block labelled 'Fan model'.

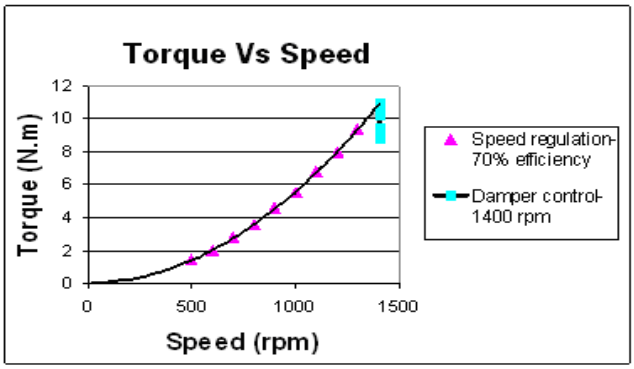

Fig. 6.1 Torque-speed of the theoretical fan

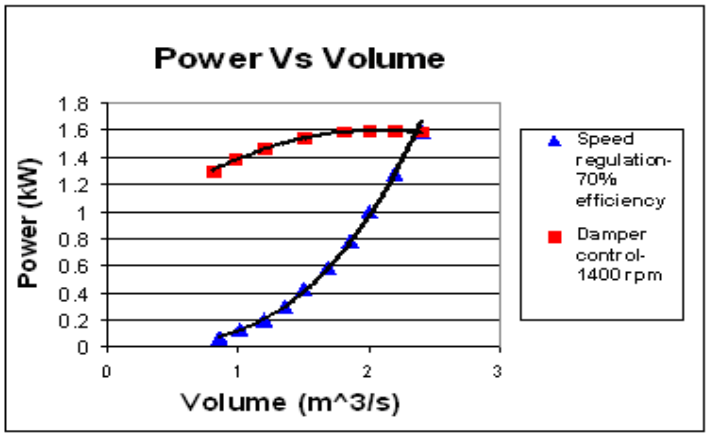

Fig. 6.2 Power-flow of the theoretical fan

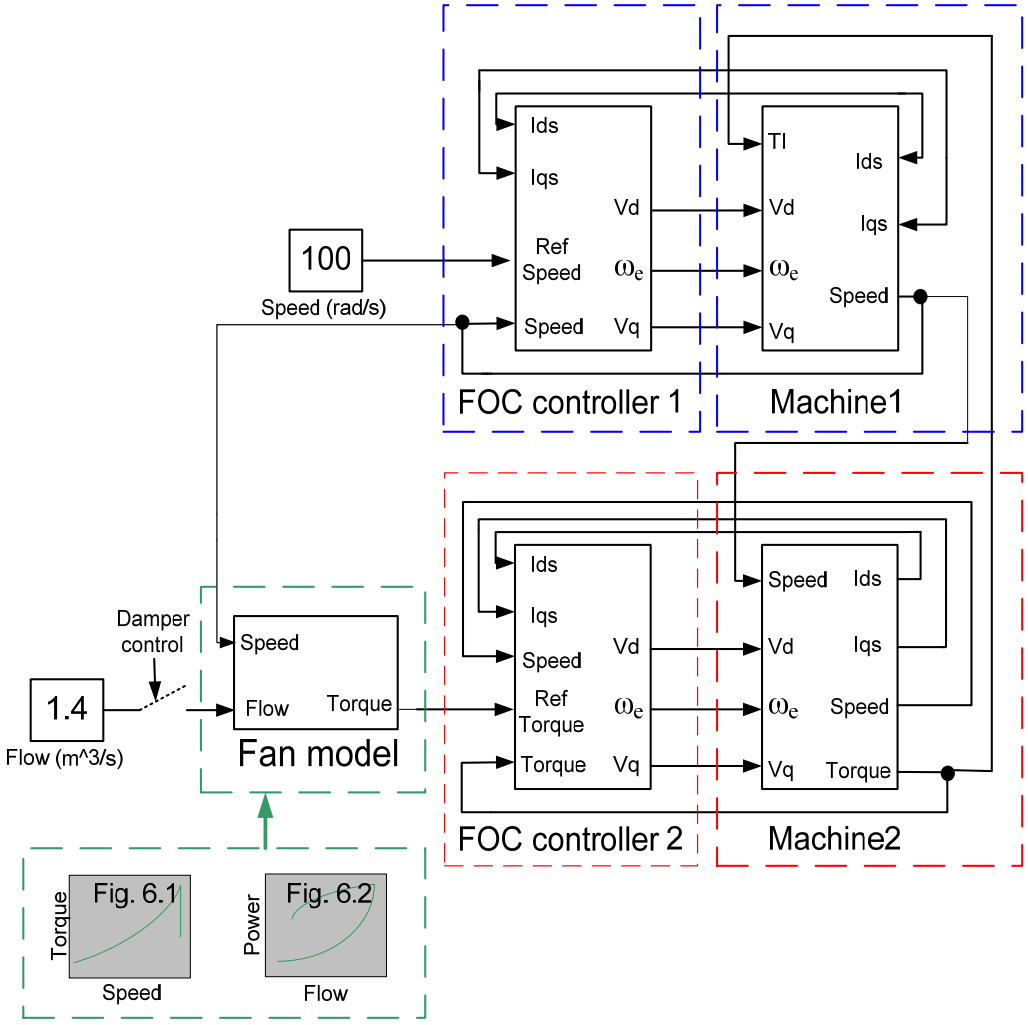

Fig. 6.3 Simulink™ block diagram for the test bed simulation of the theoretical fan

6.2.1 Simulink™ simulation results of the test bed replicating the theoretical fan

To simulate the test bed replicating the theoretical fan under variable speed, the speed of the test bed was ramped through the speed range shown in Fig. 6.4. To simulate the test bed replicating the theoretical fan under damper operation, the speed of the test bed remained fixed (Fig. 6.4) as the flow rate was ramped through the range from 0 m^3/s to 2.4 m^3/s as shown in Fig. 6.5.

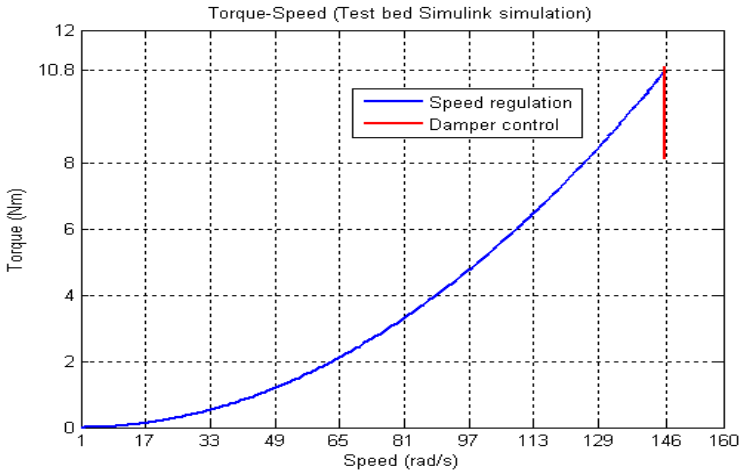

Fig. 6.4 Simulink™ simulated torque-speed curves of the test bed replicating the theoretical fan under both damper operation and speed regulation

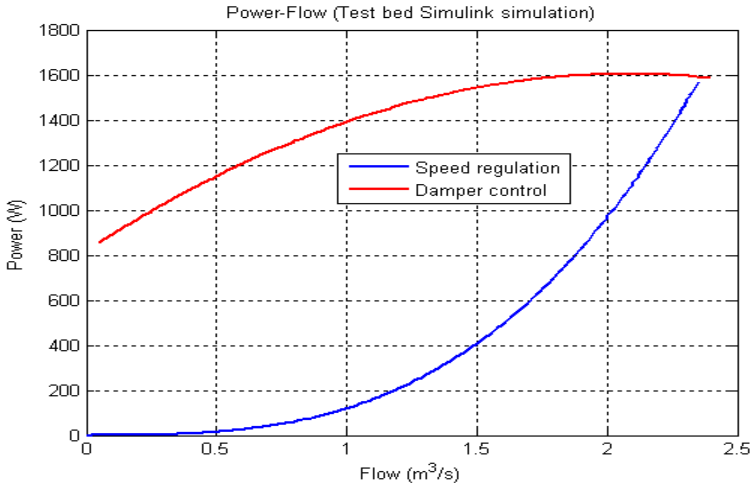

Fig. 6.5 Simulink™ simulated power-flow curves of the test bed replicating the theoretical fan under both damper operation and speed regulation

The Simulink™ simulated responses of the test bed replicating the theoretical fan are shown in Fig. 6.4 and Fig. 6.5. To verify the accuracy of the Simulink™ simulations, the operation of

the theoretical fan as discussed in Chapter 3 is compared to the Simulink™ simulations as shown in Fig. 6.6 and Fig. 6.7.

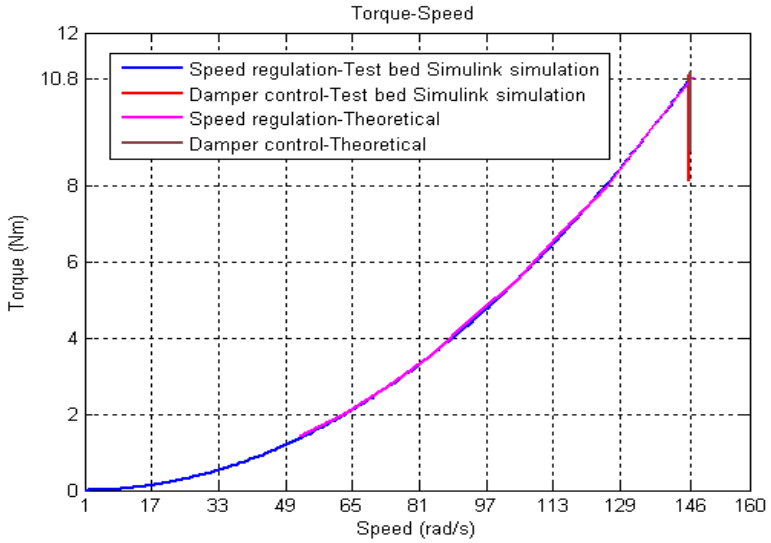

Fig. 6.6 Comparison of the theoretically calculated and Simulink™ simulated torque-speed curves

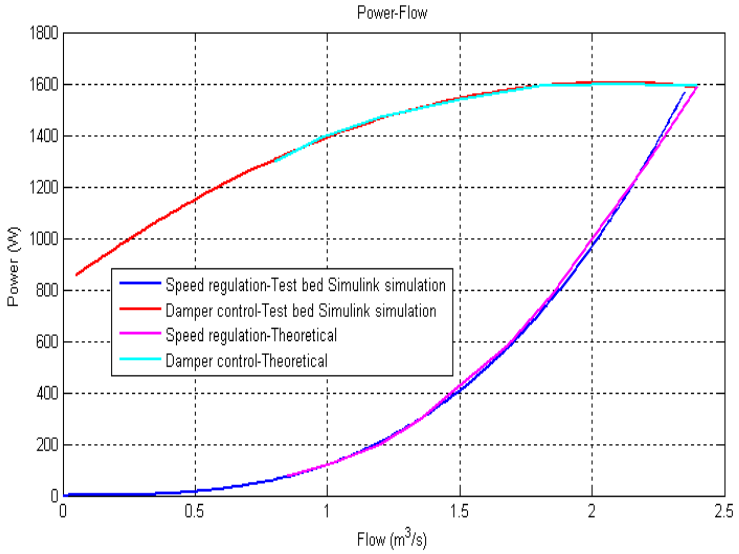

Fig. 6.7 Comparison of the theoretically calculated and Simulink™ simulated power-flow curves

The theoretically calculated fan responses and the Simulink simulated test bed responses shown in both Fig. 6.6 and Fig. 6.7 correspond closely, therefore the Simulink™ simulation of the test bed replicating the theoretical fan is correct. The actual test bed was then programmed and the practical results gained from the test bed are shown in the next section.

6.3 Test bed practical results-replication of the theoretical fan

With reference to Fig. 6.8, the torque-speed and power-flow curves shown in Fig. 6.1 and Fig. 6.2 were programmed in the PLC and the calculated speed and torque setpoints sent to VFD1 and VFD2 of the test bed via PROFIBUS. The speed transducer mounted on Machine2 of the test bed provided speed feedback from the system. Torque feedback from the system was calculated by VFD2 and sent to the PLC via a 4-20 mA current interface.

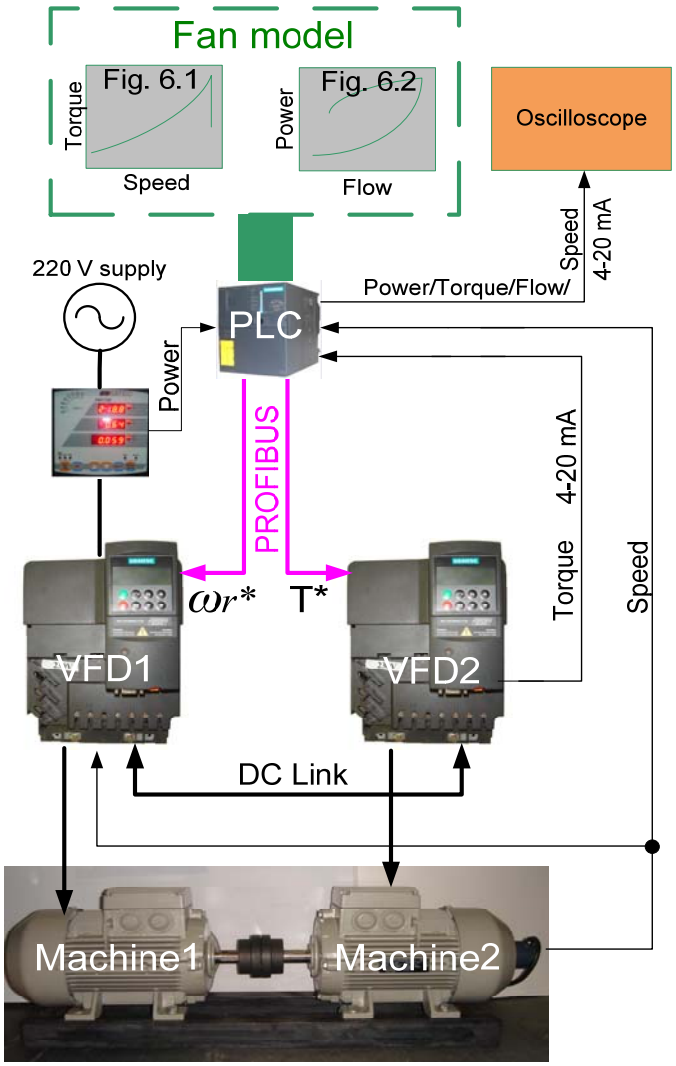

Fig. 6.8 Test bed hardware and software integration

To replicate variable speed operation of the fan, the speed of the test bed was ramped up to 1400 rpm. To replicate the damper torque-speed characteristic of the fan, the torque reference

was ramped from 8.8 Nm to 10.8 Nm and to replicate the damper power-flow characteristic of the fan the flow rate reference was ramped from 0.8 m^3/s to 2.4 m^3/s.

The actual output signals obtained from the test bed were output to an oscilloscope and imported to Matlab as shown in Fig. 6.9 and Fig. 6.10.

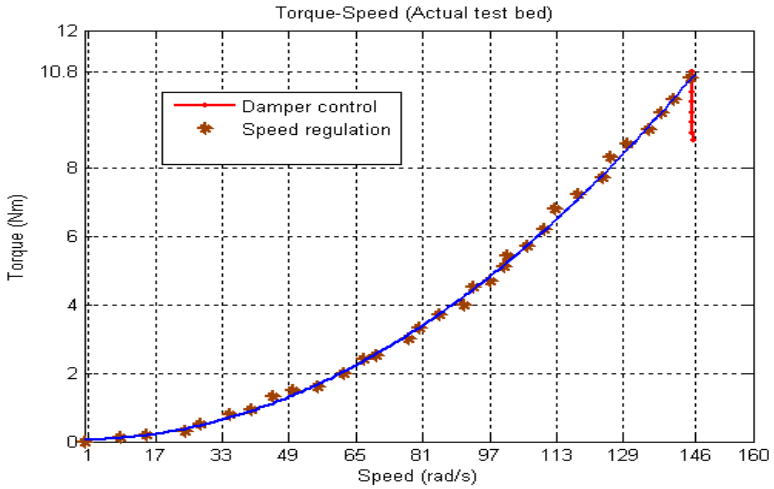

Fig. 6.9 Torque-speed for both speed regulation and damper control of the fan

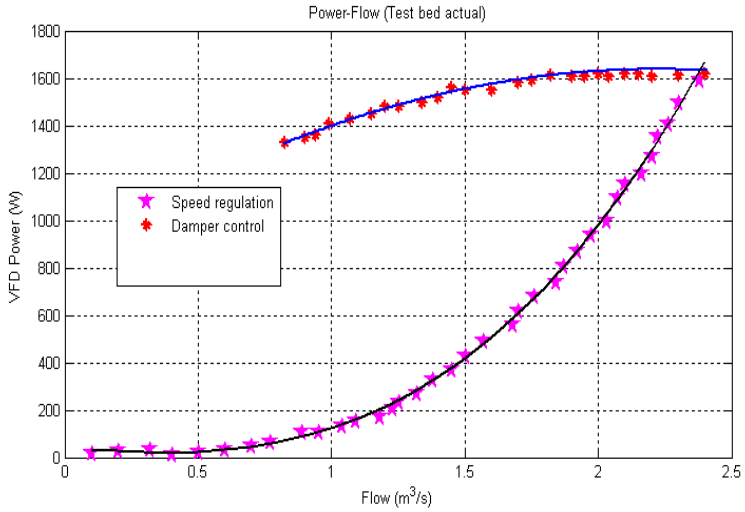

Fig. 6.10 VFD power-flow for both speed regulation and damper control of the fan

The practical results from the test bed shown in Fig. 6.9 and Fig. 6.10 are compared to the theoretically calculated responses of the fan and the Simulink™ simulated responses of the test bed replicating the theoretical fan in Fig. 6.11 and Fig. 6.12 to verify the accuracy of the test bed.

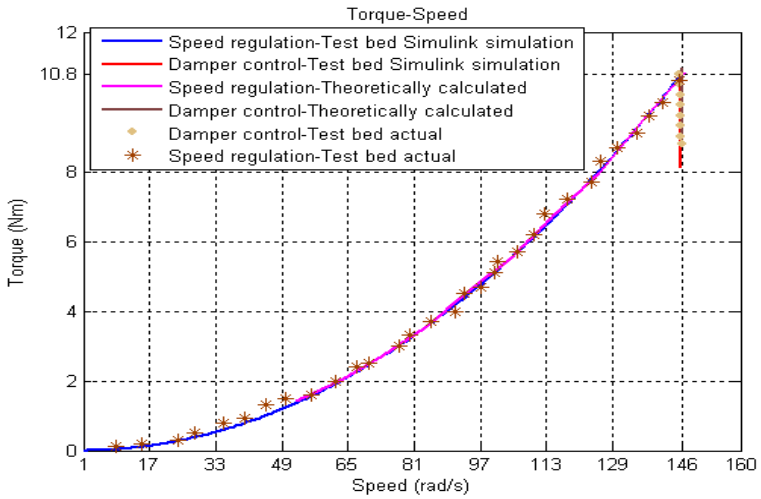

Fig. 6.11 Comparisons of the theoretically calculated, Simulink™ simulated test bed and actual test bed torque-speed responses

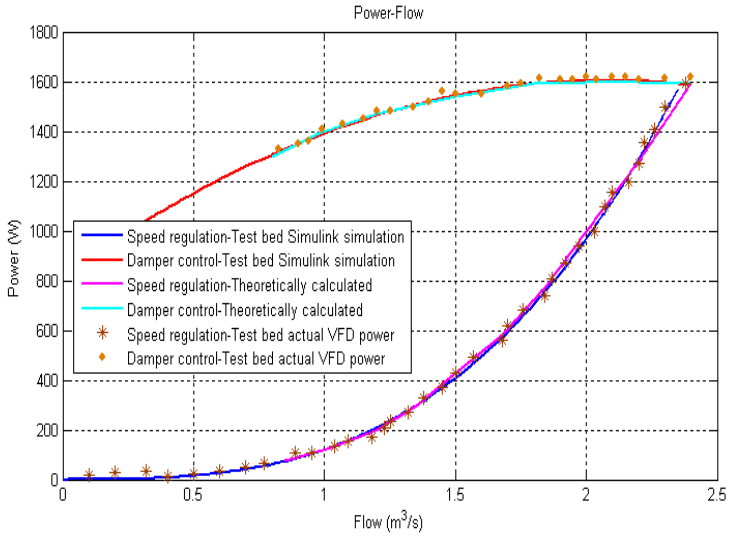

Fig. 6.12 Comparisons of the theoretically calculated, Simulink™ simulated test bed and actual test bed power-flow responses

The torque-speed results shown in Fig. 6.11 and the power-flow results shown in Fig. 6.12 correspond closely and show that the actual test bed is able to correctly replicate the operation of the theoretical centrifugal fan.

6.4 Conclusion

This chapter showed how a fan's characteristics can be simulated. The theoretically calculated torque-speed and power-flow curves of the theoretical fan were simulated by the test bed in both Simulink™ and practically. The results gained from the simulations were then compared to the theoretically calculated results showing the responses corresponding closely. This proves that the test bed is operating correctly and will be able to replicate any fan system accurately.

The next chapter discusses the construction and testing of the 1.1 kW fan system at the UKZN.

CHAPTER 7

SIMULATION OF A 1.1 kW FAN BY THE TEST BED

7.1 Introduction

After commissioning the test bed in Chapter 5 an arbitrary fan load was simulated by the test bed in Chapter 6. The data from Vlaklaagte was still not available at this stage therefore a smaller 1.1 kW centrifugal fan system having a similar characteristic to the fan system at Vlaklaagte was setup in the laboratory as shown in Fig. 7.1. A 3 kW induction machine similar to the induction machines used in the test bed was used to operate the centrifugal fan. Refer to Appendix A.1 for the nameplate data of the induction machine. The centrifugal fan shown in Fig. 7.1 is referred to as a 1.1 kW fan system throughout this thesis for the simple reason being that at approximately 1500 rpm the fan draws approximately 1.1 kW of power.

This chapter presents the hardware of the 1.1 kW fan system and the results obtained from testing the fan system. The results gained from the test bed simulating the 1.1 kW fan system in Simulink™ are then discussed followed by the practical results gained from the test bed.

7.2 1.1 kW fan construction and components

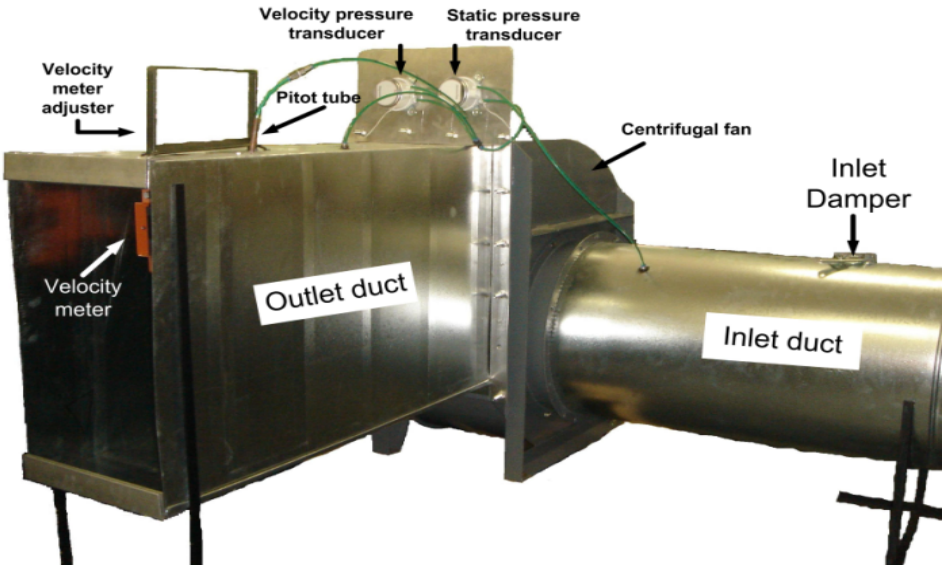

Fig. 7.1 Centrifugal fan with measurement transducers

The centrifugal fan with aluminium ducting attached to the inlet and outlet of the fan, together with pressure and air-flow transducers is shown in Fig. 7.1. The ducting allows for a more uniform flow of air at the inlet and outlet of the fan for the purpose of measurements.

Fig. 7.2 (a) Inlet damper open

Fig. 7.2 (b) Inlet damper closing

An inlet damper mounted in the inlet duct of the fan is shown in Fig. 7.2. Fig. 7.2 (a) and Fig. 7.2 (b) show the inlet damper in an open and in a partially closed position respectively. The closing action of the inlet damper is similar to that of a hinged door. The inlet damper allows for variable air-flow rates to be achieved without an adjustment of the fan speed. The control mechanism of the inlet damper is shown in Fig. 7.3.

Fig. 7.3 Control mechanism of the inlet damper

The entire fan system is shown schematically in Fig. 7.4. It comprises the centrifugal fan with a speed encoder attached to the shaft of the fan, VFD (VFD1), power supply for the PLC, the PLC, high speed counter module, analogue input module for the velocity and pressure transducers, RS 485 to RS 232 signal converter, RS 232C communication module and power meter to monitor VFD1's input power. The velocity and pressure measurement transducers are discussed in Section 7.2.1. The remaining control and monitoring equipment utilised in the fan system are not discussed, since the test bed also utilised the same equipment. This equipment was discussed in Chapter 4.

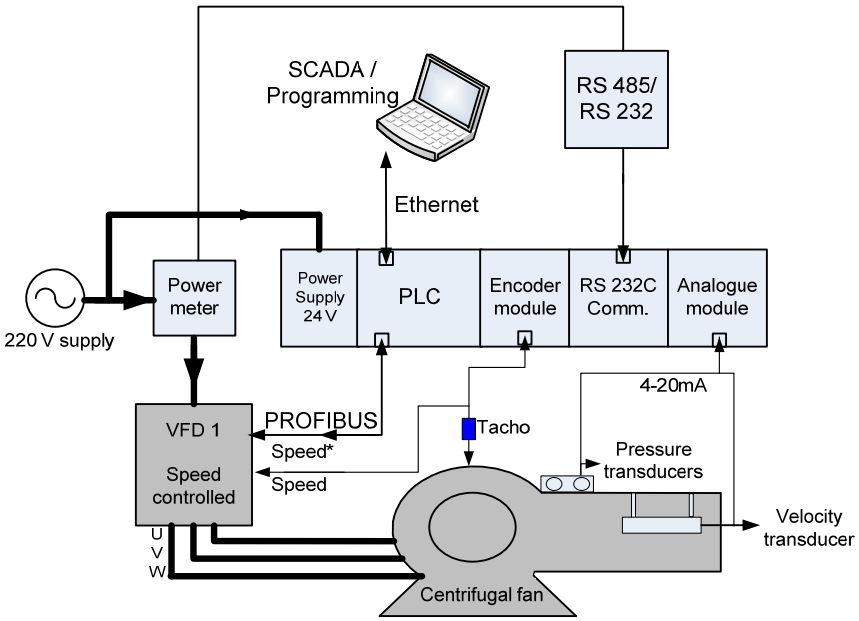

Fig. 7.4 Schematic of the fan system

7.2.1 Measurement transducers

- **Velocity transducer**

Fig. 7.5 Safdy air velocity transducer

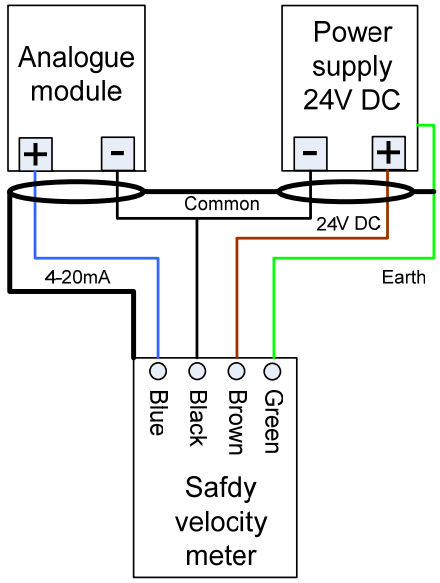

Fig. 7.6 Connection diagram for the velocity transducer

A Safdy air velocity transducer was mounted in the outlet duct of the fan as shown in Fig. 7.1. The air velocity transducer shown in Fig. 7.5 was not mounted in a fixed position but rather an adjustable bracket was made so that the air velocity transducer could be positioned where optimum air-flow occurred. The transducer measures air velocity in meters per second with a measuring range of 0-15 m/s [26] and an accuracy of +-1 % [26]. The measured air velocity is transmitted in the form of a 4-20 mA signal into the analogue module of the PLC as shown in Fig. 7.6.

- **Pressure transducers**

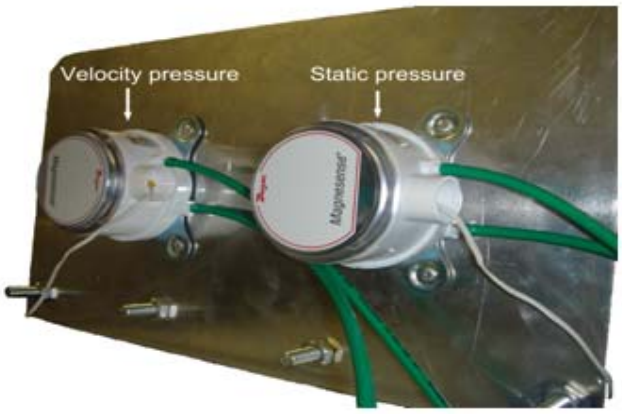

Fig. 7.7 Differential pressure transducers

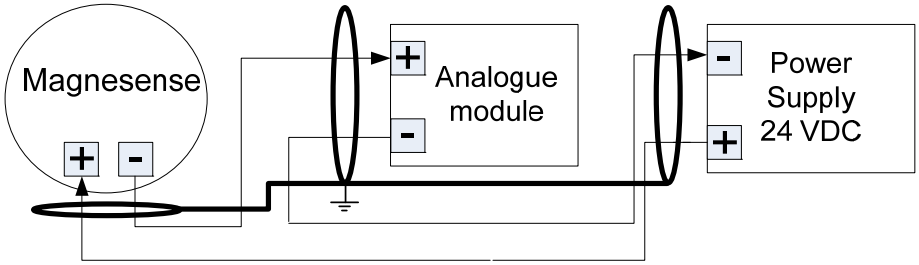

Fig. 7.8 Electrical connection diagram for the pressure transducers

Two Magnesense differential pressure transducers were mounted on a plate attached to the fan as shown in Fig. 7.1 and Fig. 7.7. One measures the static pressure across the fan whilst the other measures the velocity pressure in the outlet duct of the fan (see labels in Fig. 7.9). The plastic pipes going into both transducers were kept as short as possible to prevent additional resistance and losses in pressure. The two transducers measure air pressure in Pascals having a measuring range of 0-1250 Pa [27] and an accuracy of +-1 % [27]. The measured pressures are transmitted in the form of 4-20 mA signals into the analogue module of the PLC as shown schematically in Fig. 7.8. The maximum pressure that the transducers can handle is 6.9 kPa before bursting [27]. To measure the velocity pressure, a pitot tube was designed out of a copper pipe and bent in a 'L' shape as shown schematically in Fig. 7.9. The connection of the pipes from the pressure points of measurement into the pressure transducers are shown schematically in Fig. 7.9.

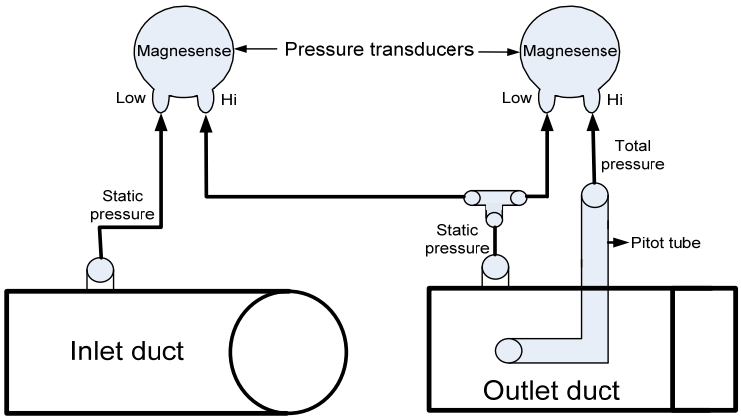

Fig. 7.9 Schematic displaying the pressure transducers and pressure points of measurement

7.3 Operating characteristics of the 1.1 kW fan system

Once the fan system had been designed, commissioned and found to be operating as expected, the next step was to conduct tests under both damper and variable speed operation.

In order to determine whether the ducting increased the work (hence an increase in torque and power) done by the fan, the torque and speed of the fan were first measured with and without the ducting present.

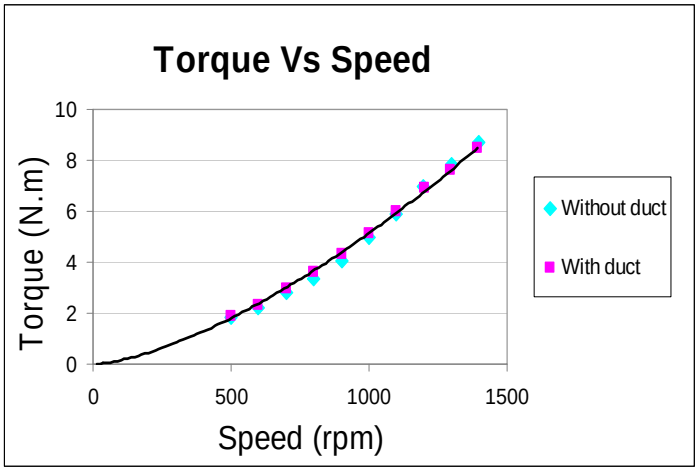

Fig. 7.10 Measured torque and speed of the fan with and without ducting present

Fig. 7.10 shows the torque-speed characteristic of the fan with and without the inlet and outlet ducts mounted on and as can be seen there is minimal difference. It is therefore safe to assume

that the ducting has no effect on the work that the fan had to do. This was due to the fact that the ducting had no bends or obstructions in it resulting in no significant new additional restrictions in the air-flow path.

7.3.1 Characteristic curves

To determine the characteristic curves of the 1.1 kW fan further tests were conducted which are discussed next.

Fan characteristic

The fan characteristic curves were determined by adjusting the inlet damper (Fig. 7.2) from a fully open position to an almost fully closed position while the fan operated at a certain fixed speed. Referring to Fig. 7.11, the blue blocks indicate the results that were recorded as the damper position was changed at a certain fixed speed. The fixed speeds shown in Fig. 7.11 range between 500 rpm and 1500 rpm.

System characteristic

The system characteristic curve was determined by keeping the damper in a fixed position while the speed of the fan was varied. The damper was first set to 100 % open while the speed of the fan was varied between 500 rpm and 1500 rpm as indicated by the purple triangles in Fig. 7.11. To then show how a system characteristic curve changes when a system physically changes, the damper was set to 50 % closed and again the speed of the fan was varied between 500 rpm and 1500 rpm as shown by the red circles in Fig. 7.11.

Operating points of the fan

Referring to Fig. 7.11, the fan would operate at points where the fan characteristic curve intersects the system characteristic curve. For the test bed to later on simulate the 1.1 kW fan, the test bed will need to replicate the operating points of the fan.

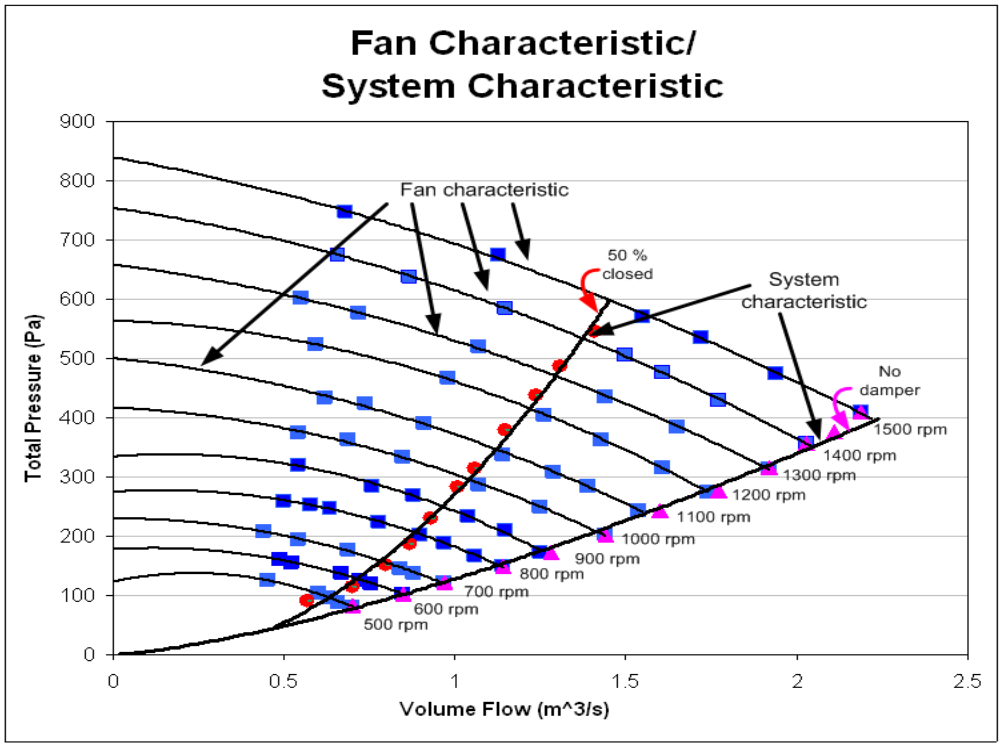

Fig. 7.11 Operating points of the fan

The torque-speed characteristic of the fan under damper operation and variable speed was then determined. For the damper control torque-speed characteristic of the fan, the speed of the fan remained at 1400 rpm while the inlet damper was adjusted from a fully open, to a fully closed position. For the variable speed torque-speed characteristic of the fan, the inlet damper was then left fully open while the speed of the fan was increased from 300 rpm to 1400 rpm. The torque-speed characteristic of the 1.1 kW fan system is shown in Fig. 7.12.

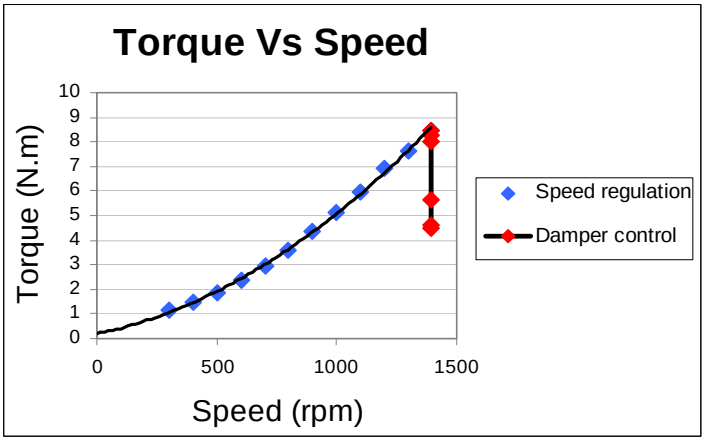

Fig. 7.12 Measured torque-speed curves of the fan using both damper control and speed regulation to vary the air-flow rate

Fig. 7.12 shows the torque remains high as the air-flow rate is varied when using damper control as compared to variable speed operation of the fan. This concludes that the power drawn by the fan should also be high since the torque is high ($P = T * \omega$).

The speed of the fan was then maintained at 1500 rpm while the inlet damper (Fig. 7.2) was again adjusted from a fully open, to a fully closed position. In this case, the power and air-flow rate of the fan were measured and plotted as shown in Fig. 7.13. The outlet damper was then left fully open and the speed of the fan was increased from 500 rpm to 1500 rpm whilst the power and air-flow rate of the fan were captured.

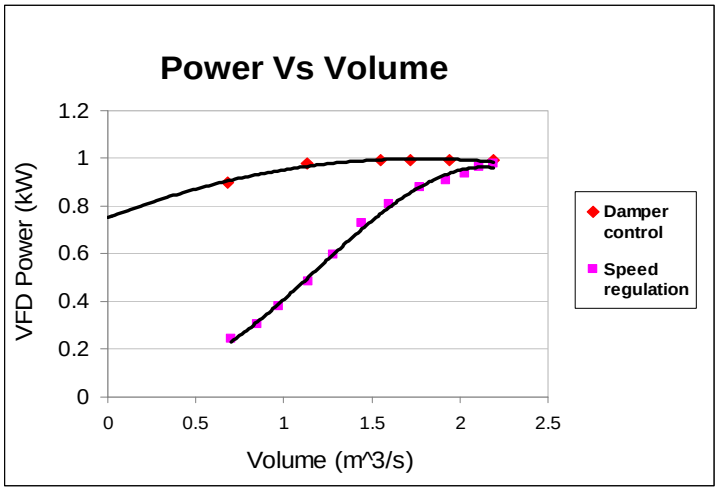

Fig. 7.13 Measured VFD power-flow curves of the fan using both damper control and speed regulation to vary the air-flow rate

Fig. 7.13 shows the power drawn by the fan is significantly lower when speed regulation is used to vary the air flow rate of the fan.

7.4 Simulink™ simulation of the test bed replicating the 1.1 kW fan

The measured torque-speed and power-flow curves of the 1.1 kW fan were shown in Fig. 7.12 and Fig. 7.13 respectively. These curves need to be simulated by the test bed for the operation of the 1.1 kW fan system to be replicated. Before the test bed could be programmed to replicate the 1.1 kW fan system, the test bed was first simulated in Simulink™. The same Simulink™ block diagram that was used to simulate the arbitrary fan in Chapter 6 is used to simulate the 1.1 kW fan system. The contents of the block labelled 'Fan model' shown in Fig. 7.14 are different and is presented in Appendix E.2.

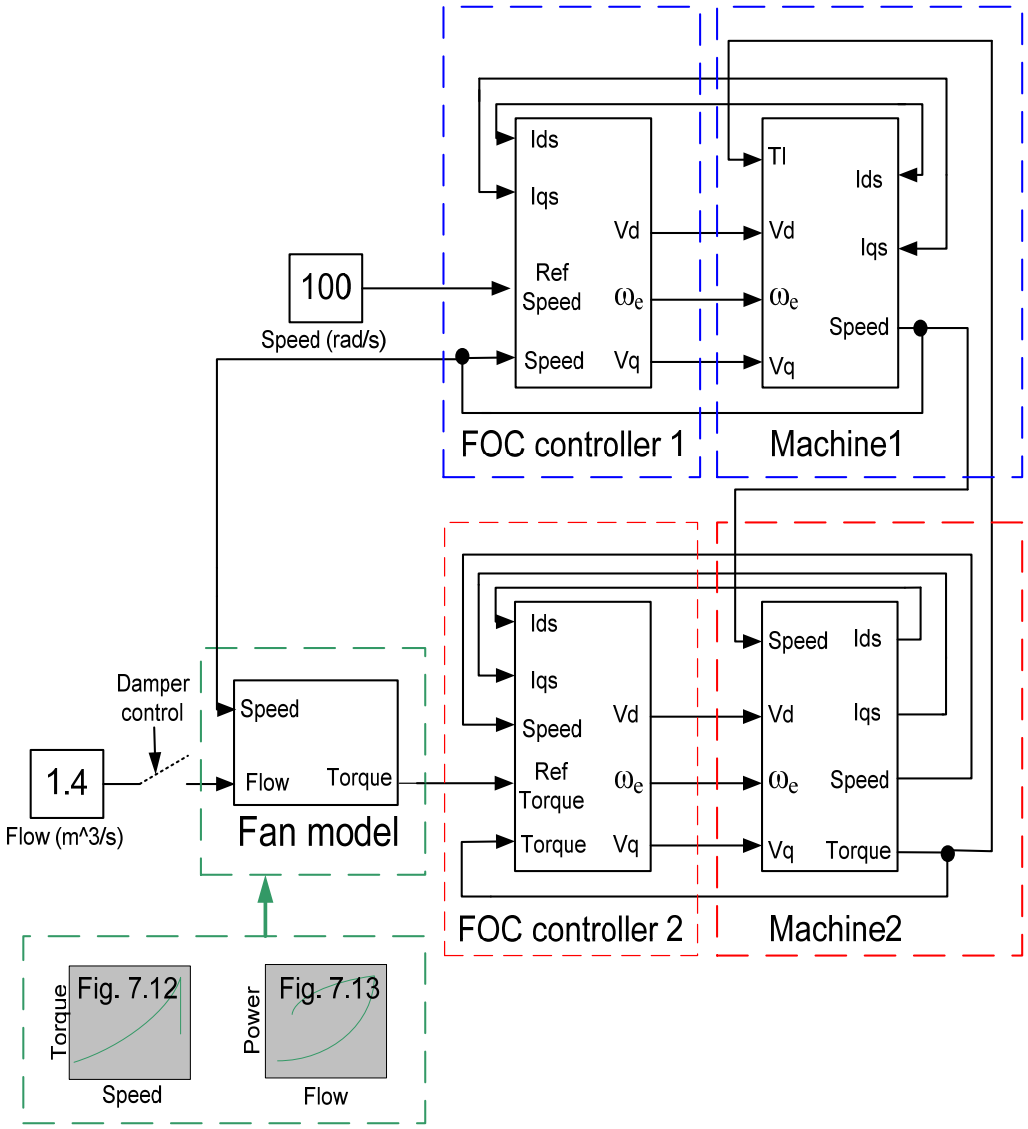

Fig. 7.14 Simulink™ block diagram for the test bed simulation of the 1.1 kW fan

7.4.1 Simulink™ simulation results of the test bed replicating the 1.1 kW fan

The results obtained from the Simulink™ simulation of the test bed replicating the 1.1 kW fan system are shown in Fig. 7.15 and Fig. 7.16.

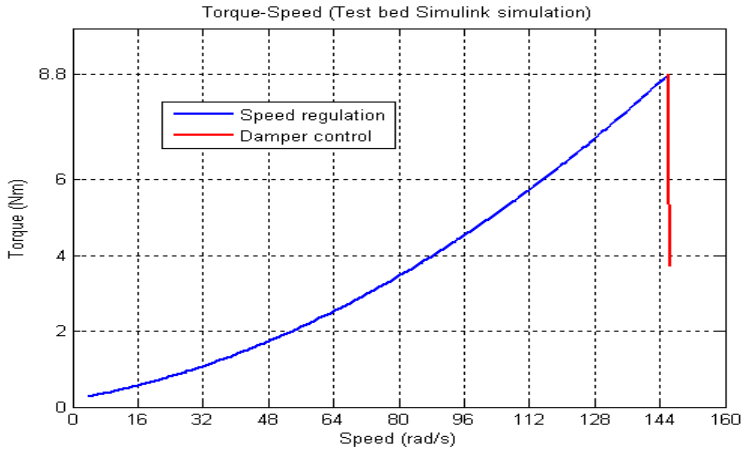

Fig. 7.15 Simulink™ simulated torque-speed curves of the test bed replicating the 1.1 kW fan under both damper operation and speed regulation

The test bed was ramped up to 146 rad/s as shown in Fig. 7.15 to simulate the variable speed torque-speed characteristic of the replicated fan, while under damper operation the reference torque was ramped to 8.8 Nm.

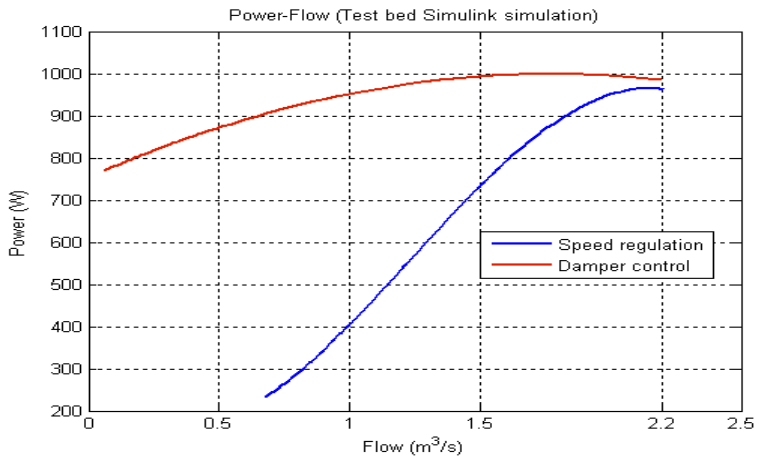

Fig. 7.16 Simulink™ simulated power-flow curves of the test bed replicating the 1.1 kW fan under both damper operation and speed regulation

To simulate the variable speed power-flow characteristic of the replicated fan, the reference speed was varied up to 157 rad/s. Under damper operation the speed of the simulated test bed remained fixed at 157 rad/s while the air-flow rate was ramped to 2.2 m^3/s as shown in Fig. 7.16.

To verify the accuracy of the Simulink™ simulations, the simulated data is compared to the measured data as shown in the next section.

7.4.2 Simulink™ simulation verification

The measured torque-speed (Fig. 7.12) and power-flow (Fig. 7.13) curves of the fan are compared to the Simulink™ simulated results shown in Section 7.4.1 to verify the accuracy of the simulations as shown in Fig. 7.17 and Fig. 7.18.

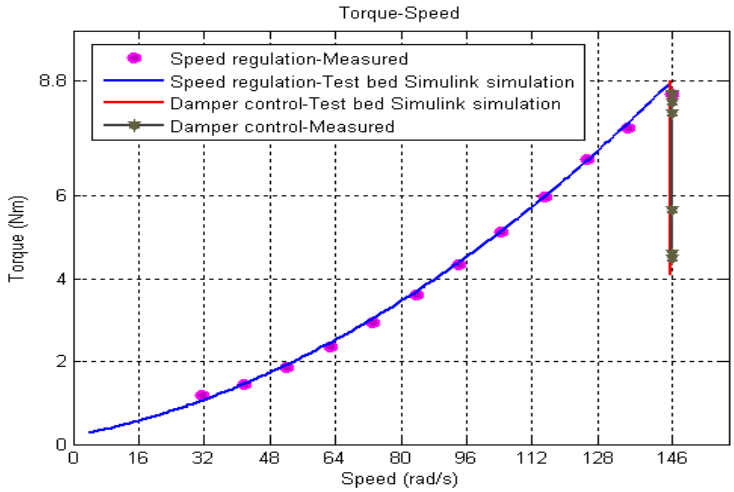

Fig. 7.17 Comparison of the actual measured and Simulink™ simulated test bed torque-speed responses

The actual and Simulink™ simulated torque-speed curves shown in Fig. 7.17 match justifying the replication of the 1.1 kW fan system as correct.

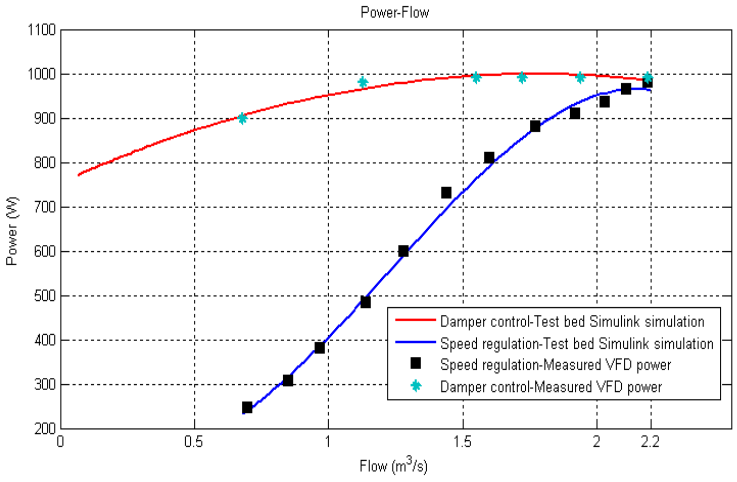

Fig. 7.18 Comparison of the actual measured and Simulink™ simulated test bed power-flow responses

Referring to Fig. 7.18, the actual measured and Simulink™ simulated power-flow curves match proving the simulation of the test bed.

The next section shows the practical results gained from the test bed that had been captured on an oscilloscope and imported to Matlab.

7.5 Test bed practical results-replication of the 1.1 kW fan system

With reference to Fig. 7.19, the measured torque-speed and power-flow curves shown in Fig. 7.12 and Fig. 7.13 respectively were programmed in the PLC enabling the actual test bed to simulate the 1.1 kW fan system. The calculated speed and torque setpoints were sent to VFD1 and VFD2 of the test bed via PROFIBUS. The speed transducer mounted on Machine2 of the test bed provided speed feedback from the system while torque feedback was calculated by VFD2 and sent to the PLC via a 4-20 mA signal.

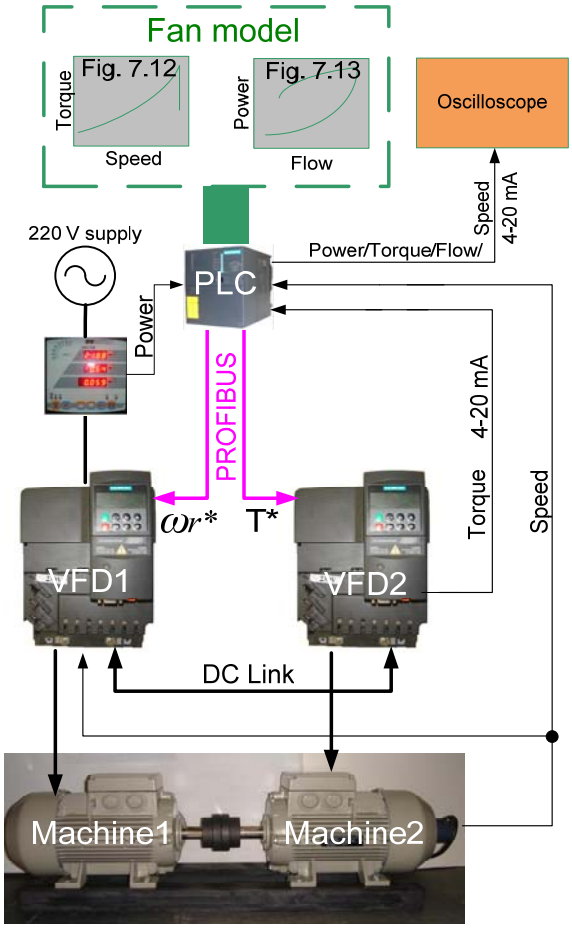

Fig. 7.19 Test bed hardware and software integration

Variable speed operation of the fan was replicated by ramping the test bed up to 1400 rpm for the torque-speed characteristic replication and up to 1500 rpm for the power-flow characteristic replication. To replicate damper torque-speed operation of the fan, the reference torque was ramped from 4 Nm to 8.8 Nm. To replicate fixed speed damper power-flow operation of the fan, the air-flow rate was ramped from 0.7 m^3/s to 2.2 m^3/s. The practical results gained from the test bed were captured on an oscilloscope and imported to Matlab as shown in Fig. 7.20 and Fig. 7.21.

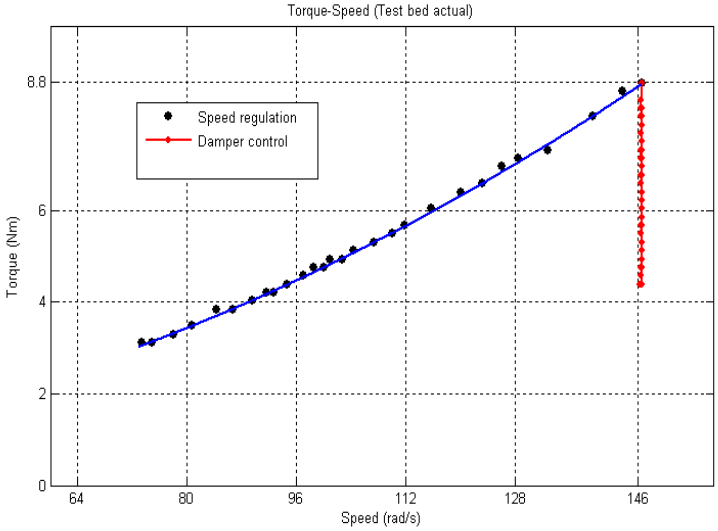

Fig. 7.20 Torque-speed of the replicated fan under both damper operation and speed regulation

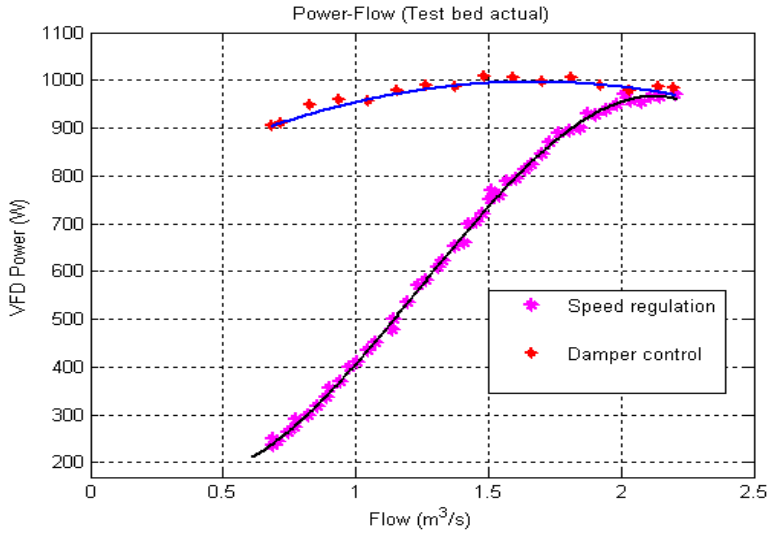

Fig. 7.21 VFD power-flow of the replicated fan under both damper operation and speed regulation

The actual simulated torque-speed and power-flow curves of the fan are shown in Fig. 7.20 and Fig. 7.21 respectively. To verify the accuracy of the actual test bed, the results shown in Fig. 7.20 and Fig. 7.21 are compared to the previously shown actual measured and Simulink™ simulated test bed results. This verification of data is shown in Fig. 7.22 and Fig. 7.23.

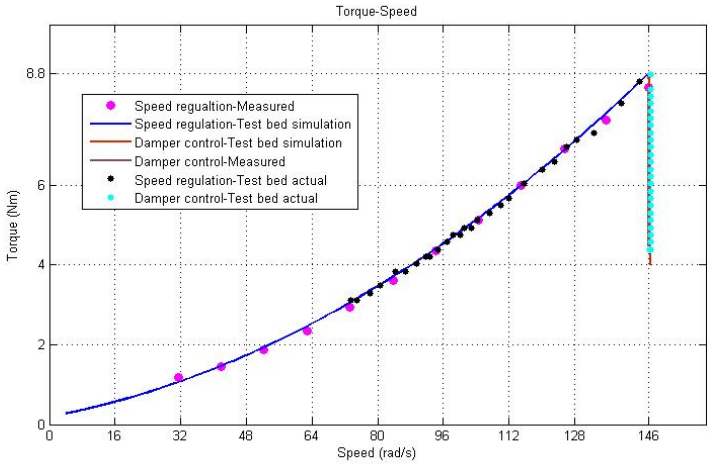

Fig. 7.22 Comparisons of the actual measured, Simulink™ simulated test bed and actual test bed torque-speed responses

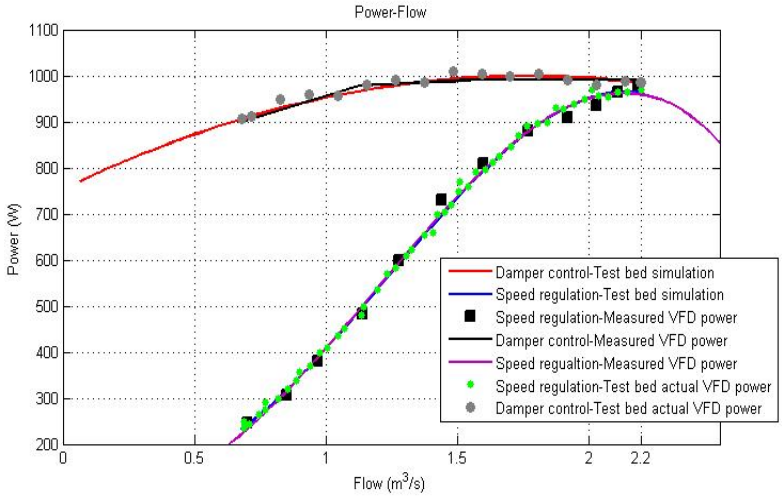

Fig. 7.23 Comparisons of the actual measured, Simulink™ simulated test bed and actual test bed power-flow responses

The torque-speed results shown in Fig. 7.22 correspond to each other and the power-flow results shown in Fig. 7.23 correspond to each other displaying the accuracy of the test bed.

7.6 Conclusion

A 1.1 kW fan system was constructed and tested. The results gained from testing the fan clearly show that variable speed operation instead of damper control utilises less power, hence less energy. The 1.1 kW fan was accurately simulated by the test bed as shown by the Simulink™ responses and the actual data gained from the test bed.

The next chapter discusses the hardware and operating characteristics of the 785 kW fan system. The ability of the test bed to mimic this fan system is first simulated in Simulink™, followed by the practical results gained from the test bed.

CHAPTER 8

SIMULATION OF A 785 kW FAN BY THE TEST BED

8.1 Introduction

Both a theoretical fan system and a 1.1 kW fan system were successfully replicated by the test bed in Chapters 6 and 7 and both showed that variable speed operation of a fan will utilise less power compared to damper operation. At this stage the data from Vlaklaagte was still not available. Anglo Coal South Africa's Greenside colliery commissioned a centrifugal fan driven air ventilation system in 2008 which may be either damper controlled or speed controlled. The new ventilation system replaced two other centrifugal fan units which were 164 kW and 190 kW respectively with three centrifugal fan units driven by induction machines having a power rating of 785 kW each. During Nov 2008 one fan unit operated at 85 % of its full potential comfortably meeting the colliery's needs. Only one centrifugal fan was tested by me at this site, hence the Greenside colliery fan system is referred to as a 785 kW fan system throughout this thesis.

This chapter describes the hardware and operating characteristics of the 785 kW centrifugal fan driven air ventilation system at Greenside. This 785 kW fan is then simulated by the test bed in Simulink™ followed by the practical results gained from the test bed.

8.2 785 kW fan system hardware

The 785 kW air ventilation system located at Anglo Coal Greenside is shown schematically in Fig. 8.1 and pictorially in Fig. 8.2. Fig. 1.1 is repeated here as Fig. 8.1.

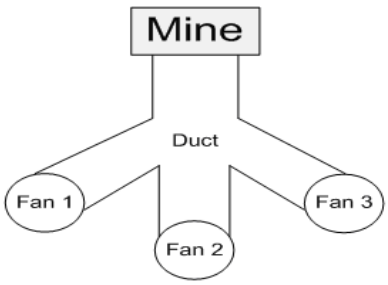

Fig. 8.1 Schematic of the air ventilation system at Greenside

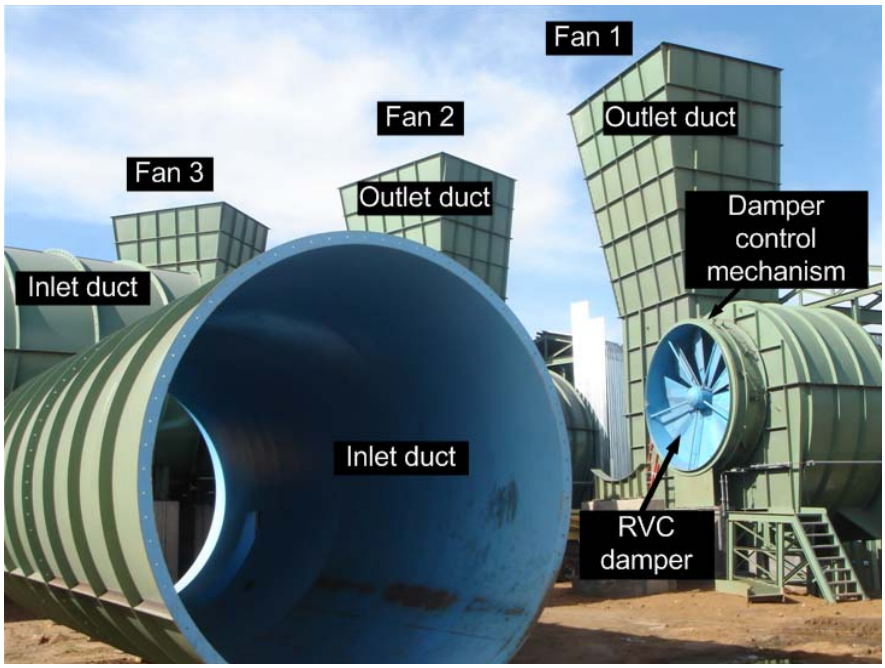

Fig. 8.2 Air ventilation system at Greenside

Fig. 8.3 (a) and Fig. 8.3 (b) depicts the control mechanisms of the inlet RVC damper (Fig. 8.2).

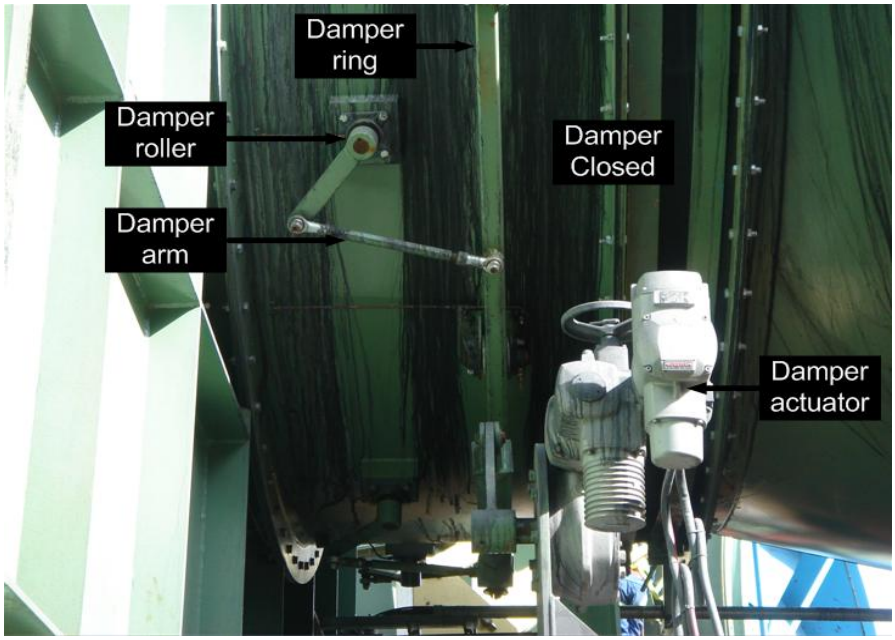

Fig. 8.3 (a) RVC damper closed

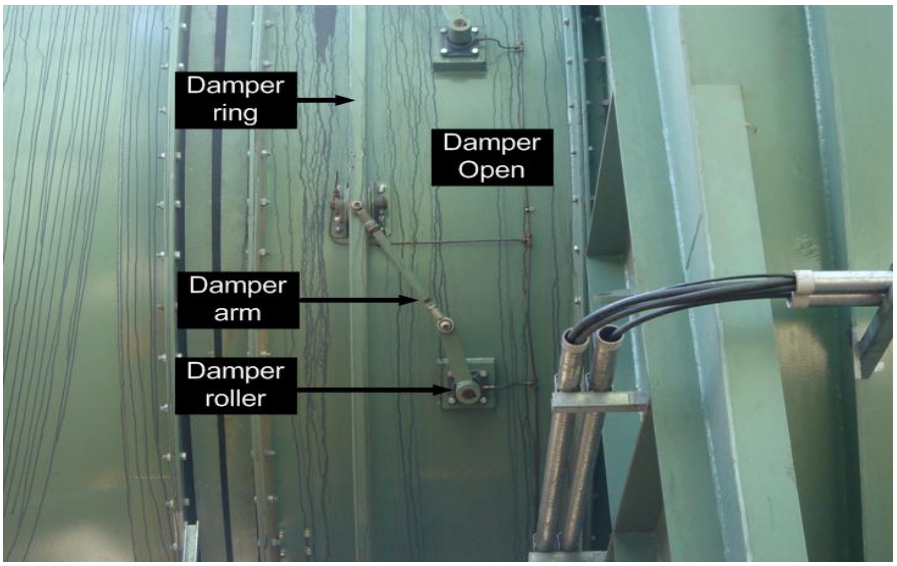

Fig. 8.3 (b) RVC damper open

Fig. 8.3 (a) shows the control arm attached to the damper ring in an almost 90˚ shape resulting in the inlet RVC damper being closed, whereas in Fig. 8.3 (b) the control arm is straight indicating that the inlet RVC damper is open.

Fig. 8.4 shows the mechanical equipment involved in driving a single centrifugal fan.

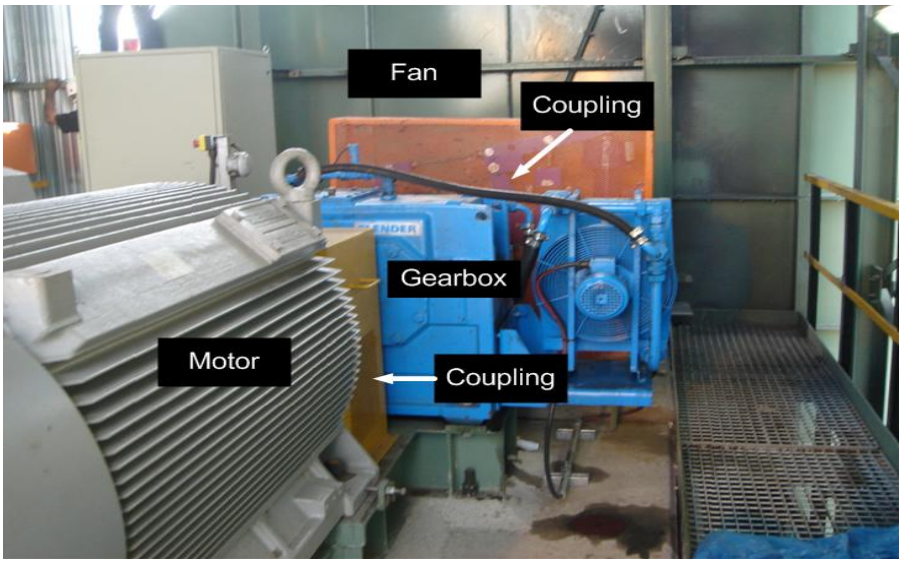

Fig. 8.4 (a) Hardware driving the fan-left view

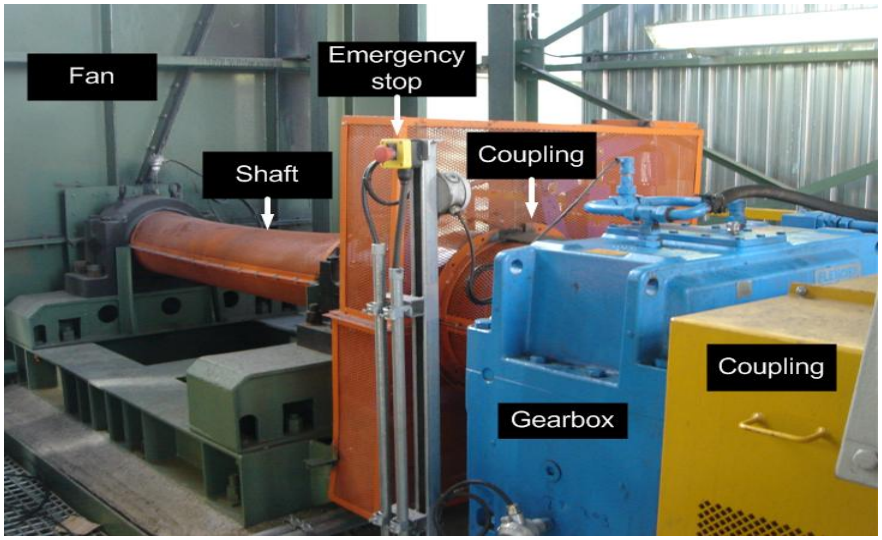

Fig. 8.4 (b) Hardware driving the fan-right view

Referring to Fig. 8.4, a 785 kW, 690 V delta connected Sinamics machine is coupled to a Flender gearbox. The gearbox ratio is 4:1. The gearbox is coupled to a shaft which fits onto the impeller of the fan.

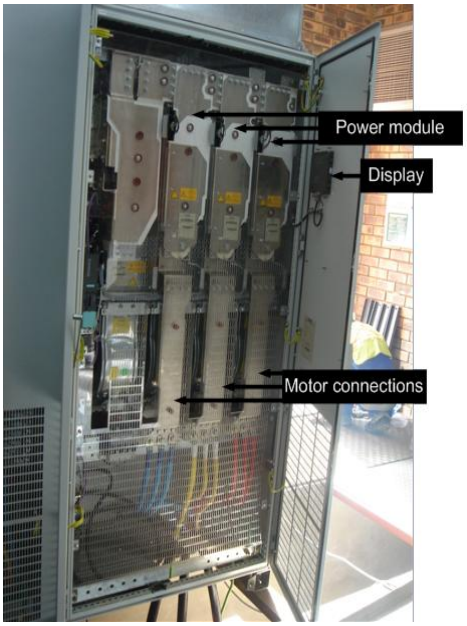

Fig. 8.5 800 kW Sinamics VFD

An 800 kW Sinamics VFD shown in Fig. 8.5 operates the fan under Sensorless Field Oriented Speed Control. The drive operates at a voltage of approximately 690 V. The display panel shown in Fig. 8.5 displays the actual power consumed by the machine, speed of the machine, current and frequency output of the drive.

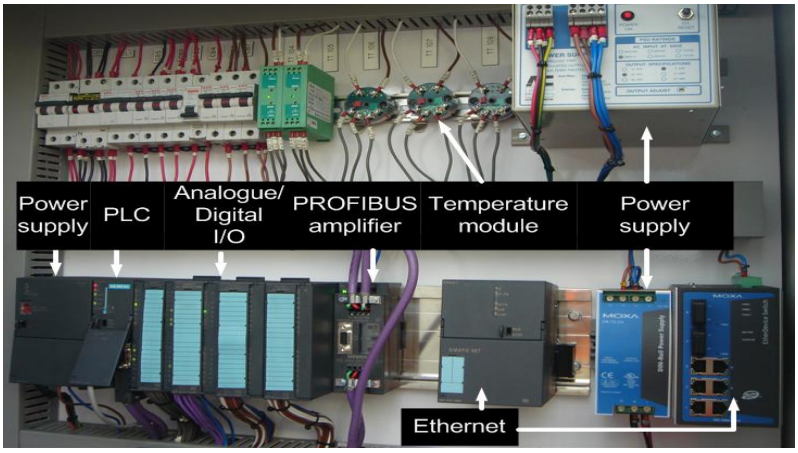

Fig. 8.6 Control equipment

Fig. 8.6 displays the control equipment of the 785 kW fan system. The PLC communicates with the VFD via PROFIBUS. The temperature modules are used to measure the temperature of the machine and gearbox. The Ethernet modules link the fan system to a Supervisory Control And Data Acquisition (SCADA) program; this was not commissioned during the time of the site visit (May 2008).

8.3 Operating characteristics of the 785 kW fan system

This section presents the results obtained from testing Fan 2 shown in Fig. 8.2. The 785 kW fan system is new as previously stated and during the time of testing only the power and speed of the machine and the air-flow rate of the system were available. Pressure transducers which were setup to measure only the static pressure at a point in the inlet duct of the fan system were not commissioned during the time of testing.

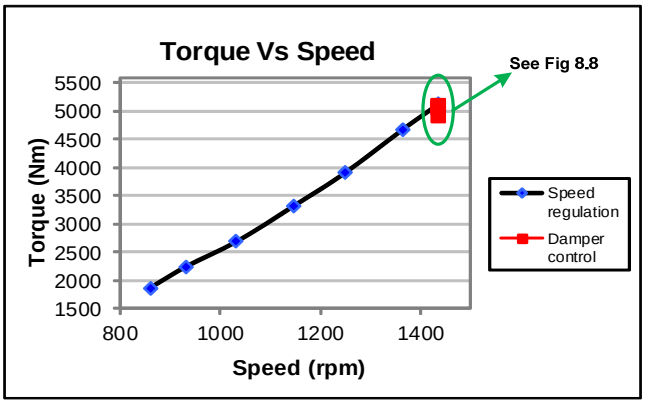

Fig. 8.7 Measured torque-speed of the fan under variable speed and damper control

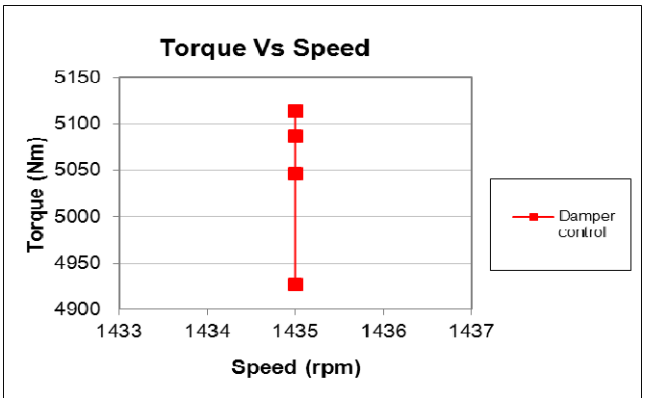

Fig. 8.8 Exploded view of Fig. 8.7 showing damper control data only

Fig. 8.7 depicts the torque speed response of the 785 kW machine under speed regulation and damper control. The speed of the machine was only varied between 800 rpm and 1435 rpm due to safety limitations that were implemented. Below 800 rpm there were doors that were mounted in the inlet duct which automatically shut preventing the fan from creating air flow through the mine and preventing the fan from becoming unstable due to any of the other two fans (Fig. 8.2) that would be on. Under damper operation only a few measurements of speed, power and air-flow rate were obtained due to the dislocation of the damper ring from its guides; see Fig. 8.9. This caused the doors in the inlet duct to shut and the fan was stopped. This was a mechanical problem which prevented further testing of the fan system.

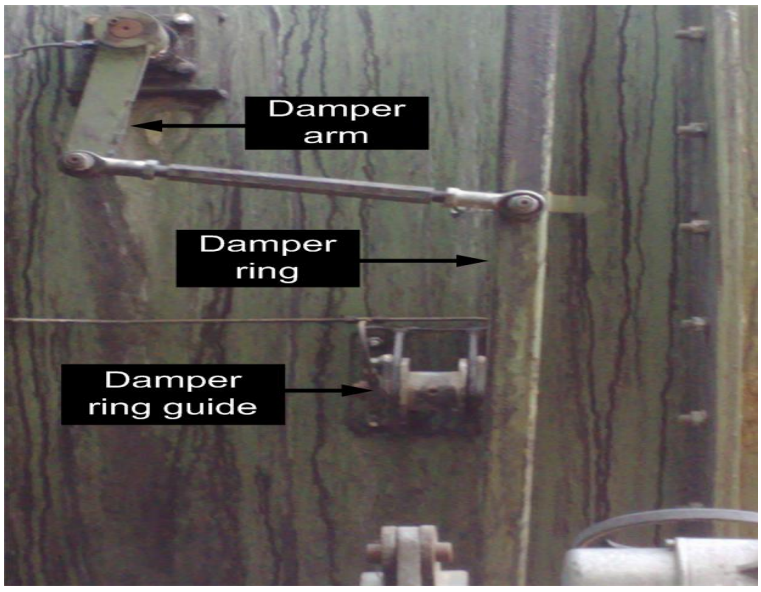

Fig. 8.9 RVC damper ring detached from its guide

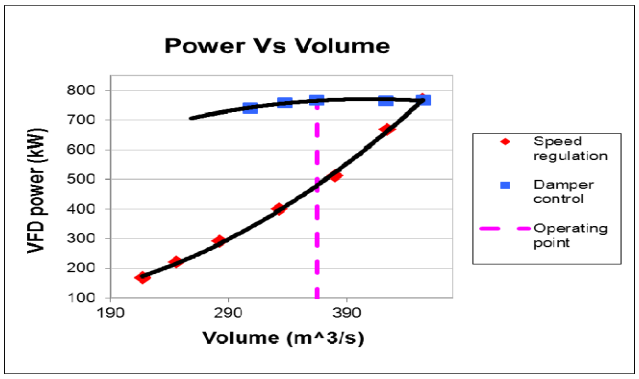

Fig. 8.10 Measured VFD power-flow of the fan using both damper control and speed regulation to vary the air-flow rate

Fig. 8.10 depicts the power drawn by the machine and the air-flow rate produced by the fan whilst operating under damper control and variable speed. The fan operates (Nov 2008) at 85 % of its full potential resulting in an air flow rate of 365 m^3/s and power of 484 kW under variable speed as shown by the operating point line in Fig. 8.10. Under damper control the machine would utilise 768 kW of power at the same air flow rate of 365 m^3/s. This results in a power saving of 284 kW.

8.4 Simulink™ simulation of the test bed replicating the 785 kW fan

This section presents the Simulink™ simulation of the test bed replicating the 785 kW fan system. The test bed has an operating range of up to 3 kW, therefore for the test bed to simulate the 785 kW fan system, certain variables from the measured fan system data needs to be scaled down. The 785 kW fan system has a speed range of 0 rpm to 1500 rpm which matches the speed range of the test bed therefore this variable is not scaled. The785 kW fan systems flow rate is not scaled because this variable is not measured by the test bed. The torque and power of the 785 kW fan system has to be scaled down to match the operating range of the test bed. By simply scaling down the measured torque and power of the 785 kW fan system by 300 as shown in Fig. 8.11 and Fig. 8.13, the test bed should now be able to replicate the 785 kW fan system. The efficiency of a large fan system is much higher than the efficiency of a small fan system. It is assumed that the test bed is 78 % efficient and the 785 kW fan system is 85 % efficient therefore the test bed will use more electrical power to simulate the 785 kW fan system. The test bed power therefore has to be reduced by 7 %.

The same test bed Simulink™ simulation model that was used in Chapter 6 (Fig. 6.3) and Chapter 7 (Fig. 7.14) to simulate the theoretical and the 1.1 kW fan systems is used to simulate

the scaled down 785 kW fan system. The test bed Simulink™ simulation model is repeated here as Fig. 8.14. The contents of the block labelled 'Fan model' in Fig. 8.14 are different and are presented in Appendix E.3.

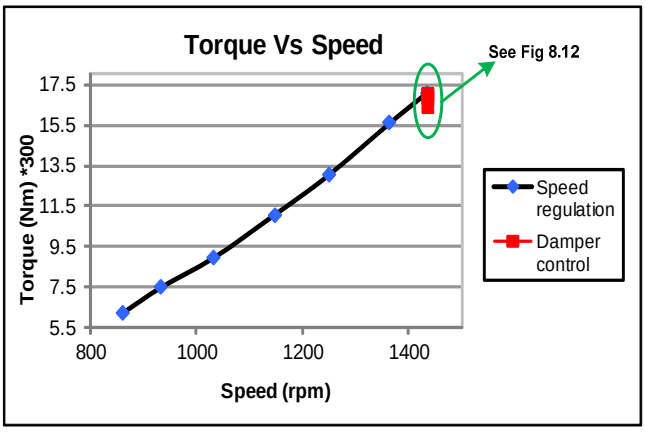

Fig. 8.11 Fig. 8.7 is repeated here showing the torque of the 785 kW fan scaled down by 300

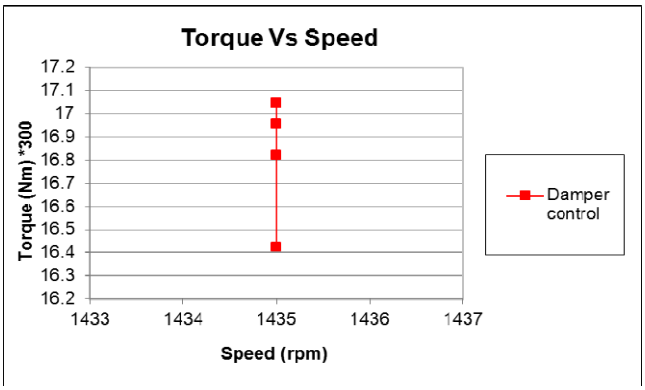

Fig. 8.12 Exploded view of Fig. 8.11 showing damper control data only

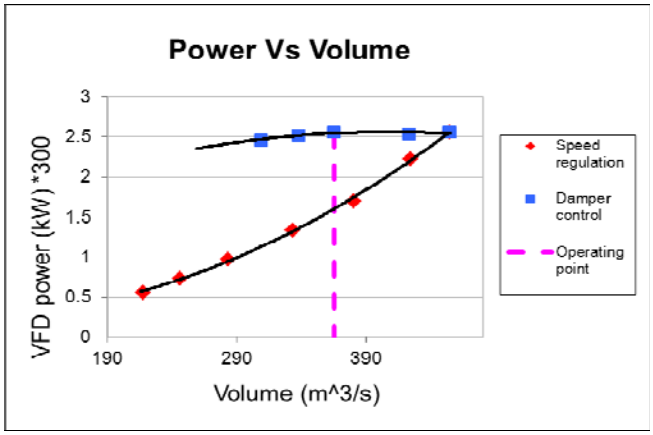

Fig. 8.13 Fig. 8.10 is repeated here showing the VFD power of the 785 kW fan scaled down by 300

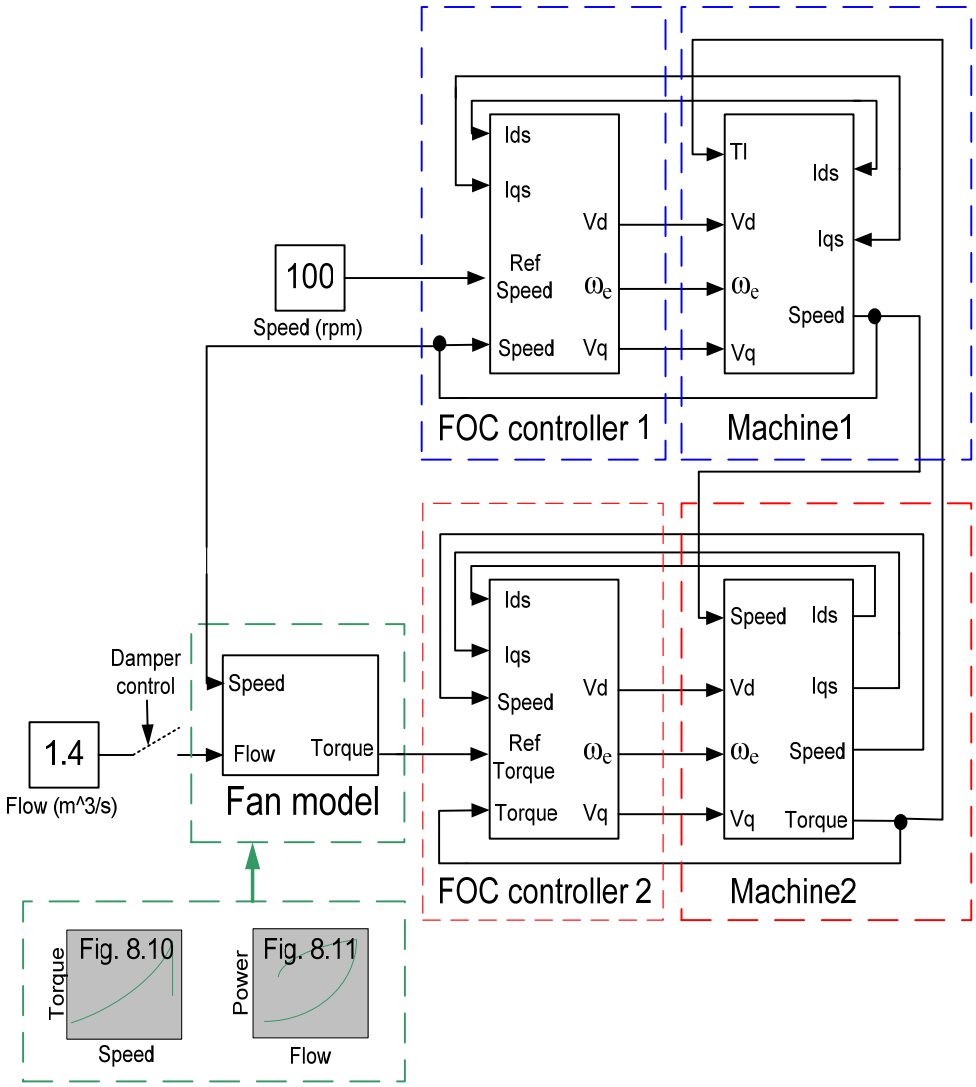

Fig. 8.14 Simulink™ block diagram for the test bed simulation of the scaled down 785 kW fan

8.4.1 Simulink™ simulation results of the test bed replicating the 785 kW fan

The results obtained from the Simulink™ test bed simulation of the scaled down 785 kW fan under damper control and speed regulation are shown in this section.

The torque-speed and power-flow responses of the simulated scaled down 785 kW fan are shown in Fig. 8.15 and Fig. 8.16 respectively. The speed of Machine1 in the test bed Simulink™ model was ramped up to 1435 rpm to replicate variable speed operation of the scaled down fan, while under damper control the speed of Machine1 remained fixed (1435 rpm) while the air-flow rate was varied from 256 m^3/s to 454 m^3/s as shown in Fig. 8.16.

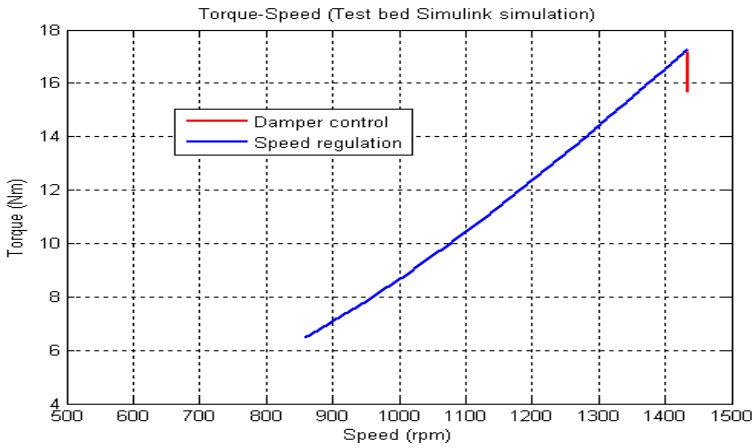

Fig. 8.15 Simulink™ simulated torque-speed curves of the test bed replicating the 785 kW fan under both damper operation and speed regulation

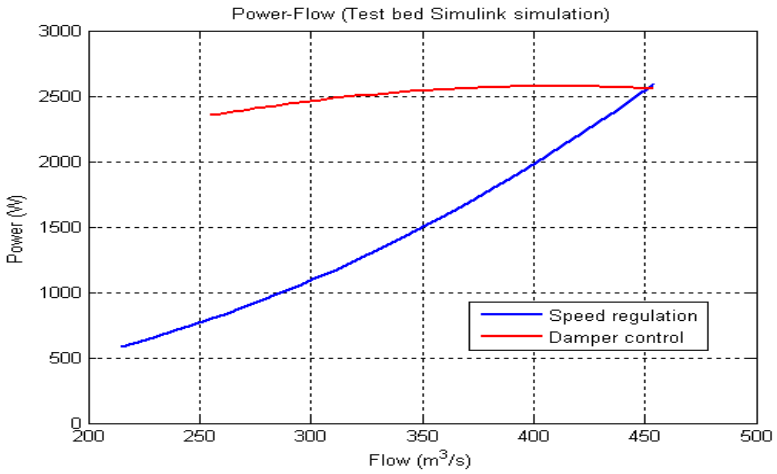

Fig. 8.16 Simulink™ simulated power-flow curves of the test bed replicating the 785 kW fan under both damper operation and speed regulation

To verify the accuracy of the Simulink simulations, the simulated data (Fig. 8.15 and Fig. 8.16) are compared to the measured data (Fig. 8.11 and Fig. 8.13) as shown in the next section.

8.4.2 Simulink™ simulation verification

The actual measured scaled down torque-speed (Fig. 8.11) and power-flow curves (Fig. 8.13) are compared to the Simulink™ simulated test bed replicated torque-speed and power-flow curves to verify the accuracy of the simulations as shown in Fig. 8.17 and Fig. 8.18.

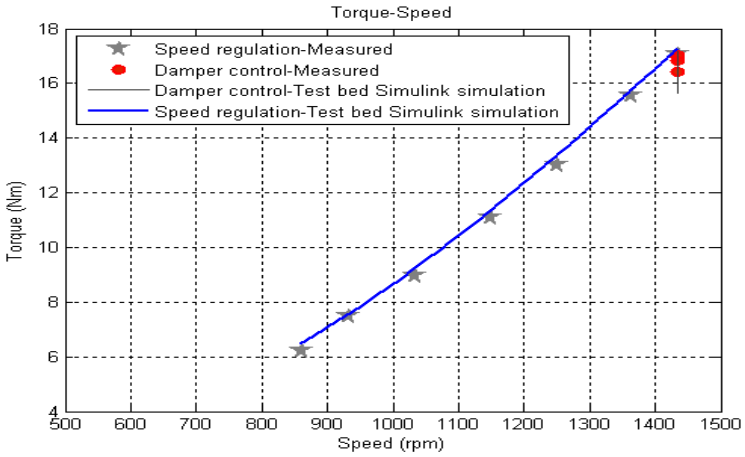

Fig. 8.17 Comparison of the actual measured and Simulink™ simulated test bed torque-speed responses

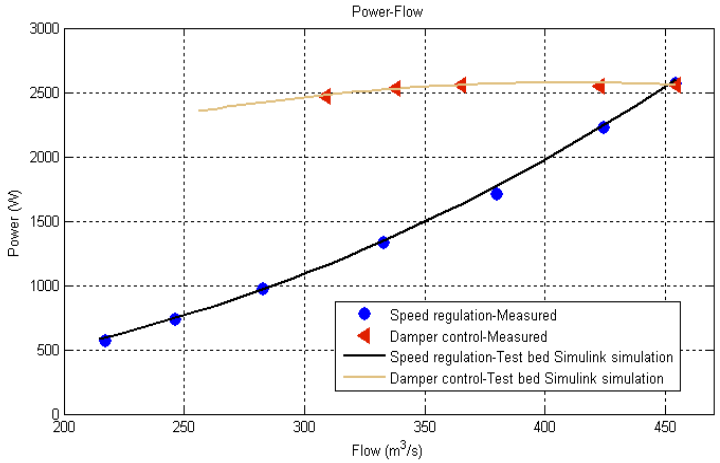

Fig. 8.18 Comparison of the actual measured and Simulink™ simulated test bed power-flow responses

The actual measured and Simulink™ simulated scaled down data correspond closely, justifying the Simulink™ simulations as correct. The actual test bed was then programmed and the results gained from the test bed are shown in the next section.

8.5 Test bed practical results-replication of the 785 kW fan system

The test bed accurately simulated the scaled down 785 kW fan in Simulink™ as shown in the previous section. The measured torque-speed and power–flow curves of the scaled down 785 kW fan were then programmed in the PLC and the relevant speed and torque setpoints were

sent to VFD1 and VFD2 via PROFIBUS respectively as shown in Fig. 8.19. Speed feedback was received from the the speed transducer mounted on Machine2 of the test bed and torque feedback was calculated by VFD2 and sent to the PLC via a 4-20 mA signal.

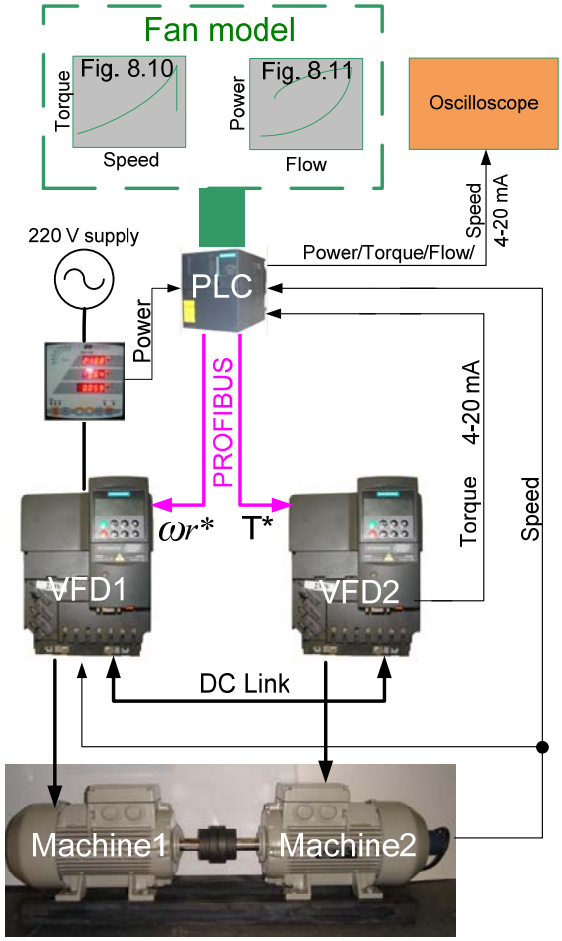

Fig. 8.19 Test bed hardware and software integration

The practical results gained from the test bed while it replicated variable speed and damper operation of the scaled down 785 kW fan were captured on an oscilloscope and imported to Matlab as shown in Fig. 8.20 and Fig. 8.21. The actual test bed replication data from Fig. 8.20 and Fig. 8.21 are then compared to the actual scaled down measured fan data (Fig. 8.11 and Fig. 8.13) and Simulink™ simulation data (Fig. 8.15 and Fig. 8.16) to verify the accuracy of the test bed as shown in Fig. 8.22 and Fig. 8.23.

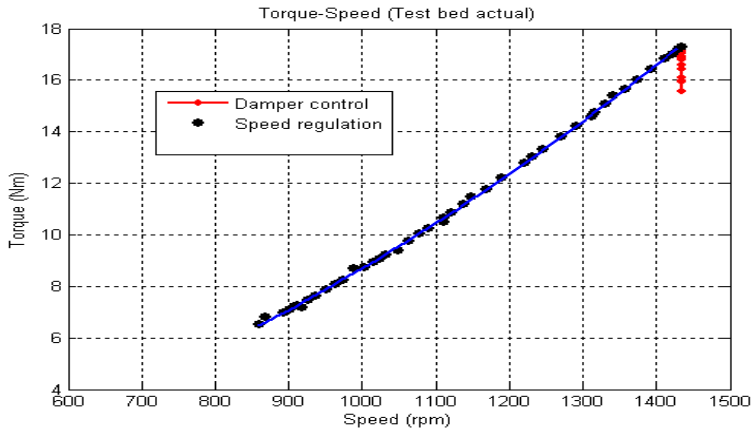

Fig. 8.20 Torque-speed of the replicated scaled down fan under both damper operation and speed regulation

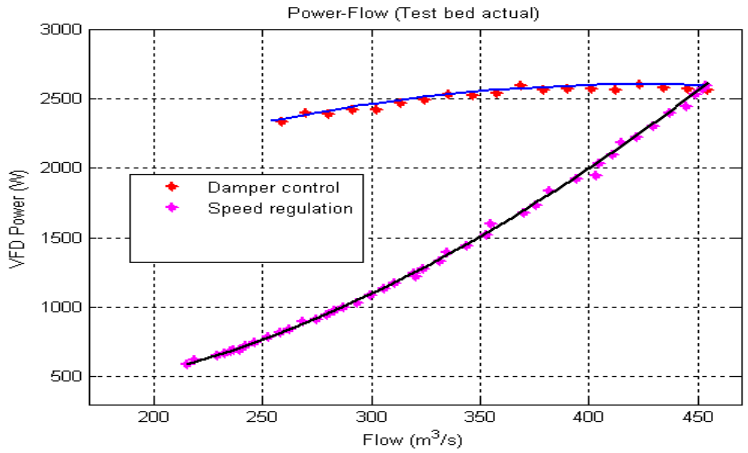

Fig. 8.21 VFD power-flow of the replicated scaled down fan under both damper operation and speed regulation

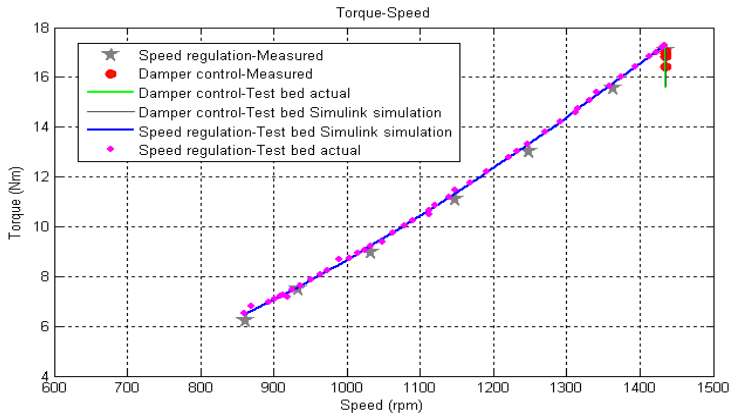

Fig. 8.22 Comparisons of the actual measured, Simulink™ simulated test bed and actual test bed torque-speed responses

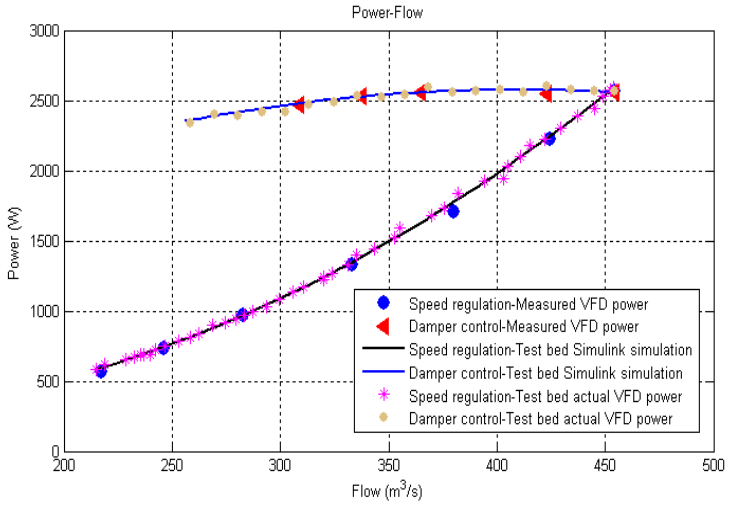

Fig. 8.23 Comparisons of the actual measured, Simulink™ simulated test bed and actual test bed power-flow responses

The torque-speed results shown in Fig. 8.22 correspond to each other and the power-flow results shown in Fig. 8.23 correspond to each other justifying the replication of the scaled down 785 kW fan system as correct.

8.6 Conclusion

This chapter described the hardware and operating characteristics of the 785 kW fan system located at Anglo Coal Greenside. This fan system was then successfully replicated by the test bed.

The next chapter presents an energy cost indicator which is then simulated in Simulink™ and in the PLC. Air flow control through speed control of the 1.1 kW fan is also presented.

CHAPTER 9

ENERGY COST INDICATOR AND AIR FLOW CONTROL

9.1 Introduction

The test bed was commissioned in Chapter 5. A theoretical fan, 1.1 kW fan and 785 kW fan were then replicated by the test bed as shown in Chapters 6, 7 and 8. All three fan systems showed from their power-flow curves that variable speed operation of the fans will consume less power compared to damper operation of the fans. To then calculate the cost of energy consumed by the replicated fans a tariff structure was simulated in Simulink™ and in the PLC. In addition to proving the energy savings achievable through speed control of fans, NPC had also requested the UKZN to determine whether variable speed operation might afford more consistent air flow rates throughout a mine air ventilation system based on an air flow feedback control system. The VFD at Vlaklaagte was not installed therefore this air flow feedback control system could not be implemented. However to demonstrate the principal of trying to achieve more consistent air flow rates through speed control of a fan, air flow control through speed control of the 1.1 kW fan was implemented.

In this chapter energy cost simulations are presented followed by the results gained from implementing air flow control of the 1.1 kW fan system.

9.2 Energy simulations in Simulink™

Once the test bed was fully operational an energy cost indicator was simulated in Simulink™ following Eskom's Megaflex weekday tariff structure; Anglo Coal South Africa follows the same tariff structure. There are three time periods which exist in the tariff structure; off peak, standard and peak periods as shown in Fig. 9.1. Fig. 9.1 and Table 9.1 show the equivalent cost of energy of each specific time period.

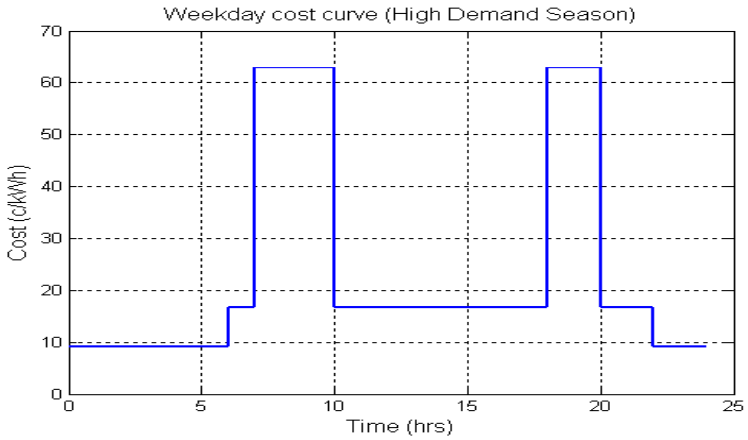

Fig. 9.1 Timing diagram for Eskom's Time Of Use Megaflex structure

Hour in the day	Time period	Cost
00-06	Off peak	9.06 c/kWh
06-07	Standard	16.67 c/kWh
07-10	Peak	63.04 c/kWh
10-18	Standard	16.67 c/kWh
18-20	Peak	63.04 c/kWh
20-22	Standard	Ia4K:y(
22-24	Off peak	9.06 c/kWh

Table 9.1: Megaflex weekday tariff rates for a specific time period [20]

The energy cost indicator runs for 24 hrs which in simulation time is equivalent to 2 min; hence 1 hr is equivalent to 5s. This is accomplished by accelerating the energy usage of the system as shown by Eq. 9.1.

$$energy = \int Power \frac{d}{dt} \times Gain \tag{9.1}$$

Referring to Table 9.1 based on the time of day, the energy is individually accumulated for each time period. There are seven time periods according to Table 9.1.

For the first *off peak* time period, from 00:00 am to 06:00 am which in simulation time is 0s to 30s, the energy is accumulated according to Eq. 9.2 for 30s.

$$kWh1 = energy \tag{9.2}$$

For the second *standard* time period from 06:00 am to 07:00 am which in simulation is 30s to 35s, the energy is accumulated according to Eqs. 9.3 and 9.4 for 5s.

$$energy2 = energy \tag{9.3}$$

$$kWh2 = \frac{1}{2}(energy2 - kWh1) \tag{9.4}$$

For the remaining four time periods the energy is accumulated according to Eqs. 9.3 and 9.4 where only the variables *energy2, kWh2 and kWh1* change. Please refer to appendix E for the remaining time period energy algorithms.

The cost of energy for each individual time period is then calculated according to Eq. 9.5.

$$Cost = kWh * Unit\ price\ of\ energy\ of\ a\ specific\ time\ period \tag{9.5}$$

The total cost is then calculated by adding the individual costs calculated in each time period as shown in Eq. 9.6.

$$Total\ Cost = Cost1 + Cost2 + Cost3 + Cost4 + Cost5 + Cost6 + Cost7 \tag{9.6}$$

The cost of energy Simulink™ model shown in Fig. 9.2 is similar to the test bed Simulink™ models used to replicate the theoretical fan (Fig. 6.3), 1.1 kW fan (Fig. 7.14) and 785 kW fan (Fig. 8.11). The algorithms (Eqs. 9.1 to Eq. 9.6) were implemented in the Simulink™ block labelled 'Cost calculation' shown in the block diagram in Fig. 9.2. Refer to Appendix E.4 for the contents of the 'Cost calculation' block. The results gained from simulating the 1.1 kW fan system and the 785 kW fan system using the Simulink™ model in Fig. 9.2 are shown next.

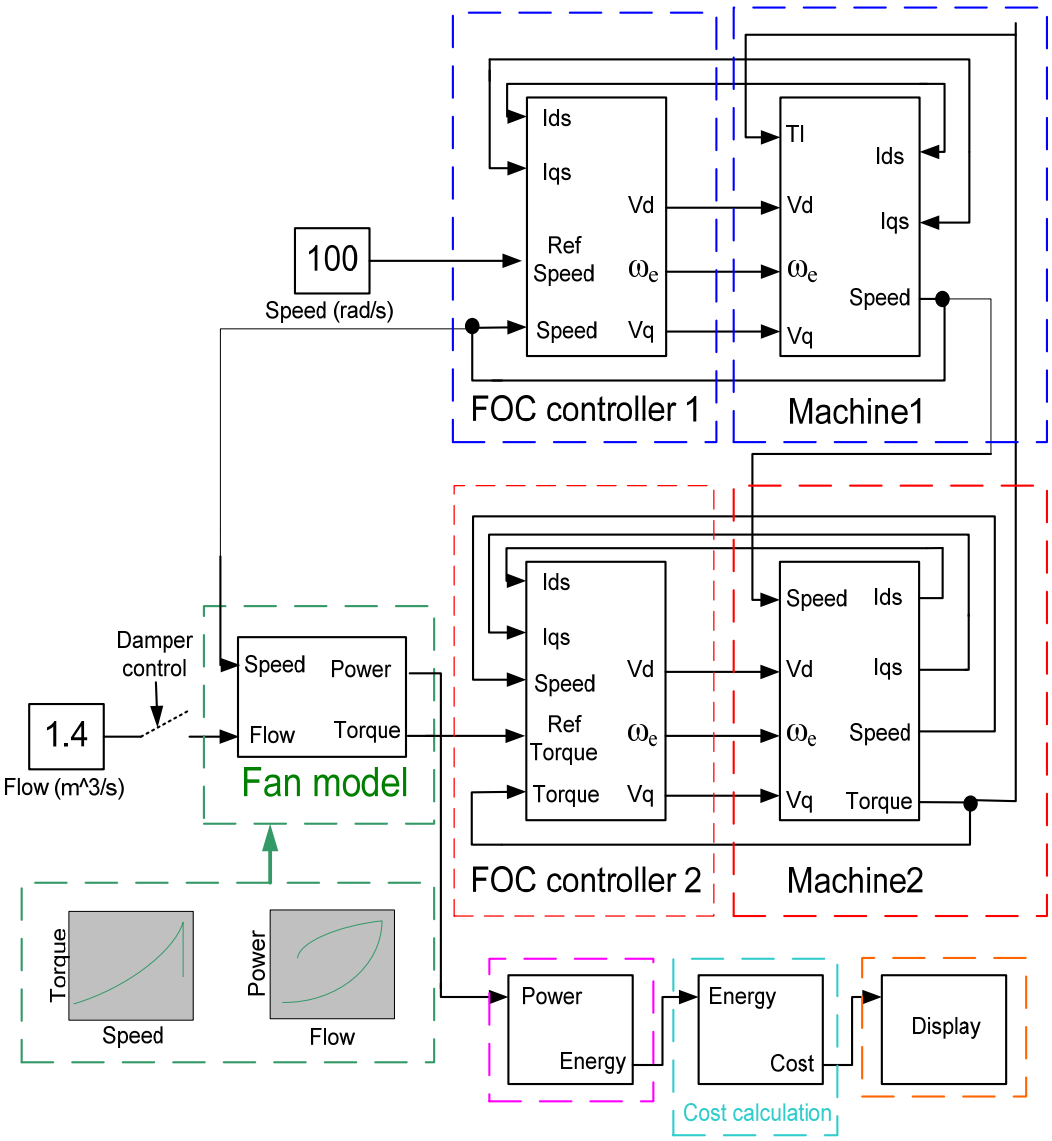

Fig. 9.2 Simulink™ model used to calculate the cost of energy per weekday

9.2.1 Energy simulations of the 1.1 kW fan system in Simulink™

The energy usage and cost of energy of the 1.1 kW fan system are simulated in this section in Simulink™. To enable energy usage and cost of energy comparisons based on a particular air flow rate to be made between damper operation and variable speed operation, consistency with regard to choosing the operating point of the fan from its power-flow curves is maintained. Considering the 1.1 kW fan system, an operating point that resulted in the fan system to be 45 % damped was chosen since most of Anglo Coal's mines were found to be 45 % damped by NPC. The operating point of the 1.1 kW fan whilst having its damper 45 % closed is shown in Fig. 9.3. Fig. 7.13 is repeated here as Fig. 9.3.

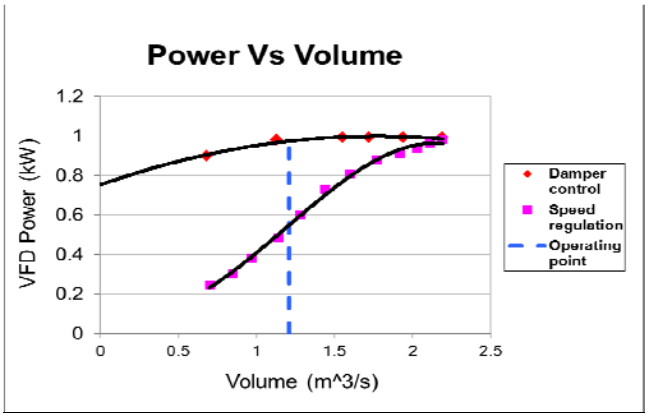

Fig. 9.3 VFD power-flow of the 1.1 kW fan

With reference to Fig. 9.3, the equivalent air-flow rate and power of the 1.1 kW fan under damper operation at the operating point is 1.21 m^3/s and 0.973 kW respectively. Under variable speed operation of the fan, the equivalent power at the same air-flow rate of 1.21 m^3/s is 0.543 kW.

Fig. 9.4 and Fig. 9.5 show the Simulink™ simulated cost of energy results for variable speed and damper operation of the fan. Only part of the full Simulink™ model (Fig. 9.2) is shown in Fig. 9.4 and Fig. 9.5 for clarity purposes. The outputs and inputs labelled 'Machine1' and 'Machine2' shown in Fig. 9.4 and Fig. 9.5 correspond accordingly to the same outputs and inputs shown in the full simulation model (Fig. 9.2).

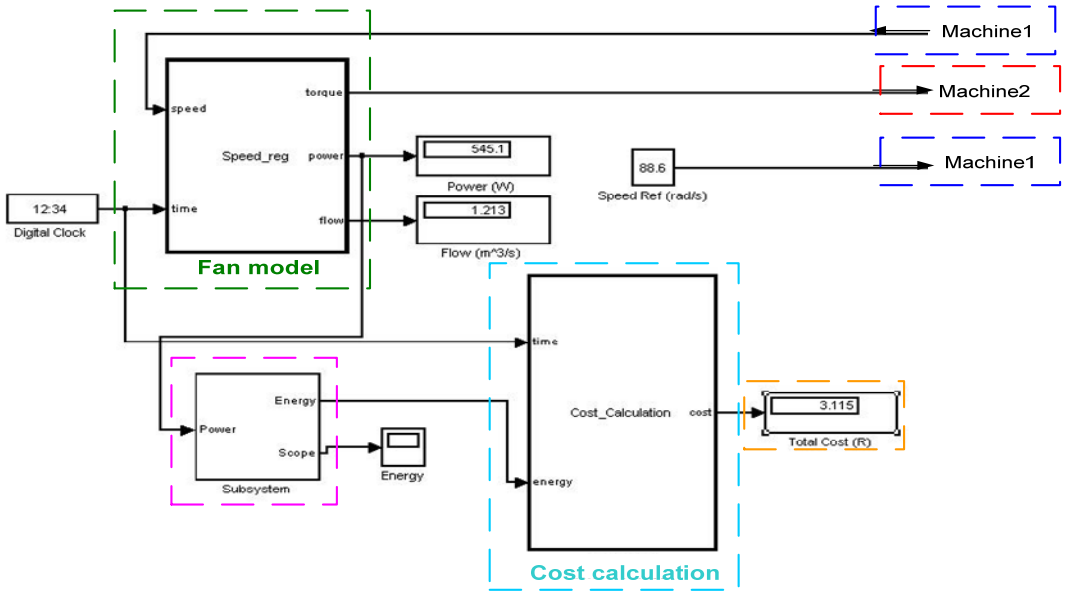

Fig. 9.4 Speed regulation Simulink™ model and results

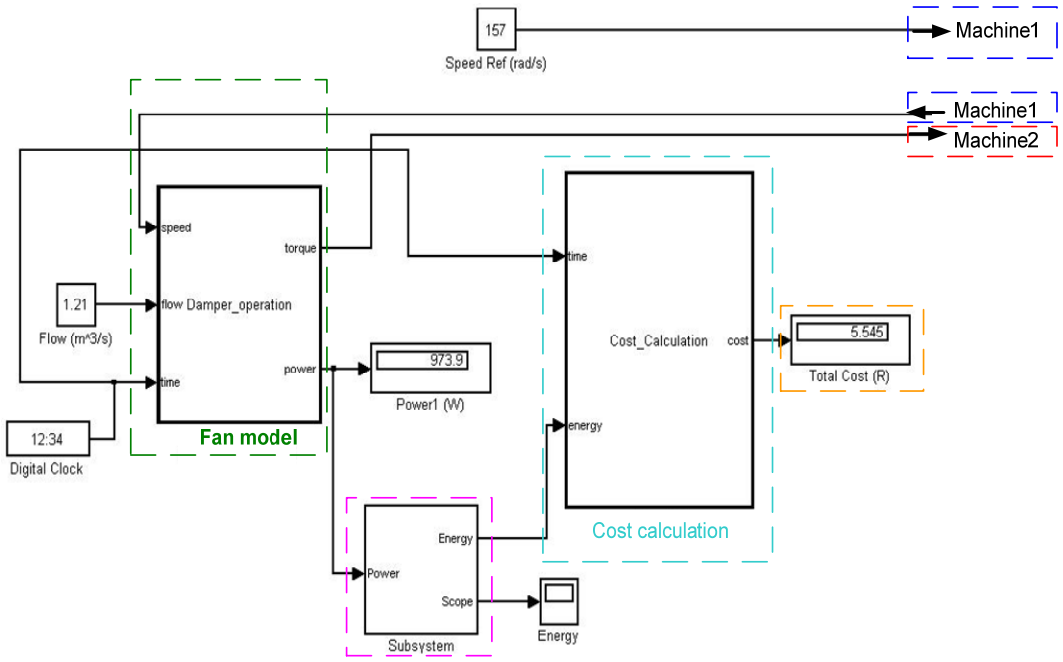

Fig. 9.5 Damper control Simulink™ model and results

Referring to Fig. 9.4, under variable speed operation of the 1.1 kW fan at a speed of 88.6 rad/s, the power drawn by the fan at an air flow rate of 1.213 m^3/s is 545.1 W. The simulated energy accumulated for the day is shown in Fig. 9.6. The cost of energy is shown in Fig. 9.4 amounting to R 3.12. Referring to Fig. 9.5, under fixed speed damper operation of the 1.1 kW fan at an air flow rate of 1.21 m^3/s the power drawn by the fan is 973.9 W. The simulated cost of energy per weekday at a power of 973.9 W is R 5.55. The monetary savings per day through variable speed operation of the fan at an air flow rate of 1.21 m^3/s is R 2.43.

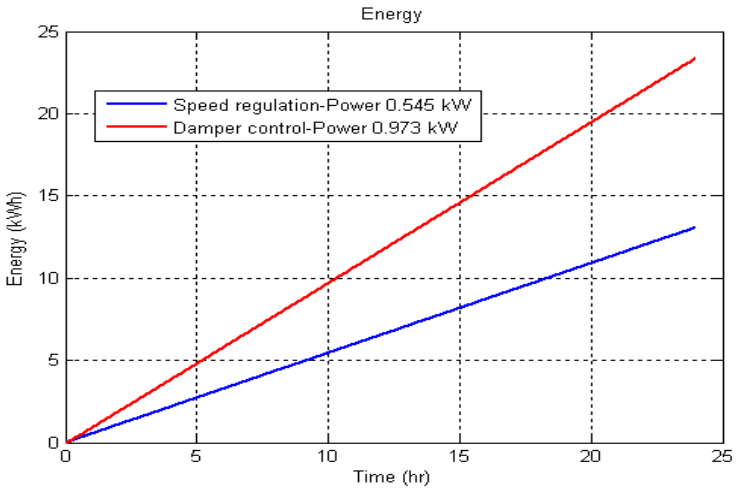

Fig. 9.6 Simulink™ simulated energy accumulated for the day

The Simulink™ simulated cost of energy per weekday while the fan was simulated under variable speed is clearly lower compared to when the fan was simulated under damper operation as shown in Fig. 9.6. The energy savings per day through variable speed operation of the fan at an air flow rate of 1.21 m^3/s amounts to 10.272 kWh.

9.2.2 Energy simulations of the 785 kW fan system in Simulink™

The energy usage of the scaled down 785 kW fan system is simulated in this section in Simulink™. To show comparisons based on a particular air-flow rate between damper operation and variable speed operation, the operating point of the scaled down 785 kW fan is maintained. The measured power-flow data of the scaled down 785 kW fan was shown in Fig. 8.11 and is repeated here in Fig. 9.7.

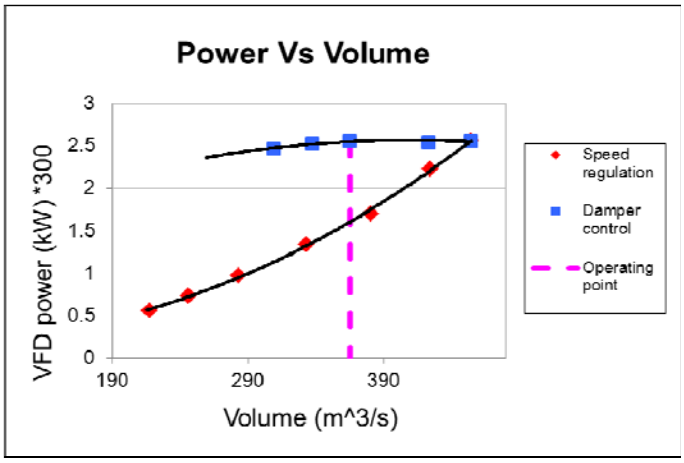

Fig. 9.7 VFD power-flow of the scaled down 785 kW fan

Referring to Fig. 9.7, the fan operated at 85 % rated speed of the machine in Nov 2008 resulting in an air flow rate of 365 m^3/s at a scaled down power of 1.613 kW. At the same air flow rate of 365 m^3/s under damper control the scaled down power drawn by the fan is 2.56 kW.

Fig. 9.8 and Fig. 9.9 show the Simulink™ results obtained from simulating the energy consumed by the scaled down fan per day under variable speed and damper control. The outputs and inputs labelled ‘Machine1’ and ‘Machine2’ shown in Fig. 9.8 and Fig. 9.9 correspond accordingly to the same outputs and inputs shown in the full simulation model (Fig. 9.2).

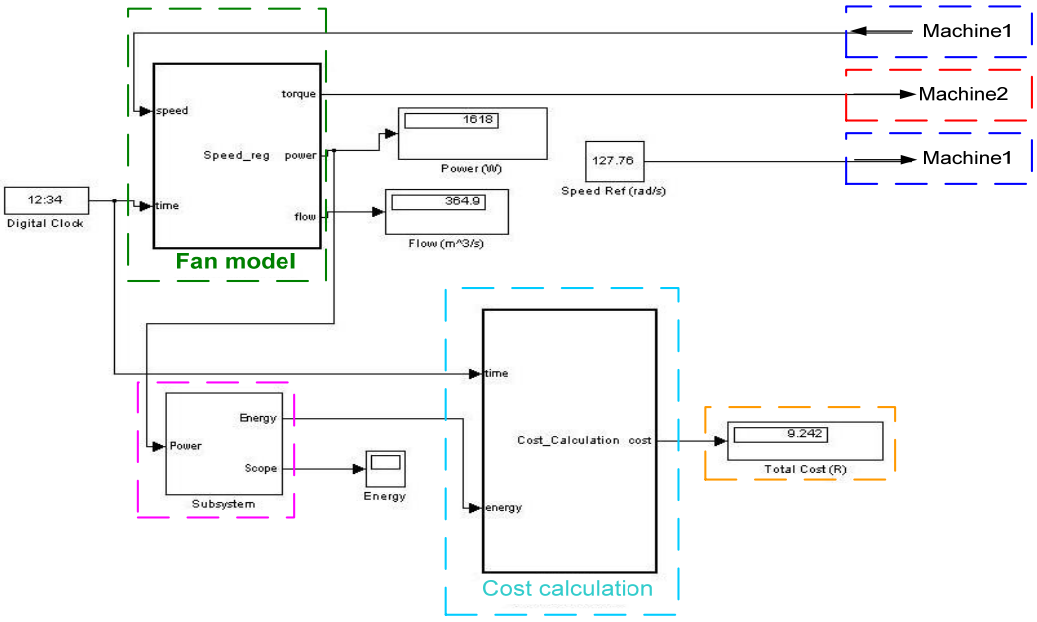

Fig. 9.8 Speed regulation Simulink™ model and results-power scaled down by 300

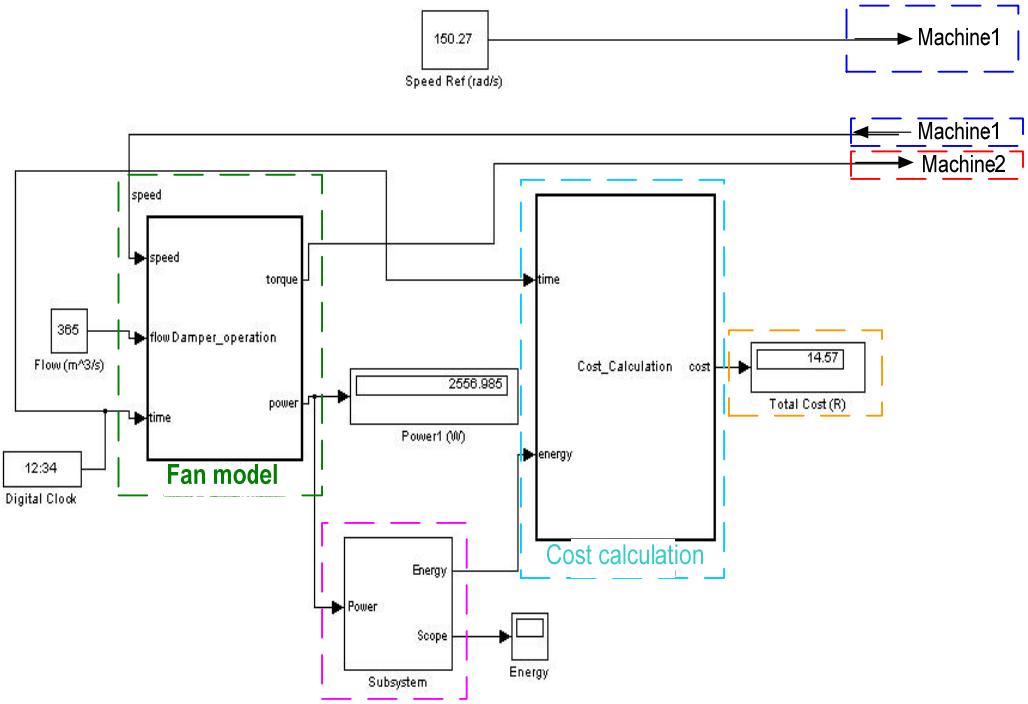

Fig. 9.9 Damper control Simulink™ model and results-power scaled down by 300

The simulated cost of energy for the scaled down fan operating under variable speed producing an air-flow rate of 364.9 m^3/s is shown in Fig. 9.8 costing R 9.24. Under fixed speed damper control the cost of energy for the scaled down fan at an air-flow rate of 365 m^3/s is R 14.57 as

shown in Fig. 9.9. Under variable speed operation the monetary savings per day for the scaled down fan is R 5.33.

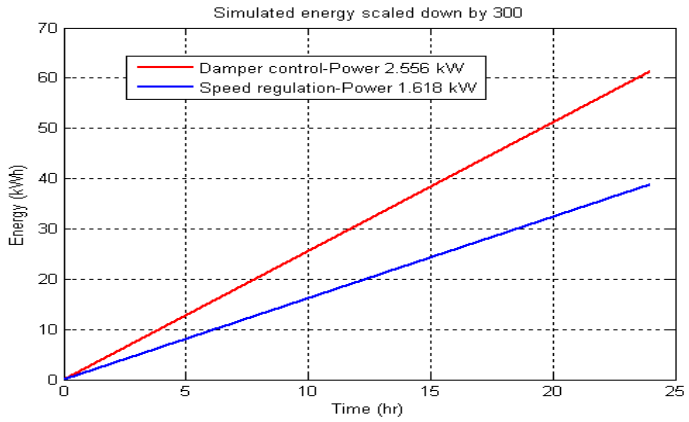

Fig. 9.10 Scaled down Simulink™ simulated energy accumulated for the day

The Simulink™ simulated energy accumulated for the day while the scaled down fan operated under damper control and variable speed is shown in Fig. 9.10. There is a significant increase in the simulated energy utilised by the fan operating under damper control compared to variable speed controlled.

The simulated unscaled cost of energy utilised by the fan per day amounts to R 2772 under variable speed operation and R 4371 under damper operation. The simulated unscaled energy consumed by the fan per day under damper control amounted to 18.4032 MWh at a power of 766.8 kW and under variable speed operation 11.6496 MWh at a power of 485.4 kW. This results in a power saving of 281.4 kW and energy savings of 6.7536 MWh per day and 2,465.064 MWh per year at the current duty cycle (85 % rated machine speed) of the fan.

After successfully simulating the energy costs of both fan systems in Simulink™, the PLC was programmed to simulate the energy costs of the test bed replicated fan systems.

9.3 Energy simulations in the PLC

In Section 9.2 the energy consumed per day by the fan systems were simulated in Simulink™. The PLC was also programmed to simulate the energy consumed by these test bed replicated fan systems per day. The PLC simulated cost of energy results of the replicated 1.1 kW fan system and the 785 kW fan system are shown via logged data.

9.3.1 Energy simulations of the 1.1 kW fan system in the PLC

This section shows the energy usage and cost of energy per weekday of the replicated 1.1 kW fan system simulated in the PLC. The cost of energy is calculated for a 45 % damped fan and its equivalent air-flow rate under variable speed so that the PLC simulated energy data can be compared to the Simulink^{TM} simulated energy data.

Fig. 9.11 depicts the cost of energy of the replicated 1.1 kW fan per weekday as the energy costs escalated. The final cost of energy per weekday for the replicated fan operating under damper control (R 5.56) is much higher compared to variable speed (R 3.15) operation of the fan to achieve the same desired air-flow rate of 1.21 m^3/s.

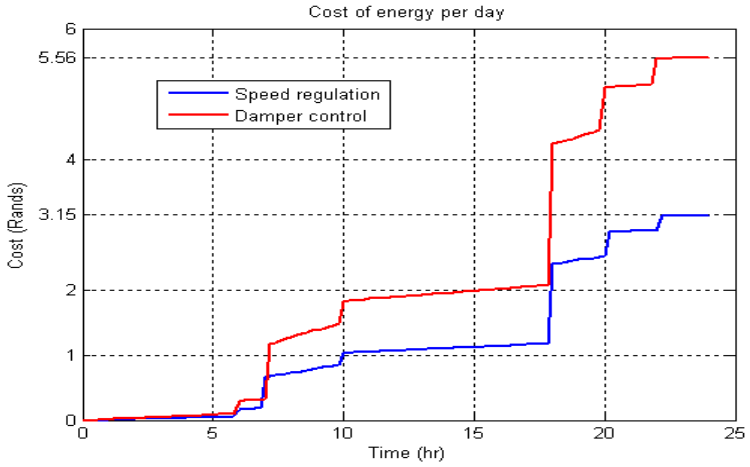

Fig. 9.11 Cost of energy per weekday of the 1.1 kW fan system

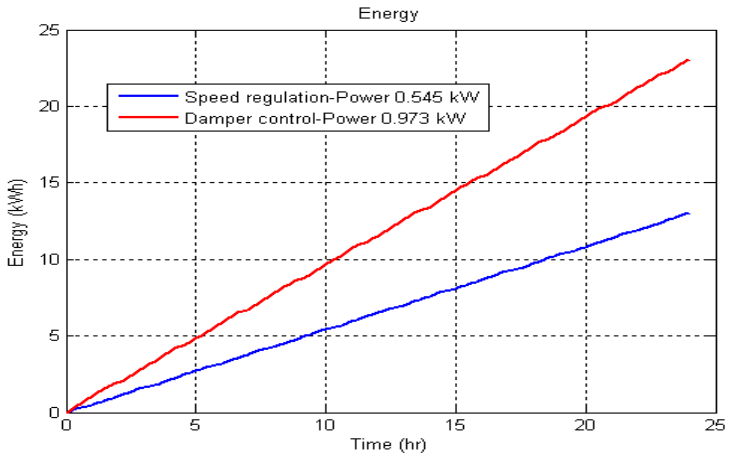

Fig. 9.12 Energy usage per day of the 1.1 kW fan system

The VFD power of the replicated fan system under damper control was approximately 973 W and under speed regulation was approximately 545 W. The energy usage per day of the 1.1 kW fan system at an air-flow rate of 1.21 m^3/s for both damper and variable speed operation is shown in Fig. 9.12 clearly depicting the energy savings achieved through variable speed operation of the fan.

The Simulink™ simulated results (Fig. 9.6) showing the accumulation of energy for both fixed speed damper operation and variable speed operation of the 1.1 kW fan are compared to the PLC simulated results (Fig. 9.12) in Fig. 9.13 to verify the accuracy of the PLC simulations.

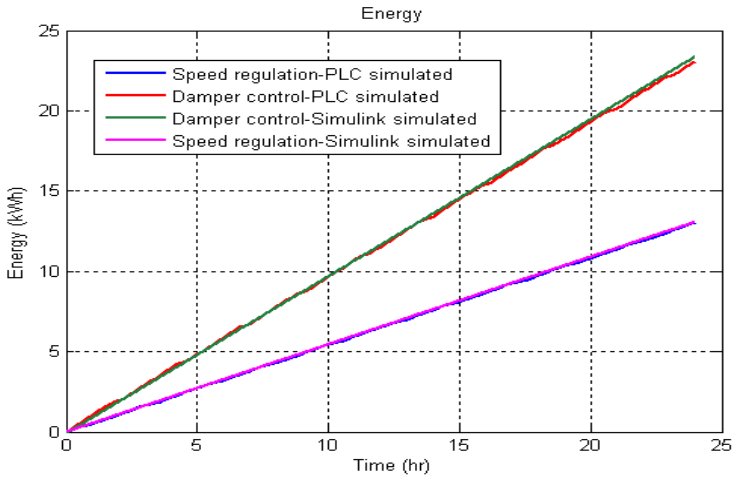

Fig. 9.13 Comparison between the Simulink™ simulated and PLC simulated energy accumulated

Referring to Fig. 9.13, the Simulink™ simulated and PLC simulated results correspond closely. The Simulink™ simulated costs of energy at an air-flow rate of 1.21 m^3/s for damper operation (973.9 W) and speed regulation (545.1 W) of the 1.1 kW fan system were R 5.55 and R 3.12 respectively. The PLC simulated costs of energy while the test bed replicated the 1.1 kW fan system at an air-flow rate of 1.21 m^3/s under damper control (approximately 0.973 kW) was R 5.56 and under speed regulation (approximately 0.545 kW) was R 3.15. The discrepancies in the final costs of energy per weekday are because the measured VFD power varied unlike in the Simulink™ simulation models which had a constant power.

9.3.2 Energy simulations of the 785 kW fan system in the PLC

The PLC simulated costs of energy and the energy accumulated while the actual test bed replicated the scaled down 785 kW fan system are shown in this section via logged data.

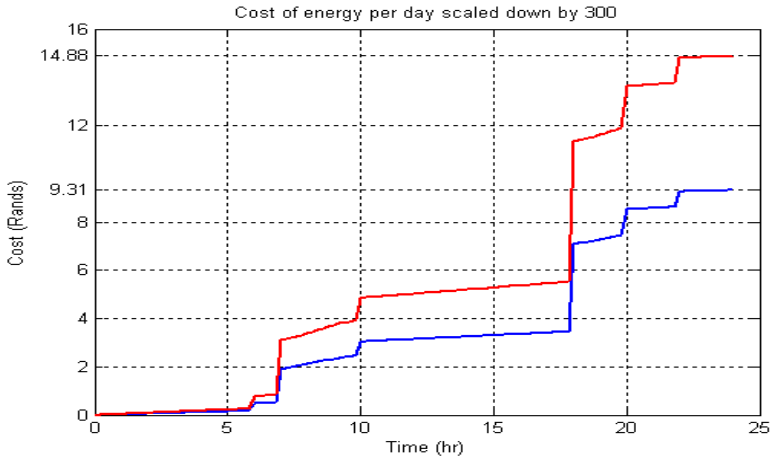

Fig. 9.14 Scaled down cost of energy per weekday of the 785 kW fan system

The scaled down cost of energy of the scaled down 785 kW fan system at an air-flow rate of 365 m^3/s is shown in Fig. 9.14 for both damper control (approximately 2.557 kW) and speed regulation (approximately 1.625 kW). Under speed regulation the scaled down cost per weekday amounted to R 9.31 while under damper control the scaled down cost accumulated to R 14.88.

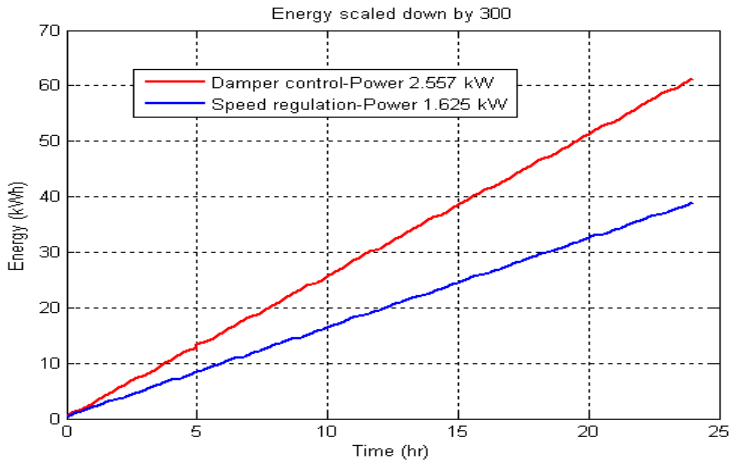

Fig. 9.15 Scaled down energy usage per day of the 785 kW fan system

The scaled down energy accumulated for the day of the scaled down 785 kW fan system is shown in Fig. 9.15 for both damper operation (approximately 2.557 kW) and variable speed operation (approximately 1.625 kW) of the fan.

The scaled down energy data simulated in the PLC (Fig. 9.15) is compared to the Simulink™ simulated scaled down energy data (Fig. 9.10) to verify the accuracy of the PLC simulations as shown in Fig. 9.16.

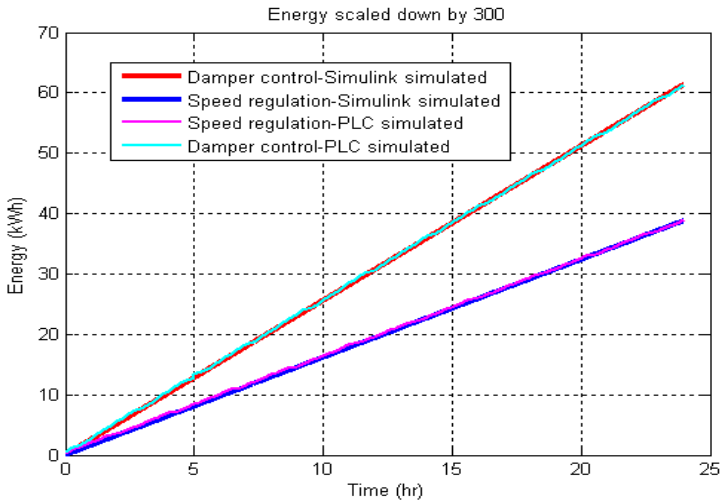

Fig. 9.16 Comparison between the Simulink™ simulated and PLC simulated energy accumulated per day of the scaled down 785 kW fan system

Referring to Fig. 9.16, both the Simulink™ simulated (Fig. 9.10) and PLC simulated (Fig. 9.15) scaled down energy results of the scaled down 785 kW fan system correspond closely. The final Simulink™ simulated scaled down costs of energy per weekday under damper control (2.556 kW) and variable speed operation (1.618 kW) of the scaled down fan at an air-flow rate of 365 m^3/s amounted to R 14.57 and R 9.24 respectively. The PLC simulated scaled down costs of energy for the replicated scaled down fan under damper control (approximately 2.557 kW) was R 14.88 and under speed regulation (approximately 1.625 kW) was R 9.31. The discrepancies between the Simulink™ simulated and PLC simulated scaled down cost of energy results are due to the VFD power varying in the actual test bed unlike in the Simulink™ simulation models which had a constant power.

9.4 Air flow control

After proving the energy savings achievable through speed control of centrifugal fans, NPC had also requested the UKZN to determine whether variable speed operation might afford more consistent air flow rates throughout a mine air ventilation system using an air feedback system. Since the VFD was not yet installed at Vlaklaagte, air flow control through speed control of the 1.1 kW fan was implemented. To explain how the air flow controller was implemented Fig. 9.17 is used.

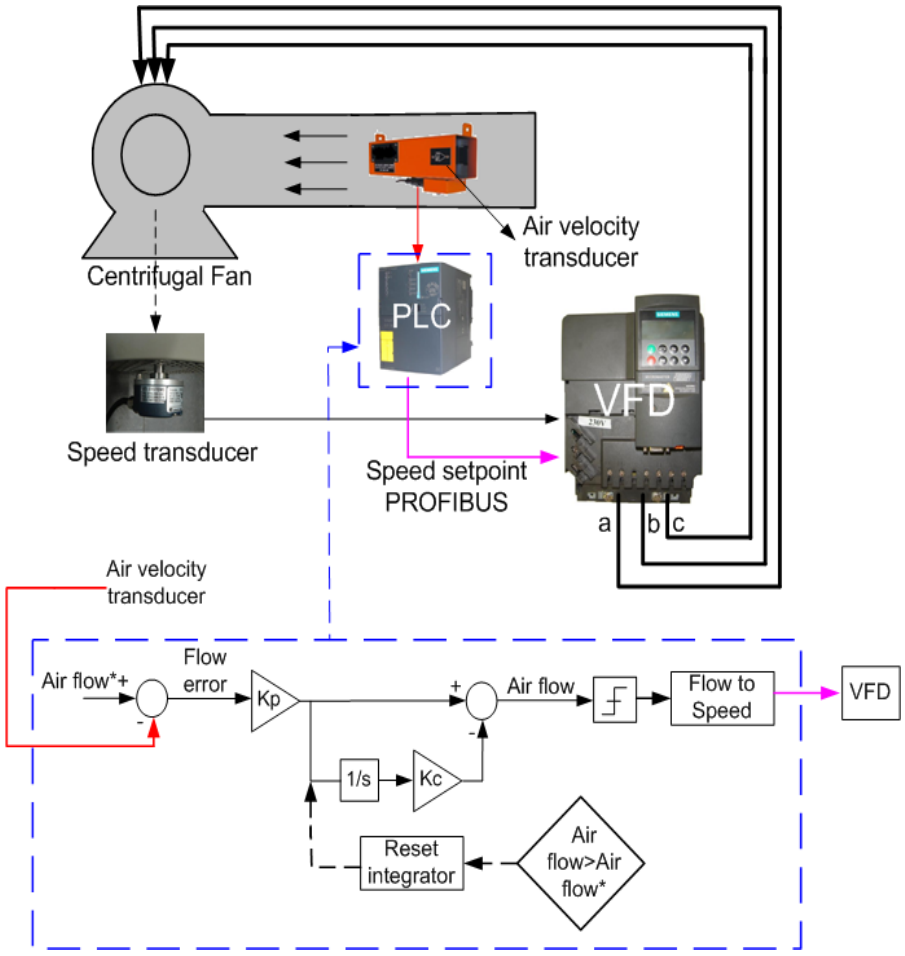

Fig. 9.17 Air flow controller hardware and software interfacing

Referring to Fig. 9.17, the air flow control loop was programmed in the PLC and facilitated via a timed interrupt to implement PI control. Air flow feedback was received from the air velocity transducer and sent to the PLC. The air flow setpoint is converted to a speed setpoint in the PLC and sent to the VFD via PROFIBUS. Speed control was implemented internally in the VFD achieving speed feedback from the speed transducer.

To convert the air-flow setpoint to a speed setpoint in the PLC, the relationship between speed and air-flow of the 1.1 kW fan was experimentally determined as shown in Fig. 9.18.

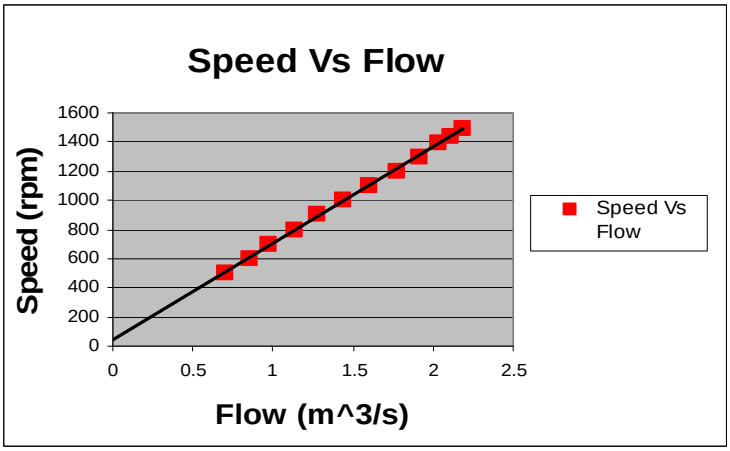

Fig. 9.18 Speed-flow of the 1.1 kW fan

To then implement the PI air-flow controller, Zeigler-Nichols rules [22] were used to provide a starting point for the tuning of the PI controller since the mathematical model of the fan system cannot be easily derived. The response produced by following the Zeigler Nichols rules were not satisfactory; there were large overshoots in both the speed and air-flow rate; however the system finally did settle to the setpoint air-flow rate as shown in Fig. 9.19. According to theory, Zeigler-Nichols rules only apply to a first order system with lag [22], and since the air-flow response was not a perfect first order system, further tuning was accomplished intuitively. The tuning of the flow control parameters (Proportional gain *kp*, Integral gain *kc* and Integral time *Ti*) was done so as not to result in excessive overshoot of the fan speed and air-flow rate, with a quick rise time and good performance during disturbances. The velocity transducer did not respond as fast as the speed transducer due to the dead band in it. This had to also be taken into account whilst tuning the controller.

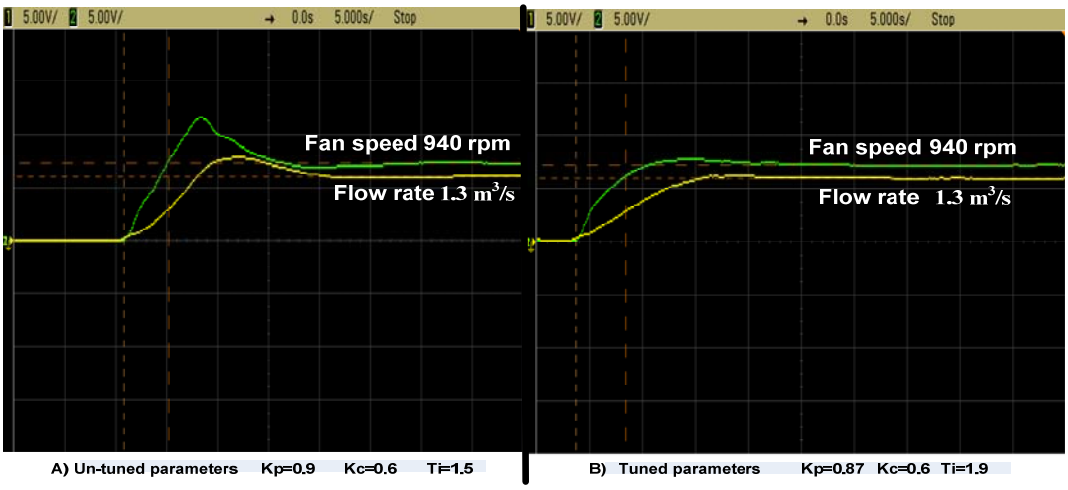

Fig. 9.19 Start-up response of the system

The system response before and after tuning is apparent in Fig. 9.19 for a 1.3 m^3/s step in flow rate. The parameters of the PI controller which resulted in these system responses are provided in Table 9.2.

	Untuned	**Tuned**
Proportional gain *Kp*	0.9	0.87
Integral gain *Kc*	0.6	0.6
Integral time *Ti (secs)*	1.5	1.9

Table 9.2: Parameters of the PI controller

Once the parameters of the controller where tuned to provide a fast response with minimum overshoot of the fan's speed and air flow rate, the fan's response to disturbances were analysed.

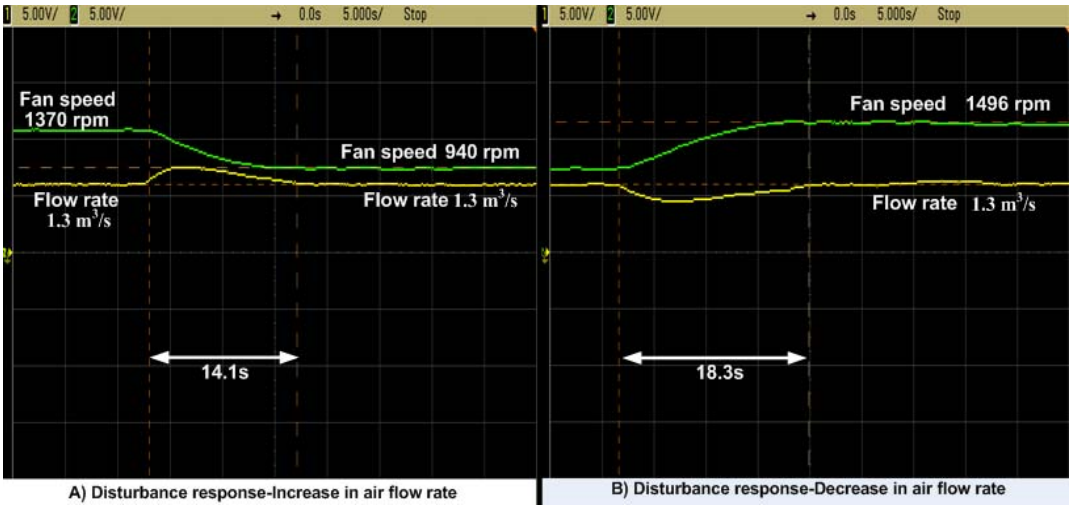

Fig. 9.20 Disturbance responses for both an increase and decrease in air-flow rate

Fig. 9.20 (a) and Fig. 9.20 (b) displays the response of the fan for both an increase and decrease in air flow rate respectively. The fan system takes 14.1s to recover from the increase in flow rate disturbance and 18.3s to recover from the decrease in flow rate disturbance. The fan system is slow as a result of the dead band in the flow transducer.

9.5 Conclusion

This chapter presented results from simulating an energy cost indicator in Simulink™ and in the PLC. Both the 1.1 kW fan system and the 785 kW fan system showed energy and monetary savings for when speed regulation was used instead of damper control to regulate the air-flow rate. Air-flow control of the 1.1 kW fan was then implemented showing that variable speed operation will achieve more consistent air flow rates.

The next chapter presents a summary and conclusion of the work performed. The progress at Vlaklaagte, a business case and recommendations for future work are provided.

CHAPTER 10

SUMMARY AND CONCLUSIONS

10.1 General

Anglo Coal South Africa currently (2008) deploys centrifugal fan driven air ventilation systems used for the extraction of methane gas underground and to properly circulate air to working faces. These centrifugal fan driven air ventilation systems operate at a fixed speed continuously throughout the year having the air flow controlled via a RVC. NPC found the air ventilation systems on most mines to be 45 % damped which is greatly inefficient. Further contributing to the inefficiency are fissures in the underground rock face resulting in variable air flow rates throughout the air ventilation system.

NPC therefore proposed a variable speed fan driven air ventilation system which according to theory [9] should result in the fan operating at a lower power if the speed of the fan is reduced. NPC therefore approached the UKZN to prove the energy savings achievable through the proposed air ventilation system at Anglo Coal's Vlaklaagte colliery.

To demonstrate the operation of the existing and proposed air ventilation systems to Anglo Coal, a test bed that could replicate the operation of these air ventilation systems was developed based on previous research [1] at the UKZN. The test bed hardware was based on similar hardware used at Anglo Coal South Africa. The hardware comprised a S7-300 PLC that could communicate via PROFIBUS to two VFDs. The control of the test bed was done through software called Step 7, available for use with a Siemens PLC. A Siemens SCADA program was then developed to provide a graphical user interface for controlling the test bed and to demonstrate to an engineer the operation of the test bed.

Due to the data from Anglo Coal Vlaklaagte being unavailable a theoretical fan system, 1.1 kW fan system and 785 kW fan system were studied. These fan systems were successfully simulated by the test bed in both Simulink and the PLC. It was shown that the power usage of all three fan systems operating under fixed speed damper control utilises almost the same amount of power throughout the damping range. The implementation of a variable speed controlled air ventilation system will always result in energy savings if the fan runs at less than full output. The amount of energy savings achievable depends greatly on the flow rate and duty cycle of the air

ventilation system. The lower the flow rate required and the longer the fan runs at reduced speed, the greater the energy savings. On large fan systems such as the 785 kW air ventilation system at Anglo Coal Greenside, even though the fan operates at 85 % its full potential, power savings of 281.4 kW were still achieved through variable speed operation of the fan. This results in energy savings of 2,465.064 MWh per year. Air flow control of the 1.1 kW fan also showed that variable speed operation of the fan does afford more consistent air flow rates.

The next section discusses the progress thus far at Vlaklaagte.

10.2 Proposed ventilation system progress at Vlaklaagte

The progress with regard to implementing the variable speed fan driven air ventilation system at Vlaklaagte thus far (Dec 2008) is presented in this section. The existing air ventilation system and equipment was shown in Chapter 1.

Additional monitoring equipment has since been installed as shown in Fig. 10.1 to Fig. 10.3.

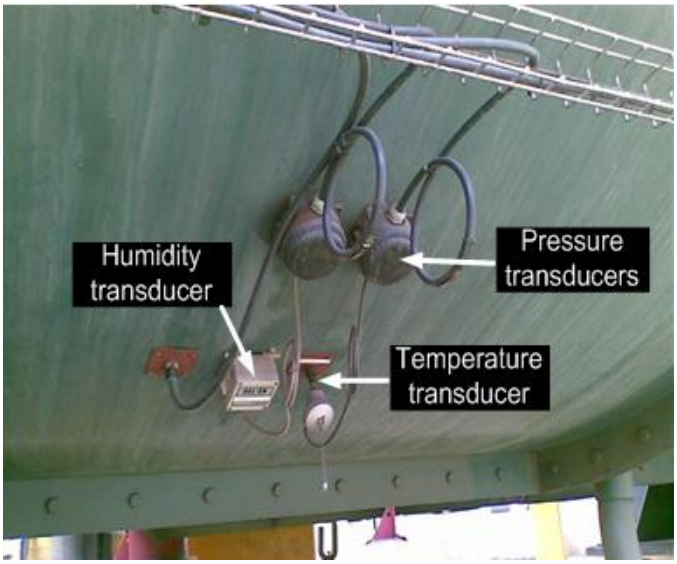

Fig. 10.1 Inlet duct transducers

The measurement transducers located on the inlet duct of the fan are shown and labelled accordingly in Fig. 10.1.

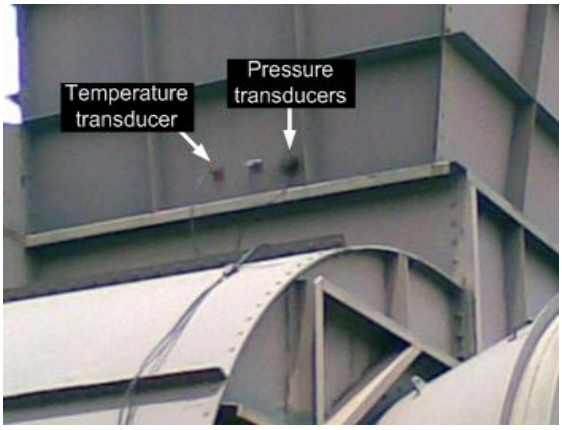

Fig. 10.2 Outlet duct transducers

In the outlet duct of the fan only pressure and temperature are measured as shown by the measurement transducers depicted in Fig. 10.2.

Fig. 10.3 PLC and interface equipment

Fig. 10.3 depicts a S7-300 PLC together with communication modules. Fibre optic is used as the communication channel between the PLC and a SCADA program which displays and logs the measured data.

Further continuation of the project is awaiting funding. An 800 kW Sinamics VFD and an 800 kW Siemens motor is proposed to replace the existing 1.2 MW slip ring induction motor and gearbox system. The changing of the fan blade from steel to carbon fibre is also being considered. A business case is presented in Tables 10.1 to 10.3 based on the fact that the air ventilation system at Vlaklaagte is 45 % damped. Once actual data is available and evaluated by the test bed, the business case will be reengineered for submission to Anglo Coal.

A power saving of 540 kW is proposed at Vlaklaagte once the damper controlled air ventilation system is replaced with a variable speed controlled air ventilation system. Table 10.1 presents the monetary value of the energy savings per annum based on Eskom's Megaflex tariff structure. The tariff structure is broken down into two seasons called Low demand season and High demand season. Low demand season refers to the months September to May in which the demand for energy is low therefore the cost of energy is low. High demand season refers to the months June to August in which the demand for energy is high therefore the cost of energy is high. The energy costs for these two seasons are given in Table 10.1. The time periods peak, off peak and standard have been discussed in Chapter 9, Section 9.2. The total rand value for each specific time period is calculated according to Eq. 10.1.and the total energy monetary savings per year is calculated according to Eq. 10.2.

$$Total\_rands = kW * Hours * Unit\_price \quad (10.1)$$

Total energy monetary savings per year = Low demand season Total(R)(Peak + Standard + Off peak) + High demand season Total(R)*(Peak + Standard + Off peak)* (10.2)

Energy monetary savings per annum				
Low demand season		**Unit Price**	**Power saved**	**Total (R)**
	Hours		**kW**	
Peak	1365.00	R 0.4013	540.00	R 295,798.23
Standard	3003.00	R 0.2458	540.00	R 398,594.20
Off peak	2184.00	R 0.1719	540.00	R 202,731.98
Total hours	6552.00			R 897,124.41
High demand season		**Unit Price**	**Power saved**	**Total (R)**
	Hours		**kW**	
Peak	460.00	R 1.4377	540.00	R 357,124.68
Standard	1012.00	R 0.3736	540.00	R 204,164.93
Off peak	736.00	R 0.1996	540.00	R 79,329.02
Total hours	2208.00			R 640,618.63
Total energy monetary savings per year				**R 1,537,743.04**

Table 10.1: Monetary savings per annum

Table 10.2 presents the inputs to the business case model shown in Table 10.3. Referring to Table 10.2, the capital required to implement the variable speed controlled air ventilation system is R 3 609 392. The energy monetary savings per annum are R 1 537 743.04 as calculated in Table 10.1. The annual energy cost increase which has been proposed by Eskom is 24.8 % for the next three years. The discounted present value which is the rate used to discount future cash flows to their present values is 12 %. The annual maintenance cost is assumed to be 2.6 % of the initial capital cost.

Capital	R 3 609 392.00
Energy savings (R)	R 1 537 743.04
Annual energy cost increase – 3 years	24.8 %
Discounted present value	12 %
Annual maintenance cost	2.6 %

Table 10.2: Inputs for the business case model

Table 10.3 presents the business case model which shows the cash outflows and inflows for a ten year period. After the ten year period the Net Present Value (NPV) and the Internal Rate of Return (IRR) of the project is calculated. The NPV shows the difference between the Present Value (PV) of cash inflows and the PV of cash outflows. The IRR shows the interest rate at which the NPV of costs (negative cash flows) of the investment equal the NPV of the benefits (positive cash flows) of the investment.

According to Table 10.3 the NPV of the project is R 12 093 538.37 and the IRR of the project is 56%. Should Vlaklaagte invest the capital in example a bank, the rate of return from the bank would be between 8 % and 10 %. Should Vlaklaagte invest the capital in this project they would receive a return of 56 %. A return of 56 % is associated with a 2 year pay back on the capital invested therefore investing in this project is very favourable from a business perspective.

GH VLAKLAAGTE VENTILATION FAN OPTIMIZATION - BUSINESS CASE

YEAR	yr 0	yr 1	yr 2	yr 3	yr 4	yr 5	yr 6	yr 7	yr 8	yr 9	yr 10	NPV	IRR
CASH OUTFLOWS													
Capital	R -3,609,392.00												
Annual maintenance cost		-93844.19	-105105.50	-117718.15	-131844.33	-147665.65	-165385.53	-185231.80	-207459.61	-232354.76	-260237.34		
OUTFLOWS TOTAL	**-3609392.00**	**-93844.19**	**-105105.50**	**-117718.15**	**-131844.33**	**-147665.65**	**-165385.53**	**-185231.80**	**-207459.61**	**-232354.76**	**-260237.34**		
YEAR	**yr 0**	**yr 1**	**yr 2**	**yr 3**	**yr 4**	**yr 5**	**yr 6**	**yr 7**	**yr 8**	**yr 9**	**yr 10**	**NPV**	**IRR**
CASH INFLOWS													
Energy savings		**R 1,537,743.04**	R 1,919,103.32	R 2,395,040.94	R 2,682,445.85	R 3,004,339.35	R 3,364,860.08	R 3,768,643.29	R 4,220,880.48	R 4,727,386.14	R 5,294,672.47		
INFLOWS TOTAL		**R 1,537,743.04**	**R 1,919,103.32**	**R 2,395,040.94**	**R 2,682,445.85**	**R 3,004,339.35**	**R 3,364,860.08**	**R 3,768,643.29**	**R 4,220,880.48**	**R 4,727,386.14**	**R 5,294,672.47**		
NET CASH FLOW	**R -3,609,392.00**	**R 1,443,898.85**	**R 1,813,997.82**	**R 2,277,322.78**	**R 2,550,601.52**	**R 2,856,673.70**	**R 3,199,474.54**	**R 3,583,411.49**	**R 4,013,420.87**	**R 4,495,031.37**	**R 5,034,435.14**	**R 12,093,538.37**	**56%**
Discounted Present value (12%)	R -3,609,392.00	R -2,320,196.60	R -874,088.64	R 746,864.73	R 2,367,818.11	R 3,988,771.49	R 5,609,724.86	R 7,230,678.24	R 8,851,631.61	R 10,472,584.99	R 12,093,538.37		

Table 10.3: Business case model

10.3 Advantages of using VFD's to drive fans

The main advantage of using a VFD to drive a centrifugal fan is energy savings. Other advantages that can also be considered:

1. The air flow rate is much easier to control and can be changed almost immediately online by adjusting the speed of the fan.

2. The fan can be started and stopped easily resulting in less mechanical stress on the fan, therefore maintenance of the fan is reduced.

3. The release of methane gas underground increases with a drop in atmospheric pressure. By changing the speed of the VSD driven fan, the air flow rate can be increased easily and immediately online to decrease the release of methane gas.

4. In an emergency the amount of ventilation required underground can be changed immediately. Example if a fire starts underground ventilation can be decreased automatically.

10.4 Recommendations for future work

1. To evaluate and simulate the data from Vlaklaagte. To resubmit the business case based on actual data.

2. To evaluate the power usage of the new variable speed fan driven air ventilation system at Vlaklaagte once the VFD and motor is installed.

3. To determine where the air flow transducers will be placed in the mine for air flow control to be implemented. To then determine limits for the deviations between the desired and actual air flow rates that will allow for the speed of the fan to change.

4. To develop a SCADA program for the new variable speed fan driven air ventilation system at Vlaklaagte.

5. To use the test bed to measure the power usage of pump systems.

APPENDIX A

MACHINE NAMEPLATE DATA AND HYBRID MODEL

A.1 Induction machine nameplate data

Manufacturer	Siemens
Machine type	1LA7107-4AA10-Z
Mass	24 kg
Power	3 kW
Voltage	230 V Δ or 400V Y
Current	11.1 A in Δ or 6.4 A in Y
Speed	1420 rpm
Frequency	50 Hz

A.2 Hybrid model

The d-q model equations [7] of the induction machine on an arbitrary reference frame are shown here as Eq. A.1 and Eq. A.2.

$$\begin{bmatrix} v_{ds} \\ v_{qs} \\ v_{dr} \\ v_{qr} \end{bmatrix} = \begin{bmatrix} R_1 + L_{11}p & -\omega L_{11} & L_m p & -\omega L_m \\ \omega L_{11} & R_1 + L_{11}p & \omega L_m & L_m p \\ L_m p & -L_m s\omega & R_2 + L_{22}p & -L_{22}s\omega \\ L_m s\omega & L_m p & L_{22}s\omega & R_2 + L_{22}p \end{bmatrix} \begin{bmatrix} i_{ds} \\ i_{qs} \\ i_{dr} \\ i_{qr} \end{bmatrix} \quad \text{(A.1)}$$

$$\begin{bmatrix} \lambda_{ds} \\ \lambda_{dr} \\ \lambda_{qs} \\ \lambda_{qr} \end{bmatrix} = \begin{bmatrix} L_{11} & 0 & L_m & 0 \\ L_m & 0 & L_{22} & 0 \\ 0 & L_{11} & 0 & L_m \\ 0 & L_m & 0 & L_{22} \end{bmatrix} \begin{bmatrix} i_{ds} \\ i_{qs} \\ i_{dr} \\ i_{qr} \end{bmatrix} \quad \text{(A.2)}$$

Inverting Eq. A.2 results in Eq. A.3.

$$\begin{bmatrix} i_{ds} \\ i_{dr} \\ i_{qs} \\ i_{qr} \end{bmatrix} \quad \begin{bmatrix} \frac{L_{22}}{\sigma} & 0 & -\frac{L_m}{\sigma} & 0 \\ 0 & \frac{L_{22}}{\sigma} & 0 & -\frac{L_m}{\sigma} \\ -\frac{L_m}{\sigma} & 0 & \frac{L_{11}}{\sigma} & 0 \\ 0 & -\frac{L_m}{\sigma} & 0 & \frac{L_{11}}{\sigma} \end{bmatrix} \begin{bmatrix} \lambda_{ds} \\ \lambda_{qs} \\ \lambda_{dr} \\ \lambda_{qr} \end{bmatrix} \tag{A.3}$$

where:

$$\sigma = 1 - \frac{L_m{}^2}{(L_{11}L_{22})} \tag{A.4}$$

Combining Eq. A.1 with Eq. A.3 results in the Hybrid model [7] as shown in Eq. A.5 and Eq. A.6 having the stator currents and the rotor flux linkages as the states. The rotor windings in a squirrel cage induction machine are short circuited, therefore the rotor voltages (v_{dr} and v_{qr}) are set to zero.

$$\begin{bmatrix} v_{ds} \\ v_{qs} \\ 0 \\ 0 \end{bmatrix} = \begin{bmatrix} R_1 + L_{11}\sigma p & -\omega L_{11}\sigma & \frac{L_m}{L_{22}} p & -\omega L_m \\ \omega L_{11}\sigma & R_1 + L_{11}\sigma & \omega \frac{L_m}{L_{22}} & \frac{L_m}{L_{22}} p \\ -R_2 \frac{L_m}{L_{22}} & 0 & \frac{R_2}{L_{22}} + p & -s\omega \\ 0 & -R_2 \frac{L_m}{L_{22}} & s\omega & \frac{R_2}{L_{22}} + p \end{bmatrix} \begin{bmatrix} i_{ds} \\ i_{qs} \\ \lambda_{dr} \\ \lambda_{qr} \end{bmatrix} \tag{A.5}$$

$$\underline{v} = [[R]p + [L]p + [F]\omega_e + [G]\omega_r]\underline{h} \tag{A.6}$$

where:

$$\underline{v} = \left[v_{ds}, v_{qs}, 0, 0 \right]^{t} \tag{A.7}$$

$$\underline{h} = \left[i_{ds}, i_{qs}, \lambda_{dr}, \lambda_{qr} \right]^{t} \tag{A.8}$$

$$\left[R \right] = \begin{bmatrix} R_1 & 0 & 0 & 0 \\ 0 & R_1 & 0 & 0 \\ -R_2 \frac{L_m}{L_{22}} & 0 & \frac{R_2}{L_{22}} & 0 \\ 0 & -R_2 \frac{L_m}{L_{22}} & 0 & \frac{R_2}{L_{22}} \end{bmatrix} \tag{A.9}$$

$$\left[L \right] = \begin{bmatrix} \sigma L_{11} & 0 & \frac{L_m}{L_{22}} & 0 \\ 0 & \sigma L_{11} & 0 & \frac{L_m}{L_{22}} \\ 0 & 0 & 1 & 0 \\ 0 & 0 & 0 & 1 \end{bmatrix} \tag{A.10}$$

$$\left[F \right] = \begin{bmatrix} 0 & -\sigma L_{11} & 0 & -\frac{L_m}{L_{22}} \\ \sigma L_{11} & 0 & \frac{L_m}{L_{22}} & 0 \\ 0 & 0 & 0 & -1 \\ 0 & 0 & 1 & 0 \end{bmatrix} \tag{A.11}$$

$$\left[G \right] = \begin{bmatrix} 0 & 0 & 0 & 0 \\ 0 & 0 & 0 & 0 \\ 0 & 0 & 0 & 1 \\ 0 & 0 & -1 & 0 \end{bmatrix} \tag{A.12}$$

APPENDIX B

RATED ROTOR FLUX LINKAGE

The procedure for calculating the rated rotor flux linkage of an induction machine is presented in this appendix.

A sinusoidal winding flux linkage is defined according to Eq. B.1.

$$\lambda = \lambda_{max}\, cos(\omega_e t + \psi_\lambda) \tag{B.1}$$

The rate of change of flux in a winding is the induced emf into the winding as shown by Eq. B.2.

$$e = p\lambda \tag{B.2}$$

Substituting Eq. B.1 into Eq. B.2 results in the induced emf per winding as given in Eq. B.3.

$$\begin{aligned} e &= p[\,\lambda_{max}\, cos(\omega_e t + \psi_\lambda)] \\ &= \omega_e \lambda_{max}\, sin(\omega_e t + \psi_\lambda) \\ &= E_m\, sin(\omega_e t + \psi_\lambda) \end{aligned} \tag{B.3}$$

where:

$E_m = \omega_e \lambda_{max}$ …..the amplitude of the induced winding emf.

Eqs. B.1 to B.3 can now be applied to an induction machine to establish the rated rotor flux linkage of the machine. The rated amplitude of the rotor flux linkage per phase using Eq. B.3 is calculated here in Eq. B.4.

$$\begin{aligned} \lambda_{max} &= \frac{E_m}{\omega_e} \\ &= \frac{\sqrt{2}E_{RMS}}{\sqrt{3}}\left(\frac{1}{\omega_e}\right) \end{aligned} \tag{B.4}$$

$$= \frac{\sqrt{2}(230)}{\sqrt{3}}\left(\frac{1}{314.16}\right)$$

$$= 0.598$$

The rated rotor flux linkage in the d-q reference frame is given in Eq. B.5.

$$\left|\overline{\lambda_r}\right| = \sqrt{\frac{3}{2}}\lambda_{\max} \tag{B.5}$$

$$= \sqrt{\frac{3}{2}}0.598$$

$$= 0.73$$

The magnitude of $\overline{\lambda_r}$ is defined below in Eq. B.6.

$$\left|\overline{\lambda_r}\right| = \sqrt{\lambda^2{}_{dr} + \lambda^2{}_{qr}} \tag{B.6}$$

Under FOC the q-axis rotor flux linkage is zero ($\lambda_{qr}=0$) therefore Eq. B.6 reduces to $\left|\overline{\lambda_r}\right| = \lambda_{dr}$.

The rated d-axis current (i_{ds}) is now given by Eq. B.7.

$$i_{ds} = \frac{\lambda_{dr}}{L_m} \tag{B.7}$$

$$= \frac{0.73}{0.199}$$

$$= 3.68$$

APPENDIX C

FOC CONTROLLER GAINS

In this appendix the various controller gains required to simulate the two 3 kW induction machines of the test bed under FOC, following the controller design procedure as discussed in Chapter 2, Section 2.5 are calculated. The Matlab optimised parameters (Table C.1) from Chapter 5, Section 5.6 are used to calculate the various controller gains required for the implementation of FOC.

Optimised parameters		
Parameter name	**Parameter symbol**	**Value**
Stator resistance	R_1	2.35 Ω
Rotor resistance	R_2	1.49 Ω
Stator leakage inductance	L_1	0.01 H
Rotor leakage inductance	L_2	0.009987 H
Mutual inductance	L_m	0.199 H
Inertia	J	0.0046 kg-m^2
Frictional damping coefficient	B	0.0008926 N.m.s/rad

Table C.1: Optimised machine parameters

$$\sigma = 1 - \frac{L_m{}^2}{L_{11}L_{22}} \qquad \text{(C.1)}$$

$$= 1 - \frac{(0.1999)^2}{0.209 \times 0.209}$$

$$= 0.093$$

C.1 The q-axis current controller

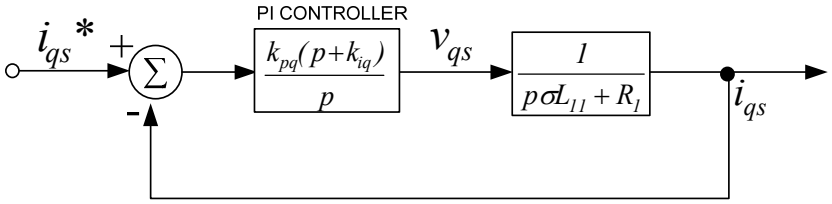

Fig. C. 1 Block diagram of the q-axis current controller

$$k_{iq} = \frac{R_1}{\sigma L_{11}} \tag{C.2}$$

$$= \frac{2.35}{0.093 \times (0.209)}$$

$$= 120.9$$

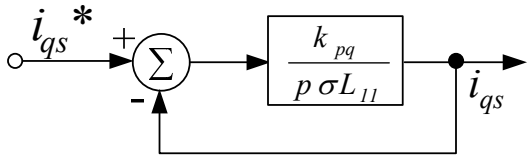

Fig. C. 2 q-axis K_{pq} transfer function

$$k_{pq} = \frac{\sigma L_{11}}{1 \times 10^{-3} \times 314.14} \tag{C.3}$$

$$= \frac{0.093 \times 0.209}{1 \times 10^{-3} \times 314.14}$$

$$= 0.062$$

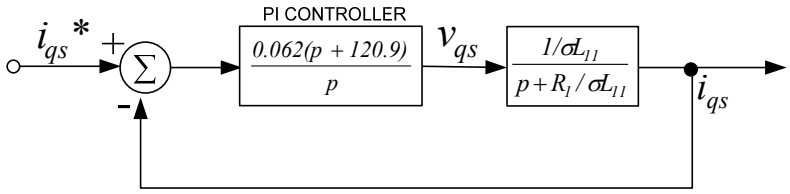

Fig. C. 3 Resultant block diagram together with the controller gains

C.2 The d-axis current controller

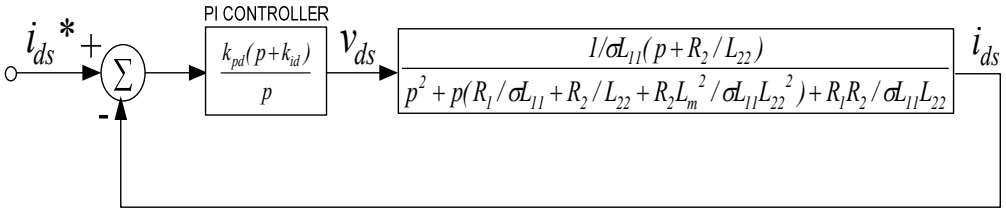

Fig. C. 4 Block diagram of the d-axis current controller

The optimised parameters of the 3 kW induction machine are substituted in the transfer function appearing in Fig. C. 4 resulting in the transfer function shown in Fig. C. 5.

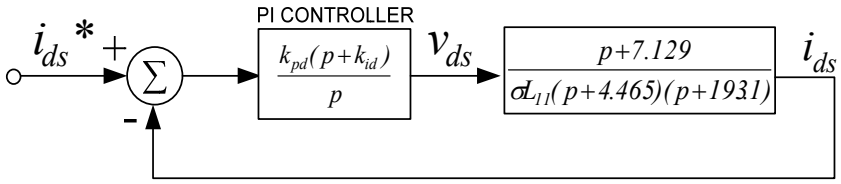

Fig. C. 5 d-axis transfer function with the substituted parameters of the machine

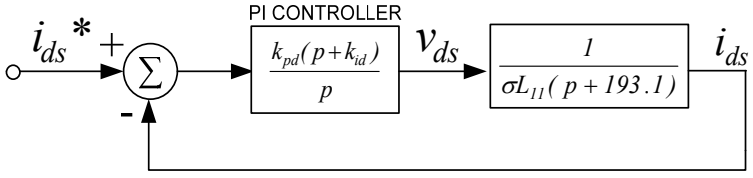

Fig. C. 6 d-axis transfer function

The d-axis current controller shown in Fig. C. 6 can now be designed in a similar manner to that of the q-axis current controller shown in Fig. C. 1 since the transfer functions are similar.

$k_{id} = 193.1$ (C.4)

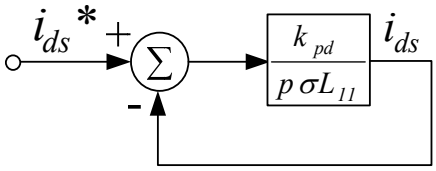

Fig. C. 7 d-axis K_{pd} transfer function

The transfer function in Fig. C. 7 looks identical to the q-axis current controller transfer function in Fig. C. 2, therefore the proportional gain K_{pd} can be chosen to be the same as the proportional gain K_{pq}.

$$k_{pd} = 0.062 \tag{C.5}$$

C.3 Speed controller

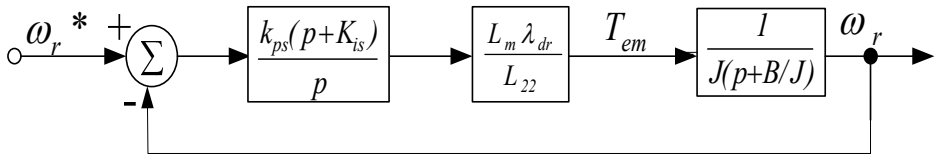

Fig. C. 8 Speed controller

$$k_{is} = \frac{B}{J} \tag{C.6}$$
$$= \frac{0.0008926}{0.0046}$$
$$= 0.194$$

Referring to Appendix B, the rated rotor flux linkage (λ_{dr}) for a Delta connected induction machine is 0.73 Wb.

$$k_{ps} = \frac{JL_{22}}{L_m \lambda_{dr} (10 \times 10^{-3})} \tag{C.7}$$
$$= \frac{0.0046 \times 0.209}{(0.199) \times 0.73 \times (10 \times 10^{-3})}$$
$$= 0.662$$

C.4 The q-axis voltage pre-compensator

The q-axis stator signal path together with its pre-compensating controller is shown in Fig. C. 9.

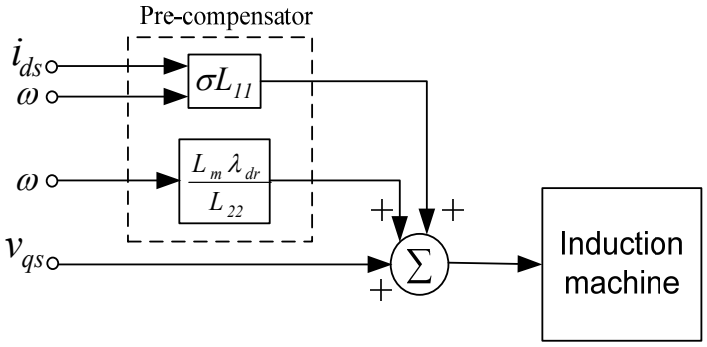

Fig. C. 9 The q-axis voltage pre-compensating controller

$$\sigma L_{11} = 0.01944 \tag{C.8}$$

$$\frac{L_m \lambda_{dr}}{L_{22}} = \frac{0.199 \times 0.73}{0.209} = 0.695 \tag{C.9}$$

C.5 The d-axis voltage pre-compensator

The d-axis stator signal path together with its pre-compensating controller is shown in Fig. C. 10.

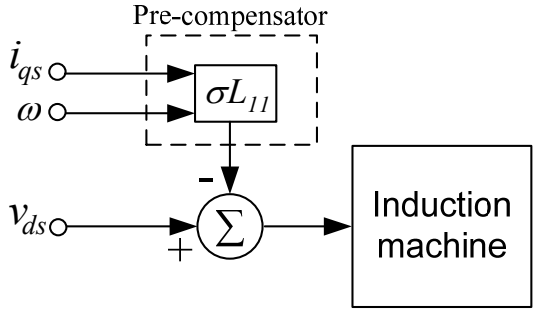

Fig. C. 10 The d-axis voltage pre-compensating controller

$$\sigma L_{11} = 0.01944 \tag{C.10}$$

APPENDIX D

INDUCTION MACHINE TESTS

This appendix describes the tests performed on an induction machine to determine its per phase equivalent circuit and mechanical parameters. The induction machine was tested at room temperature (20˚ C) using the IEEE Standard Test Procedure for Polyphase Induction Machines and Generators (Std 112-1984) [6]. The power terminals of the machine were connected in delta directly to a 220 V three phase supply. The power and current were measured with analogue meters having an accuracy of 0.5 %, whilst the voltage was measured with a digital meter having an accuracy of 0.1 %.

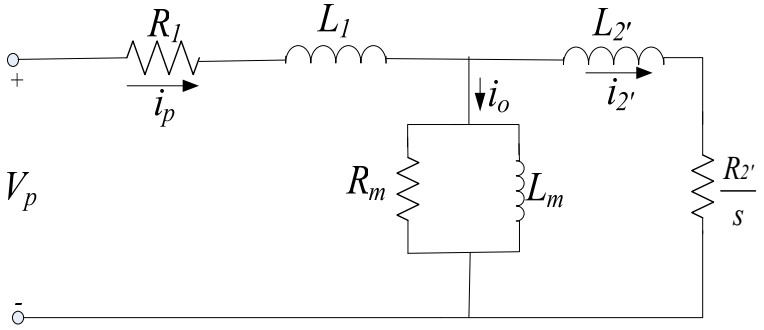

Fig. D. 1 Per phase equivalent circuit of the induction machine

The per phase equivalent circuit of the induction machine is shown in Fig. D. 1.

D.1 No load test

The no load test is performed to determine the core loses (R_m) and the mutual inductance (L_m) of the induction machine. The rated voltage (220 V) was applied to the machine which ran on no load for the test. When the machine runs on no load, the slip (s) is approximately zero and the current (I_2') in the equivalent circuit shown in Fig. D. 1 is also approximately zero; the circuit in Fig. D. 1 is taken to be open circuited and the equivalent circuit for this condition is depicted in Fig. D. 2. The parameters R_m and L_m are calculated by measuring the voltage, current and power per phase.

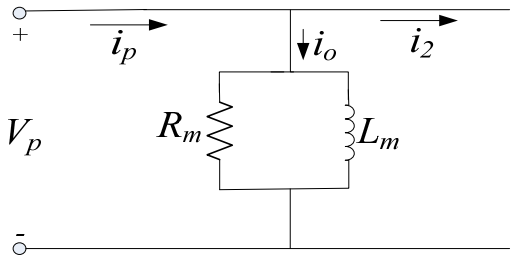

Fig. D. 2 No load equivalent circuit

$$R_m = \frac{V_p^{\,2}}{P_{ph}} \tag{D.1}$$

$$X_m = \frac{V_p^{\,2}}{\sqrt{V_p^{\,2} I^2 - P_{ph}^{\,2}}} \tag{D.2}$$

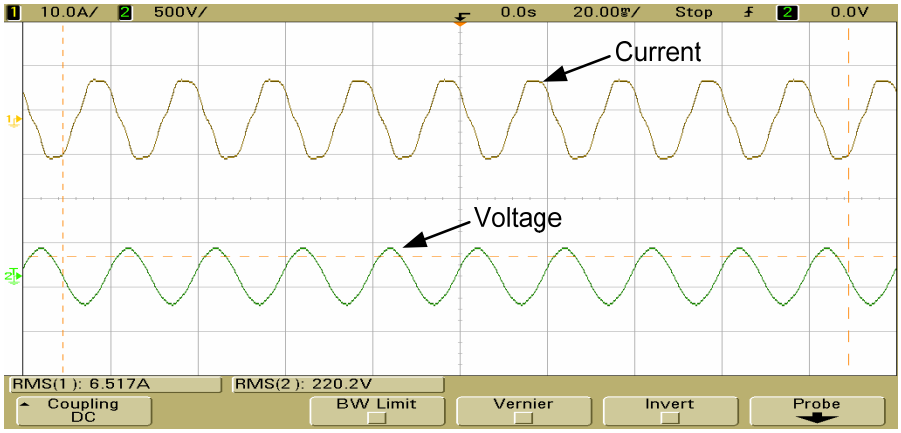

Fig. D. 3 No load current and voltage captured on an oscilloscope

Vp (V)	Ip (A)	Pph (W)	Rm (Ω)	Xm (Ω)
220.2	3.763	80	605.55	58.77

Table D.1: No load test results

$$L_m = \frac{X_m}{2 \times \pi \times f} \tag{D.3}$$

$$L_m = \frac{58.77}{2 \times 3.14 \times 50} = 0.187 H$$

D.2 Locked rotor

The locked rotor test is performed to determine the parameters R_e and L_e. R_e represents both the stator (R_1) and referred rotor resistance (R_2') and L_e represents both the stator (L_1) and referred rotor (L_2') inductance. A reduced voltage was applied to the machine until the rated current (11.1 A) flowed in its stator windings. At the reduced voltage, the current (I_o in Fig. D. 1) is approximately zero and the slip is one, thus the circuit in Fig. D. 1 reduces to the circuit depicted in Fig. D. 4.

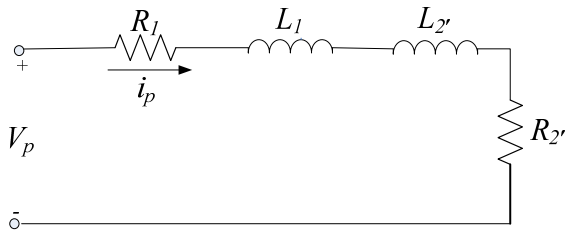

Fig. D. 4 Locked rotor equivalent circuit

$$R_e = R_1 + a^2 R_2 \tag{D.4}$$

$$R_e = \frac{P_{ph}}{I^2} \tag{D.5}$$

$$L_e = L_1 + a^2 L_2 \tag{D.6}$$

$$X_e \frac{\sqrt{V_p{}^2 I^2 - P_{ph}{}^2}}{I^2} \tag{D.7}$$

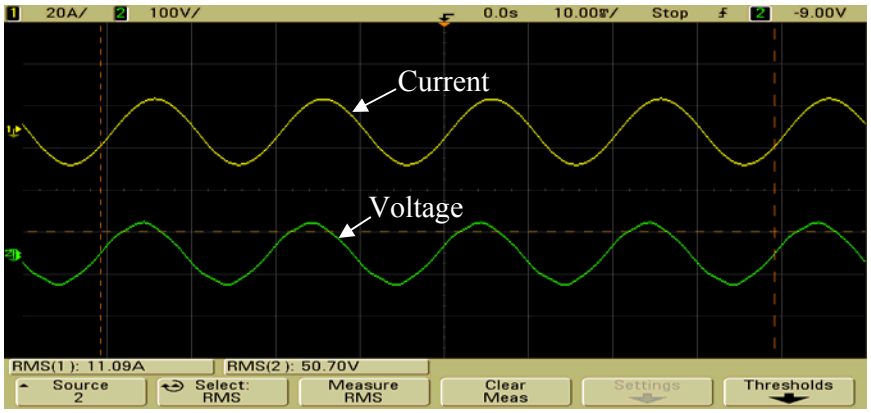

Fig. D. 5 Locked rotor current and voltage

Vp (V)	Ip (A)	Pph (W)	Re (Ω)	Xe (Ω)
50.7	6.4	153.33	3.740199	6.979388

Table D.2: Locked rotor test results

$$R_2' = R_e - R_1 \quad \text{(D.8)}$$

$$R_2' = 3.740199 - 2.3 = 1.440199\Omega$$

$$L_e = \frac{X_e}{2 \times \pi \times f} \quad \text{(D.9)}$$

$$L_e = \frac{6.979388}{2 \times 3.14 \times 50} = 0.022227H$$

$$L_1 = L_2' = \frac{L_e}{2} = 0.01111H$$

D.3 Windage and Friction loss

This test is performed to determine the power lost due to windage and friction while the machine runs on no load. The power, voltage and current were recorded while the stator voltage was reduced from the rated voltage (220 V) of the machine to zero.

Stator core losses are then subtracted from the input power and the result is plotted against the input voltage [6]. The resultant curve is then extended to the point where the voltage is zero; that point of interception on the *y* axis (Input Power-Stator losses) is the windage and friction loss [6]. A graph of voltage squared instead of voltage [6] is plotted for more accurate results.

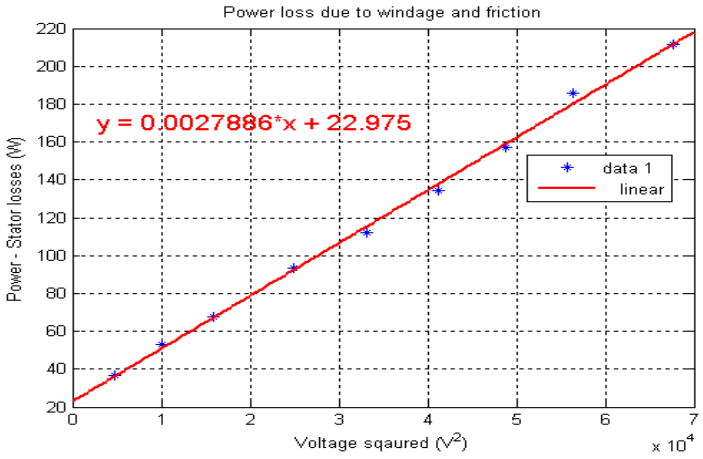

Fig. D. 6 Power loss due to windage and friction

The *y* intercept of the curve in Fig. D. 6 was found by linear curve fitting. This *y* value of 22.975 is the equivalent windage and friction power loss (P_{wf}).

D.4.1 Inertia *J* - Method 1

This section describes the first method used to determine the machine's mechanical parameters *J* and *B* i.e. the machine's inertia and frictional damping coefficients respectively. An incremental encoder mounted at the back of the machine was used to measure the machine's speed. The machine when supplied with its rated voltage (220 V) ran at no load speed (approximately 157 rad/s). The supply voltage was then removed and the speed decay of the machine was recorded as shown in Fig. D. 7.

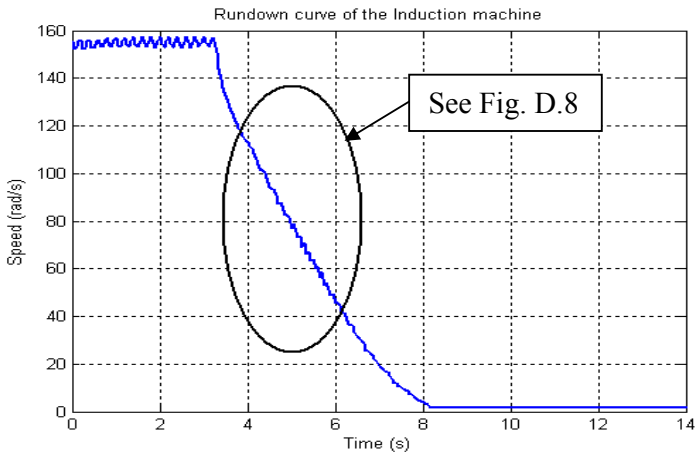

Fig. D. 7 Rundown curve of the induction machine

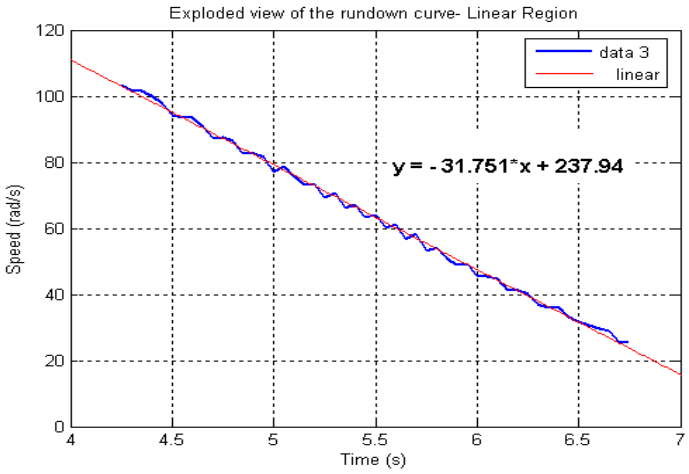

Fig. D. 8 Exploded view of Fig. D. 7 from 4s to 7s

Fig. D. 7 depicts the machine decelerating from no load speed to zero speed in 8.25s. Part of the curve in Fig. D. 7 was replotted and shown in Fig. D. 8 illustrating a change of speed from 103 rad/s to 25 rad/s. In this region, the rate of change of speed is approximately constant. A tangent line is therefore drawn in this approximately constant region; the gradient of the line found by linear curve fitting is the rate of change of speed.

Rate of change of speed ($p\omega_r$)= -31.751 rad/s^2

The electromagnetic torque (T_e) of an induction machine is given by Eq. D.10.

$$T_e = Jp\omega_r + \beta\omega_r + T_l \qquad \text{(D.10)}$$

As soon as the power supply is removed the electromagnetic torque produced by the machine does not exist and since the machine runs on no load, load torque T_l is zero therefore Eq. D.10 reduces to:

$$Jp\omega_r = -\beta\omega_r \qquad \text{(D.11)}$$

To calculate the inertia of the machine as shown in Eq. D.13, the torque due to windage and friction is first calculated using Eq. D.12. The power loss due to windage and friction was calculated in Section D.3 as 22.975 W. The speed of the machine was approximately 157 rad/s.

$$T_{wf} = \frac{P_{wf}}{\omega_r} = \frac{22.975}{157} = 0.146\,Nm \qquad \text{(D.12)}$$

$$J = \frac{-T_{wf}}{P\omega_r} = \frac{-0.146}{-31.751} = 0.00459 kg.m^2 \quad \text{(D.13)}$$

Calculating the inertia of the induction machine using the above described method is accurate and can be used to determine the inertia of any size of induction machine provided that a speed transducer is installed on the machine.

D.4.2 Inertia *J* - Method 2

This section describes the second method used to calculate the inertia of the machine. This method does not require the use of a speed transducer and can be considered for use on small machines.

The machine was stripped and the rotor was taken out. The total mass of the rotor was measured to be 5 kg. The lengths and diameters of the different sections that contributed to the structure of the rotor were measured and are presented below in Fig. D. 9.

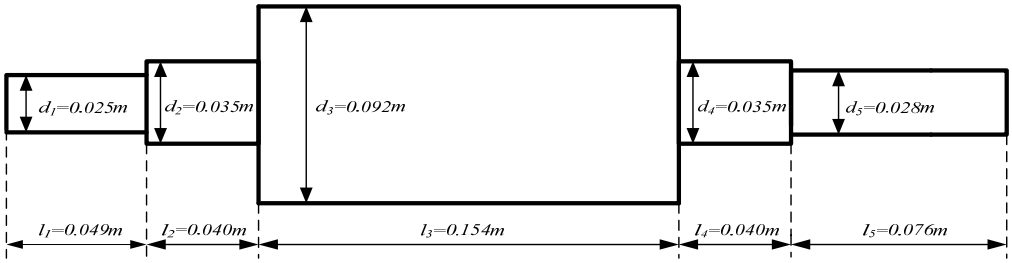

Fig. D. 9 Structure of the rotor

Assuming a uniform density allows for the calculation of mass distribution throughout the rotor, if the volume is known.

*Mass * Volume = Density* (D.14)

The volume (*V*) of each section of the rotor is calculated using Eq. D.15 with the lengths (*l)* and diameters (*d*) corresponding to the ones shown in Fig. D. 9.

$$V = \frac{\pi d^2 l}{4} \quad \text{(D.15)}$$

Table D.3 illustrates the resultant volumes of each section of the rotor shown in Fig. D. 9.

Volume 1 (mm^3)	**Volume 2** (mm^3)	**Volume 3** (mm^3)	**Volume 4** (mm^3)	**Volume 5** (mm^3)	**Volume Total** (mm^3)
2.41×10^{-5}	3.85×10^{-5}	1.024×10^{-3}	3.85×10^{-5}	4.68×10^{-5}	1.172×10^{-3}

Table D.3: Resultant volume calculated as per Eq. D.15

The volume of any single section of the rotor, divided by the total volume (V_t) of the entire rotor, multiplied by the total mass (m) of the rotor, will result in the mass of that specific section of the rotor as given by Eq. D.16.

$$m = \frac{V}{V_t} 5kg \tag{D.16}$$

The mass of each section of the rotor in Fig. D. 9 is calculated according to Eq. D.16 and is shown in Table D.4.

Mass 1 (kg)	**Mass 2** (kg)	**Mass (3)** (kg)	**Mass 4** (kg)	**Mass 5** (kg)	**Total mass** (kg)
0.1028	0.164	4.3691	0.164	0.19966	4.999

Table D.4: Resultant mass calculated as per Eq. D.16

The moment of inertia (J) for a solid cylinder is given by Eq. D.17.

$$J = \frac{1}{2} mr^2 \tag{D.17}$$

The moment of inertia of each section of the rotor in Fig. D. 9 is calculated according to Eq. D.17 and the results are shown in Table D.5.

Inertia 1 ($kg.m^2$)	Inertia 2 ($kg.m^2$)	Inertia 3 ($kg.m^2$)	Inertia 4 ($kg.m^2$)	Inertia 5 ($kg.m^2$)	Total Inertia ($kg.m^2$)
8.03×10^{-6}	2.51×10^{-5}	4.623×10^{-3}	2.51×10^{-5}	1.957×10^{-5}	0.0047

Table D.5: Resultant inertia calculated as per Eq. D.17

This method is also accurate but can not be used on large induction machines as it is difficult to dismantle a large induction machine.

D.5 Frictional damping Coefficient - *B*

The frictional dampening coefficient is calculated according to Eq. D.18.

$$B = \frac{T_{wf}}{\omega_r} = \frac{0.146}{157} = 0.00093 Nms/rad \quad \text{(D.18)}$$

Eq. D.18 finds *B* at no load speed only. *B* varies since the torque due to windage and friction varies with changes in speed.

D.6 Final measured induction machine parameters

Measured parameters		
Parameter name	**Parameter symbol**	**Value**
Stator resistance	R_1	2.3 Ω
Referred rotor resistance	R_2'	1.440199 Ω
Stator leakage inductance	L_1	0.01111 H
Referred rotor leakage inductance	L_2'	0.01111 H
Magnetising resistance	R_m	605.55 Ω
Mutual inductance	L_m	0.187 H
Inertia - Method 1	J	0.00459 kg-m^2
Inertia - Method 2	J	0.0047 kg-m^2
Frictional damping coefficient	B	0.00093 N.m.s/rad

Table D.6: Measured machine parameters

APPENDIX E

MATLAB EMBEDDED FUNCTIONS

This appendix presents the C code that was written into the embedded Simulink simulation blocks. The code used to simulate the theoretical fan, the 1.1 kW fan and the 785 kW fan are shown in sections E.1 to E.3 respectively. In section E.4 the C code that was written into the cost of energy calculation block is shown.

E.1 Theoretical fan

Torque-Speed

Variable speed

```
function [torque, power] = Speed_reg(speed,time)
% This block supports an embeddable subset of the MATLAB language.
% See the help menu for details.

power=0;                              % initializing variable to zero
torque=0;                             % initializing variable to zero
speedrpm=0;                           % initializing variable to zero
flow=0;                               % initializing variable to zero

if time < 0.005
    speed=1;
else
speedrpm=speed*(60/(2*pi));           % Converts rad/s to rpm
torque=(10.85/(1400^2))*(speedrpm^2);% Equation of the torque-speed
                                      % curve (Fig. 6.1)
power=power*1000;                     % kilowatts to Watts
torque=power/speed;
end
```

Power-Flow

Variable speed

```
function [torque, power, flow] = Speed_reg(speed,time)
% This block supports an embeddable subset of the MATLAB language.
% See the help menu for details.

power=0;                              % initializing variable to zero
torque=0;                             % initializing variable to zero
speedrpm=0;                           % initializing variable to zero
flow=0;                               % initializing variable to zero

if time < 0.005
    speed=1;
else
speedrpm=speed*(60/(2*pi));
flow=(2.38/1400)*speedrpm;            % Equation of the speed-flow
                                      % curve
power=power*1000;                     % kilowatts to Watts
power=torque*speed;
end
```

Fixed speed

```
function [torque,power] = Damper_operation(speed,time,flow)
% This block supports an embeddable subset of the MATLAB language.
% See the help menu for details.

power=0;                              % initializing variable to zero
torque=0;                             % initializing variable to zero

if time < 0.005
    speed=1;
else
power = -0.1837*(flow^2) + 0.7616*flow +0.8145; % Equation of the
                                      % power-flow curve (Fig. 6.2)
power=power*1000;                     % kilowatts to Watts
torque=power/speed;
end
```

E.2 1.1 kW fan

Torque-Speed

Variable speed

```
function [torque, power, flow] = Speed_reg(speed,time)
% This block supports an embeddable subset of the MATLAB language.
% See the help menu for details.

power=0;                              % initializing variable to zero
torque=0;                             % initializing variable to zero
speedrpm=0;                           % initializing variable to zero

if time < 0.005
    speed=1;
else
speedrpm=speed*(60/(2*pi));           % Converts rad/s to rpm
torque=3E-6*(speedrpm^2)+0.002*speedrpm+0.1928; % Equation of the
                                      % torque-speed curve (Fig. 7.12)
end
```

Power-Flow

Variable speed

```
function [torque, power, flow] = Speed_reg(speed,time)
% This block supports an embeddable subset of the MATLAB language.
% See the help menu for details.

power=0;                              % initializing variable to zero
torque=0;                             % initializing variable to zero
speedrpm=0;                           % initializing variable to zero
flow=0;                               % initializing variable to zero

if time < 0.005
    speed=1;
else
speedrpm=speed*(60/(2*pi));           % Converts rad/s to rpm
```

```
flow=((speedrpm-47.6)/658.43);      % Equation of the speed-flow curve
                                    % (Fig. 9.35)
power= -0.2692*(flow^3)+0.9933*(flow^2)-0.5503*flow+0.2318; % Equation
                                    %of the power-flow curve(Fig.7.13)
power=power*1000;                   % kilowatts to Watts
torque=power/speed;
end
```

Fixed speed

```
function [torque,power] = Damper_operation(speed,flow,time)
% This block supports an embeddable subset of the MATLAB language.
% See the help menu for details.

power=0;                            % initializing variable to zero
torque=0;                           % initializing variable to zero

if time < 0.005
    speed=1;
else
power = -0.0779*(flow^2) + 0.2766*flow - 0.7533; % Equation of the
                                    % power-flow curve (Fig. 7.13)
power=power*1000;                   % kilowatts to Watts
torque=power/speed;
end
```

E.3 785 kW fan

Torque-Speed

Variable speed

```
function [torque, power] = Speed_reg(speed,time)
% This block supports an embeddable subset of the MATLAB language.
% See the help menu for details.

power=0;                            % initializing variable to zero
torque=0;                           % initializing variable to zero
```

```
speedrpm=0;                          % initializing variable to zero
flow=0;                              % initializing variable to zero

if time < 0.005
    speed=1;
else
speedrpm=speed*(60/(2*pi));          % Converts rad/s to rpm
torque= 7E-6*(speedrpm^2)+0.001*speedrpm-0.673; % Equation of the
                                     torque-speed curve (Fig. 8.9)
power=power*1000;                    % kilowatts to Watts
torque=power/speed;
end
```

Power-Flow

Variable speed

```
function [torque, power, flow] = Speed_reg(speed,time)
% This block supports an embeddable subset of the MATLAB language.
% See the help menu for details.

power=0;                             % initializing variable to zero
torque=0;                            % initializing variable to zero
speedrpm=0;                          % initializing variable to zero
flow=0;                              % initializing variable to zero

if time < 0.005
    speed=1;
else

speedrpm=speed*(60/(2*pi));          % Converts rad/s to rpm
flow=((speedrpm-343.36)/2.4027);     % Equation of the speed-flow curve
power= 0.0000159*(flow^2)-0.0023*flow+0.34; % Equation of the power-
                                     % flow curve (Fig. 8.10)
power=power*1000;                    % kilowatts to Watts
torque=power/speed;
end
```

Fixed speed

```
function [torque,power] = Damper_operation(speed,flow,time)
% This block supports an embeddable subset of the MATLAB language.
% See the help menu for details.

power=0;                                % initializing variable to zero
torque=0;                               % initializing variable to zero

if time < 0.005
    speed=1;
else
power = -0.0000094*(flow^2) + 0.0077*flow+0.9988; % Equation of the
                                        % power-flow curve (Fig. 8.10)
power=power*1000;                       % kilowatts to Watts
torque=power/speed;
end
```

E.4 Energy cost calculation

```
function cost   = Cost_Calculation (time,energy)
% This block supports an embeddable subset of the MATLAB language.
% See the help menu for details.

cost1=0;                                % initializing variable to zero
cost2=0;                                % initializing variable to zero
cost3=0;                                % initializing variable to zero
cost4=0;                                % initializing variable to zero
cost5=0;                                % initializing variable to zero
cost6=0;                                % initializing variable to zero
cost7=0;                                % initializing variable to zero

kwh1=0;                                 % initializing variable to zero
kwh2=0;                                 % initializing variable to zero
kwh3=0;                                 % initializing variable to zero
kwh4=0;                                 % initializing variable to zero
kwh5=0;                                 % initializing variable to zero
```

```
kwh6=0;                                 % initializing variable to zero
kwh7=0;                                 % initializing variable to zero

energy2=0;                              % initializing variable to zero
energy3=0;                              % initializing variable to zero
energy4=0;                              % initializing variable to zero
energy5=0;                              % initializing variable to zero
energy6=0;                              % initializing variable to zero
energy7=0;                              % initializing variable to zero

if ((time>=0)&& (time<=30))             % 00hr-06hr
    kwh1 = energy,cost1 = kwh1*0.0906; % energy accumulation and off-
                                        % peak energy cost calculation
end

if ((time>=30)&& (time<=35))            % 06hr-07hr
energy2= energy,kwh2 = (1/2*(energy2-kwh1)),cost2 = kwh2*0.1667;
% energy accumulation and standard energy cost calculation
end

if ((time>=35)&& (time<=50))            % 07hr-10hr
energy3= energy,kwh3 = (1/2*(energy3-kwh2)),cost3 = kwh3*0.6304;
% energy accumulation and peak energy cost calculation
end

if ((time>=50)&& (time<=90))            % 10hr-18hr
energy4= energy,kwh4 = (1/2*(energy4-kwh3)),cost4 = kwh4*0.1667;
% energy accumulation and standard energy cost calculation
end

if ((time>=90)&& (time<=100))           % 18hr-20hr
energy5= energy,kwh5 = (1/2*(energy5-kwh4)),cost5 = kwh5*0.6304;
% energy accumulation and peak energy cost calculation
end

if ((time>=100)&& (time<=110))          % 20hr-22hr
energy6= energy,kwh6 = (1/2*(energy6-kwh5)),cost6 = kwh6*0.1667;
% energy accumulation and standard energy cost calculation
```

```
end

if ((time>=110)&& (time<=120))      % 22hr-24hr
energy7= energy,kwh7 = (1/2*(energy7-kwh6)),cost7 = kwh7*0.0906;
% energy accumulation and off-peak energy cost calculation
end

cost=cost1+cost2+cost3+cost4+cost5+cost6+cost7;
% final cost of energy for the day
end
```

APPENDIX F

SIMATIC STEP7 PROGRAMS

The programs written in the PLC to control both the test bed and the 1.1 kW fan system are shown in this Appendix. The PLC was programmed using Siemens Step7 software and the programming was done using both ladder logic and statement list languages. In Step7 the code is broken down into different Organisational Blocks (OB's), Functions (FC's), Data Blocks (DB's), Function Blocks (FB's), User Defined Data Types (UDT's), System Function Blocks (SFB's) and System Functions (SFC's). Only the code written in the OB's and FC's are presented below as this is where the main control programs are written. The DB's and UDT's are used for variable declaration and as data storage areas. The two FB's used for serial communication are freely available from Siemens. The SFB's and SFC's are special blocks that provide specific functionality also developed by Siemens.

F.1 Organisational Blocks

F.1.1 OB1 Cyclical execution block

SIMATIC mine data\SIMATIC 06/17/2008 04:06:18 PM
300(1)\CPU 315F-2 PN/DP\...\OB1 - <offline>

OB1 - <offline>

"CYCL_EXC" Cycle Execution
Name: OB1 Family:
Author: Ashvir.H Version: 0.1
Block version: 2
Time stamp Code: 06/17/2008 04:06:12 PM
Interface: 02/15/1996 04:51:12 PM
Lengths (block/logic/data):00624 00460 00022

Name	Data Type	Address	Comment
TEMP		0.0	
OB1_EV_CLASS	Byte	0.0	Bits 0-3 = 1 (Coming event), Bits 4-7 = 1 (Event class 1)
OB1_SCAN_1	Byte	1.0	1 (Cold restart scan 1 of OB 1), 3 (Scan 2-n of OB 1)
OB1_PRIORITY	Byte	2.0	Priority of OB Execution
OB1_OB_NUMBR	Byte	3.0	1 (Organization block 1, OB1)
OB1_RESERVED_1	Byte	4.0	Reserved for system
OB1_RESERVED_2	Byte	5.0	Reserved for system
OB1_PREV_CYCLE	Int	6.0	Cycle time of previous OB1 scan (milliseconds)
OB1_MIN_CYCLE	Int	8.0	Minimum cycle time of OB1 (milliseconds)
OB1_MAX_CYCLE	Int	10.0	Maximum cycle time of OB1 (milliseconds)
OB1_DATE_TIME	Date_And_Time	12.0	Date and time OB1 started

Block: OB1 "Main Program Sweep (Cycle)"

Network: 1

Compare integer

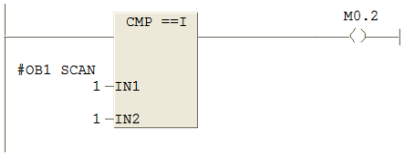

Network: 2

Call FC1

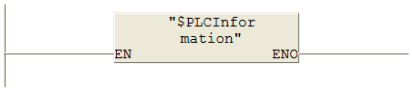

SIMATIC mine data\SIMATIC 06/17/2008 04:06:18 PM
300(1)\CPU 315F-2 PN/DP\...\OB1 - <offline>

Network: 3

Setting up power meter comms.

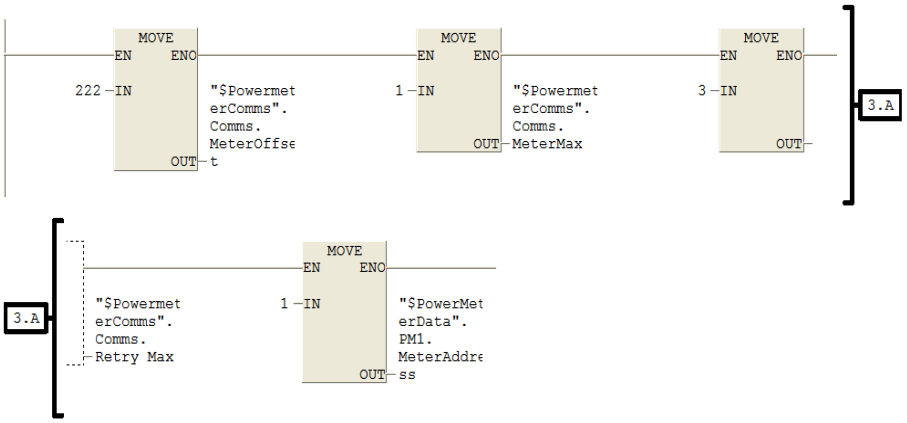

Network: 4 1 = Retrieve Demand Register Sets. DB & UDT MUST be set loaded.

Retrieve Demand Register Sets. DB & UDT MUST be set loaded.
Perform a time sync of the meter from the PLC Clock

SIMATIC mine data\SIMATIC 06/17/2008 04:06:18 PM
300(1)\CPU 315F-2 PN/DP\...\OB1 - <offline>

Network: 5

Setting Vmax, Imax, Pmax

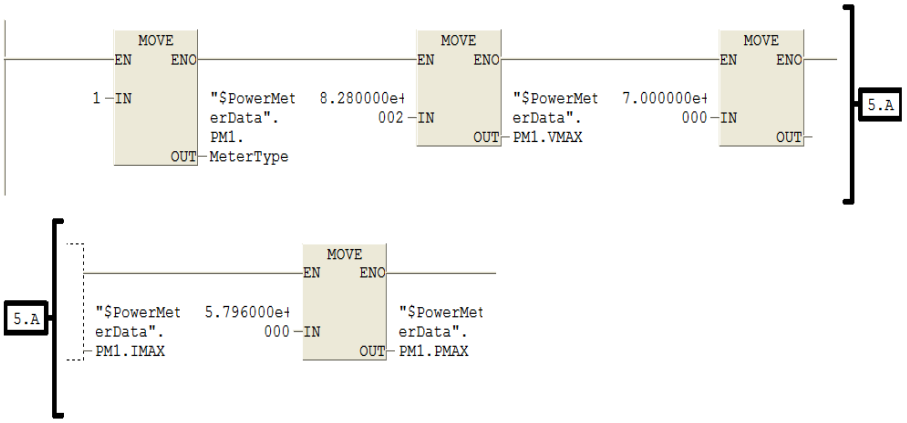

Network: 6 1 = Perform a time sync of the meter from the PLC Clock

Perform a time sync of the meter from the PLC Clock

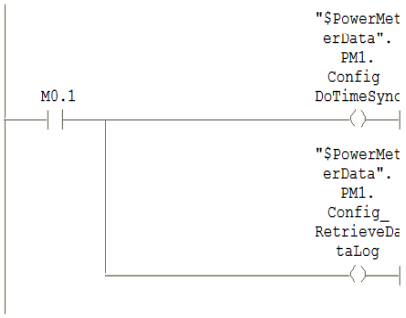

Network: 7

Call FC150

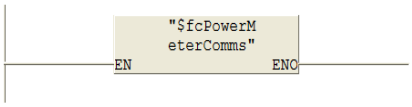

Network: 8

Call FC3

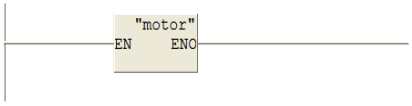

SIMATIC mine data\SIMATIC 06/17/2008 04:06:19 PM
300(1)\CPU 315F-2 PN/DP\...\OB1 - <offline>

Network: 9

Call FC6 if switch is OFF

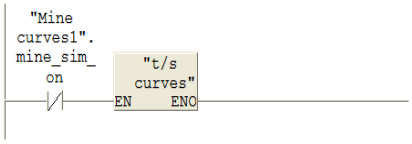

Network: 10

Call FC8

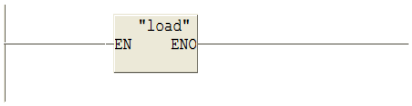

Network: 11

Call FC9

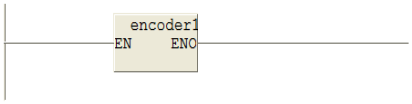

Network: 12

Call FC10

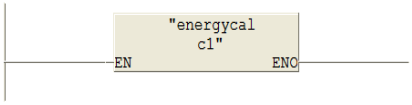

Network: 13

Call FC5

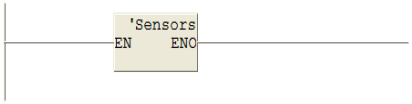

Network: 14

Call FC7 if switch is OFF

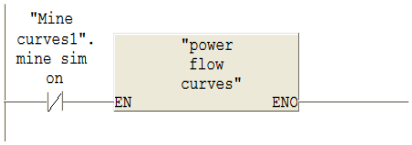

SIMATIC mine data\SIMATIC 06/17/2008 04:06:19 PM
300(1)\CPU 315F-2 PN/DP\...\OB1 - <offline>

Network: 15

Call FC23

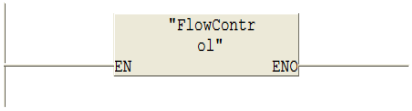

Network: 16

Call FC24

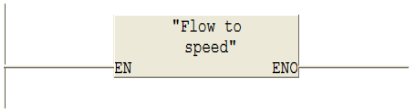

Network: 17

Call FC12

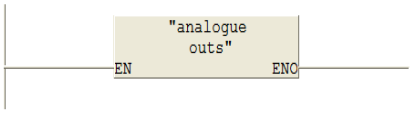

Network: 18

Call FC14 if switch is ON

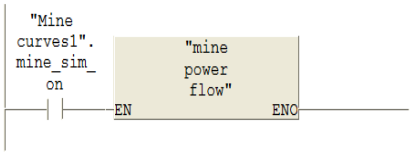

F.1.2 OB35 Cyclical interrupt block

SIMATIC mine data\SIMATIC 12/08/2008 10:48:57 PM
300(1)\CPU 315F-2 PN/DP\...\OB35 - <offline>

OB35 - <offline>

"CYC_INT5" Cyclic Interrupt 5
Name: OB35 Family:
Author: Ashvir.H Version: 0.1
Block version: 2
Time stamp Code: 12/08/2008 10:47:57 PM
Interface: 02/15/1996 04:51:11 PM
Lengths (block/logic/data):00556 00410 00022

Name	Data Type	Address	Comment
TEMP		0.0	
OB35_EV_CLASS	Byte	0.0	Bits 0-3 = 1 (Coming event), Bits 4-7 = 1 (Event class 1)
OB35_STRT_INF	Byte	1.0	16#36 (OB 35 has started)
OB35_PRIORITY	Byte	2.0	Priority of OB Execution
OB35_OB_NUMBR	Byte	3.0	35 (Organization block 35, OB35)
OB35_RESERVED_1	Byte	4.0	Reserved for system
OB35_RESERVED_2	Byte	5.0	Reserved for system
OB35_PHASE_OFFSET	Word	6.0	Phase offset (msec)
OB35_RESERVED_3	Int	8.0	Reserved for system
OB35_EXC_FREQ	Int	10.0	Frequency of execution (msec)
OB35_DATE_TIME	Date_And_Time	12.0	Date and time OB35 started

Block: OB35 "Cyclic Interrupt 10ms"

Network: 1 Torque ramped down

Ramp torque, torque-speed curve
Ramp from 8.46 to 4.49
When click for damper control in SCADA set DB53.DBD54 to 8.46
Damper button in SCADA reset DB53.DBX52.0 and reset DB53.DBX52.1
Flow will decrease to 0.68 and then speed regulation will occur

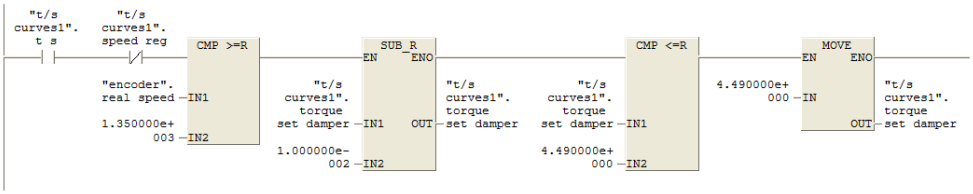

SIMATIC mine data\SIMATIC 12/08/2008 10:48:57 PM
300(1)\CPU 315F-2 PN/DP\...\OB35 - <offline>

Network: 2 1.1 kW system - Flow ramped down

Ramp flow for power Vs flow damper y = -0.0779x2 + 0.2766x + 0.7533
Ramp from 2.19 to 0.68
Click for damper control on scada set DB57.DBD12 to 2.19
Damper button in SCADA reset DB53.DBX52.0 and reset DB53.DBX52.1
Flow will decrease to 0.68

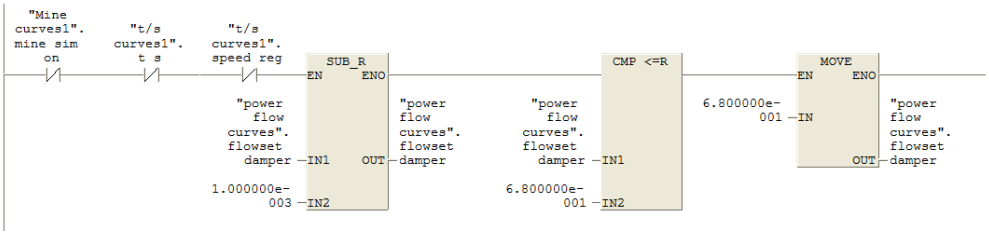

Network: 3 785 kW system - flow ramped down

Ramp flow for power Vs flow damper control from 454.34 to 365

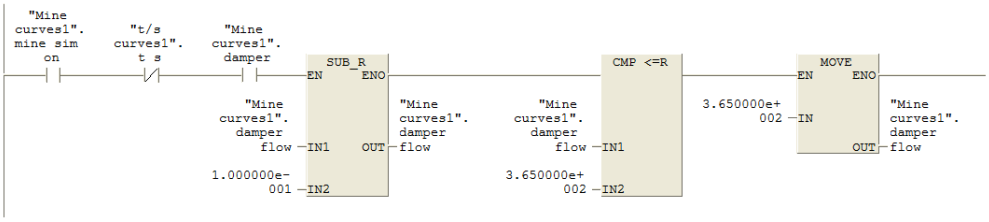

Network: 4

Cycle time max = 15 and interrupt =10 ms every 150ms perform function

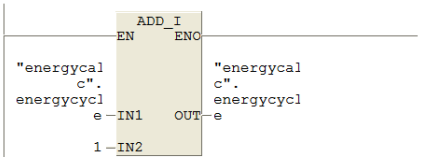

SIMATIC mine data\SIMATIC 12/08/2008 10:48:57 PM
300(1)\CPU 315F-2 PN/DP\...\OB35 - <offline>

Network: 5

Accumalate the energy used

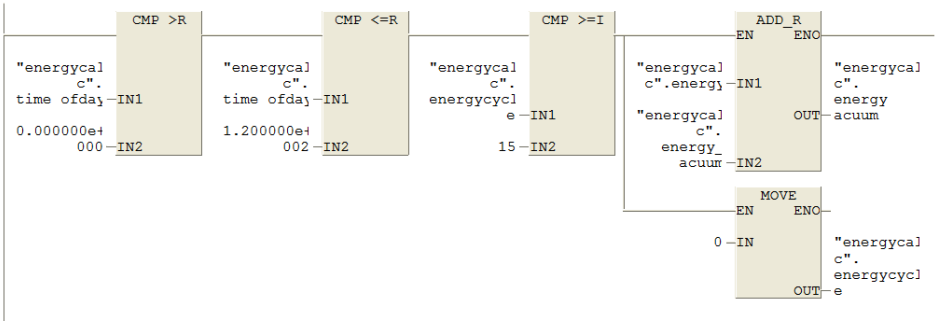

F.2 Functions

F.2.1 FC1 PLC information

SIMATIC mine data\SIMATIC 06/17/2008 02:39:50 PM
300(1)\CPU 315F-2 PN/DP\...\FC1 - <offline>

FC1 - <offline>

"$PLCInformation"
Name: FC1 **Family:**
Author: Ashvir.H **Version:** 0.1
Block version: 2
Time stamp Code: 06/15/2008 11:07:58 PM
Interface: 03/02/2006 10:18:33 AM
Lengths (block/logic/data): 00816 00580 00054

Name	Data Type	Address	Comment
IN		0.0	
OUT		0.0	
IN_OUT		0.0	
TEMP		0.0	
tINT1	Int	0.0	
Temp_word	Word	2.0	
Temp_busy	Bool	4.0	
tDINT1	DInt	6.0	
tDiNT2	DInt	10.0	
tDINT3	DInt	14.0	
tDINT4	DInt	18.0	
INT5	DInt	22.0	
INT6	DInt	26.0	
Temp_INT1	Int	30.0	
Temp_INT2	Int	32.0	
Temp_DINT1	DInt	34.0	
tempdt	Date_And_Time	38.0	
RETURN		0.0	
RET_VAL		0.0	

Block: FC1 PLC time and date information

Network: 1

Logic_0 and Logic_1

Network: 2

One second pulse M1.0

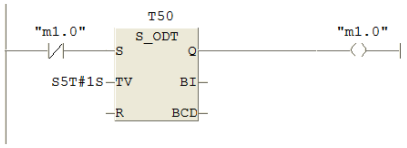

SIMATIC mine data\SIMATIC 06/17/2008 02:39:50 PM
300(1)\CPU 315F-2 PN/DP\...\FC1 - <offline>

Network: 3

Read PLC Date and Time

```
L     T      1
T     DB1.DBD   96
R     T      1
```

Network: 4

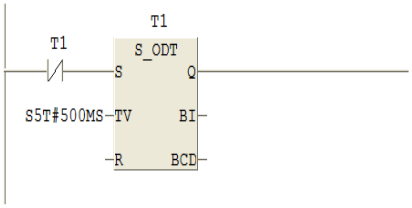

Network: 5

Read PLC clock

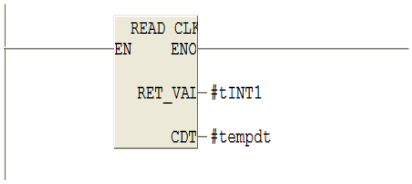

SIMATIC mine data\SIMATIC 06/17/2008 02:39:50 PM
300(1)\CPU 315F-2 PN/DP\...\FC1 - <offline>

Network: 6

Get PLC information

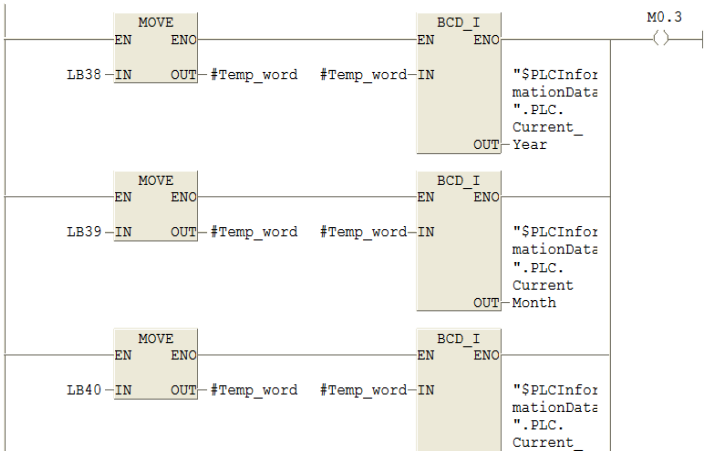

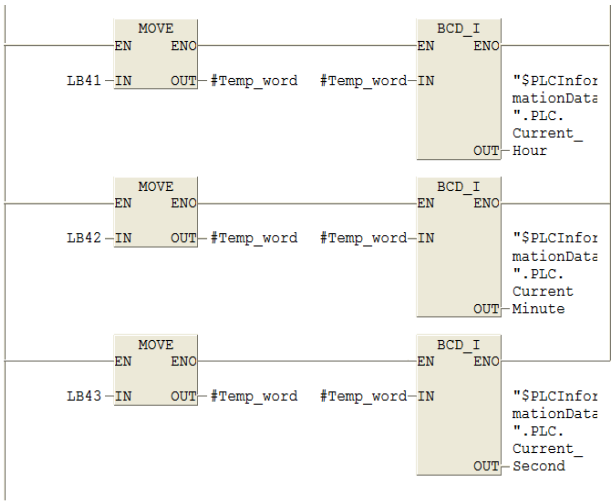


```
Network: 7
Get Hours,Minutes,Seconds and Convert to HHMMSS

      OPN   "$PLCInformationData"

      L     DBW   16
      T     #tDINT1

      L     DBW   18
      T     #tDiNT2

      L     DBW   20
      T     #tDINT3

      L     #tDINT1
      L     L#10000
      *D
      T     #tDINT1

      L     #tDiNT2
```

```
SIMATIC                          mine data\SIMATIC              06/17/2008 02:39:50 PM
                        300(1)\CPU 315F-2 PN/DP\...\FC1 - <offline>

      L     L#100
      *D
      T     #tDiNT2

      L     #tDINT1
      L     #tDiNT2
      +D
      L     #tDINT3
      +D
      T     DBD   34
```

```
Network: 8
Get year,month & day and Convert to YYYYMMDD

      OPN   "$PLCInformationData"


      L     DBW   10
      T     #tDINT4

      L     DBW   12
      T     #INT5

      L     DBW   14
      T     #INT6

      L     #tDINT4
      L     L#10000
      *D
      T     #tDINT4
      L     #tDINT4
      L     L#20000000
      +D
```

```
      T     #tDINT4

      L     #INT5
      L     L#100
      *D
      T     #INT5

      L     #tDINT4
      L     #INT5
      +D
      L     #INT6
      +D
      T     DBD   30
```

Network: 9

Set data and time, M100.0 being the time sync bit

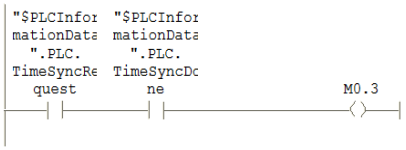

Network: 10

F.2.2 FC 3 Control of the Fan machine and Test bed Machine1

FC3 - <offline>

"motor"
Name: FC2 **Family:**
Author: Ashvir.H **Version:** 0.1
Block version: 2
Time stamp Code: 06/17/2008 03:09:34 PM
Interface: 09/18/2007 10:50:35 PM
Lengths (block/logic/data): 00564 00428 00000

Name	Data Type	Address	Comment
IN		0.0	
OUT		0.0	
IN_OUT		0.0	
TEMP		0.0	
RETURN		0.0	
RET_VAL		0.0	

Block: FC3 Fan motor or Test Bed Motor1 control

Network: 1

Motor Initialised via PROFIBUS

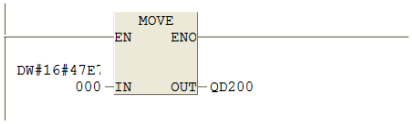

Network: 2

Motor ON via PROFIBUS

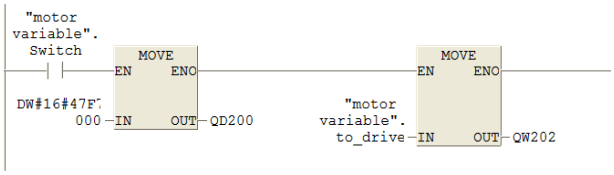

Network: 3

Speed setpoint

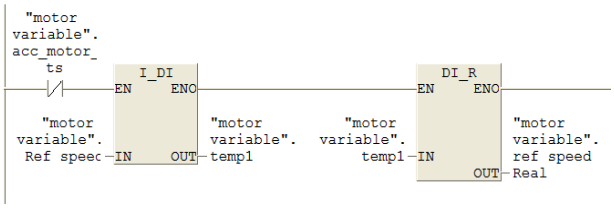

SIMATIC mine data\SIMATIC 06/17/2008 03:09:44 PM
300(1)\CPU 315F-2 PN/DP\...\FC3 - <offline>

Network: 4

Motor slip

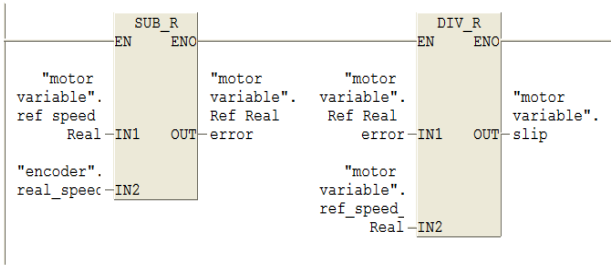

Network: 5

Accelerate motor for 1.1 kW torque-speed characteristic

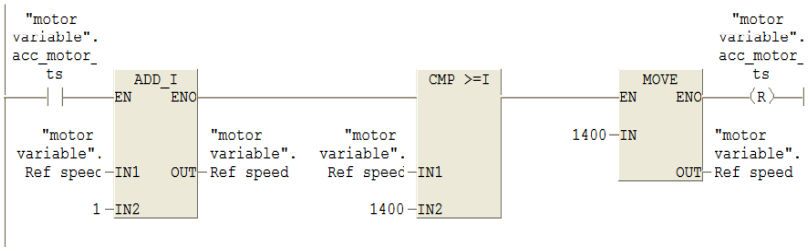

Network: 6

Accelerate motor for ~1.1 kW or ~785 kW power-flow characteristic

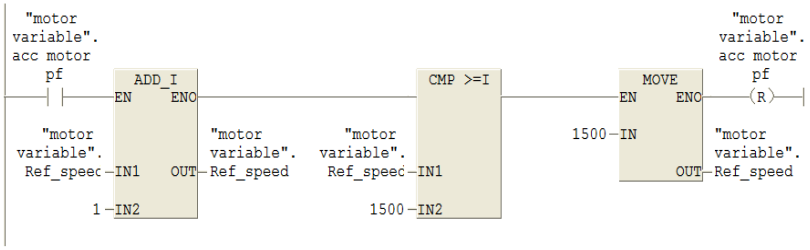

Network: 7

Send speed setpoint to VSD1 via PROFIBUS

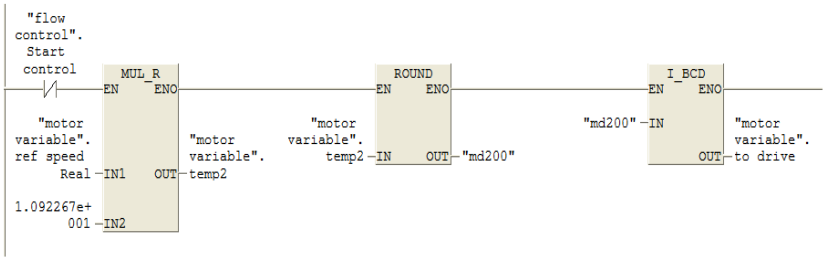

F.2.3 FC 5 Fan pressure and velocity sensors

SIMATIC mine data\SIMATIC 06/17/2008 02:43:20 PM
300(1)\CPU 315F-2 PN/DP\...\FC5 - <offline>

FC5 - <offline>

"Sensors"
Name: FC5 **Family:**
Author: Ashvir.H **Version:** 0.1
Block version: 2
Time stamp Code: 06/17/2008 02:43:11 PM
Interface: 01/31/2008 12:48:53 PM
Lengths (block/logic/data): 00578 00442 00036

Name	Data Type	Address	Comment
IN		0.0	
OUT		0.0	
IN_OUT		0.0	
TEMP		0.0	
static	Real	0.0	
flow	Real	4.0	
velocity	Real	8.0	
anaflow	Real	12.0	
anaspeed	Real	16.0	
anaspeed1	Real	20.0	
RETURN		0.0	
RET_VAL		0.0	

Block: FC5 Fan Pressure and Velocity sensors

Network: 1

Static pressure and Velocity pressure displayed value forced to zero should the fan be OFF.

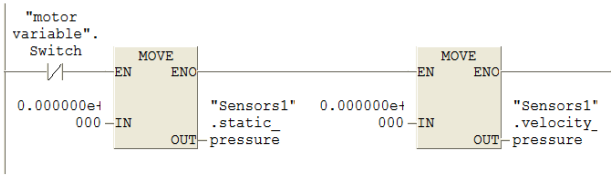

Network: 2 Air Velocity

Air Velocity received via Analogue interface
Offset by 2.19667=4mA

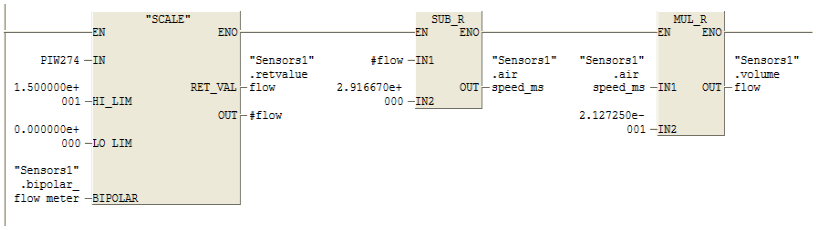

SIMATIC mine data\SIMATIC 06/17/2008 02:43:20 PM
300(1)\CPU 315F-2 PN/DP\...\FC5 - <offline>

Network: 3 Static pressure

Static pressure received via Analogue interface
Offset by 254=4mA

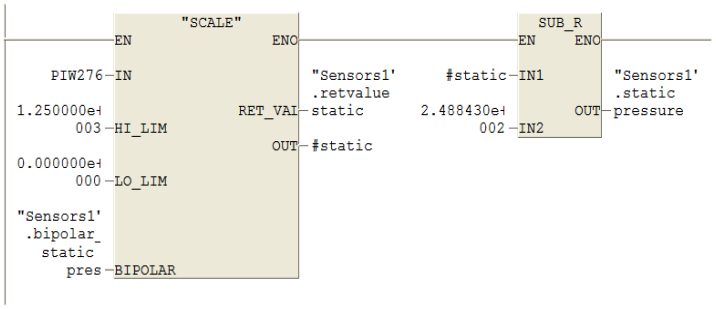

Network: 4 Velocity pressure

Velocity pressure received via Analogue interface
Offset by 219=4mA

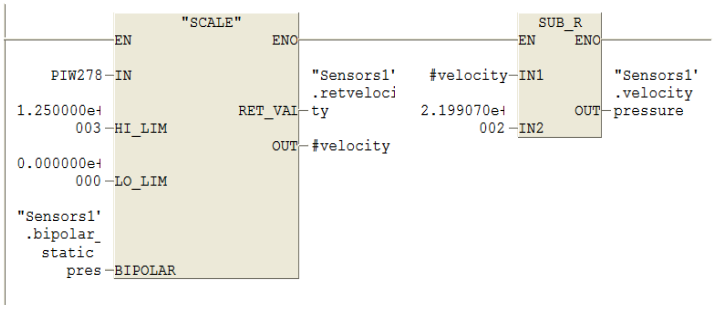

Network: 5

Total pressure = Static pressure + Velocity pressure

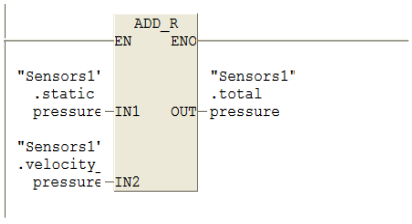

F.2.4 FC 7 Replication of the 1.1 kW fans power flow characteristic

SIMATIC mine data\SIMATIC 06/17/2008 04:03:34 PM
300(1)\CPU 315F-2 PN/DP\...\FC7 - <offline>

FC7 - <offline>

"power_flow curves"
Name: FC7 Family:
Author: Ashvir.H Version: 0.1
Block version: 2
Time stamp Code: 06/17/2008 04:03:07 PM
Interface: 02/13/2008 09:32:00 PM
Lengths (block/logic/data):01530 01304 00074

Name	Data Type	Address	Comment
IN		0.0	
OUT		0.0	
IN_OUT		0.0	
TEMP		0.0	
flow_squared	Real	0.0	
flow_cube	Real	4.0	
part1_eq2	Real	8.0	
part2_eq2	Real	12.0	
part3_eq2	Real	16.0	
temp_eq2	Real	20.0	
temp1_eq2	Real	24.0	
temp1	Real	28.0	
temp2	Real	32.0	
damper_flow_sq	Real	36.0	
part1_eq3	Real	40.0	
part2_eq3	Real	44.0	
temp_eq3	Real	48.0	
temp3	Real	52.0	
temp4	Real	56.0	
temp_eq1	Real	60.0	
flowpntreg	Real	64.0	
scale1	Real	68.0	
TEMP0	Bool	72.0	
RETURN		0.0	
RET_VAL		0.0	

Block: FC7 1.1 kW Power-flow

Network: 1 Speed to flow

Any speed value will give the equivalent flow rate according to the speed vs
flow y = 658.43x + 47.6 equation (Eq1).
Flow rate known-put flow rate in Eq2 to get the equivalent power
Power = Tw send torque setpoint to VSD2.

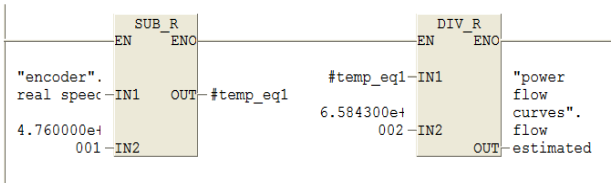

SIMATIC mine data\SIMATIC 06/17/2008 04:03:34 PM
300(1)\CPU 315F-2 PN/DP\...\FC7 - <offline>

Network: 2 Speed regulation

Equation for Power Vs Flow
Eq 2 :y = -0.2692x3 + 0.9933x2 - 0.5503x + 0.2318

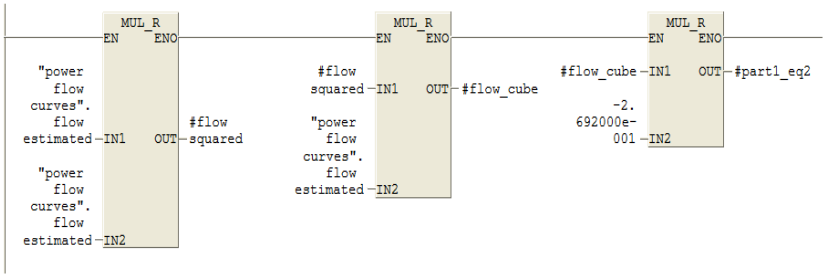

Network: 3 Speed regulation

Eq 2 :y = -0.2692x3 + 0.9933x2 - 0.5503x + 0.2318

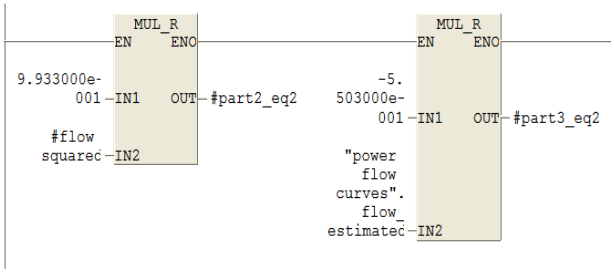

Network: 4 Speed regulation

Eq 2 :y = -0.2692x3 + 0.9933x2 - 0.5503x + 0.2318
Adding the different parts of the Eq2 from network 2 and network 3

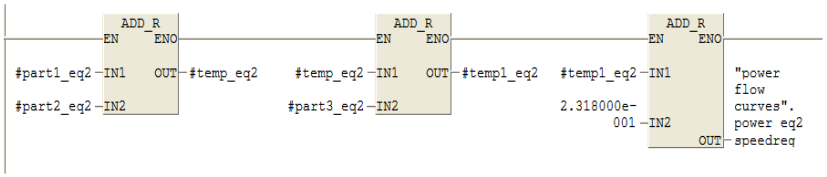

Network: 5 Speed regulation

Power= Torque*Speed
Power calculated in network 4

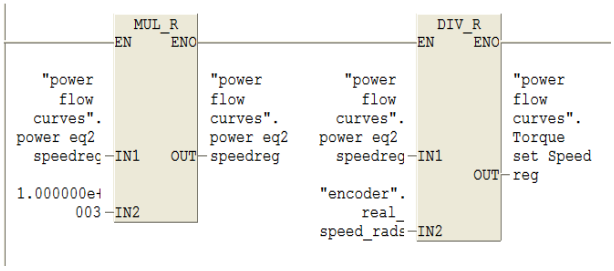

SIMATIC mine data\SIMATIC 06/17/2008 04:03:34 PM
300(1)\CPU 315F-2 PN/DP\...\FC7 - <offline>

Network: 6 Speed regulation

Sending torque from Network 5 to VSD2

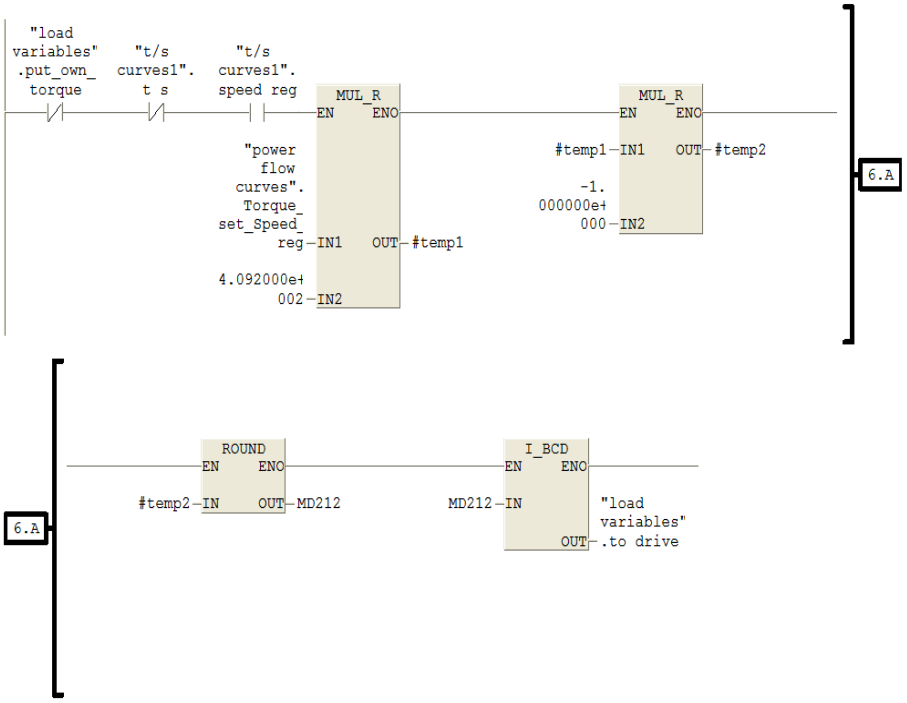

Network: 7 Damper control

Flow is decremented in OB35 network 2
Eq 3: y = -0.0779x2 + 0.2766x + 0.7533

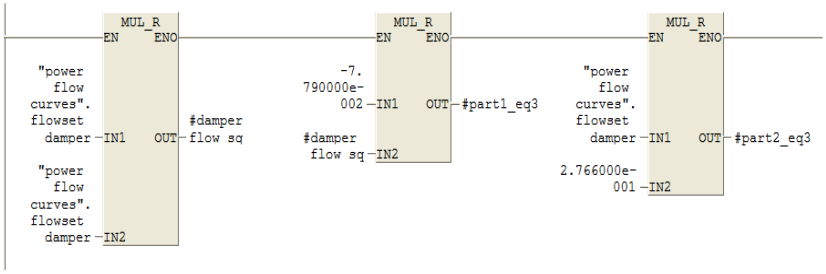

Network: 8 Damper control

eq 3: y = -0.0779x2 + 0.2766x + 0.7533
Adding the different parts of Eq3

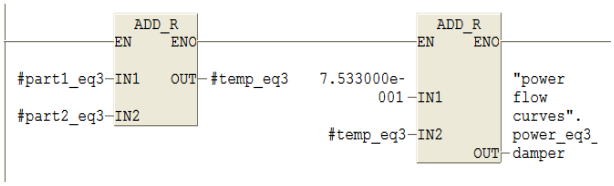

SIMATIC mine data\SIMATIC 06/17/2008 04:03:34 PM
300(1)\CPU 315F-2 PN/DP\...\FC7 - <offline>

Network: 9 Damper control

Power= Torque*Speed
Power from network 8

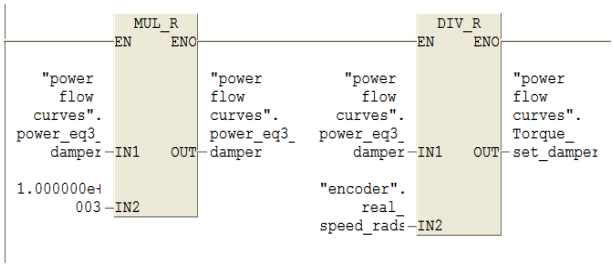

SIMATIC mine data\SIMATIC 06/17/2008 04:03:34 PM
300(1)\CPU 315F-2 PN/DP\...\FC7 - <offline>

Network: 10 Damper control

Sending torque from network 9 to VSD2

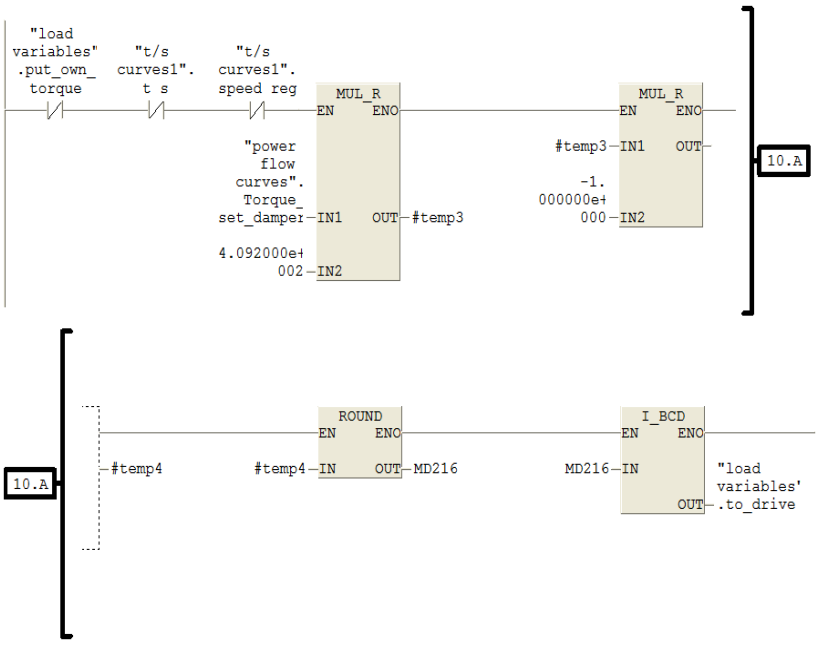

SIMATIC mine data\SIMATIC 06/17/2008 04:03:34 PM
300(1)\CPU 315F-2 PN/DP\...\FC7 - <offline>

Network: 11 Scaling for the white dot in SCADA

Speed regulation-1.1 kW simulation
DB57.DBD0
x=320

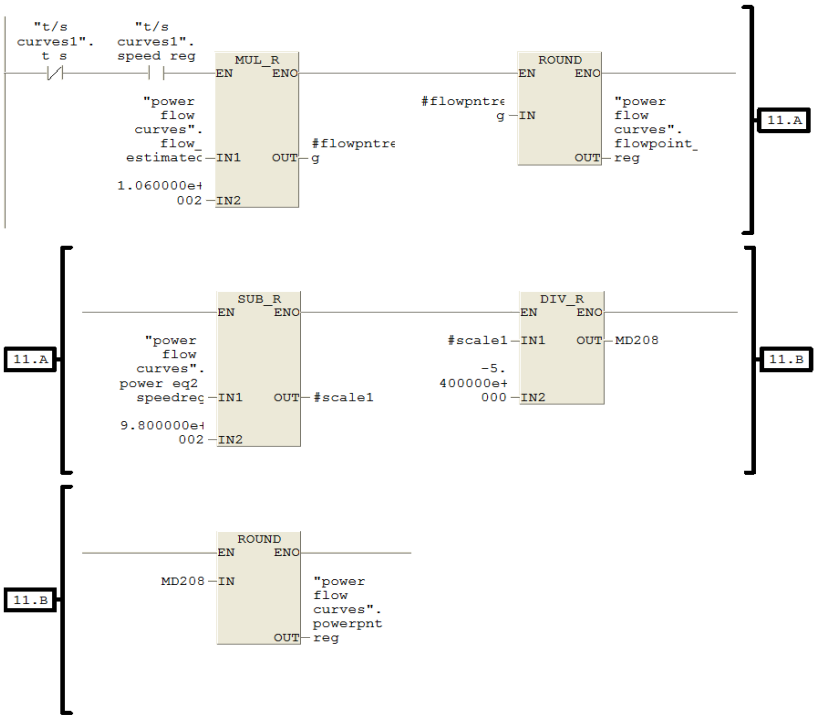

SIMATIC mine data\SIMATIC 06/17/2008 04:03:34 PM
300(1)\CPU 315F-2 PN/DP\...\FC7 - <offline>

Network: 12 Scaling for the white dot in SCADA

Damper control - 1.1 kW simulation
DB57.DBD0
x=320

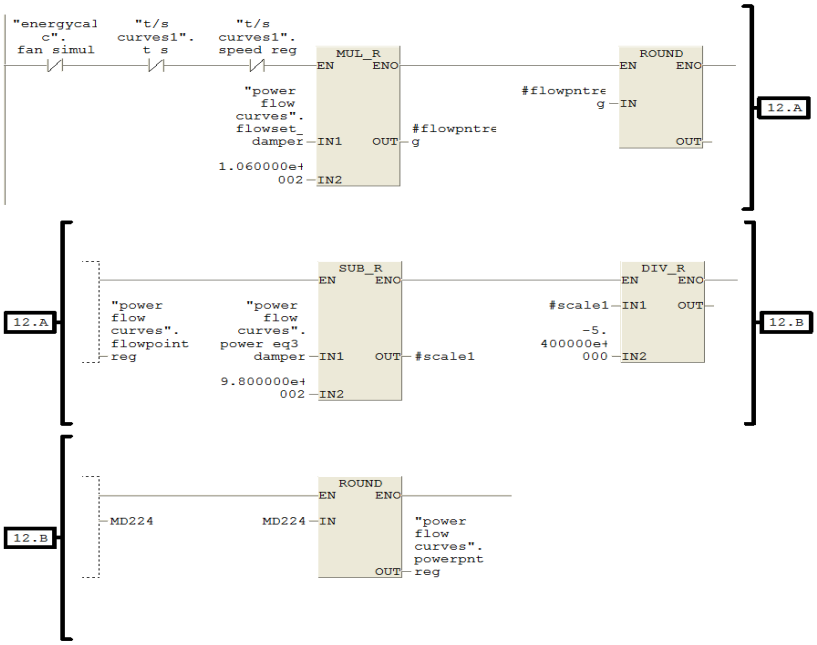

SIMATIC mine data\SIMATIC 06/17/2008 04:03:34 PM
300(1)\CPU 315F-2 PN/DP\...\FC7 - <offline>

Network: 13 Scaling for the white dot in SCADA

Speed regulation and Damper control-Actual fan
DB57.DBD0
x=320

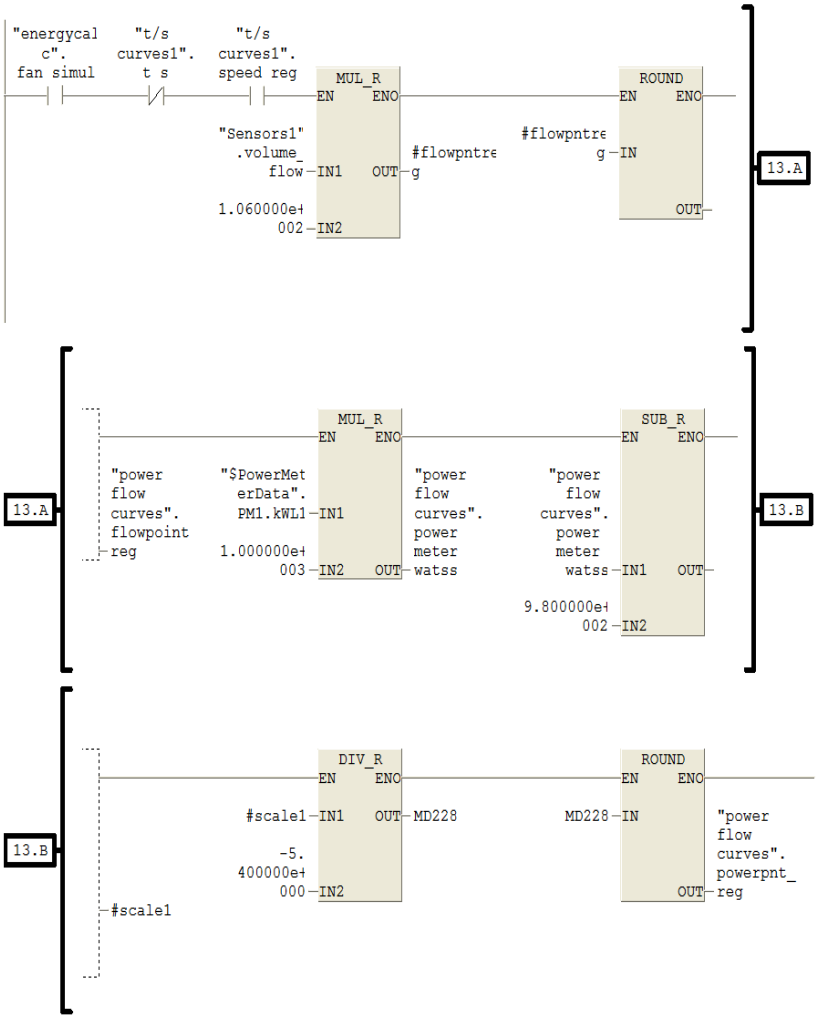

Network: 14

Converting power to watts from kW

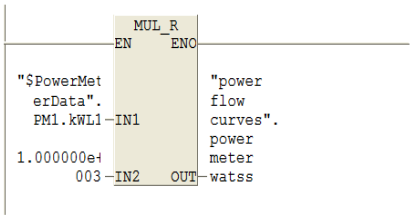

F.2.5 FC 8 Control of the Test bed Machine2

SIMATIC mine data\SIMATIC 06/17/2008 03:14:36 PM
300(1)\CPU 315F-2 PN/DP\...\FC8 - <offline>

FC8 - <offline>

"load"
Name: FC8 Family:
Author: Ashvir.H Version: 0.1
Block version: 2
Time stamp Code: 06/17/2008 02:54:48 PM
Interface: 09/18/2007 10:48:38 PM
Lengths (block/logic/data):00376 00236 00000

Name	Data Type	Address	Comment
IN		0.0	
OUT		0.0	
IN_OUT		0.0	
TEMP		0.0	
RETURN		0.0	
RET_VAL		0.0	

Block: FC8 Load - Motor2 in the test bed system

Network: 1

Load Initialised via PROFIBUS

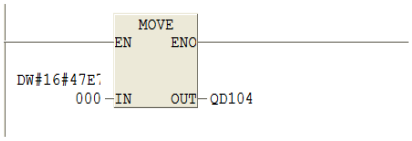

Network: 2

Load ON via PROFIBUS

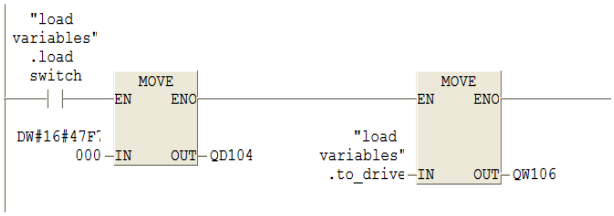

SIMATIC mine data\SIMATIC 06/17/2008 03:14:36 PM
300(1)\CPU 315F-2 PN/DP\...\FC8 - <offline>

Network: 3

User defined torque setpoint sent to VSD2

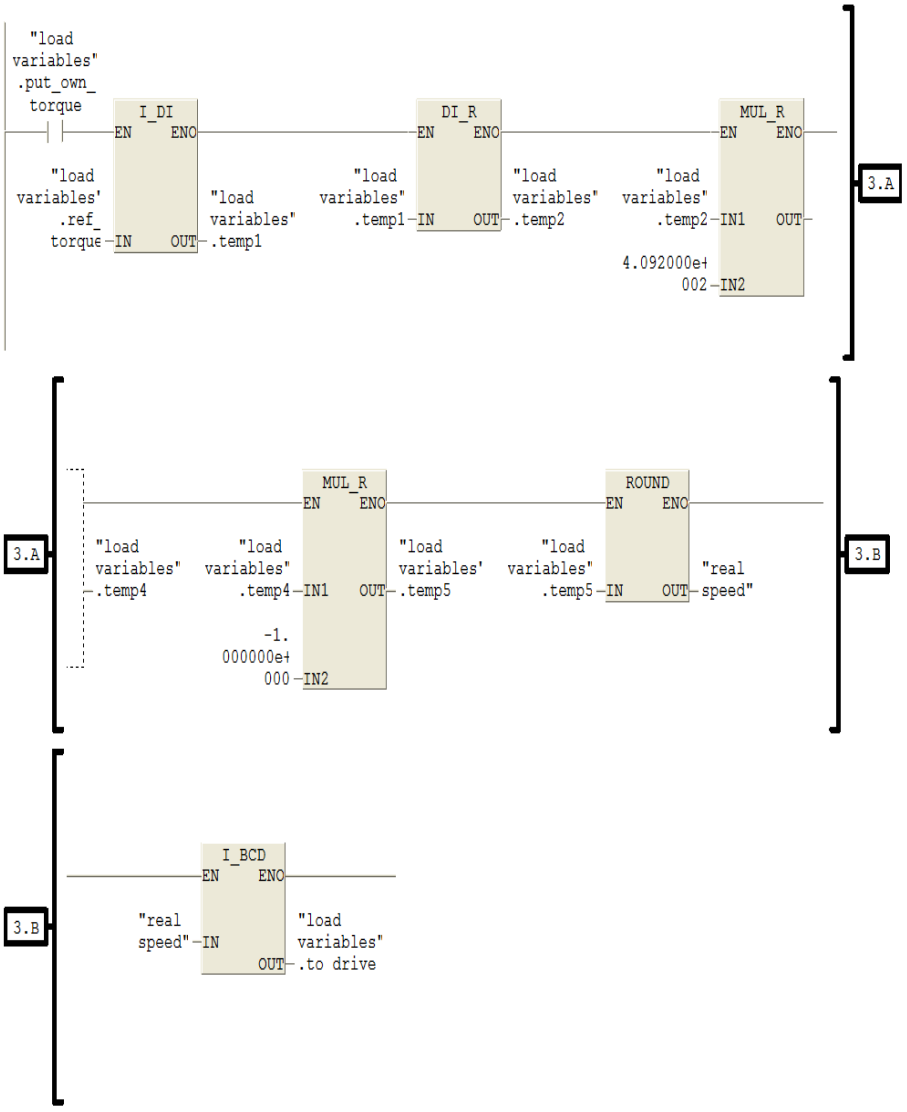

F.2.6 FC 9 High Speed Counter Control to evaluate the encoder signals

SIMATIC mine data\SIMATIC 06/17/2008 04:04:39 PM
300(1)\CPU 315F-2 PN/DP\...\FC9 - <offline>

FC9 - <offline>

"encoder1"
Name: FC9 **Family:**
Author: Ashvir.H **Version:** 0.1
Block version: 2
Time stamp Code: 06/15/2008 11:12:25 PM
Interface: 10/12/2007 02:24:50 PM
Lengths (block/logic/data): 00498 00398 00006

Name	Data Type	Address	Comment
IN		0.0	
OUT		0.0	
IN_OUT		0.0	
TEMP		0.0	
RETURN		0.0	
RET_VAL		0.0	

Block: FC9

Network: 1

Contol the High Speed Counter module

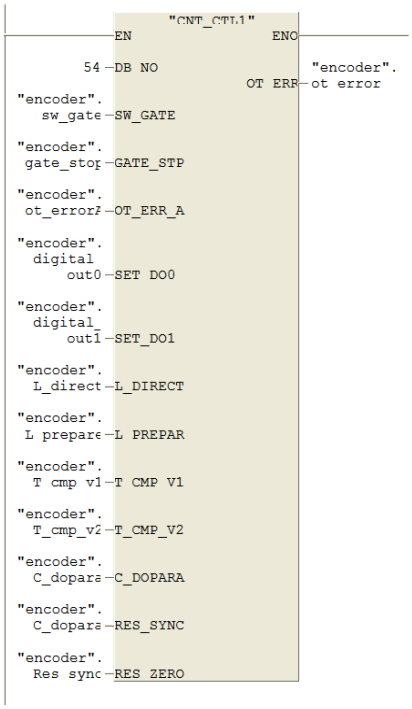

SIMATIC mine data\SIMATIC 06/17/2008 04:04:39 PM
300(1)\CPU 315F-2 PN/DP\...\FC9 - <offline>

Network: 2

Actual speeed

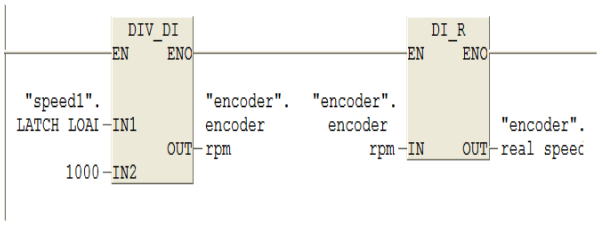

Network: 3

Actual frequency

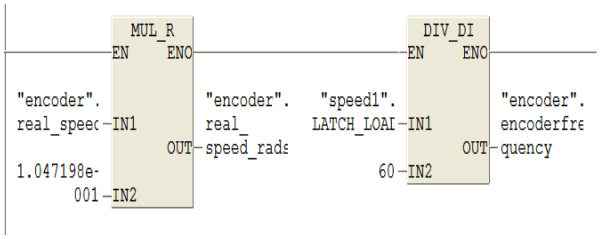

F.2.7 FC 10 Energy calculation per weekday

FC10 - <offline>
"energycalc1"
Name: FC10 **Family:**
Author: Ashvir.H **Version:** 0.1
Block version: 2
Time stamp Code: 06/17/2008 03:08:52 PM
Interface: 01/28/2008 06:40:04 PM
Lengths (block/logic/data): 02400 02142 00034

Name	Data Type	Address	Comment
IN		0.0	
OUT		0.0	
IN_OUT		0.0	
TEMP		0.0	
temp	Int	0.0	
temp1	DInt	2.0	
temp2	Real	6.0	
costtemp	Real	10.0	
costtemp1	Real	14.0	
costtemp2	Real	18.0	
costtemp3	Real	22.0	
costtemp4	Real	26.0	
powerinkw	Real	30.0	
RETURN		0.0	
RET_VAL		0.0	

Block: FC10 Cost of energy calculations

Network: 1

Sets up count for 2 mins equivalent to 24 hrs

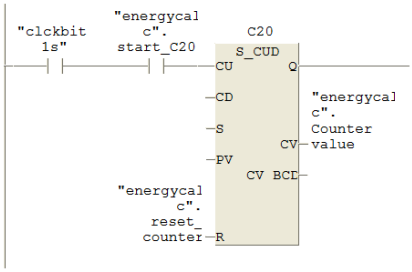

Network: 2 Temporary placeholder variable

Starts counter 20 remotely

SIMATIC mine data\SIMATIC 06/17/2008 03:34:16 PM
300(1)\CPU 315F-2 PN/DP\...\FC10 - <offline>

Network: 3 Temporary placeholder variable

Count up to 2 min and reset

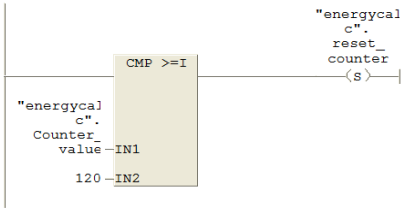

Network: 4

Getting the power from the meter for when the actual fan is running

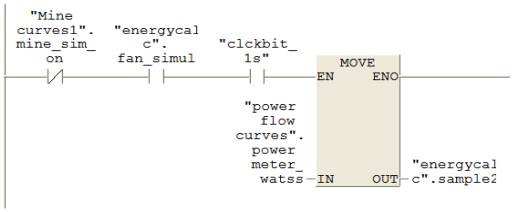

Network: 5

Simulated power for the 1.1 kW fan system as calculated in FC7

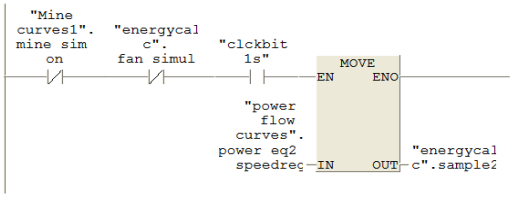

Network: 6

Simulated power for the 785 kW fan system as calculated in FC14

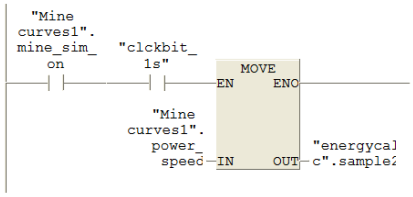

SIMATIC mine data\SIMATIC 06/17/2008 03:34:16 PM
300(1)\CPU 315F-2 PN/DP\...\FC10 - <offline>

Network: 7

Getting the time of day for the tariff structure

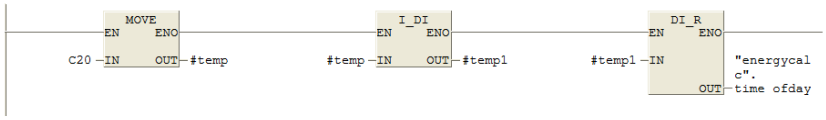

SIMATIC mine data\SIMATIC 06/17/2008 03:34:16 PM
300(1)\CPU 315F-2 PN/DP\...\FC10 - <offline>

Network: 8

Energy calculation

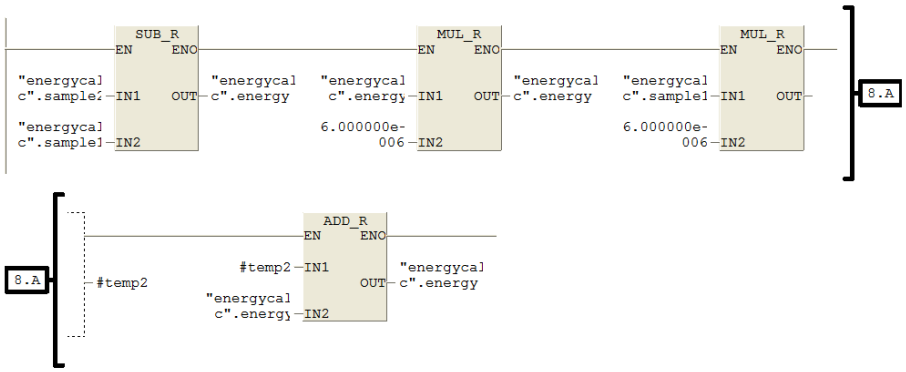

SIMATIC mine data\SIMATIC 06/17/2008 03:34:16 PM
300(1)\CPU 315F-2 PN/DP\...\FC10 - <offline>

Network: 9

Off peak 1 0-30s 0-6hr

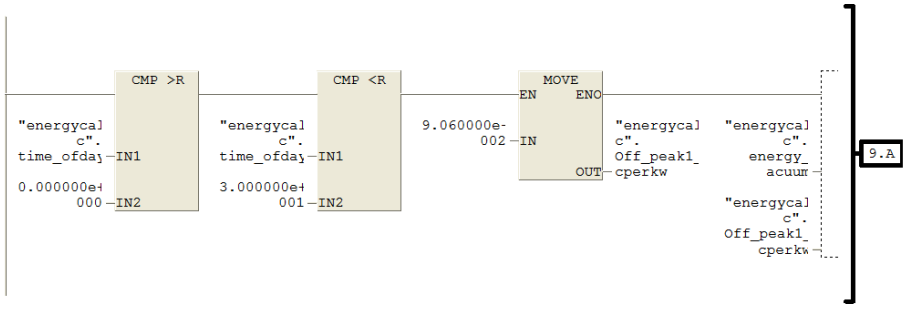

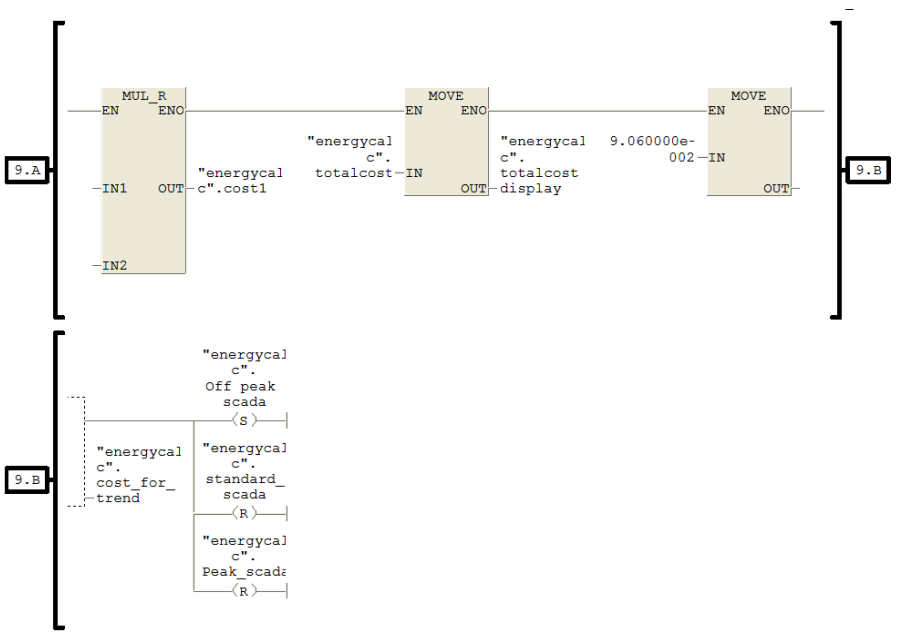

SIMATIC mine data\SIMATIC 06/17/2008 03:34:16 PM
300(1)\CPU 315F-2 PN/DP\...\FC10 - <offline>

Network: 10

Standard calculation 1 30-35s 6-7hr

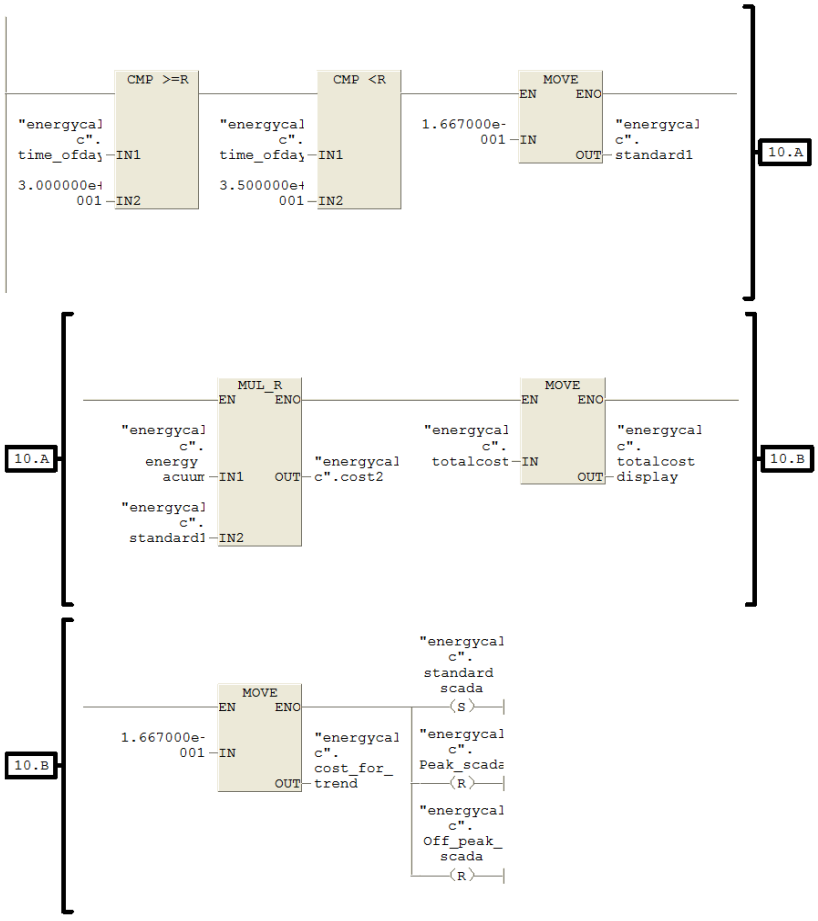

SIMATIC mine data\SIMATIC 06/17/2008 03:34:16 PM
300(1)\CPU 315F-2 PN/DP\...\FC10 - <offline>

Network: 11

Peak calculation 35-50s 7-10hr

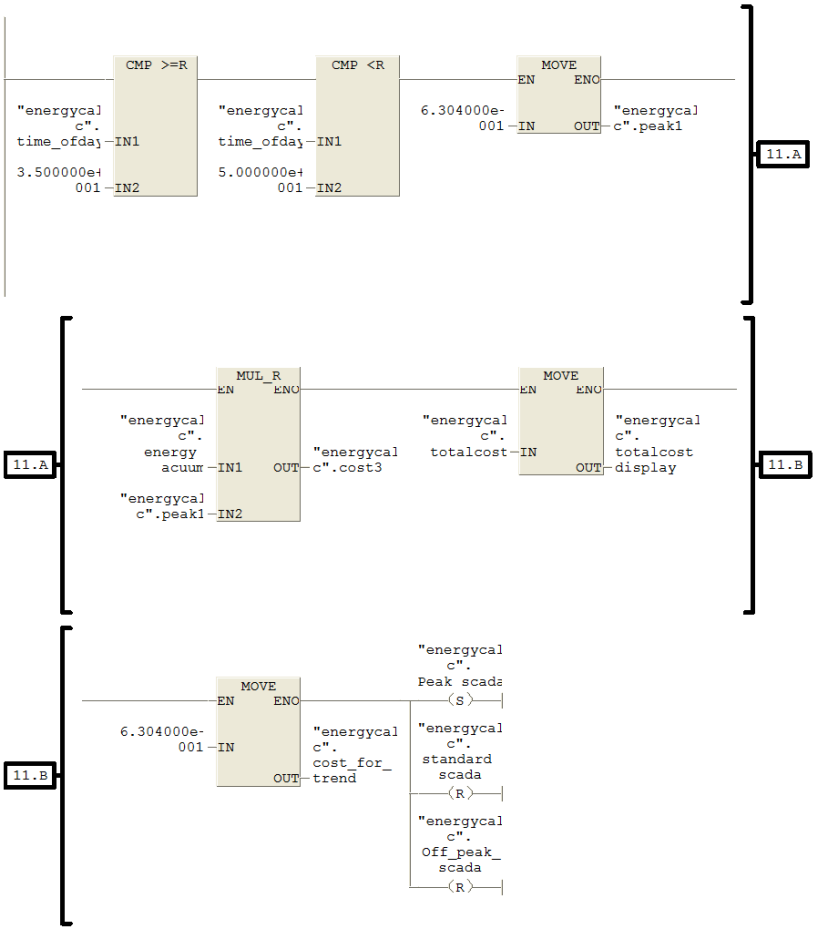

SIMATIC mine data\SIMATIC 06/17/2008 03:34:16 PM
300(1)\CPU 315F-2 PN/DP\...\FC10 - <offline>

Network: 12

Standard calculation 2 50-90s 10-18hr

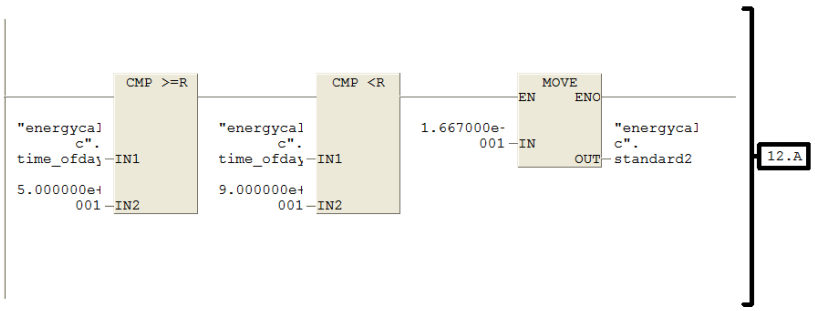

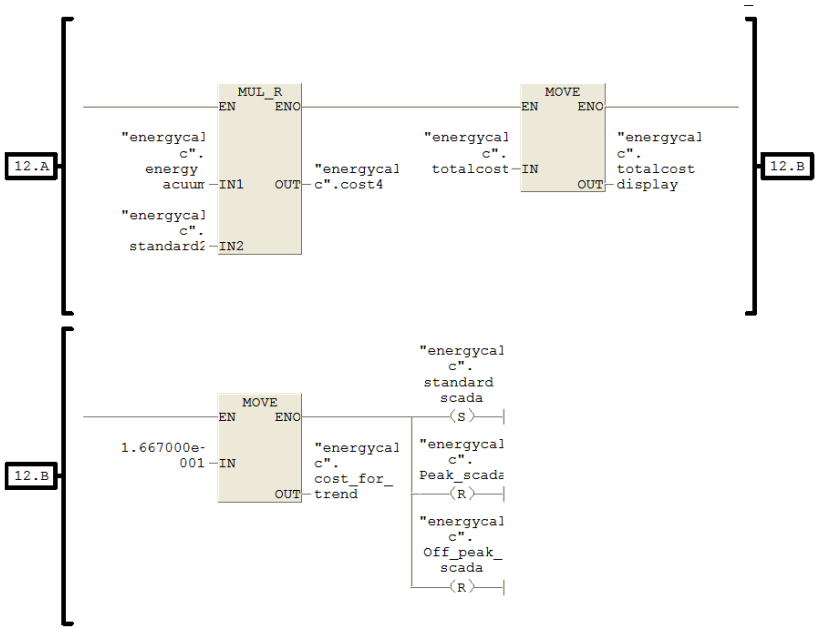

SIMATIC mine data\SIMATIC 06/17/2008 03:34:16 PM
300(1)\CPU 315F-2 PN/DP\...\FC10 - <offline>

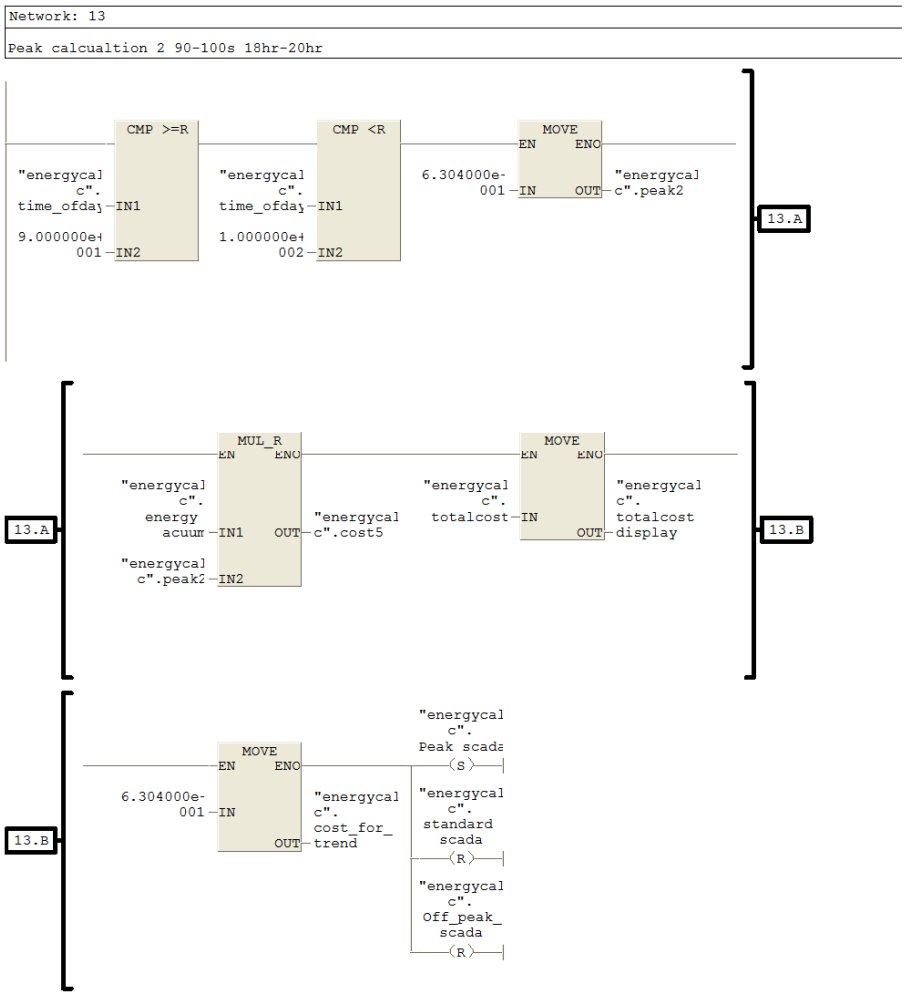

SIMATIC mine data\SIMATIC 06/17/2008 03:34:16 PM
300(1)\CPU 315F-2 PN/DP\...\FC10 - <offline>

Network: 14

Standard calculation 3 100-110s 20hr -22hr

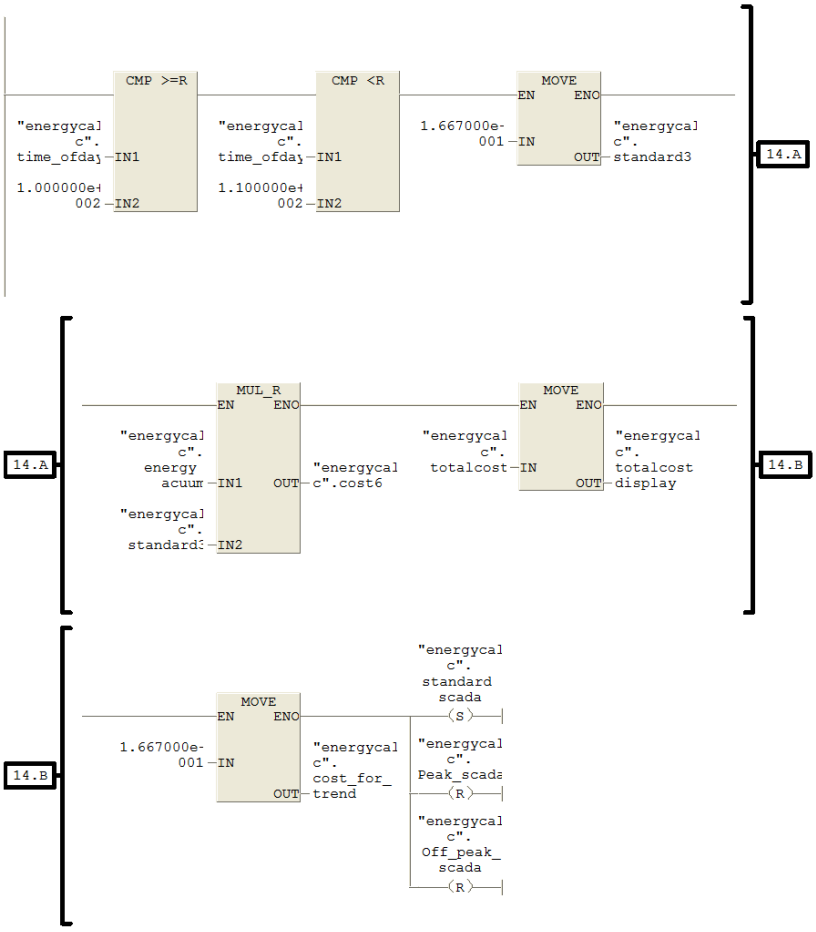

SIMATIC mine data\SIMATIC 06/17/2008 03:34:16 PM
300(1)\CPU 315F-2 PN/DP\...\FC10 - <offline>

Network: 15

Off peak 2 110s-120s 22hr-24hr

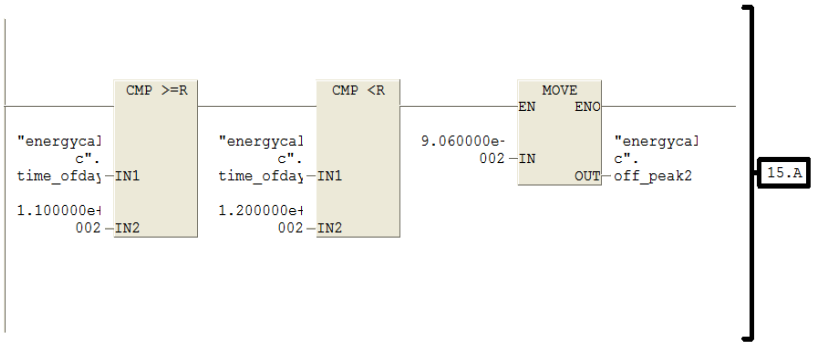

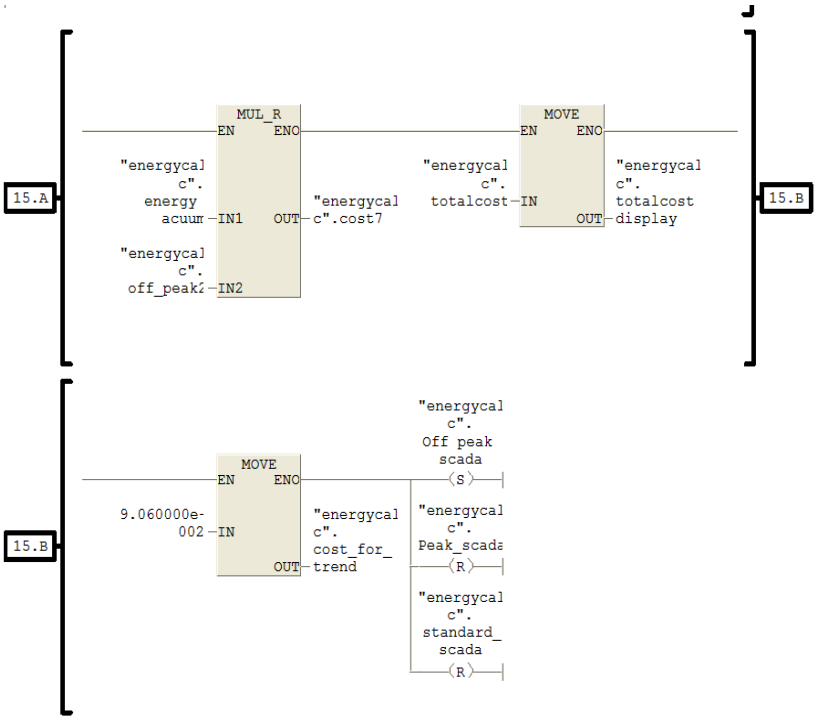

Network: 16

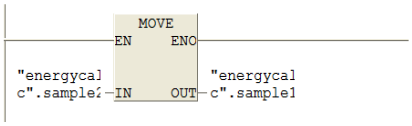

Network: 17

Total cost

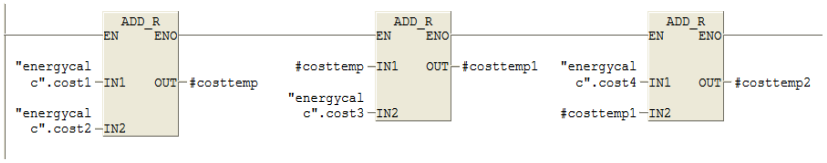

Network: 18

Total cost

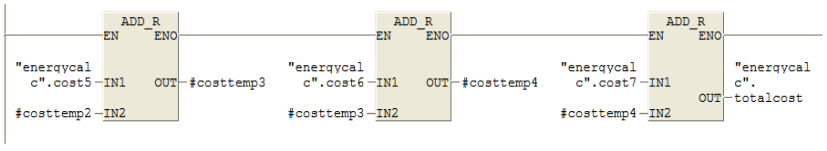

SIMATIC mine data\SIMATIC 06/17/2008 03:34:16 PM
300(1)\CPU 315F-2 PN/DP\...\FC10 - <offline>

Network: 19

Reseting

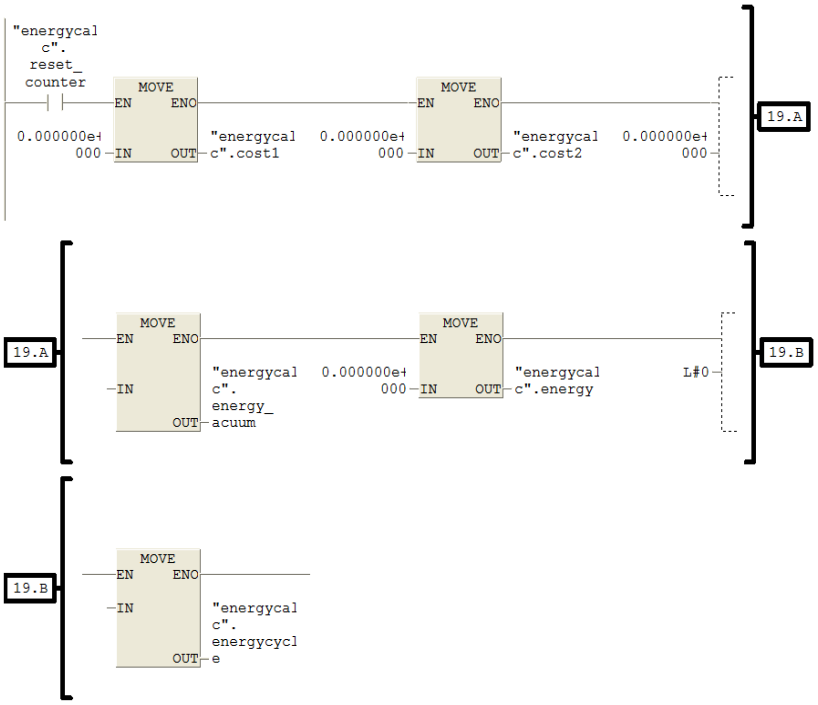

SIMATIC mine data\SIMATIC 06/17/2008 03:34:16 PM
300(1)\CPU 315F-2 PN/DP\...\FC10 - <offline>

Network: 20

Reseting

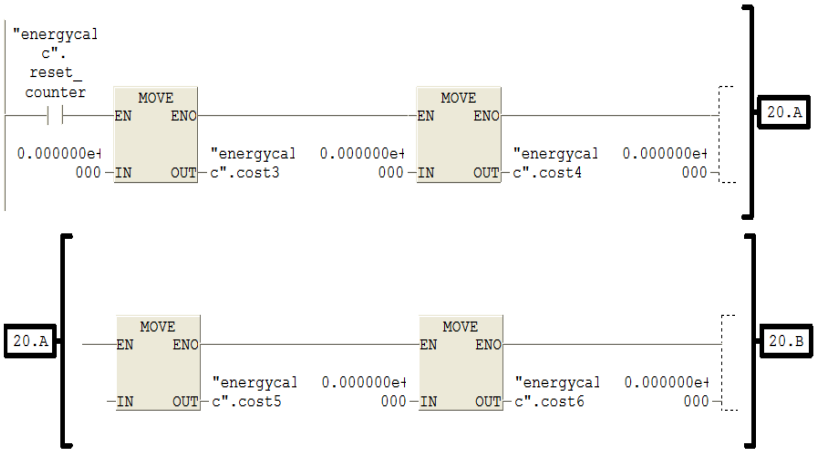

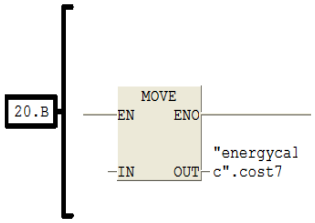

Network: 21

Cost per day and year and ten year

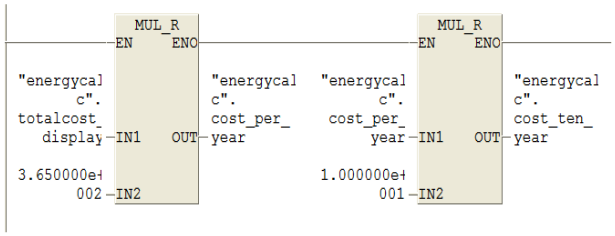

Network: 22

Saving in cost using speed regualtion for the ~1.1 kW fan system

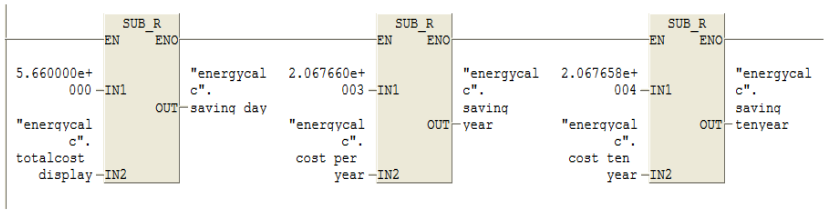

F.2.8 FC 12 Analogue outputs for display on an oscilloscope

FC12 - <offline>
"analogue outs"
Name: FC12 **Family:**
Author: Ashvir.H **Version:** 0.1
Block version: 2
Time stamp Code: 06/17/2008 04:25:23 PM
Interface: 02/21/2008 05:02:13 PM
Lengths (block/logic/data): 01048 00860 00028

Name	Data Type	Address	Comment
IN		0.0	
OUT		0.0	
IN_OUT		0.0	
TEMP		0.0	
flowfan	Real	0.0	
speedfan	Real	4.0	
speedfan1	Real	8.0	
powerfan	Real	12.0	
powerfan_1	Real	16.0	
torquefan	Real	20.0	
temptor	Real	24.0	
RETURN		0.0	
RET_VAL		0.0	

Block: FC12 Analogue outs for the oscilloscope

280 = x
282 = y

Network: 1 Flow running on fan mode

32000 = 11.50 V = 2.5 m^3/s yellow curve x axis
Flow 1m^3/s = 4.5V

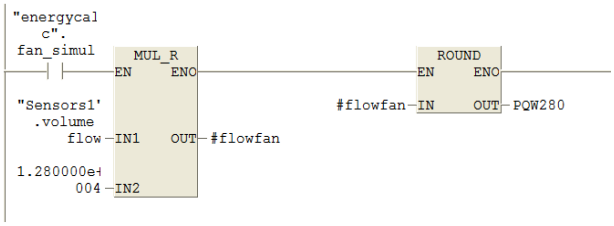

Network: 2 Speed running on fan mode

Speed 32000=11.5V
700rpm=5.5V
1000rpm=7.75V

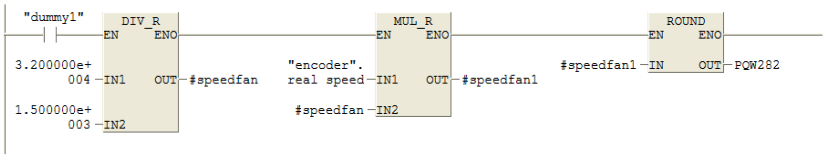

SIMATIC mine data\SIMATIC 06/17/2008 04:25:37 PM
300(1)\CPU 315F-2 PN/DP\...\FC12 - <offline>

Network: 3 power running on fan mode

Power 32000=11.5V y axis
DB57.DBD28 power watts
500 watts = 5V
100 watts = 1V

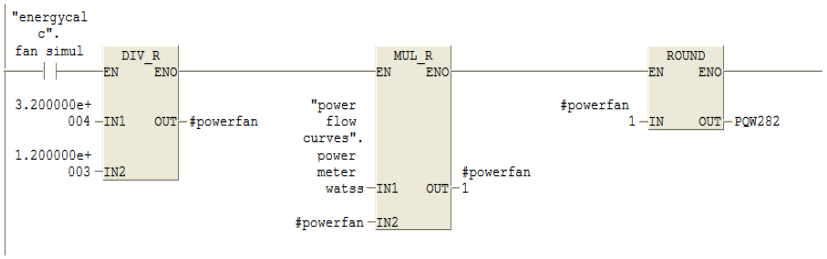

Network: 4 Speed running on simulation

Speed 32000=11.5V
DB50.DBD10=real speed
700rpm=5.5V
1000rpm=7.75V

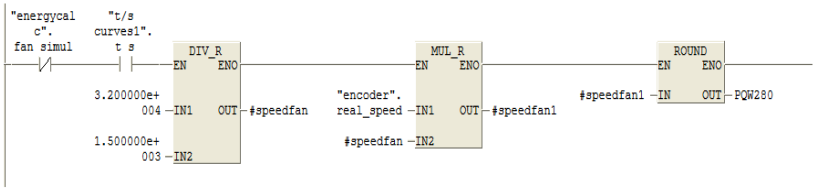

Network: 5 Torque running on simulation mode-Speed regulation

Analogue out 2 torque 0.645V=1Nm
DB53.DBD48

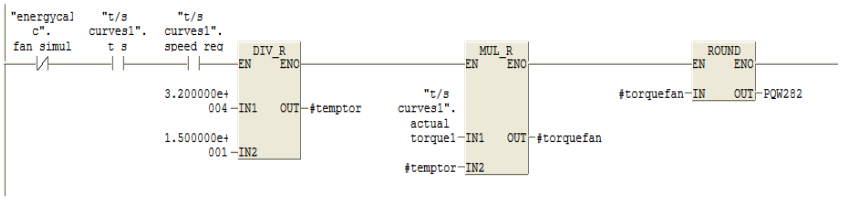

Network: 6 Torque running on simulation mode- Damper control

Analogue out 2 torque 0.645V=1Nm

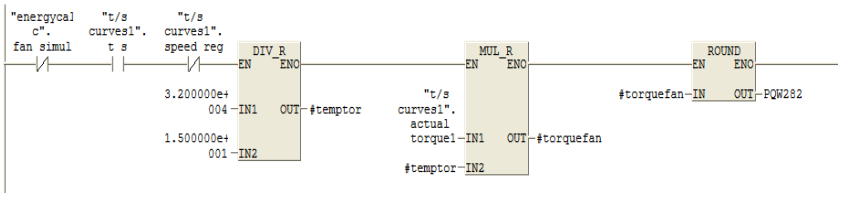

SIMATIC mine data\SIMATIC 06/17/2008 04:25:37 PM
300(1)\CPU 315F-2 PN/DP\...\FC12 - <offline>

Network: 7 Flow running on simulation mode- Speed regulation

32000 = 11.50V = 2.5 m^3/s
Flow 1m^3/s = 4.5V

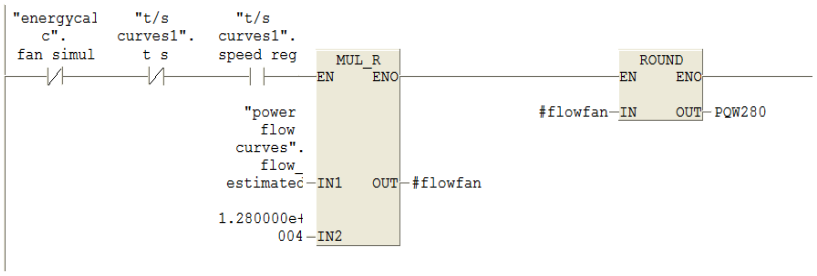

Network: 8 Flow running on simulation mode-Damper control

32000 = 11.50V = 2.5 m^3/s
Flow 1m^3/s = 4.5V

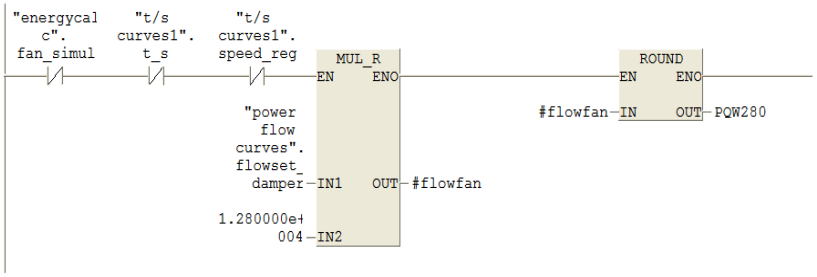

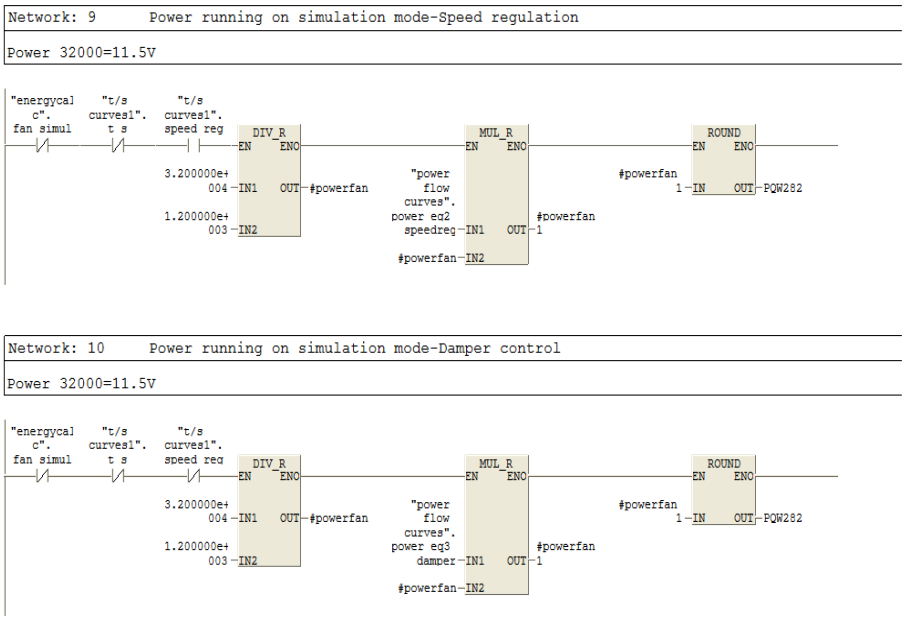

F.2.9 FC 14 Replication of the ~785 kW fans power flow characteristic

SIMATIC mine data\SIMATIC 12/08/2008 10:52:44 PM
300(1)\CPU 315F-2 PN/DP\...\FC14 - <offline>

FC14 - <offline>

"mine power flow"
Name: FC14 **Family:**
Author: Ashvir.H **Version:** 0.1
Block version: 2
Time stamp Code: 11/11/2008 02:04:55 PM
Interface: 02/13/2008 09:32:00 PM
Lengths (block/logic/data): 01752 01498 00098

Name	Data Type	Address	Comment
IN		0.0	
OUT		0.0	
IN_OUT		0.0	
TEMP		0.0	
flow_squared	Real	0.0	
flow_cube	Real	4.0	
part1_eq2	Real	8.0	
part2_eq2	Real	12.0	
part3_eq2	Real	16.0	
temp_eq2	Real	20.0	
temp1_eq2	Real	24.0	
temp1	Real	28.0	
temp2	Real	32.0	
damper_flow_sq	Real	36.0	
part1_eq3	Real	40.0	
part2_eq3	Real	44.0	
temp_eq3	Real	48.0	
temp3	Real	52.0	
temp4	Real	56.0	
temp_eq1	Real	60.0	
flowpntreg	Real	64.0	
scale1	Real	68.0	
TEMP0	Bool	72.0	
anflo	Real	74.0	
flo1	Real	78.0	

flo2	Real	82.0	
damflo	Real	86.0	
flo3	Real	90.0	
flo4	Real	94.0	
RETURN		0.0	
RET_VAL		0.0	

Block: FC14 Power flow for the 785 kW system

Network: 1

Torque input via analogue input1

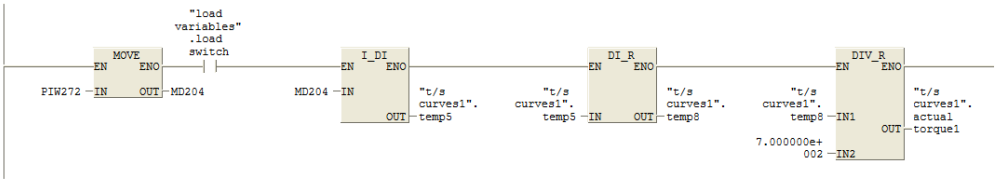

Network: 2 Speed to flow

Any speed value will give the equivalent flow rate according to speed vs flow
Eq1 y = 2.4027x + 343.36
Flow rate known put flow rate in Eq2 to get the equivalent power.
Power = Tw to get the torque setpoint

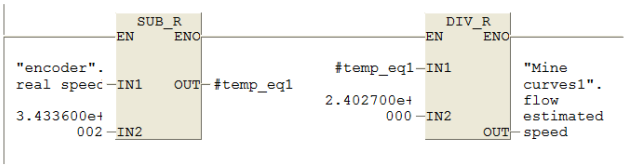

Network: 3 Speed regulation

Equation for Power Vs Flow
Eq2 y = 0.0000159x2 - 0.0023x + 0.34

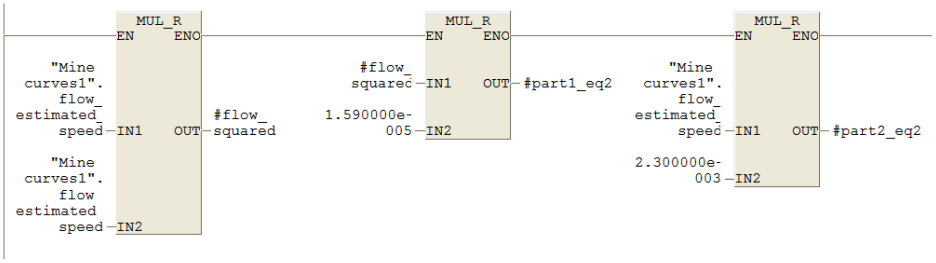

Network: 4 Speed regulation

Eq2 :y = 0.0000159x2 - 0.0023x + 0.34
Adding the different parts of Eq2.

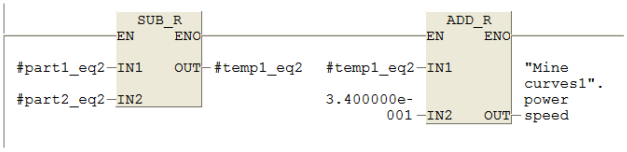

Network: 5 Speed regulation

Power= Torque*Speed
Power from network 4

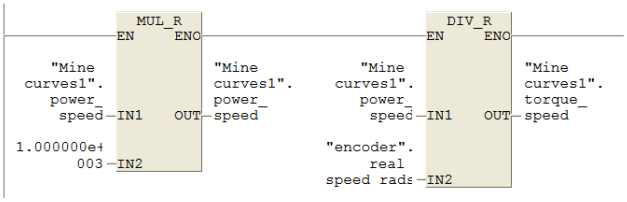

SIMATIC mine data\SIMATIC 12/08/2008 10:52:44 PM
300(1)\CPU 315F-2 PN/DP\...\FC14 - <offline>

Network: 6 Speed regulation

Sending the torque from network 5 to the drive

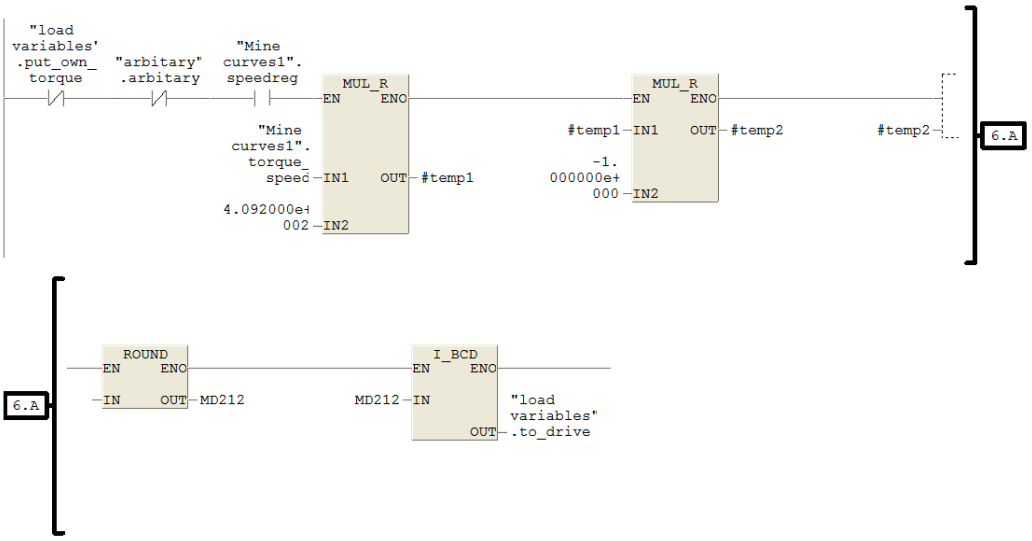

Network: 7 Damper control

The flow is decremented in OB35 network 3
Eq3 y = -0.0000094x2 + 0.0077x +0.9988

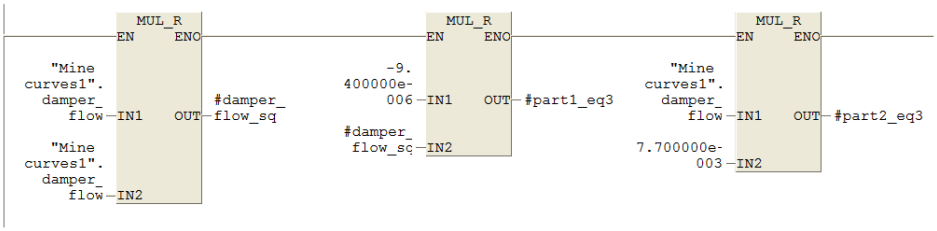

SIMATIC mine data\SIMATIC 12/08/2008 10:52:44 PM
300(1)\CPU 315F-2 PN/DP\...\FC14 - <offline>

Network: 8 Damper control

Eq3 y = -0.0000094x2 + 0.0077x +0.9988
Adding the different parts of Eq3

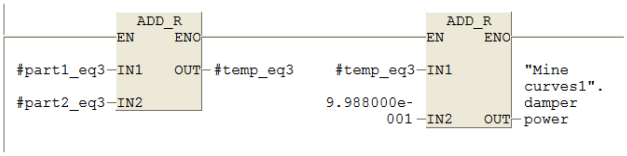

Network: 9 Damper control

Power= Torque*Speed
Power from network 8

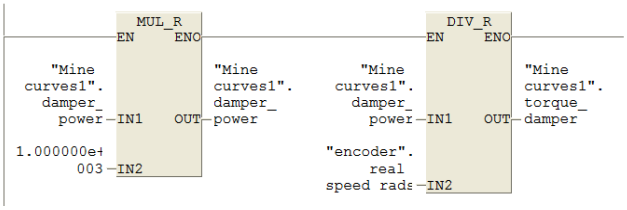

SIMATIC mine data\SIMATIC 12/08/2008 10:52:44 PM
300(1)\CPU 315F-2 PN/DP\...\FC14 - <offline>

Network: 10 Damper control

Sending the torque from network 9 to VSD2

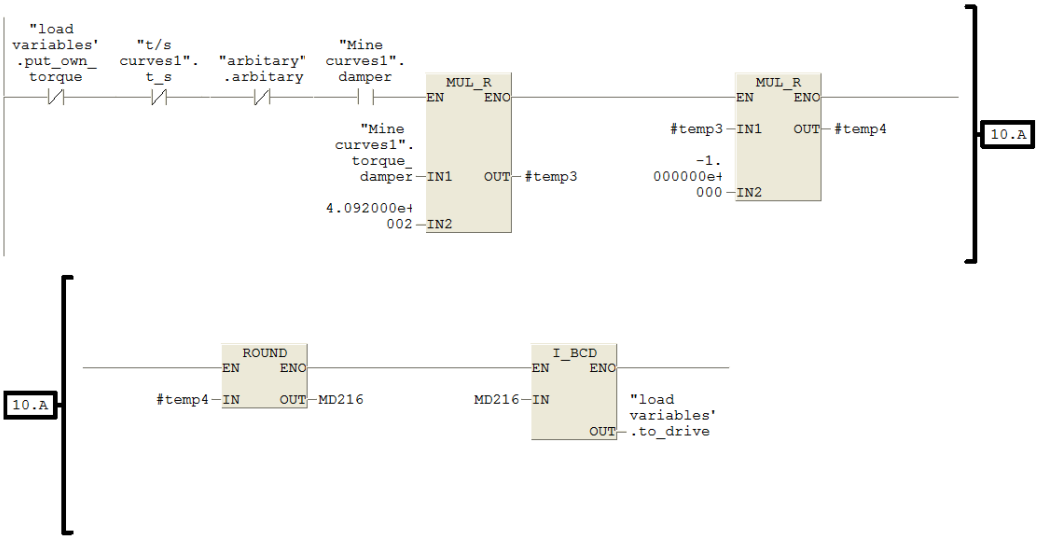

SIMATIC mine data\SIMATIC 12/08/2008 10:52:44 PM
300(1)\CPU 315F-2 PN/DP\...\FC14 - <offline>

Network: 11 Scaling for the white dot in the SCADA screens

Speed regulation
DB58.DBD2
DB58.DBD6
x=320

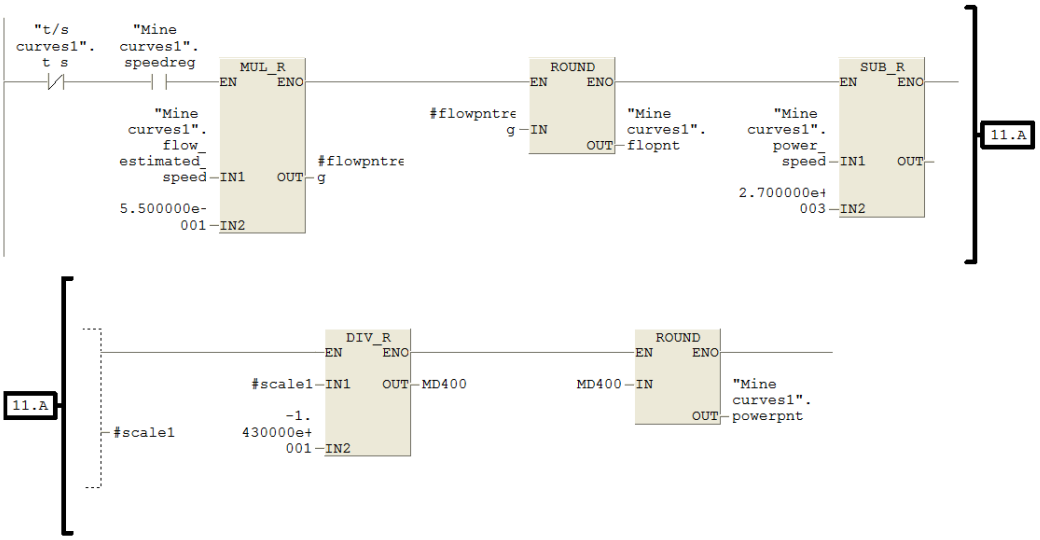

SIMATIC mine data\SIMATIC 12/08/2008 10:52:45 PM
300(1)\CPU 315F-2 PN/DP\...\FC14 - <offline>

Network: 12 Scaling for the white dot in the SCADA screens

Damper control
DB58.DBD14
DB58.DBD18
x=320

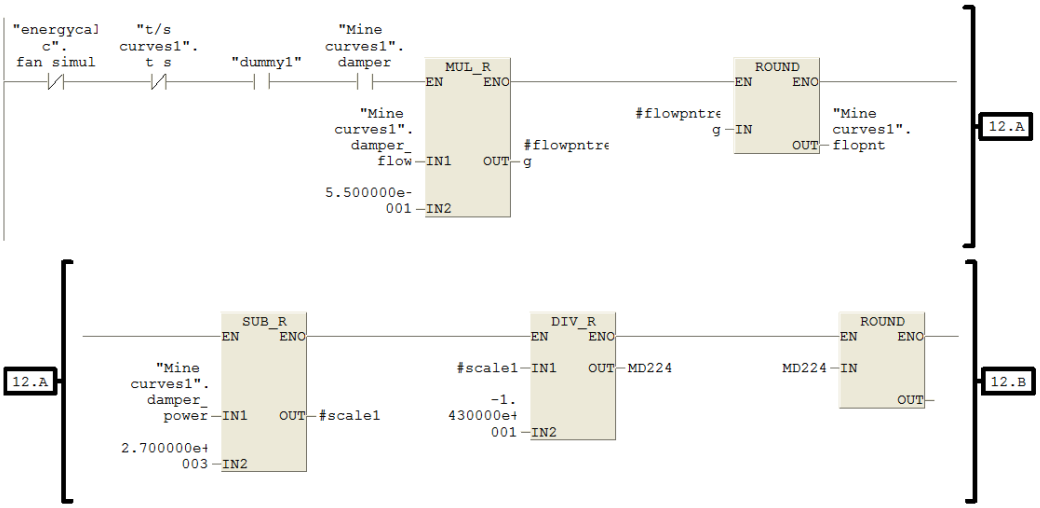

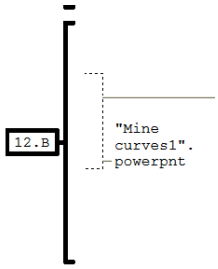

Network: 13

Converting the power from kW to watts

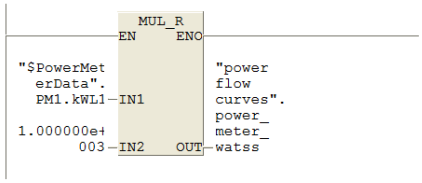

SIMATIC mine data\SIMATIC 12/08/2008 10:52:45 PM
300(1)\CPU 315F-2 PN/DP\...\FC14 - <offline>

Network: 14 Flow running on simulation mode- Speed regulation

32000 = 11.50V = 2.5 m^3/s
Flow 1m^3/s = 4.5V

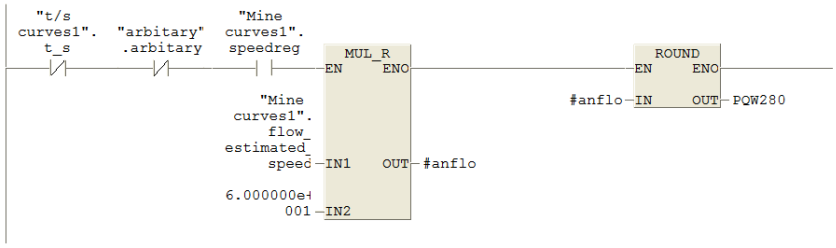

Network: 15 Flow running on simulation mode-Damper control

32000 = 11.50V = 2.5 m^3/s
Flow 1m^3/s = 4.5V

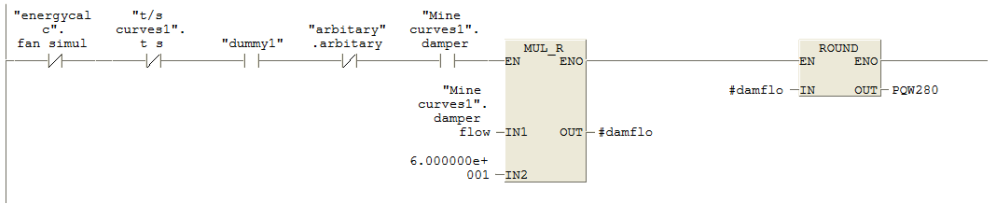

Network: 16 Power running on simulation mode-Speed regulation

Power 32000=11.5V

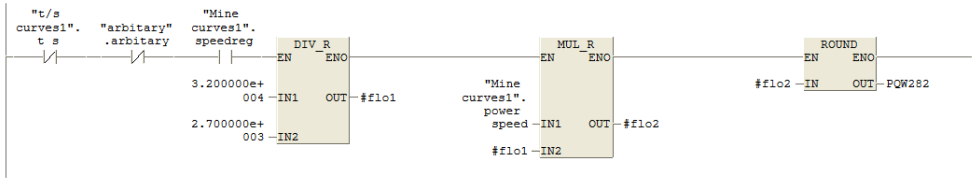

SIMATIC mine data\SIMATIC 12/08/2008 10:52:45 PM
300(1)\CPU 315F-2 PN/DP\...\FC14 - <offline>

Network: 17 Power running on simulation mode-Damper control

Power 32000=11.5V

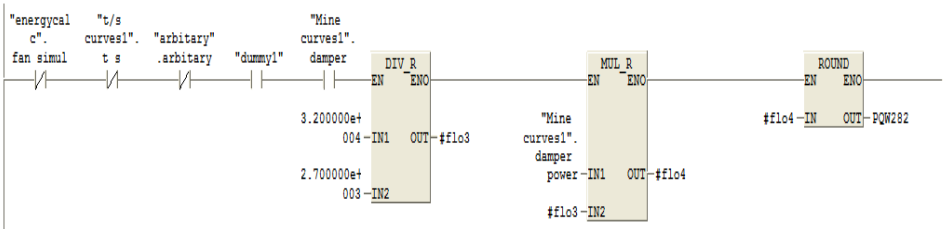

F.2.10 FC 23 Flow control implemented on the actual 1.1 kW fan

SIMATIC mine data\SIMATIC 06/17/2008 03:24:43 PM
300(1)\CPU 315F-2 PN/DP\...\FC23 - <offline>

FC23 - <offline>

"FlowControl" Flow rate setpoint control
Name: FC23 Family:
Author: Ashvir.H Version: 0.1
Block version: 2
Time stamp Code: 06/17/2008 03:24:36 PM
Interface: 10/20/2007 12:35:08 AM
Lengths (block/logic/data):00562 00424 00016

Name	Data Type	Address	Comment
IN		0.0	
OUT		0.0	
IN_OUT		0.0	
TEMP		0.0	
part1	Real	0.0	
temp	Real	4.0	
temp1	Real	8.0	
temp2	Real	12.0	
RETURN		0.0	
RET_VAL		0.0	

Block: FC23 Flow control

Network: 1

Start flow control

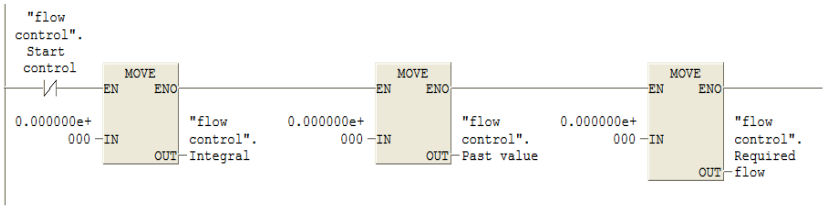

Network: 2

Reset controller if flow is too high

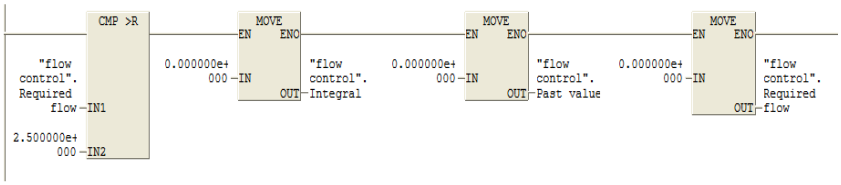

SIMATIC mine data\SIMATIC 06/17/2008 03:24:43 PM
300(1)\CPU 315F-2 PN/DP\...\FC23 - <offline>

Network: 3

Dummy flows for simulation

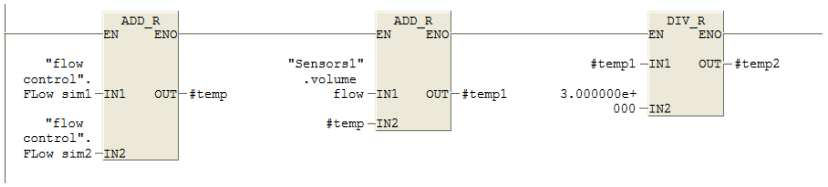

Network: 4

Error between the actual and required flow

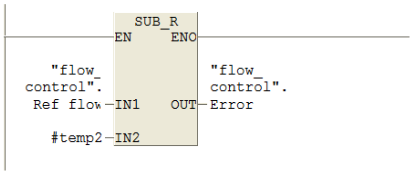

Network: 5

Proportional Gain for flow Control = 0.87

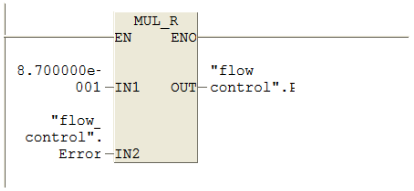

Network: 6

Integral Gain for flow Control = 0.6

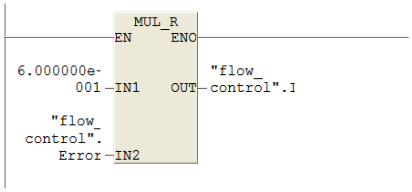

SIMATIC mine data\SIMATIC 06/17/2008 03:24:43 PM
300(1)\CPU 315F-2 PN/DP\...\FC23 - <offline>

Network: 7

Sampling Time (10ms) / Integral Time = 1.9 =gradient

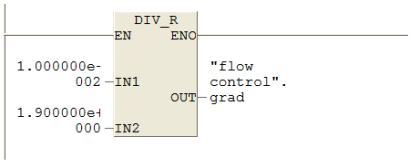

Network: 8

Integral

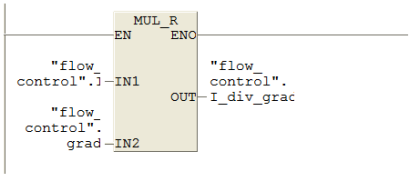

Network: 9

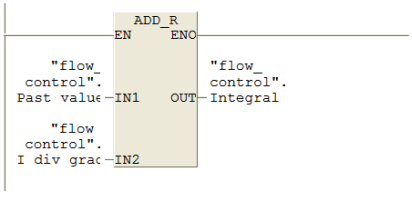

Network: 10

Final Controller Output - Flow sent to the speed to flow code FC24

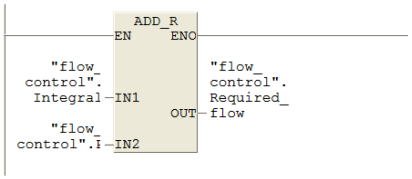

SIMATIC mine data\SIMATIC 06/17/2008 03:24:43 PM
300(1)\CPU 315F-2 PN/DP\...\FC23 - <offline>

Network: 11

Integration Step to store past errors

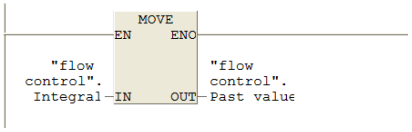

F.2.11 FC 24 Flow to speed conversion for the implementation of the flow controller

SIMATIC mine data\SIMATIC 06/17/2008 03:25:23 PM
300(1)\CPU 315F-2 PN/DP\...\FC24 - <offline>

FC24 - <offline>

"Flow to speed"
Name: FC24 **Family:**
Author: Ashvir.H **Version:** 0.1
Block version: 2
Time stamp Code: 06/17/2008 03:25:16 PM
Interface: 02/18/2008 10:13:18 AM
Lengths (block/logic/data): 00332 00214 00012

Name	Data Type	Address	Comment
IN		0.0	
OUT		0.0	
IN_OUT		0.0	
TEMP		0.0	
Part1	Real	0.0	
temp2	Real	4.0	
limit	Real	8.0	
RETURN		0.0	
RET_VAL		0.0	

Block: FC24 Flow to speed

Network: 1

y = 658.43x + 47.6

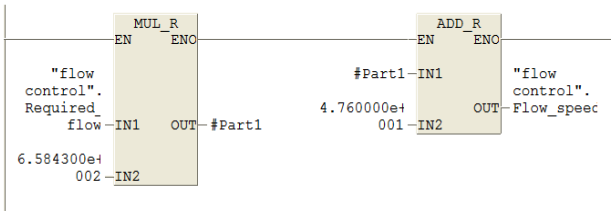

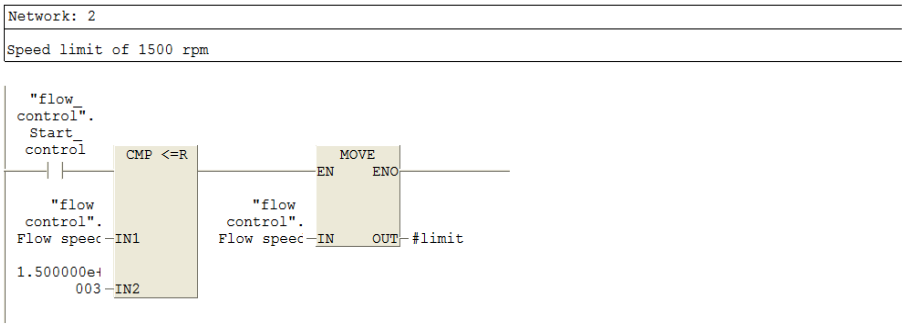

SIMATIC mine data\SIMATIC 06/17/2008 03:25:23 PM
300(1)\CPU 315F-2 PN/DP\...\FC24 - <offline>

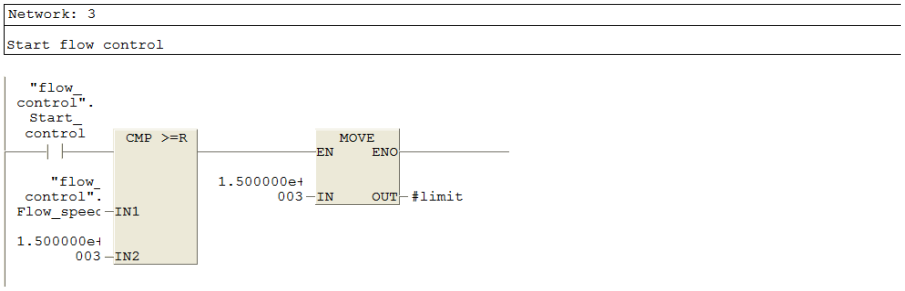

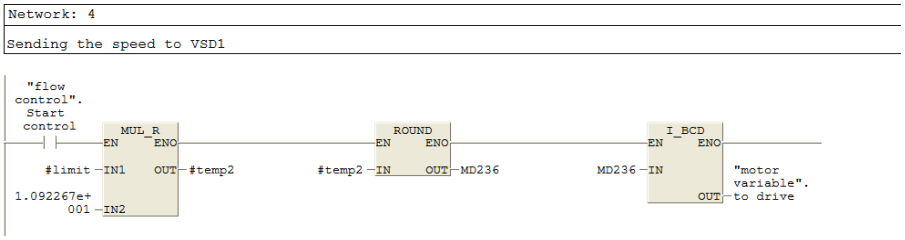

F.2.12 FC 150 Establishing communication between the RS 232C module and the power meter

SIMATIC mine data\SIMATIC 10/25/2009
300(1)\CPU 315F-2 PN/DP\...\FC150 - <offline>

FC150 - <offline>
"$fcPowerMeterComms"
Name: FC150 **Family:**
Author: Ashvir.H **Version:** 0.1
Block version: 2
Time stamp Code: 09/30/2009 07:46:47 PM
Interface: 02/20/2006 12:57:27 PM
Lengths (block/logic/data): 05792 05390 00026

Name	Data Type	Address	Comment
IN		0.0	
OUT		0.0	
IN_OUT		0.0	
TEMP		0.0	

tInt1	Int	0.0	
tInt2	Int	2.0	
tInt	Int	4.0	
tWord	Word	6.0	
tIntInt	Int	8.0	
tPointer	DInt	10.0	
RETURN		0.0	
RET_VAL		0.0	

Block: FC150 Power meter comms using the CP 340

Network: 1

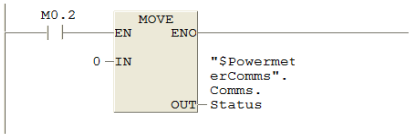

SIMATIC mine data\SIMATIC 300(1)\ 06/17/2008 03:26:45 PM
CPU 315F-2 PN/DP\...\FC150 - <offline>

Network: 2

Time synch and initialise the download requested

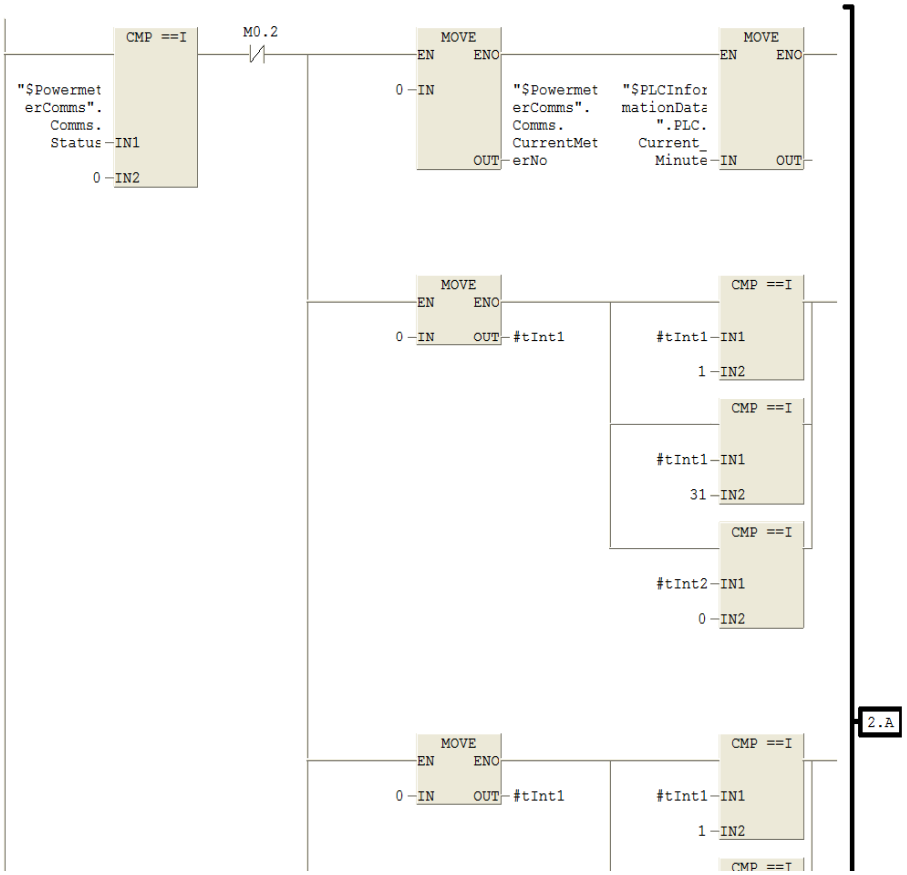

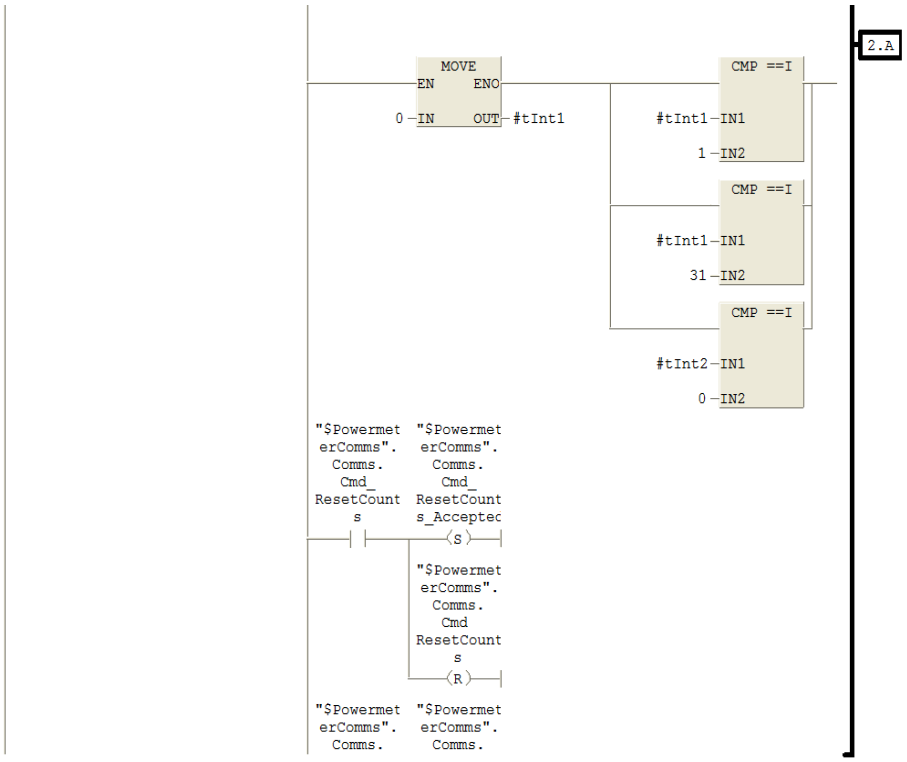

SIMATIC mine data\SIMATIC 300(1)\ 06/17/2008 03:26:45 PM
CPU 315F-2 PN/DP\...\FC150 - <offline>

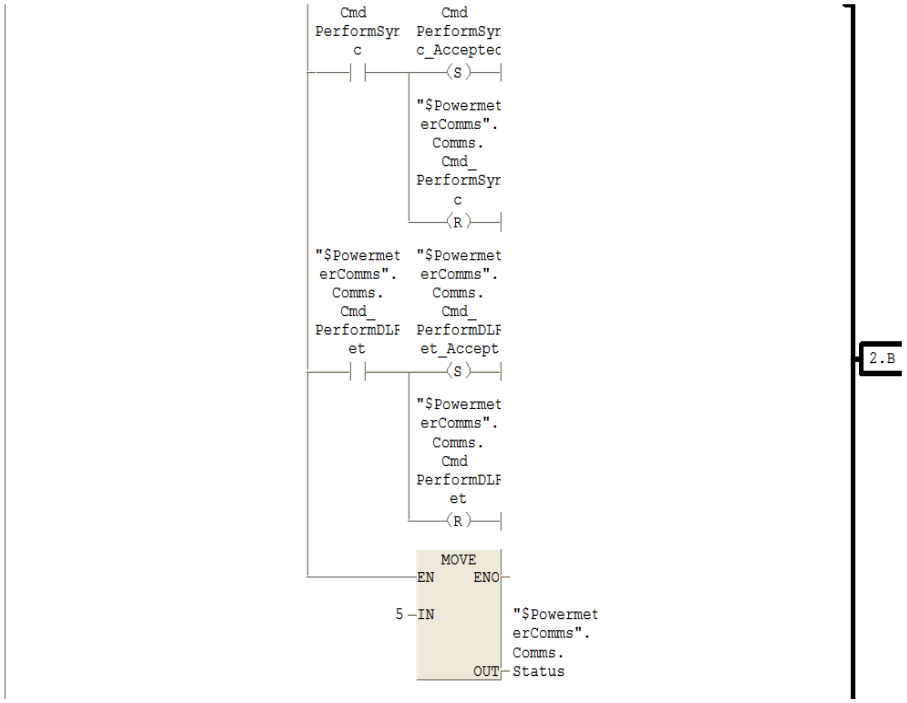

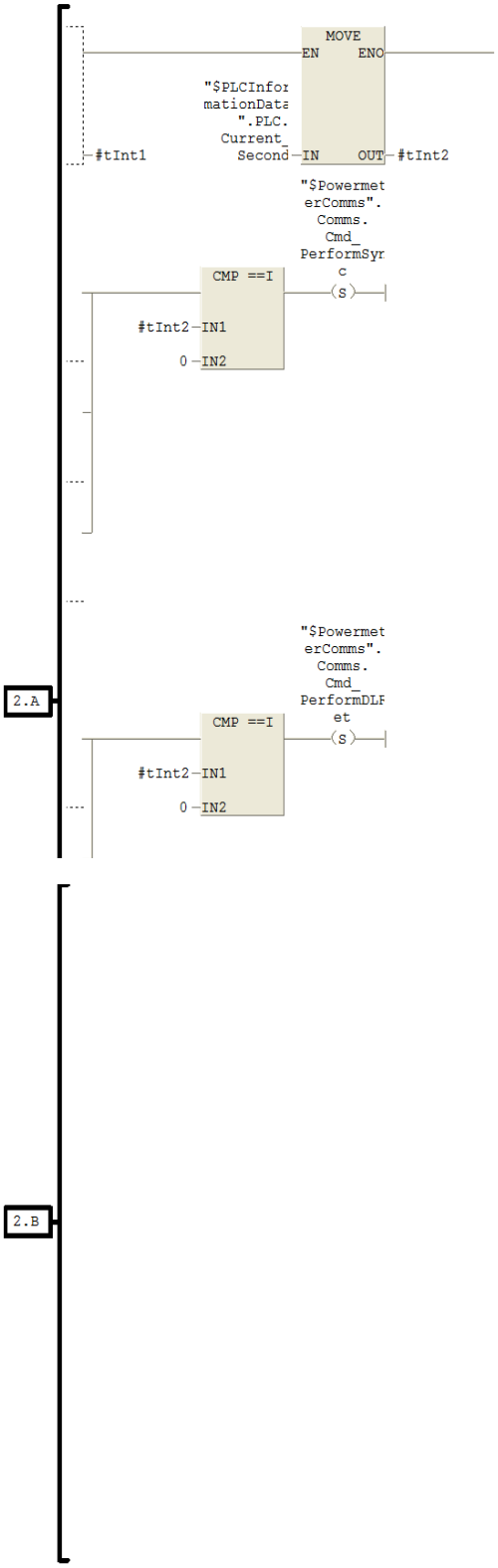
MOVE
EN
ENO
"$PLCInfor
mationData
".PLC.
Current_
Second
#tInt1
IN
OUT
#tInt2
"$Powermet
erComms".
Comms.
Cmd_
PerformSyr
c
CMP ==I
S
#tInt2
IN1
0
IN2
"$Powermet
erComms".
Comms.
Cmd_
PerformDLF
et
CMP ==I
S
#tInt2
IN1
0
IN2
2.A
2.B

```
Network: 3

Load all data relevant to current Meter

      A(
      L     "$PowermeterComms".Comms.Status
      L     5
      ==I
      )
      JNB   M001

      L     0
      T     "$PowermeterComms".Comms.CurrentFunction

      L     "$PowermeterComms".Comms.CurrentMeterNo
      L     "$PowermeterComms".Comms.MeterOffset
      *I
      T     "$PowermeterComms".Comms.CurrentMeterOffset

      L     "$PowermeterComms".Comms.CurrentMeterNo
      L     "$PowermeterComms".Comms.MeterOffset2
      *I
      T     "$PowermeterComms".Comms.CurrentMeterOffset2


      L     "$PowermeterComms".Comms.CurrentMeterOffset
      SLD   3
      T     #tPointer
      OPN   "$PowerMeterData"
      L     DBW [#tPointer]
      T     "$PowermeterComms".Comms.CurrentMeterAddress

      L     "$PowermeterComms".Comms.CurrentMeterOffset
      L     16
      +I
      SLD   3
      T     #tPointer
      OPN   "$PowerMeterData"
      L     DBW [#tPointer]
      T     DB150.DBW   50


      L     "$PowermeterComms".Comms.CurrentMeterOffset
      L     18
      +I
      SLD   3
```



```
      T     #tPointer
      OPN   "$PowerMeterData"
      L     DBW [#tPointer]
      T     "$PowermeterComms".Comms.Timeouts

      L     "$PowermeterComms".Comms.CurrentMeterOffset
      L     20
      +I
      SLD   3
      T     #tPointer
      OPN   "$PowerMeterData"
      L     DBW [#tPointer]
      T     "$PowermeterComms".Comms.Errors

      L     "$PowermeterComms".Comms.CurrentMeterOffset
      L     22
      +I
      SLD   3
      T     #tPointer
      OPN   "$PowerMeterData"
      L     DBB [#tPointer]
      OPN   "$PowermeterComms"

      T     DBB   66



M001: NOP   0
```

SIMATIC mine data\SIMATIC 300(1)\ 06/17/2008 03:26:45 PM
CPU 315F-2 PN/DP\...\FC150 - <offline>

Network: 4

Determine what functions to perform with meter

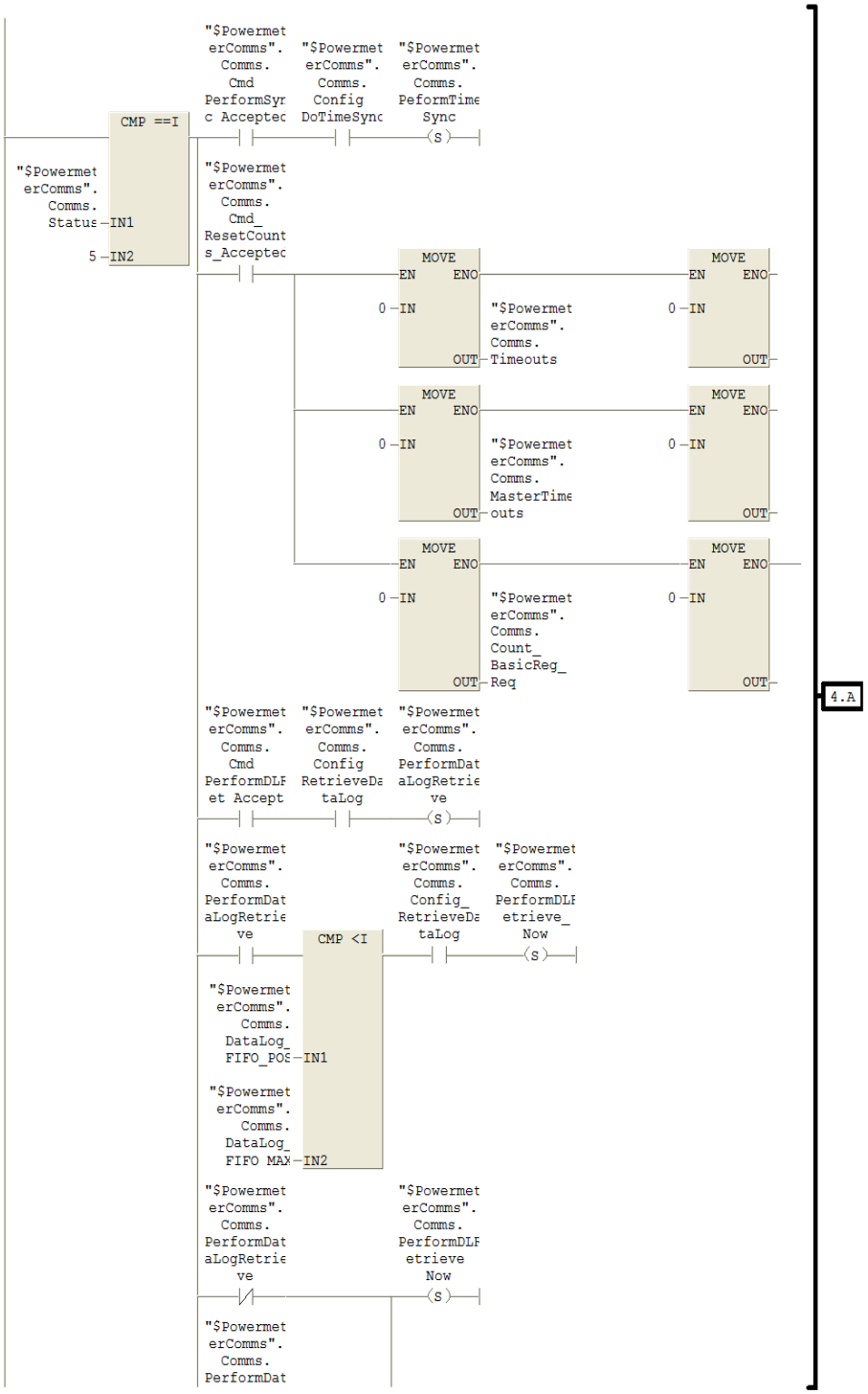

SIMATIC mine data\SIMATIC 300(1)\ 06/17/2008 03:26:45 PM
CPU 315F-2 PN/DP\...\FC150 - <offline>

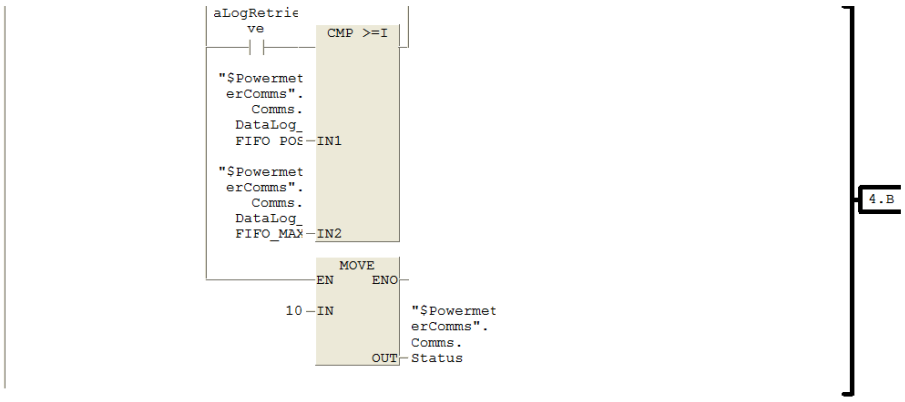

SIMATIC mine data\SIMATIC 300(1)\ 06/17/2008 03:26:45 PM
CPU 315F-2 PN/DP\...\FC150 - <offline>

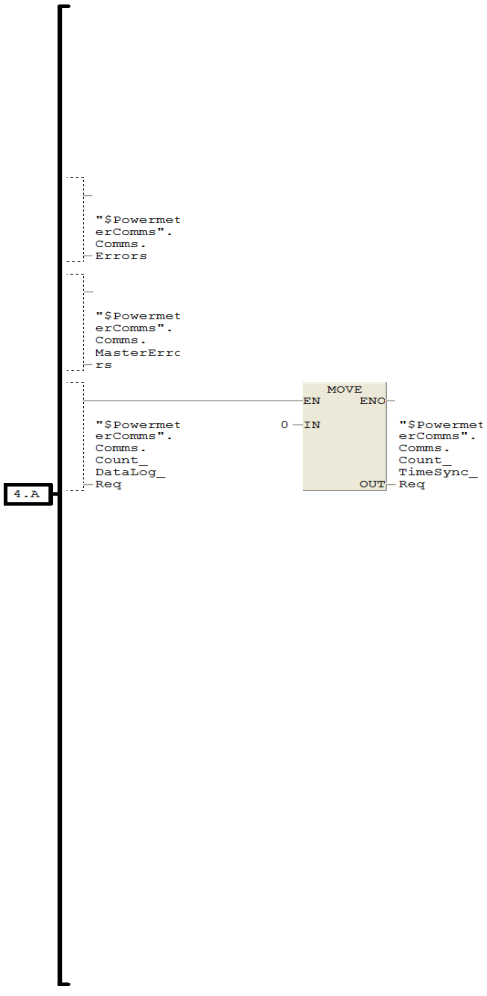

SIMATIC mine data\SIMATIC 300(1)\ 06/17/2008 03:26:45 PM
CPU 315F-2 PN/DP\...\FC150 - <offline>

Network: 5

Based on function to be performed goto appropriate section of the sequence

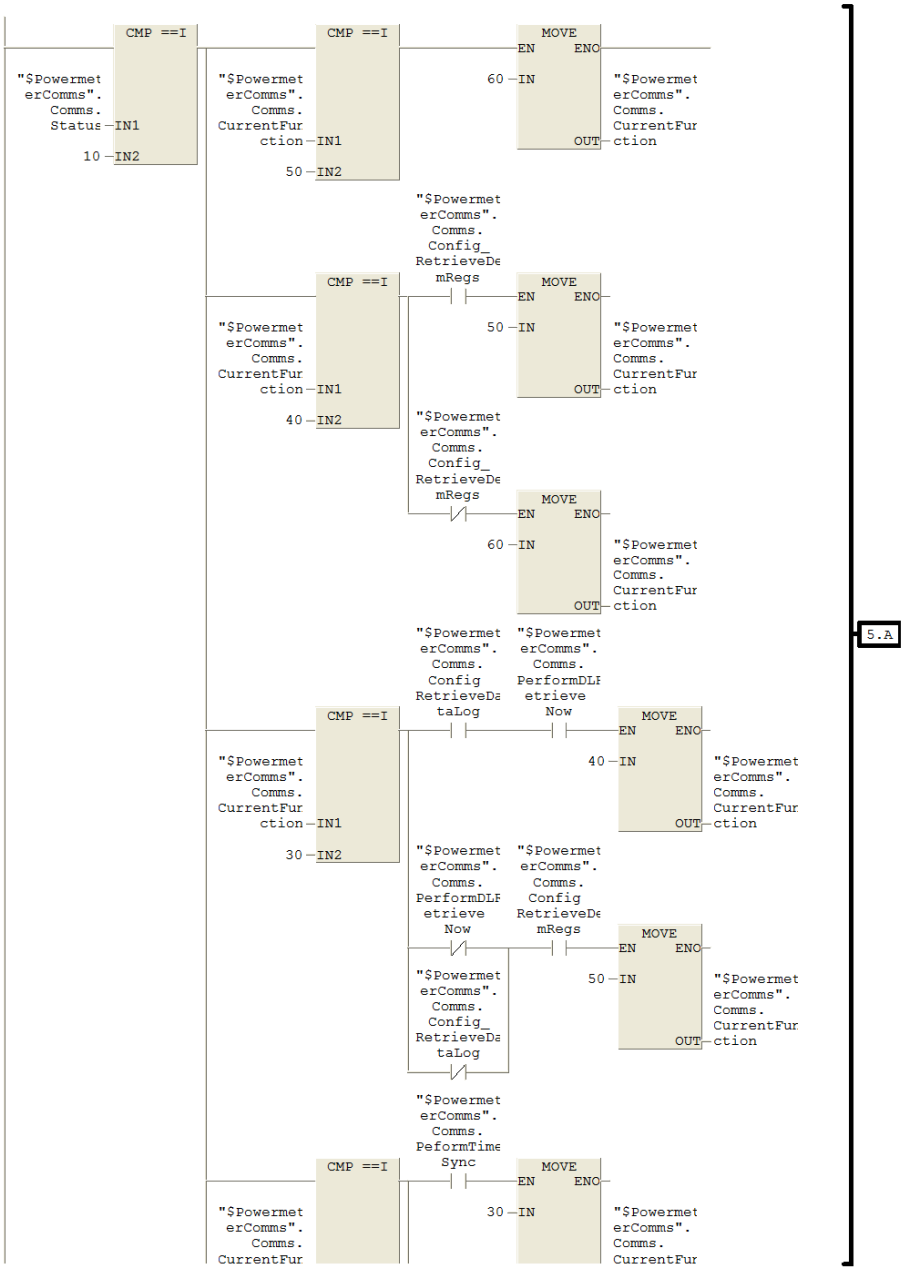

SIMATIC mine data\SIMATIC 300(1)\ 06/17/2008 03:26:45 PM
CPU 315F-2 PN/DP\...\FC150 - <offline>

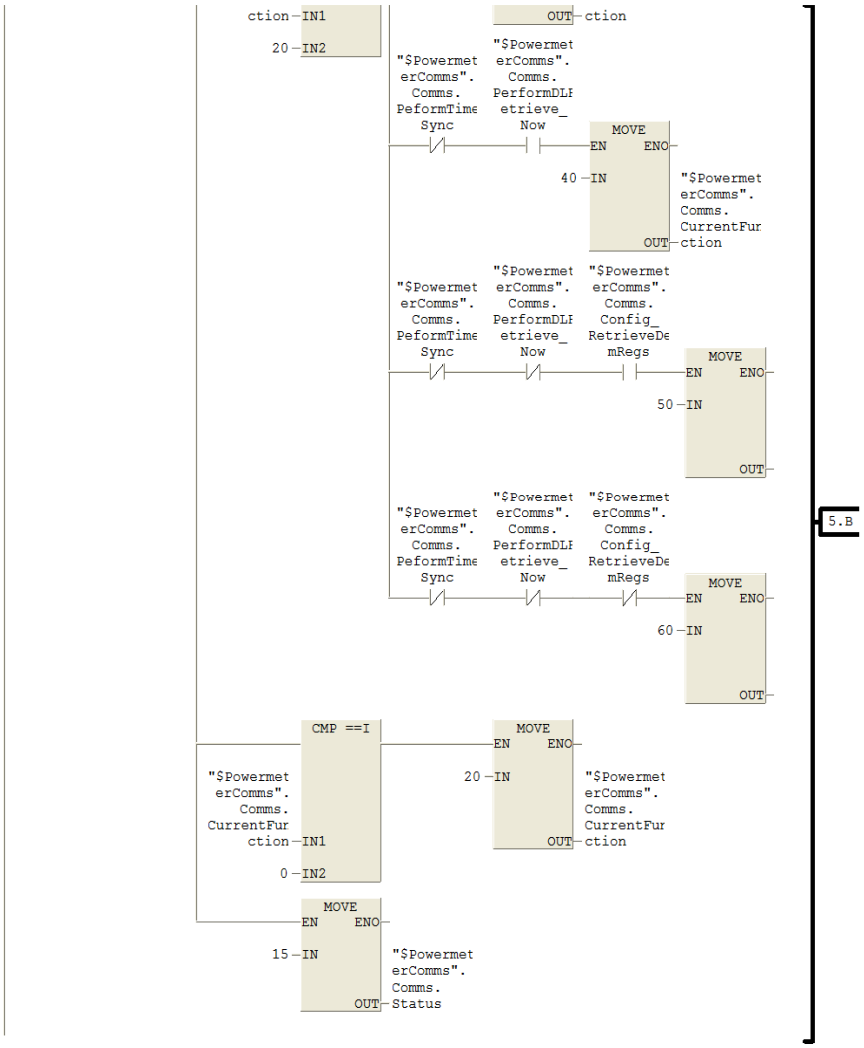

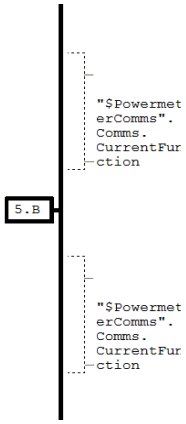

SIMATIC mine data\SIMATIC 300(1)\ 06/17/2008 03:26:45 PM
CPU 315F-2 PN/DP\...\FC150 - <offline>

Network: 6

Based on function to be performed goto appropriate section of the sequence
20 Basic Register
30 Time Sync
40 Datalogs

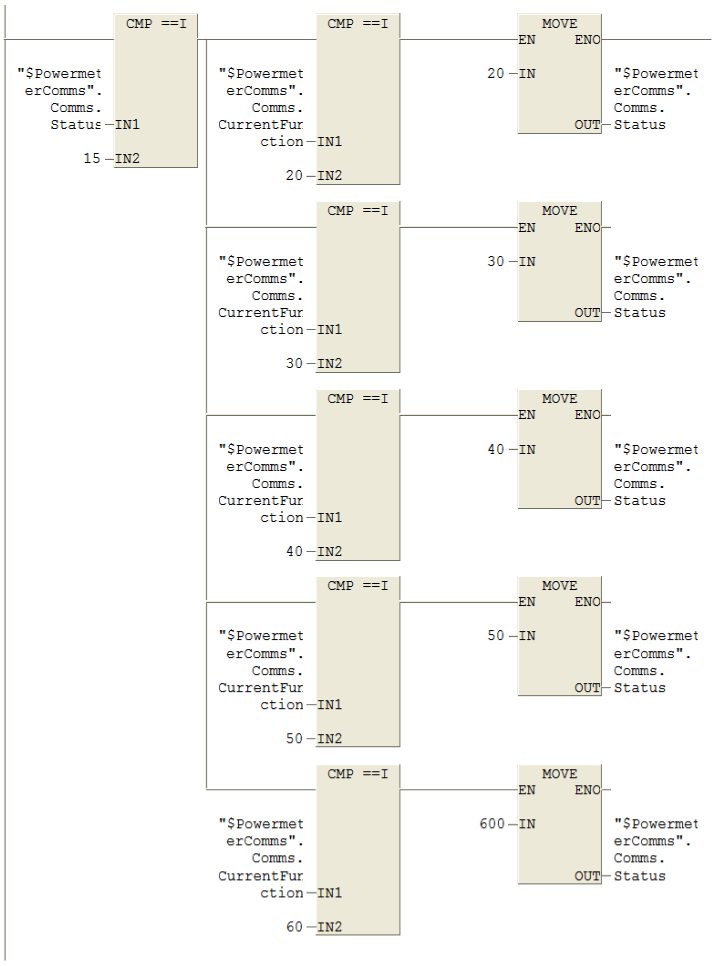

SIMATIC mine data\SIMATIC 300(1)\ 06/17/2008 03:26:45 PM
CPU 315F-2 PN/DP\...\FC150 - <offline>

Network: 7

Build "basic register request" message

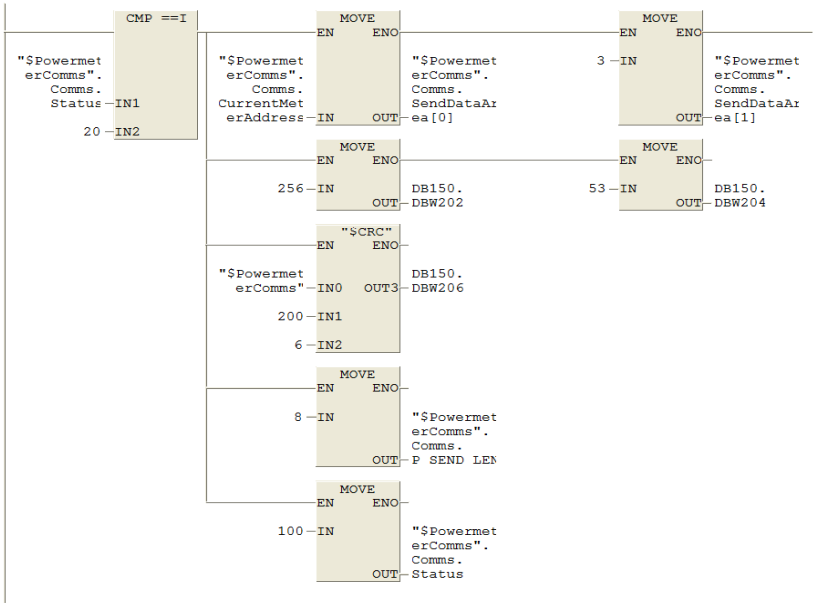

SIMATIC mine data\SIMATIC 300(1)\ 06/17/2008 03:26:45 PM
CPU 315F-2 PN/DP\...\FC150 - <offline>

Network: 8

Build "Set Realtime Clock" Message

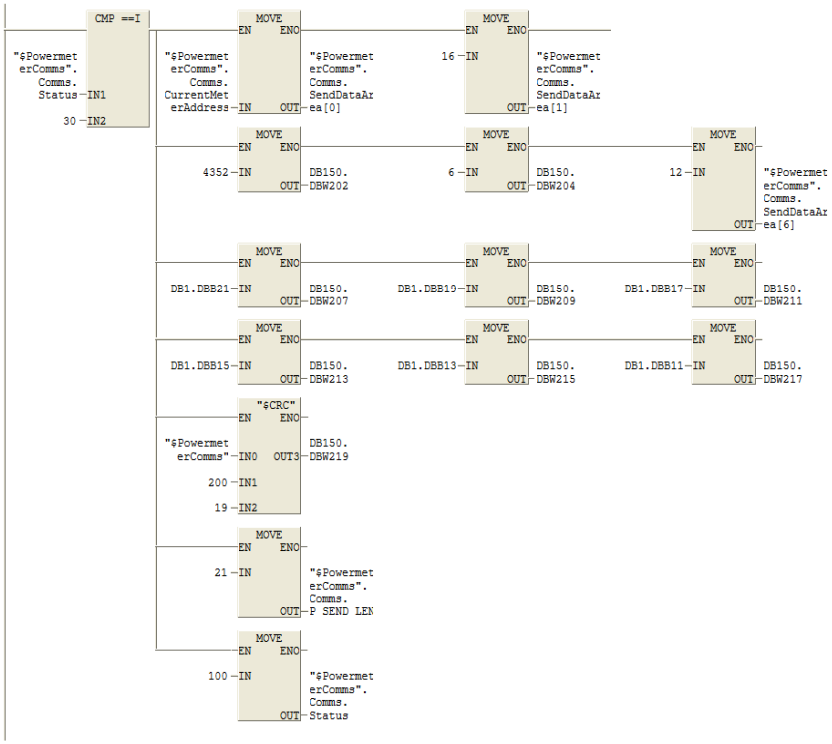

SIMATIC mine data\SIMATIC 300(1)\ 06/17/2008 03:26:45 PM
CPU 315F-2 PN/DP\...\FC150 - <offline>

Network: 9

Build "Retrieve Data Log" Message

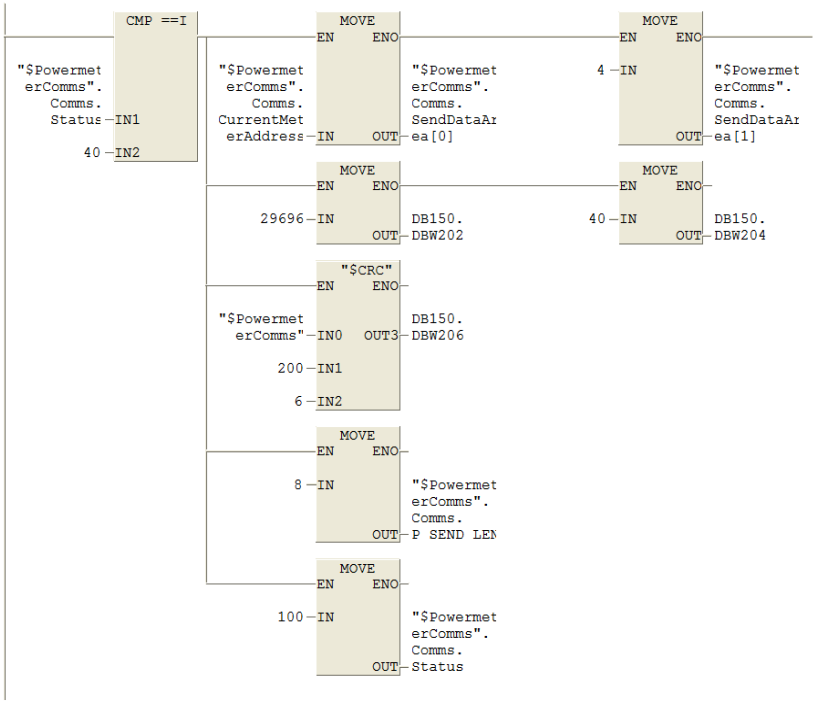

Network: 10

Build "Present Demands Register Request" message

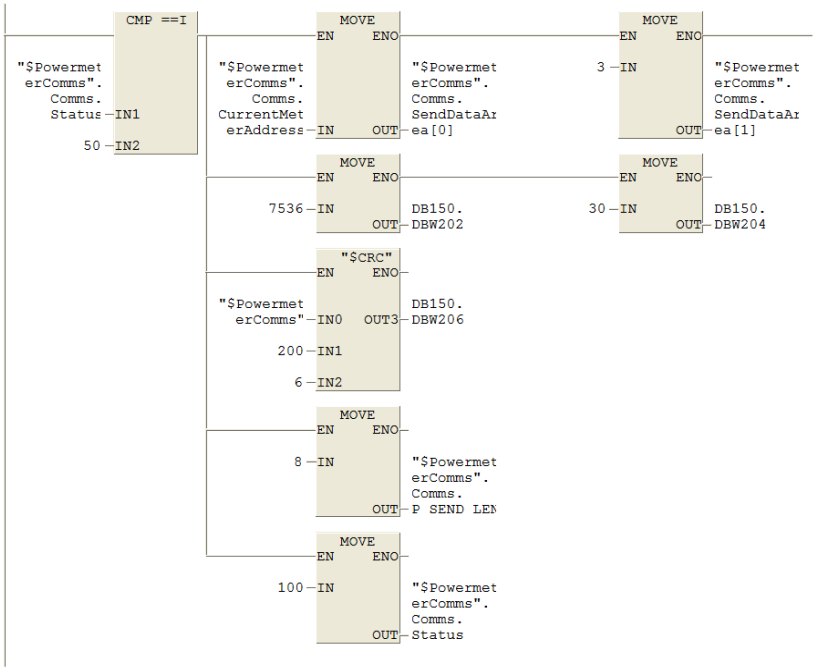

Network: 11

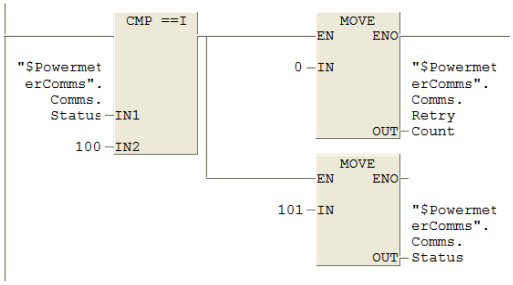

SIMATIC mine data\SIMATIC 300(1)\ 06/17/2008 03:26:45 PM
CPU 315F-2 PN/DP\...\FC150 - <offline>

Network: 12

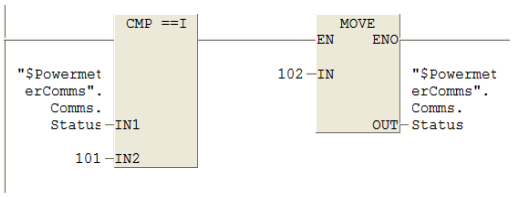

Network: 13

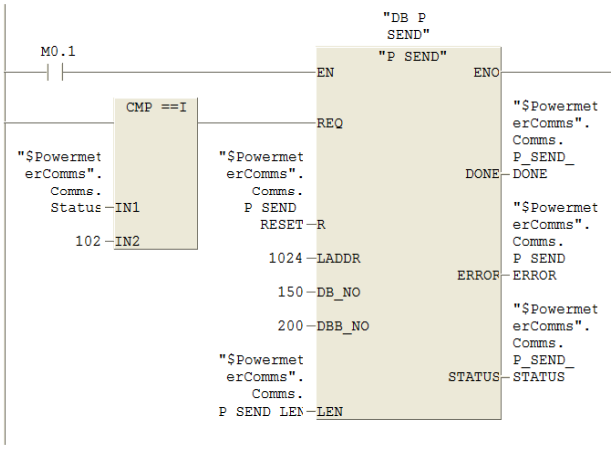

Network: 14

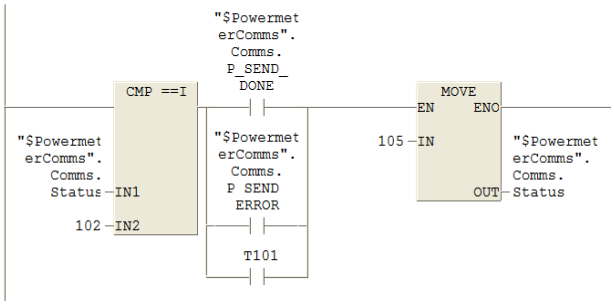

Network: 15

Receive response from the Power meter throught CP 340

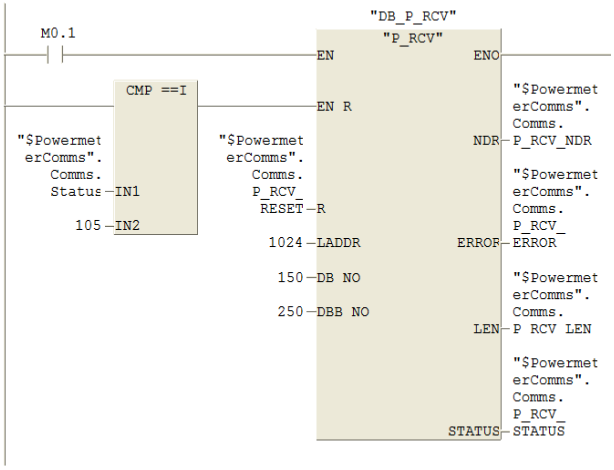

Network: 16

Check of string succesfully received 107

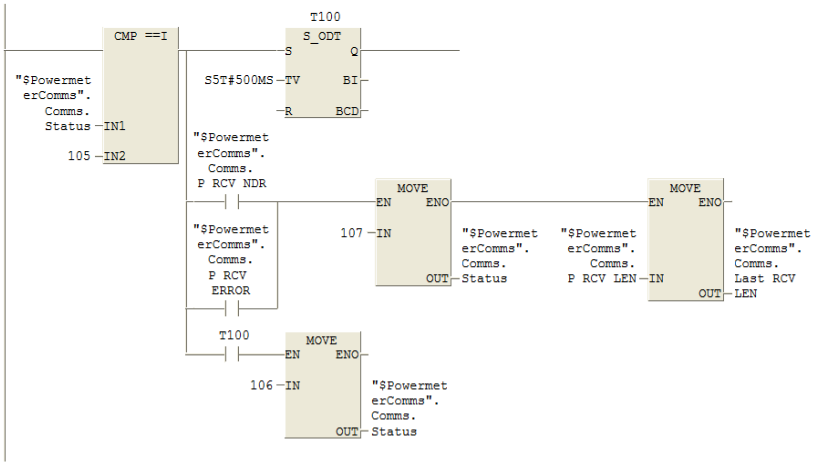

SIMATIC mine data\SIMATIC 300(1)\ 06/17/2008 03:26:45 PM
CPU 315F-2 PN/DP\...\FC150 - <offline>

Network: 17

If request timed out then retry if retry limit not yet reached

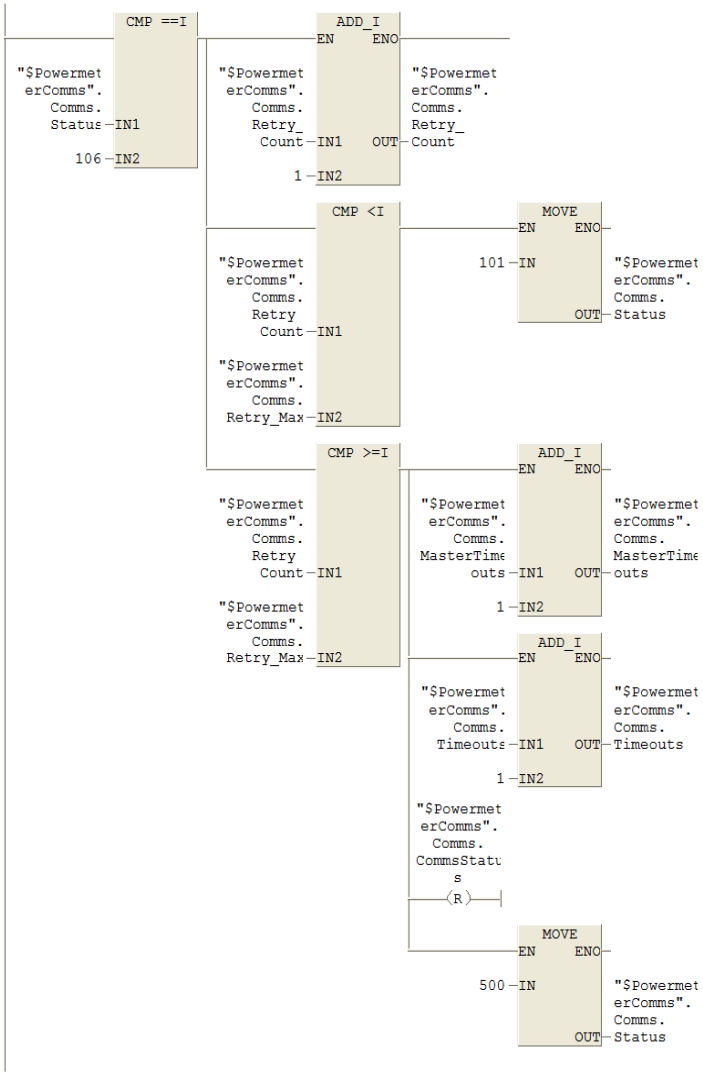

SIMATIC mine data\SIMATIC 300(1)\ 06/17/2008 03:26:45 PM
CPU 315F-2 PN/DP\...\FC150 - <offline>

Network: 18

Check crc of received string

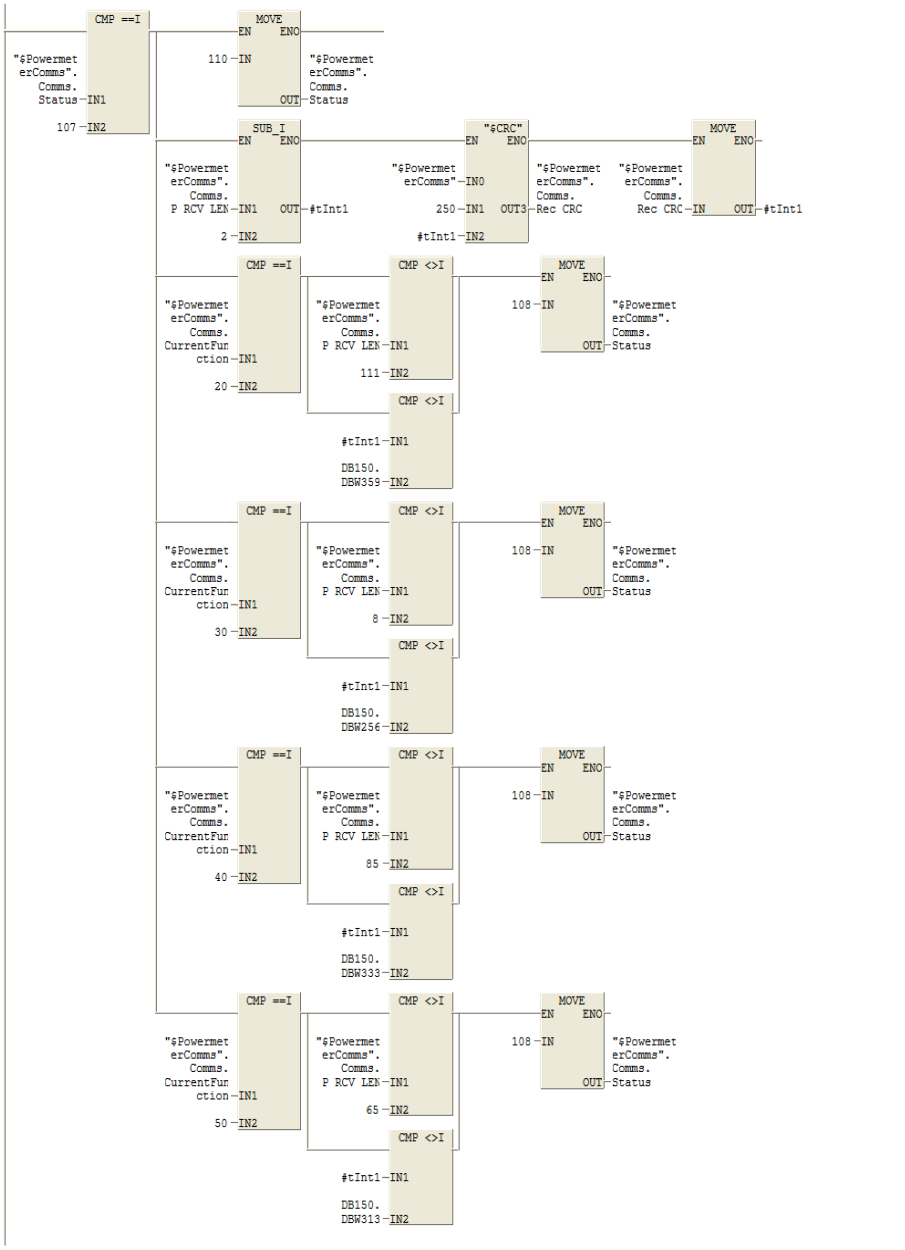

SIMATIC mine data\SIMATIC 300(1)\ 06/17/2008 03:26:45 PM
CPU 315F-2 PN/DP\...\FC150 - <offline>

Network: 19

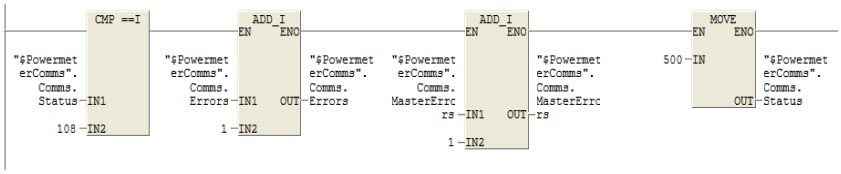

Network: 20

Message successfully received

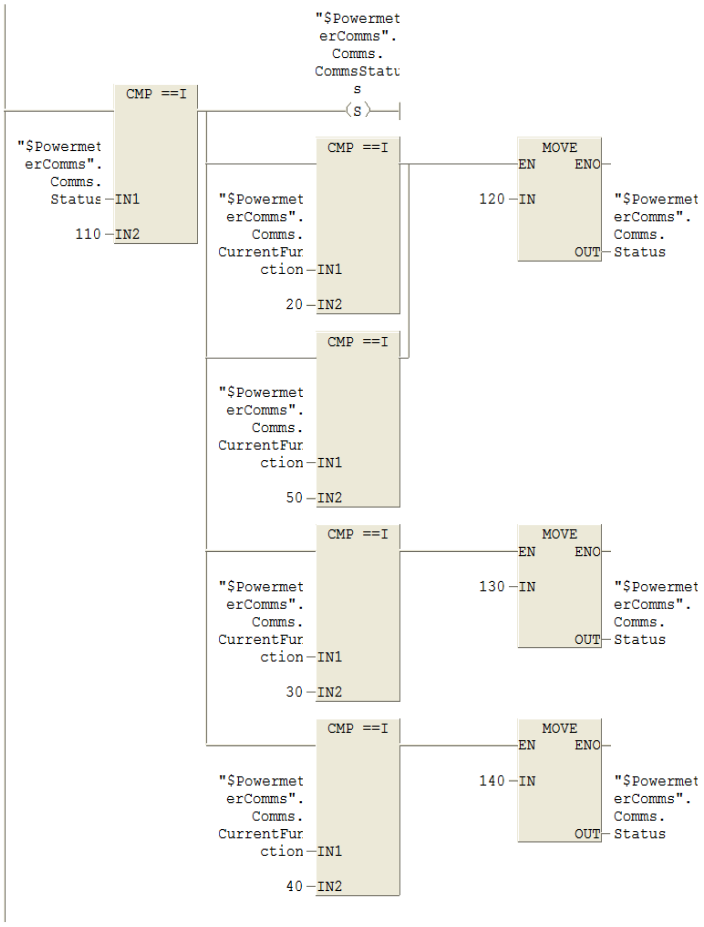

SIMATIC mine data\SIMATIC 300(1)\ 06/17/2008 03:26:45 PM
CPU 315F-2 PN/DP\...\FC150 - <offline>

Network: 21

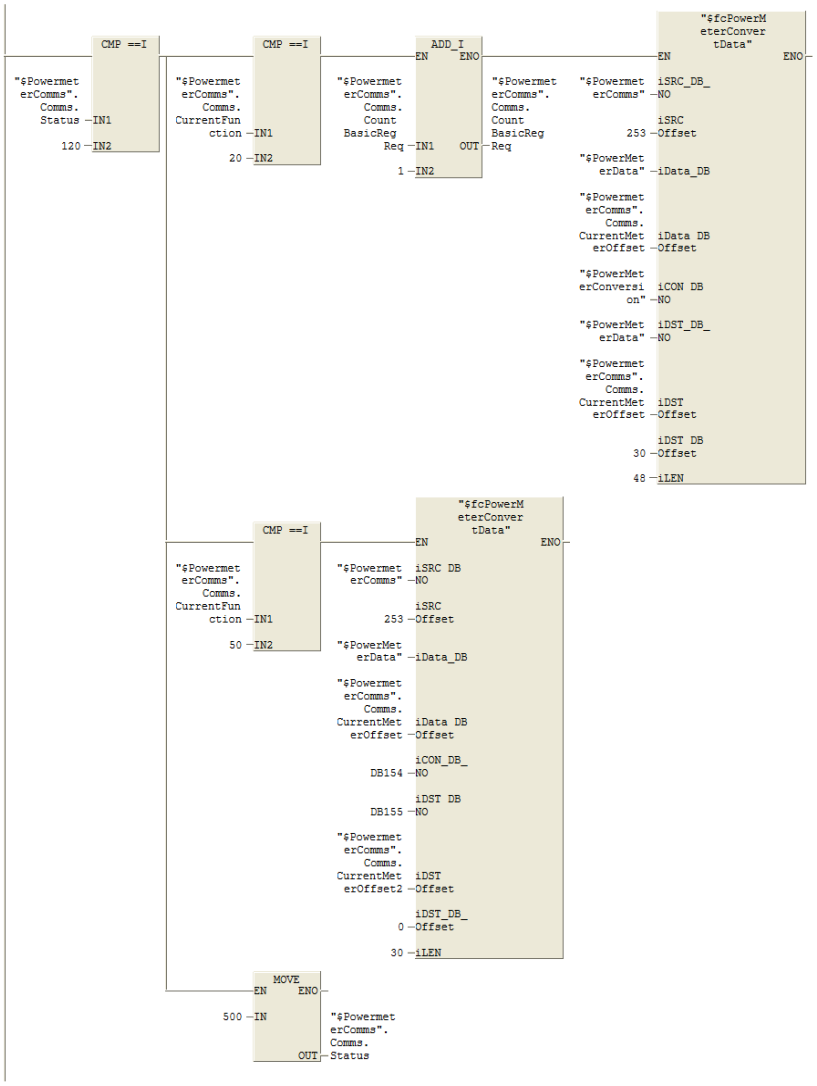

SIMATIC mine data\SIMATIC 300(1)\ 06/17/2008 03:26:45 PM
CPU 315F-2 PN/DP\...\FC150 - <offline>

Network: 22

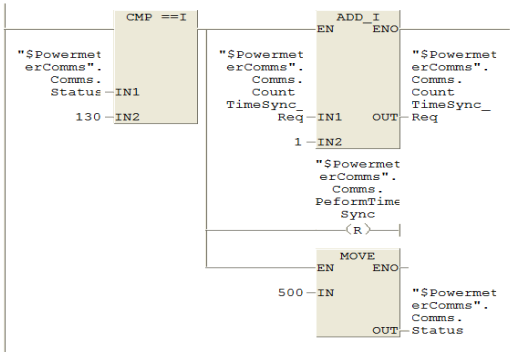

SIMATIC mine data\SIMATIC 300(1)\ 06/17/2008 03:26:45 PM
CPU 315F-2 PN/DP\...\FC150 - <offline>

Network: 23

Datalog Receipt Processing

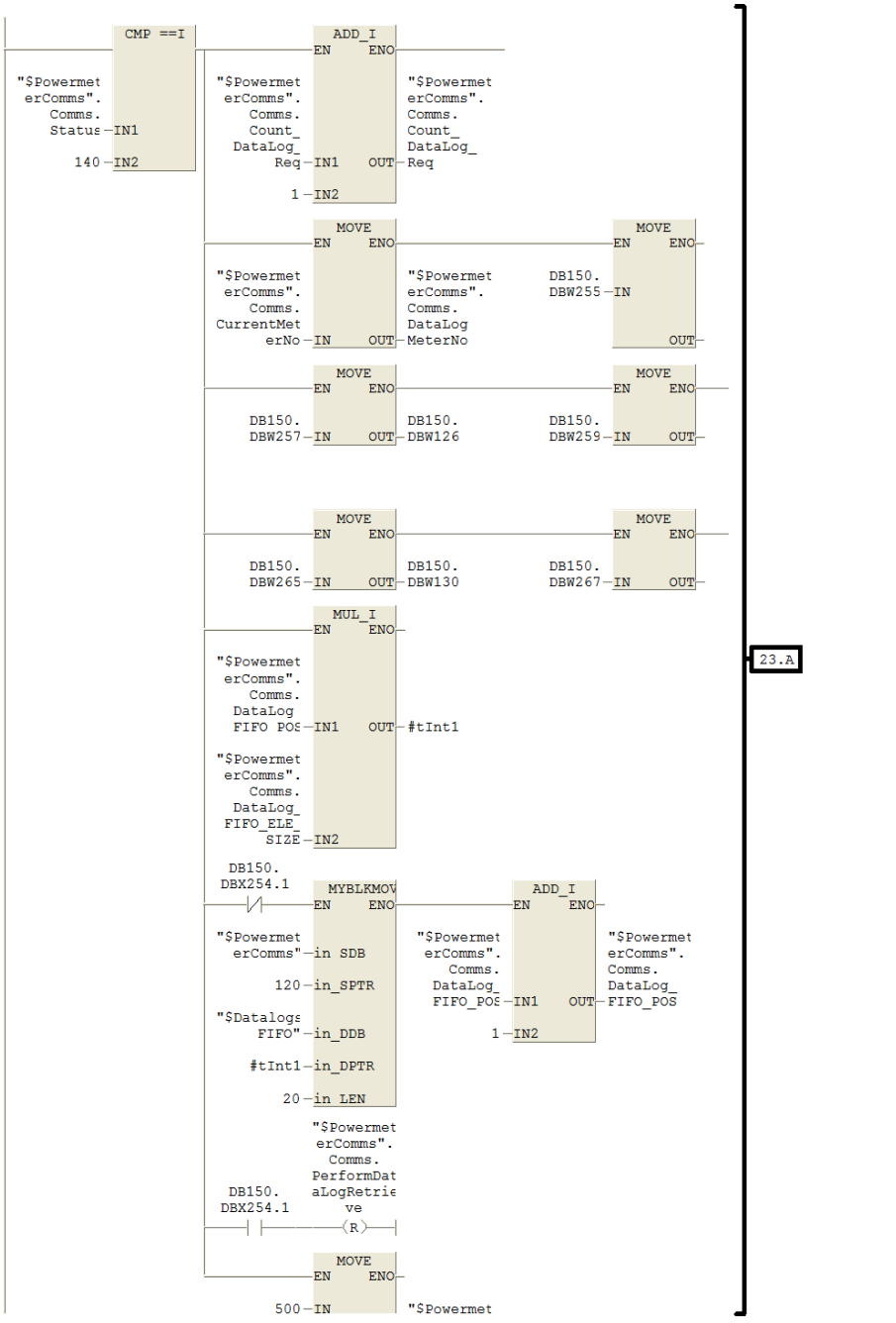

SIMATIC mine data\SIMATIC 300(1)\ 06/17/2008 03:26:45 PM
CPU 315F-2 PN/DP\...\FC150 - <offline>

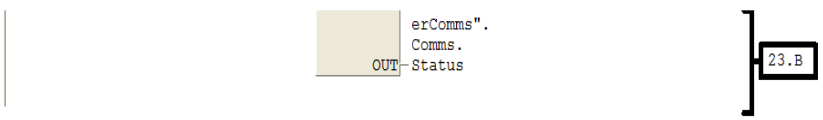

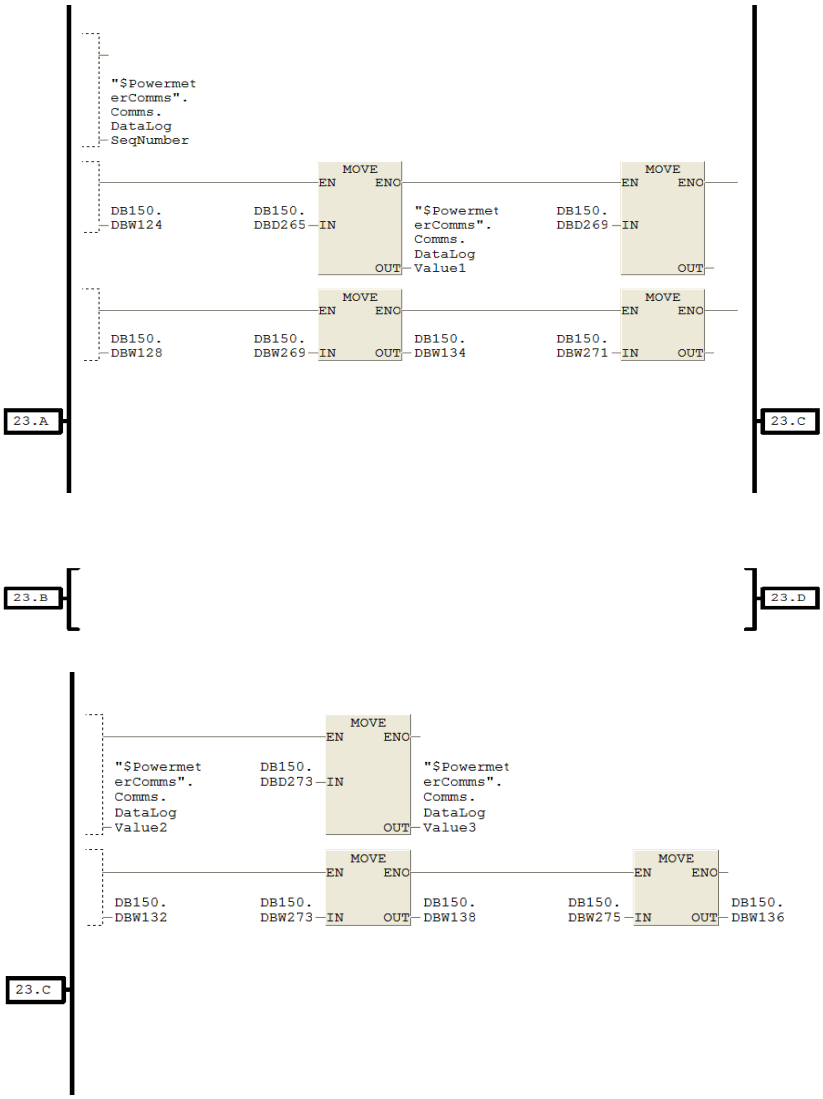
"$Powermet
erComms".
Comms.
DataLog
SeqNumber
MOVE
EN ENO
DB150.
DBW124
DB150.
DBD265
IN
"$Powermet
erComms".
Comms.
DataLog
Value1
DB150.
DBD269
OUT
MOVE
EN ENO
DB150.
DBW128
DB150.
DBW269
IN OUT
DB150.
DBW134
DB150.
DBW271
IN OUT
23.A
23.C
23.B
23.D
MOVE
EN ENO
"$Powermet
erComms".
Comms.
DataLog
Value2
DB150.
DBD273
IN
"$Powermet
erComms".
Comms.
DataLog
Value3
OUT
MOVE
EN ENO
DB150.
DBW132
DB150.
DBW273
IN OUT
DB150.
DBW138
DB150.
DBW275
IN OUT
DB150.
DBW136
23.C
23.D

Network: 24

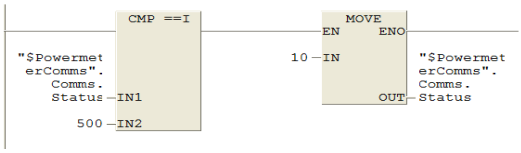
CMP ==I
"$Powermet
erComms".
Comms.
Status
IN1
500
IN2
MOVE
EN ENO
10
IN
"$Powermet
erComms".
Comms.
Status
OUT

Network: 25

```
      A(
      L     "$PowermeterComms".Comms.Status
      L     600
      ==I
      )
      JNB   M028

      L     "$PowermeterComms".Comms.CurrentMeterOffset
      L     16
      +I
      SLD   3
      T     #tPointer

      L     DB150.DBW   50
      OPN   "$PowerMeterData"
      T     DBW [#tPointer]

      L     "$PowermeterComms".Comms.CurrentMeterOffset
      L     18
      +I
      SLD   3
      T     #tPointer
      L     "$PowermeterComms".Comms.Timeouts
      OPN   "$PowerMeterData"
      T     DBW [#tPointer]

      L     "$PowermeterComms".Comms.CurrentMeterOffset
      L     20
      +I
      SLD   3
      T     #tPointer
      L     "$PowermeterComms".Comms.Errors
      OPN   "$PowerMeterData"
      T     DBW [#tPointer]

M028: NOP   0
```

Network: 26

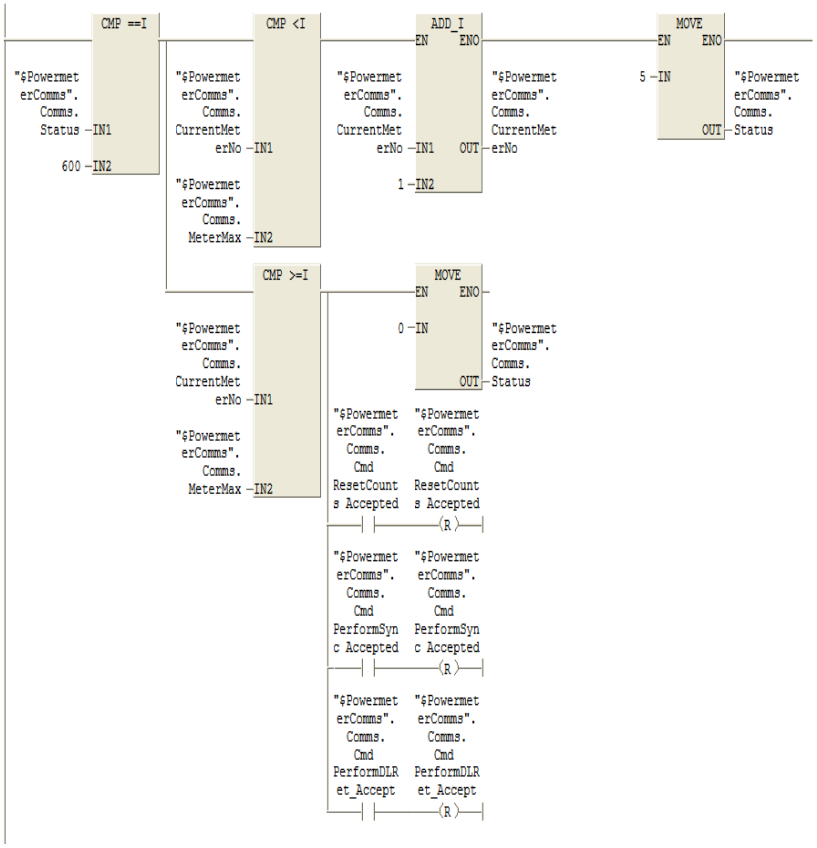

F.2.13 FC 151 Converting the raw data retrieved from the power meter into information

SIMATIC mine data\SIMATIC 10/25/2009
300(1)\CPU 315F-2 PN/DP\...\FC151 - <offline>

FC151 - <offline>
"$fcPowerMeterConvertData"
Name: FC151 **Family:**
Author: Ashvir.H **Version:** 0.1
Block version: 2
Time stamp Code: 09/30/2009 07:46:53 PM
Interface: 10/25/2006 03:32:44 PM
Lengths (block/logic/data): 01036 00844 00046

Name	Data Type	Address	Comment
IN		0.0	
iSRC_DB_NO	Block_DB	0.0	Source DB No
iSRC_Offset	Int	2.0	Source Offset (253)
iData_DB	Block_DB	4.0	
iData_DB_Offset	Int	6.0	
iCON_DB_NO	Block_DB	8.0	Conversion Data Block
iDST_DB_NO	Block_DB	10.0	Destination Data Block
iDST_Offset	Int	12.0	Destination Address Offset in DB
iDST_DB_Offset	Int	14.0	Offset in Dest DB at which values begin
iLEN	Int	16.0	Length of Address Block to be converted
OUT		0.0	
IN_OUT		0.0	
TEMP		0.0	
tPointer	DWord	0.0	
tSRC_Index	Int	4.0	Source Index
tCON_Index	Int	6.0	Conversion Data Block
tDST_Index	Int	8.0	Destination Index
tSRC_Data	Real	10.0	Source Data
tCON_Type	Byte	14.0	Conversion Type
tVMAX	Real	16.0	
tIMAX	Real	20.0	
tPMAX_POS	Real	24.0	
tPMAX_NEG	Real	28.0	
tValue	Real	32.0	
tLEN	Int	36.0	
tdint	DInt	38.0	
tValue2	Real	42.0	
RETURN		0.0	
RET_VAL		0.0	

Block: FC151

Network: 1

Convert Data block read from meter and convert to meter specific data block

```
      L     #iSRC_Offset     // Load Source DB No
      T     #tSRC_Index      // Set temp Source DB No

      L     0                // Load 0
      T     #tCON_Index      // Set temp Conversion DB to 0

      L     #iDST_Offset     // Load Destination Offset address in DB of the current meter read
      T     #tDST_Index      // Set Destination Index = Destination offset

      L     0                // Load 0
      T     #tLEN            // Set LEN to 0
```

```
      OPN   #iData_DB        // Open Destination DB
      L     #iData_DB_Offset // Load Destination Index offset address in DB
      L     4                // Load 4
      +I                     // Add 4 to Destination Index address
      SLD   3                // Shift Left Double to Create pointer address
      T     #tPointer        // Transfer pointer value to pointer
      L     DBD [#tPointer]  // Load DB Double Word from the pointer address VMAX data

      T     #tVMAX           // Transfer value to temp VMAX

      L     #iData_DB_Offset // Load Destination Index offset of current meter
      L     8                // Load 8
      +I                     // Add offset address and 8
      SLD   3                // Shift Left Double word to create pointer
      T     #tPointer        // Transfer value to pointer
      L     DBD [#tPointer]  // Load pointer address value
      T     #tIMAX           // Transfer value to temp IMAX

      L     #iData_DB_Offset
      L     12
      +I
      SLD   3
      T     #tPointer
      L     DBD [#tPointer]
      T     #tPMAX_POS
      L     -1.000000e+000
      *R
      T     #tPMAX_NEG


      L     #tDST_Index      // Load temp Destination address in open DB
      L     #iDST_DB_Offset  // Load 30
      +I                     // Add 30 to temp Destination address offet in open DB
      T     #tDST_Index      // Transfer value to destination index
```

Network: 2

Convert Data in Meter Read data block

```
M030: NOP   0

      OPN   #iSRC_DB_NO     // Open Source DB
      L     #tSRC_Index     // Load Source Data address index for current meter
      SLD   3               // Shift left double to create data pointer
      T     #tPointer       // Transfer value to data pointer
      L     DBW [#tPointer] // Load data word in source data block at pointer
      ITD                   // Integer to Double 16 bit to 32 bits
      DTR                   // Double to Real (floating point)
      T     #tSRC_Data      // Copy Data to temp Source Data

      OPN   #iCON_DB_NO     // Open Conversion Data Block
      L     #tCON_Index     // Load temp Conversion Data Block Index
      SLD   3               // Shift Left Double Word to create data pointer
      T     #tPointer       // Transfer value to data pointer
      L     DBB [#tPointer] // Load data from data block
      T     #tCON_Type      // Transfer to temp Conversion Type

      L     0
      T     #tValue         // Set temp Value to Zero

      L     #tCON_Type      // Load Conversion Type
      L     1
      ==I                   // Check for Conversion Type 1
      JC    M001

      L     #tCON_Type
      L     2
      ==I                   // Check for Conversion Type 2
      JC    M002

      L     #tCON_Type
      L     3
      ==I                   // Check for Conversion Type 3
      JC    M003

      L     #tCON_Type
      L     4
      ==I                   // Check for Conversion Type 4
      JC    M004

      L     #tCON_Type
      L     5
      ==I                   // Check for Conversion Type 5
      JC    M005
```

```
      JU    M020


M001: NOP   0               // Type 1: Low = 0, High = Vmax, Conv = LIN3
      L     #tSRC_Data
      L     9.999000e+003
      /R
      L     #tVMAX
      *R
      T     #tValue
      JU    M020

M002: NOP   0               // Type 2: Low = 0, High = Imax, Conv = LIN3
      L     #tSRC_Data
      L     9.999000e+003
      /R
      L     #tIMAX
      *R
      T     #tValue
      JU    M020

M003: NOP   0               // Type 3: Low = -Pmax, High = Pmax, Conv = LIN3
      L     #tPMAX_POS
      L     #tPMAX_NEG
      -R
      L     9.999000e+003
      /R
      L     #tSRC_Data
      *R
      L     #tPMAX_NEG
      +R
      T     #tValue
      JU    M020

M004: NOP   0               // Type 4: Low = -1, High = 1, Conv = LIN3
      L     1.000000e+000
      L     -1.000000e+000
      -R
      L     9.999000e+003
      /R
      L     #tSRC_Data
      *R
      L     -1.000000e+000
      +R
      T     #tValue
      JU    M020

M005: NOP   0               // Type 5: Low = 45, High = 65, Conv = LIN3
      L     6.500000e+001
      L     4.500000e+001
      -R
      L     9.999000e+003
      /R
      L     #tSRC_Data
      *R
      L     4.500000e+001
      +R
      T     #tValue
      JU    M020


M020: NOP   0
```

Network: 3

```
      L     #tCON_Type
      L     6
      ==I                   // Check for Conversion Type 6
      JC    M006

      L     #tCON_Type
      L     7
      ==I                   // Check for Conversion Type 7
      JC    M007

      L     #tCON_Type
      L     8
      ==I                   // Check for Conversion Type 8
      JC    M008

      L     #tCON_Type
      L     9
      ==I                   // Check for Conversion Type 9
      JC    M009
```

```
      JU    M021

M006: NOP   0               // Type 6: Low = 0, High = 9999, Conv = None
      L     9.999000e+003
      L     0.000000e+000
      L     #tSRC_Data
      T     #tValue

      L     #tSRC_Index
      L     2
      +I                    // Index Source Data by 2 registers
      T     #tSRC_Index

      L     #tCON_Index     // Skip to next low data word
      L     1
      +I                    // Index Conversion Type Data by 1 register
      T     #tCON_Index

      OPN   #iSRC_DB_NO     // Open Source DB
      L     #tSRC_Index     // Load Source Data address index for current meter
      SLD   3               // Shift left double to create data pointer
      T     #tPointer       // Transfer value to data pointer
      L     DBW [#tPointer] // Load data word in source data block at pointer
      ITD                   // Integer to Double 16 bit to 32 bits
      DTR                   // Double to Real (floating point)
      T     #tSRC_Data      // Copy Data to temp Source Data

      L     #tSRC_Data
      L     1.000000e+004   // Multiply by 10000
      *R
      T     #tValue2
      L     #tValue
      +R                    // Add high and low values
      T     #tValue

      JU    M021

M007: NOP   0               // Type 7: Low = 0, High = 999.9, Conv = LIN3
      L     9.999000e+002
      L     0.000000e+000
      -R
      L     9.999000e+003
      /R
      L     #tSRC_Data
      *R
      L     0.000000e+000
      +R
      T     #tValue

      JU    M021

M008: NOP   0               // Type 8: Low = 0, High = 100, Conv = LIN3
      L     1.000000e+002
      L     0.000000e+000
      -R
      L     9.999000e+003
      /R
      L     #tSRC_Data
      *R
      L     0.000000e+000
      +R
      T     #tValue

      JU    M021

M009: NOP   0               // Type 9: Low = 0, High = Pmax, Conv = LIN3
      L     #tSRC_Data
      L     9.999000e+003
      /R
      L     #tPMAX_POS
      *R
      T     #tValue
      JU    M021



M021: NOP   0
```

```
SIMATIC                          mine data\SIMATIC 300(1)\          06/17/2008 03:27:39 PM
                              CPU 315F-2 PN/DP\...\FC151 - <offline>

Network: 4

      OPN   #iDST_DB_NO     // Open destination data block
      L     #tDST_Index     // Load destination address in Data Block
      SLD   3               // Shift left double word to create data pointer
      T     #tPointer       // Transfer to pointer
      L     #tValue         // Load temp converted Value
      T     DBD [#tPointer] // Transfer value to destination data block



Network: 5


      L     #tLEN
      L     1
      +I
      T     #tLEN

      L     #tLEN
      L     #iLEN
      >=I
      JC    M040

      L     #tSRC_Index
      L     2
      +I
      T     #tSRC_Index

      L     #tCON_Index
      L     1
      +I
      T     #tCON_Index

      L     #tDST_Index
      L     4
      +I
      T     #tDST_Index

      JU    M030

Network: 6

M040: NOP   0
```

REFERENCES

[1] Walker ML, “Test bed system for investigating the energy usage of Variable Speed Drive Systems”, MSc Thesis, University of Natal, 2001, Durban South Africa.

[2] Kleinhans CE, “Simulation and Practical Implementation of Field Oriented Control on the Current Source Inverter-Fed Induction Machine”, MSc thesis, University of Natal, 1995, Durban, South Africa.

[3] Hao B, “Field Oriented Control of a Voltage-Fed Current Regulated Induction Motor”, MSc thesis, University of Natal, 1994, Durban, South Africa.

[4] Diana G, Harley RG, “Relationship between the Real and Complex Form of the Mathematical Model for Symmetric Induction Machinery”, University of Natal, 1985, Durban, South Africa.

[5] Theodore Wildi, “Electrical Machines, Drives and Power Systems”, 6th edition, Pearson Prentice Hall, New Jersey 2006.

[6] IEEE Power Engineering Society, “IEEE Standard Test Procedure for Polyphase Induction Motors and Generators”, Std 112-1984, IEEE, 345 East 47th Street. New York, NY 10017, copyright 1984.

[7] D.O’Kelly and Simmons, “Introduction to Generalized Electrical Machine Theory”, McGraw-Hill, 1968.

[8] Diana G, Harley RG, “An Aid for Teaching Field Oriented Control Applied to Induction Machines”, IEE Transcript On Power Systems, Vol. 4 No. 3, Aug 1989, Pg. 1258-1262.

[9] WC. OSBORNE, “Fans”, Pergamon Press, 1966, Library of Congress Catalog No. 66-18408.

[10] "Eskom annual Report 2007", Eskom, 2007.

[11] F. T. Cawood, R.C.A Minnitt, "A new royalty for South African mineral resources", The Journal of the South African Institute of Mining and Metallurgy, March/April 2001.

[12] Harcharan A, Diana G, "Development of a scaled down laboratory test bed system for use in the optimisation of an underground fan driven air ventilation system", South African Universities Power Engineering Conference (SAUPEC), Durban, South Africa, January 2008.

[13] A. Harcharan, National Power Contractors, "Southern African Energy Efficiency Convention (SAEEC)", October 2007.

[14] VSD Siemens, "MICROMASTER 440 0.12kW-250kW, Operating instructions", 6SE6400-5AW00-0BP0, October 2006.

[15] VSD Siemens, "MICROMASTER 440, Parameter list", 6SE6400-5BB00-0BP0, October 2006.

[16] PROFIBUS Siemens, "MICROMASTER PROFIBUS Optional Board, Operating instructions" 6SE6400-5AK00-0BP0, February 2002.

[17] Counter module Siemens, "SIMATIC FM 350-1 Function Module, Manual", 6ES7350-1AH00-8BG0, January 2003.

[18] Communication module Siemens, "SIMATIC S7-300 PtP coupling and configuration of CP 340, Manual", A5E00369892-01, April 2005.

[19] Power meter Satec, "Series PM110 Powermeters, Installation and Operational manual", BG0256 Rev. A3.

[20] Eskom, "Eskom Tariffs and Charges", April 2007-March 2008, Pg. 15-16.

[21] Howdin Donkin (PTY) LTD, P.O. Box 15196, Westmead 3620, South Africa.

[22] K Ogata, "Modern Control Engineering", 5th Edition, Prentice Hall International.

[23] J.D. Rozner, P.W. Meyers, C.J. Robb, “The application of Adjustable Frequency Controllers to Force Draft Fans for Improved Reliability and Energy Savings”, IEEE Transcript on Industry Applications, Vol. IA-21, No. 6, Nov/Dec 1985, pg 1482-1490.

[24] “The National Air and Space Museum”, Steven F. Udvar-Hazy Center, Photo courtesy of Dick Powers.

[26] Air velocity transducer, “Safdy Air Velocity Sensor, Model VA 316 B”, Safdy systems, P.O. Box 912870, Silverton 0127, South Africa.

[27] Pressure transducer, “Series MS Magnesense Differential Pressure Transmitter, Installation and Operating instructions”, 2007.

[28] Matlab Simulink Version 7.1, “Simulink help”, 2005.

[29] Tyson M. Murphy, “A method for evaluating the application of variable frequency drives with coal mine ventilation fans”, MSc Thesis, Virginia Polytechnic Institute and State University, 2006, Blacksburg.

[30] Mining weekly, “Coal giants keep home fires burning”, 7 September 2007.

[31] A. Harcharan, National Power Contractors, “Southern African Energy Efficiency Convention (SAEEC)”, November 2008.

[32] PC Krause, “Analysis of Electric Machinery”, McGraw-Hill, 1940.

[33] World Coal Institute, “Coal Facts 2007 Edition with 2006 data”, October 2007.

[34] G. Diana, M. W. Pickering, and R. G. Harley, "Design of a speed controller for a squirrel cage induction motor using field oriented control," Electric Power Systems Research, vol. 18, no. 3, pp. 235-245, May 1990.